Contract No:

This document was prepared in conjunction with work accomplished under Contract No. 89303321CEM000080 with the U.S. Department of Energy (DOE) Office of Environmental Management (EM).

Disclaimer:

5. RESULTS OF ANALYSIS

This chapter presents selected GW flow and radionuclide contaminant transport results from PORFLOW for the VZ and aquifer zone for each type of DU (STs, ETs, LAWV, ILV, and NRCDAs). Results for the nominal PA compliance case and various sensitivity cases are given. Results for the VZ include water saturation spatial profiles and radionuclide flux-to-the-water-table time profiles. Aquifer zone results include maximum concentration spatial contours; radionuclide concentration time profiles at the 100-meter POA; and peak concentrations at the 100-meter POA and time of occurrence for each modeled radionuclide. Dose history time profiles and preliminary disposal limits for the GW pathway are provided in Chapter 8. GoldSim® model results for the air pathway and radon flux analyses for the four types of DUs are also presented and include peak doses (air) and fluxes (radon), peak times, and dose limits. Appendices supplement the limited results included in the chapter.

- **Section 5.1** presents GW, air, and radon pathways results for STs and ETs. The GW pathway results include generic waste as well as simple and complex SWFs.
- **Section 5.2** provides GW, air, and radon pathways results for the LAWV.
- **Section 5.3** summarizes GW, air, and radon pathways results for the ILV. The GW pathway results are for generic waste and five SWFs.
- **Section 5.4** presents GW, air, and radon pathways results for the NRCDAs. GW pathway results include generic waste and SWFs.

KEY TAKEAWAYS

- ✓ The probabilistic scheme for cap subsidence implemented in STs and ETs indicates that end, central, and cap-crest hole locations are equally likely based on historical data for non-crushables. To avoid overly pessimistic assumptions, flux-to-the-water-table profiles for the three hole locations are blended equally. Early and later peaks for radionuclides like Np-237 are better represented through time. For Sr-90 with a single peak, blending is more pessimistically bounding because the dominant flux is at an end hole.
- ✓ For STs and ETs, saturation profiles demonstrate the comparative effectiveness of the final closure cap, where travel time to the water table is 50,000 to 80,000 years depending on depth to water.
- ✓ For CIG SWFs, lower infiltration from installation of a concrete mat and/or intact closure cap delays peak flux to the water table due to the lower water velocity and longer aging time for cementitious materials. For shorter-lived nuclides like Sr-90, this delay leads to a peak flux at CIG-6 and CIG-7 that is several orders of magnitude lower than the bounding subsidence case.
- ✓ A mechanistic model of concrete degradation is successfully developed for LAWV and ILV.
- ✓ For LAWV and ILV, radionuclide fluxes in the sensitivity cases peak higher and earlier than in the nominal PA and best estimate cases.
- ✓ For LAWV, ILV, and NRCDAs, peak flux at the water table and peak concentrations at the 100-meter POA are most sensitive to changes in infiltration and K_d.
- ✓ NRCDA VZ transport models correctly capture early and late releases due to hydraulic failure of bolted containers and differences in corrosion rates of activated Inconel and Zircaloy in welded casks.
- ✓ For NRCDA SWF with activated Zircaloy, all sensitivity cases show a negligible impact on peak flux because of low release rates (104,349-yr corrosion time).
- ✓ Radon flux largely depends on specific activity of parent radionuclides; secular or transient disequilibrium in decay chains leads to lower flux.
- ✓ Faster transport to surface for air-pathway nuclides does not necessarily lead to higher dose to receptors because of a shift in the POA at the end of IC from the site boundary to the 100-meter boundary.

5.1. SLIT AND ENGINEERED TRENCHES

5.1.1. Vadose Zone Model for Generic Waste Forms

PORFLOW flow and radionuclide transport models of the VZ are developed for STs and ETs to evaluate dose impacts and produce disposal limits for the ELLWF. This section presents selected flow and radionuclide contaminant transport results for the PORFLOW VZ model of STs and ETs. Appendix D contains supplemental concentration profiles of SWF radionuclides that contribute to at least 0.1% of the sum-of-fractions.

As discussed in Section 4.1.3, 3-D conceptual models of the VZ for STs and ETs for the GW pathway are developed and then implemented in PORFLOW to create the complete suite of GW flow and radionuclide contaminant transport models for PA2022 (Danielson, 2019a; 2019b; 2019c; Danielson, 2020a; 2020b). The preliminary ST and ET scoping studies summarized in Section 4.1.3 are utilized to compile best-estimate or bounding assumptions and create a workflow for implementation. Where possible, the generalizability of ST and ET model geometries is leveraged to promote computational efficiency in the models' implementation and allow for more direct comparison of flow and transport results. This approach reduces the potential for numerical artifacts of differing spatial discretizations. The primary features that have been generalized are as follows:

1. UVZ clayey material from the edges of the model domain up to the DU boundary.
2. DU geometry, including the pre- and post-dynamic compacted waste zone and backfill material for STs and ETs.
3. Spatial discretization (Table 5-1) in the X and Y planes across the model domain as well as vertical discretization within the DU volume.

Table 5-1. Spatial Discretization of Waste Zone Material Regions and Uniform X-Y Discretization Across Model Domain

Material Region	Thickness (ft)	Nodes		
		X	Y	Z
Dynamic-Compacted Boxed Waste Zone	2.5	168	43	4
Dynamic-Compacted Hybrid Waste Zone	11.1	168	43	10
Waste Zone with No Dynamic Compaction	16	168	43	6
Backfill	4	168	43	4
Domain	DU-specific	200	75	DU-specific

Notes:
Vertical discretization outside the waste zone varies based on the hydrostratigraphic grouping.

As summarized in Figure 4-42, this PA requires 17 unique VZ models from seven unique hydrostratigraphic groupings. The 17 unique 3-D PORFLOW VZ models are developed to capture the unique geometry and features of the waste zones (Sections 4.1.3.3 and 4.1.3.4) and subsurface hydrostratigraphic units (Section 4.1.3.2), as well as the chronology of facility events (Section 4.1.3.5) and infiltration boundary conditions (Section 4.1.3.6) for each trench. Radionuclide, chemical, and material properties, as well as the subsurface features represented in

the models, are obtained from the PA property data packages (SRNL, 2017; 2018; 2019a; 2019b; 2020) containing key PA data.

The features of the ST hybrid waste form and ET boxed waste form are built into all simulation meshes; PORFLOW "LOCAte" commands are used to combine the appropriately dimensioned waste zone sections.

Infiltration rate boundary conditions are specified on a per-trench-DU basis, considering both cover geometries associated with the specific DU location (i.e., central-, corner-, and edge-located trench DUs as illustrated in Figure 5-1 and Figure 5-2) and the percentage of the waste volume that contains non-crushable inventory, if any. The non-crushable inventory determines the subsidence potential of the waste zone.

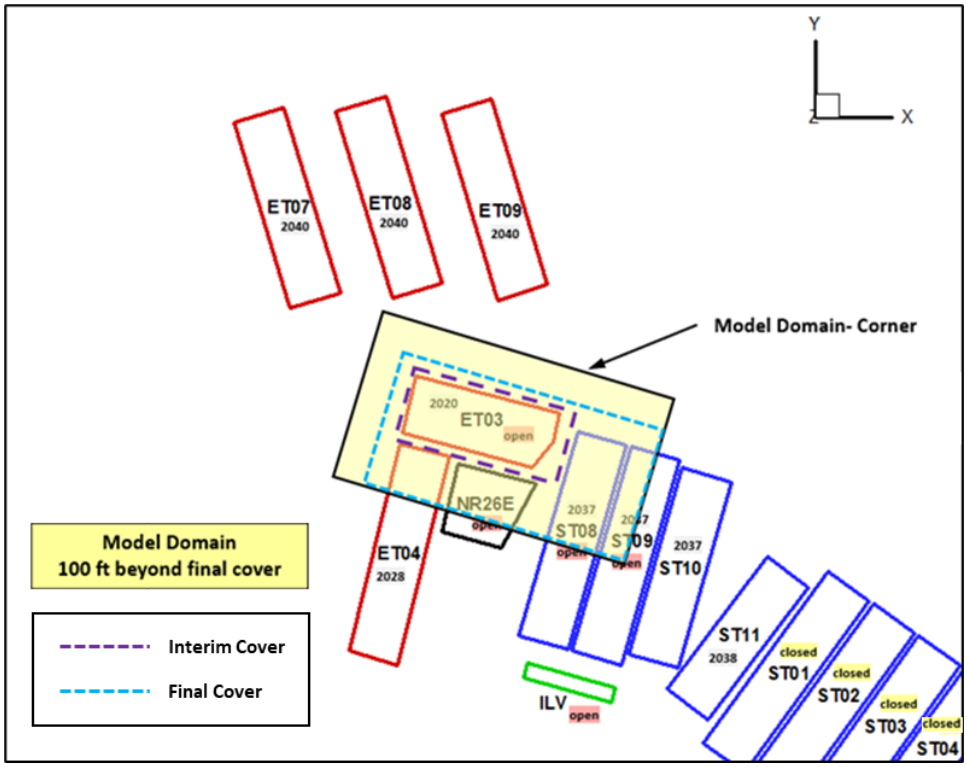

Figure 5-1. Illustration of a Corner-Located Trench Disposal Unit

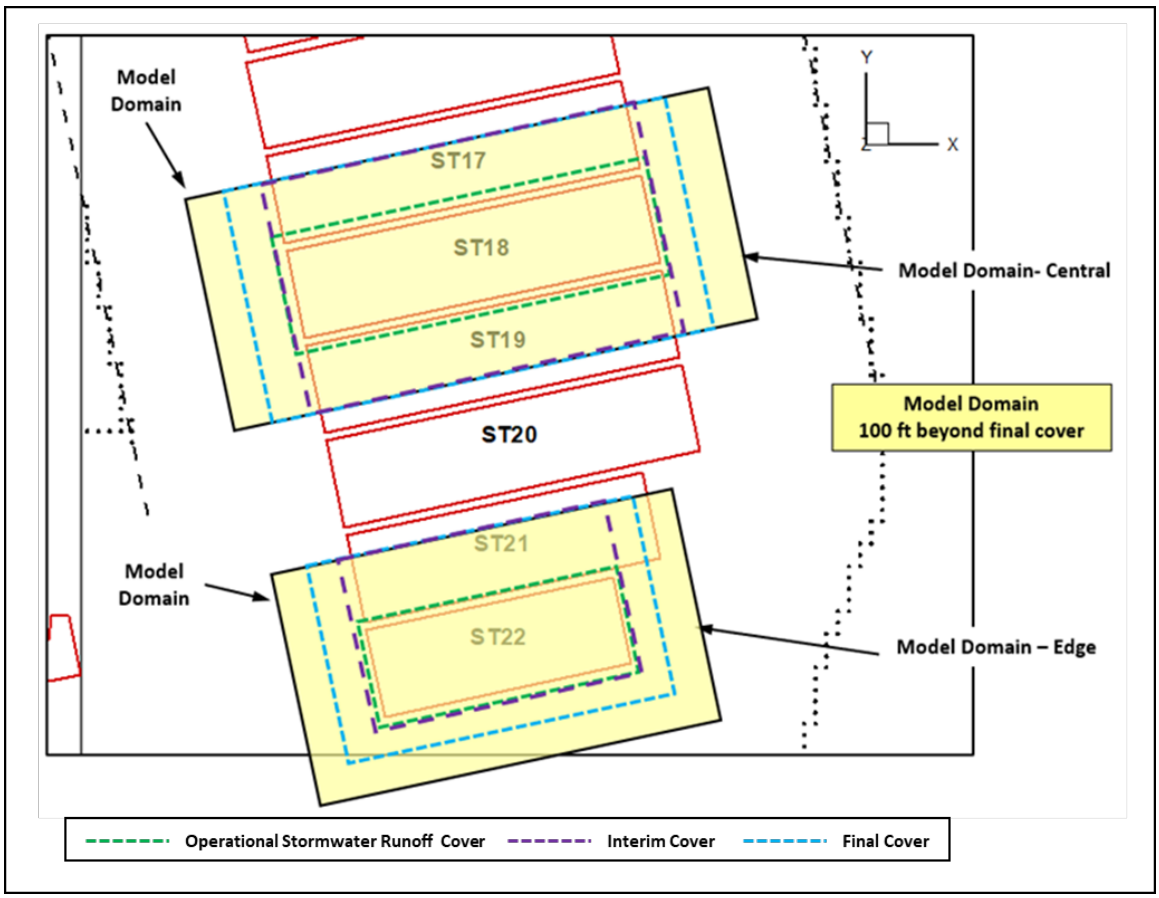

Figure 5-2. Illustration of Centrally Located and Edge-Located Trench Disposal Units

Table 5-2 provides a detailed listing of the percent subsidence and cover geometry for each ST and ET DU for the seven ST and ET VZ model hydrostratigraphic groupings. Note that ET03, ET04, and ST08, located near NR26E, receive a unique treatment at the time of the interim cover placement because the NR26E disposal pad is and will remain uncovered[1] until the final closure cap is installed.

[1] The uncovered period is before a HDPE stormwater runoff cover is placed over a filled ST or ET DU. When a section of a ST is filled, 4 feet of clean soil is placed over the waste layer to bring the ST up to grade and serve as the required operational soil cover (OSC1). Similarly, when a sufficient number of B-25 rows are placed in an ET, stockpiled clean soil is bulldozed in a single lift over a portion of the completed rows to produce a minimum 4-foot-thick, clean soil layer on top (i.e., an operational soil cover).

Table 5-2. Hydrostratigraphic Grouping, Cover Geometry, and Percent Subsidence for Slit and Engineered Trench Model Disposal Units

Hydrostratigraphic Grouping	DU	Interim Cover Geometry	Final Cover Geometry	Percent Subsidence
Group 1	ET04	Operational SW Runoff Cover[1]	Corner	2
	ST01	Central	Central	0
	ST02	Central	Central	2
	ST08	Edge	Central	2
	ST09	Central	Central	2
	ST10	Central	Central	2
	ST11	Central	Central	2
Group 2	ET03	Operational SW Runoff Cover[1]	Corner	0
	ST03	Central	Central	4.9
	ST04	Central	Central	3.6
	ST23	Central	Central	2
Group 3	ST05	Central	Central	0.54
	ST06	Central	Central	2
	ST07	Central	Central	2
	ST24	Central	Central	2
Group 4	ET01	Central	Central	2
	ST14	Central	Central	2
Group 5	ET05	Edge	Edge	2
	ET06	Edge	Edge	2
	ST17	Central	Central	2
	ST18	Central	Central	2
	ST19	Central	Central	2
	ST20	Central	Central	2
	ST21	Central	Central	2
	ST22	Central	Central	2
Group 6	ET02	Central	Central	2
Group 7	ET07	Edge	Edge	2
	ET08	Central	Central	2
	ET09	Edge	Edge	2

Notes:

[1] The interim cover in this location is assumed to have the same geometry as the operational stormwater runoff cover (i.e., 10-foot overhang on all sides) due to the proximity of the NR26E disposal pad, which remains uncovered at interim closure.

The pre-processing workflow for implementation of PORFLOW flow simulations is as follows:

1. Discretize mesh for each hydrostratigraphic grouping.
2. Separate STs and ETs.
3. Use PORFLOW LOCAte commands to assign DU-specific material properties.

4. Use PORFLOW LOCAte commands to specify location-dependent operational, interim, and final closure cap boundary condition geometries for central-, corner-, and edge-located trench DUs in all hydrostratigraphic groupings.
5. Separate intact and subsidence flow models.
6. Specify trench-specific, subsidence hole sizes (if subsidence conditions exist) using PORFLOW LOCAte commands.
7. Apply appropriate infiltration rate boundary conditions.

The resulting hierarchical file structure from this workflow is illustrated in Figure 5-3.

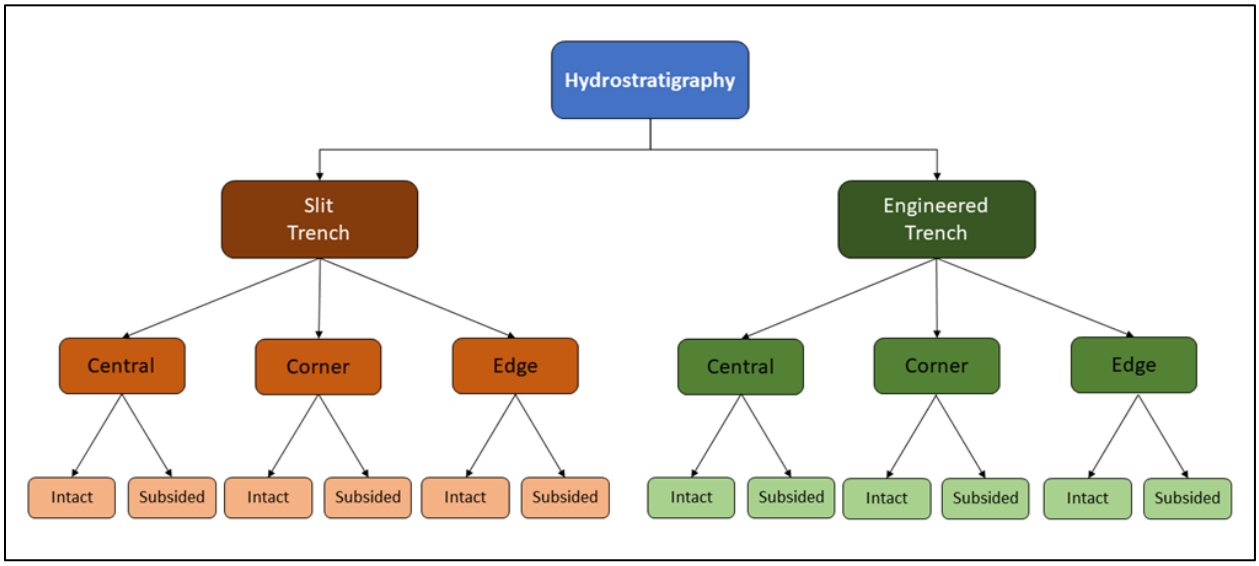

Figure 5-3. Hierarchical File Structure of Pre-Processed PORFLOW Steady-State Flow Simulations

5.1.1.1. Flow Model

For each simulation setup in the model hierarchy, a sequence of 98 flow fields are computed spanning 10,471 years and representing various stages of operational, interim, and final closure periods. Time-dependent waste form properties (i.e., pre- and post-dynamic compaction) and boundary conditions based on installation and degradation of infiltration barriers are accounted for in each simulation setup. In this section, a limited subset of the PORFLOW-computed flow fields is presented to highlight the differences of the various trench and cover geometries and the intact and subsidence boundary conditions.

5.1.1.1.1. Intact Closure Cap Boundary Condition

Figure 5-4 through Figure 5-13 present the saturation profiles for time intervals corresponding to the operational, interim, and final closure periods for ST and ET geometries under intact conditions. Note that water saturation is dimensionless (vol/vol). The saturation profiles show the impact of the various covers. For example, although the operational stormwater runoff cover and interim cover have the same infiltration rate, the spatial extent differs. As a result, when the operational stormwater runoff cover is present, more water impacts the waste zone as water suction occurs on all four sides of the ST and ET. By comparison, the interim cover for centrally located

STs and ETs extends across the model domain in the y-direction and, therefore, no suction occurs in that direction.

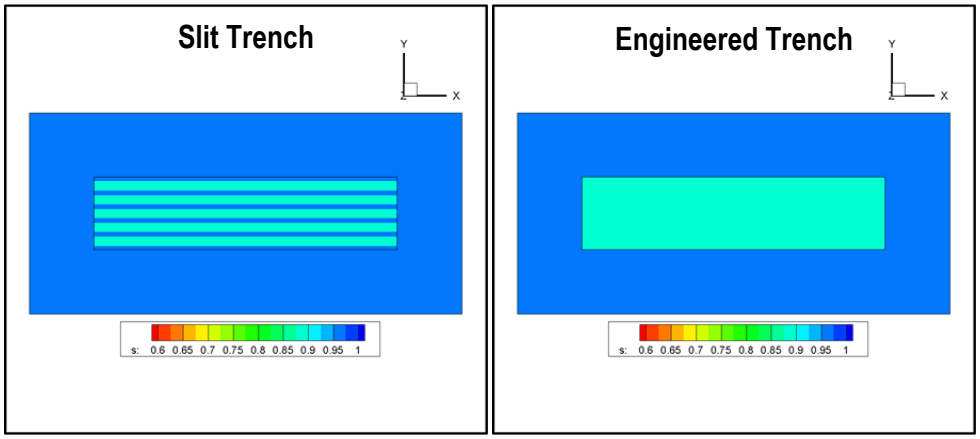

Figure 5-4. Slit Trench (left) and Engineered Trench (right) Overhead Saturation Profiles During Uncovered Period

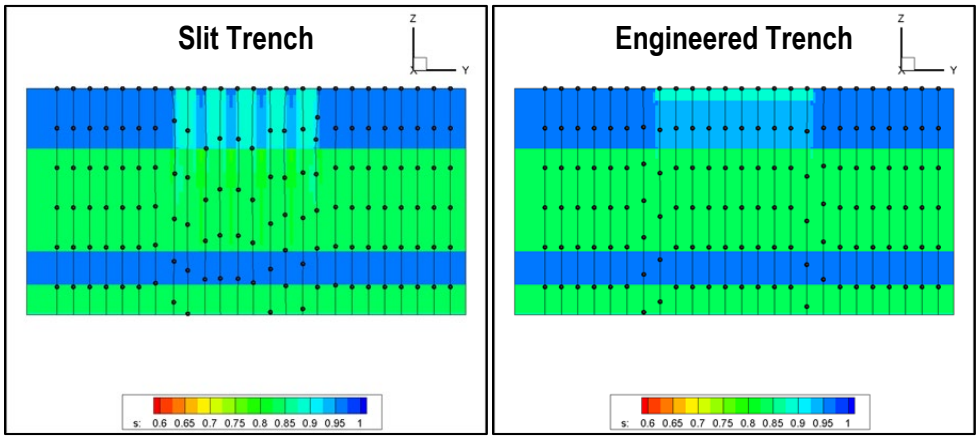

Figure 5-5. Slit Trench (left) and Engineered Trench (right) Saturation Profiles in a YZ Plane During Uncovered Period with Stream Traces Showing 10-Year Time Markers

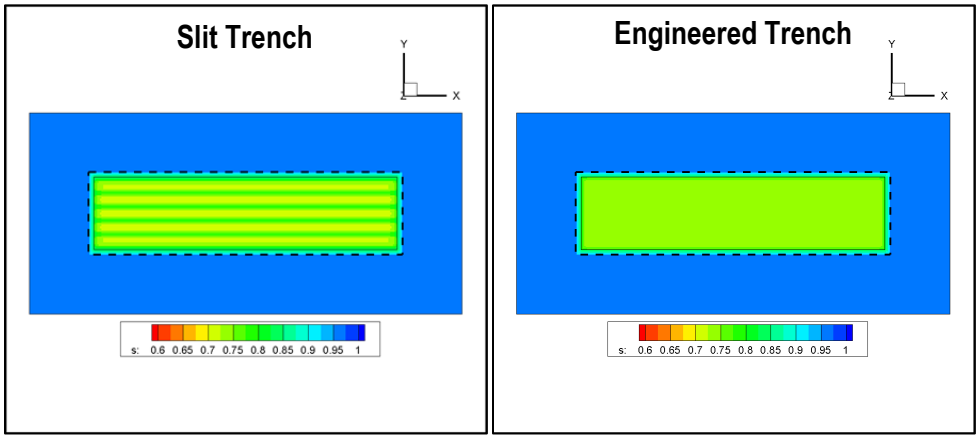

Figure 5-6. Slit Trench (left) and Engineered Trench (right) Overhead Saturation Profiles During Operational Stormwater Runoff Cover Period

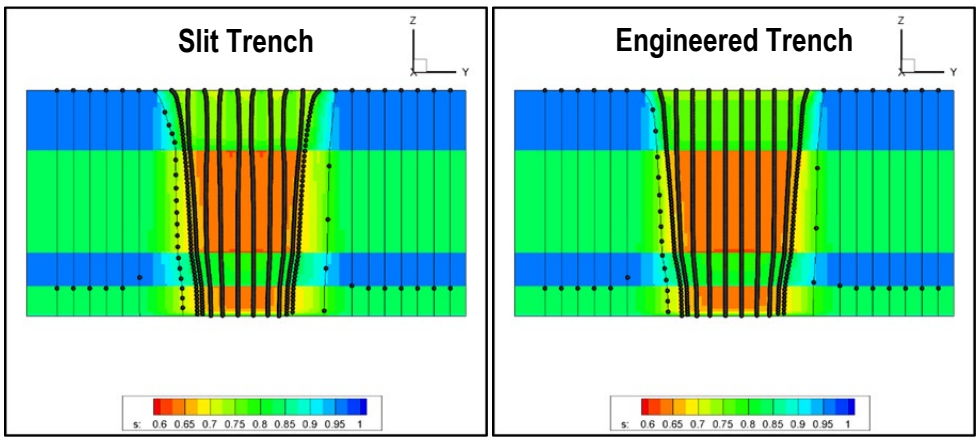

Figure 5-7. Slit Trench (left) and Engineered Trench (right) Saturation Profiles in a YZ Plane During Operational Stormwater Runoff Cover Period with Stream Traces Showing 50-Year Time Markers

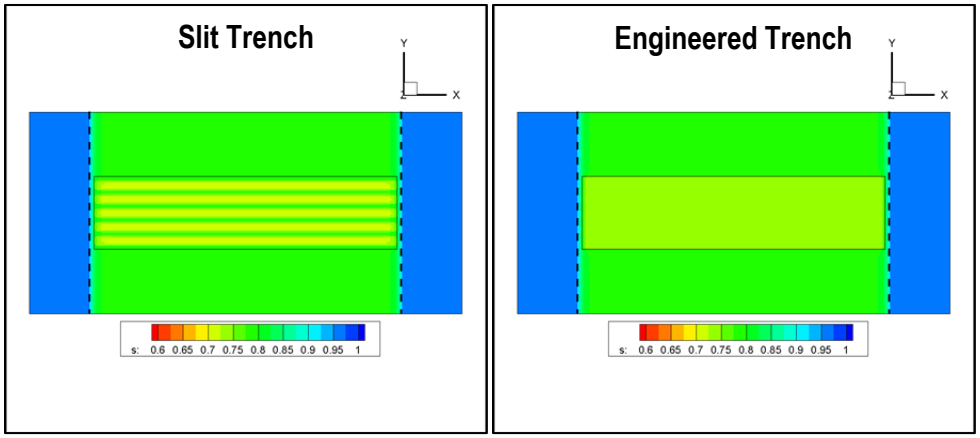

Figure 5-8. Slit Trench (left) and Engineered Trench (right) Overhead Saturation Profiles During Interim Cover Period

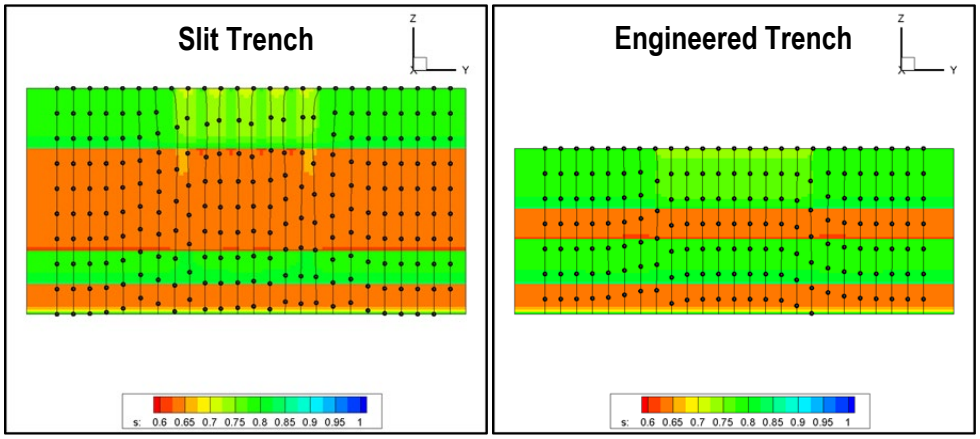

Figure 5-9. Centrally Located Slit Trench (left) and Engineered Trench (right) Saturation Profiles in YZ Plane During Interim Cover Period with Stream Traces Showing 1,000-Year Time Markers

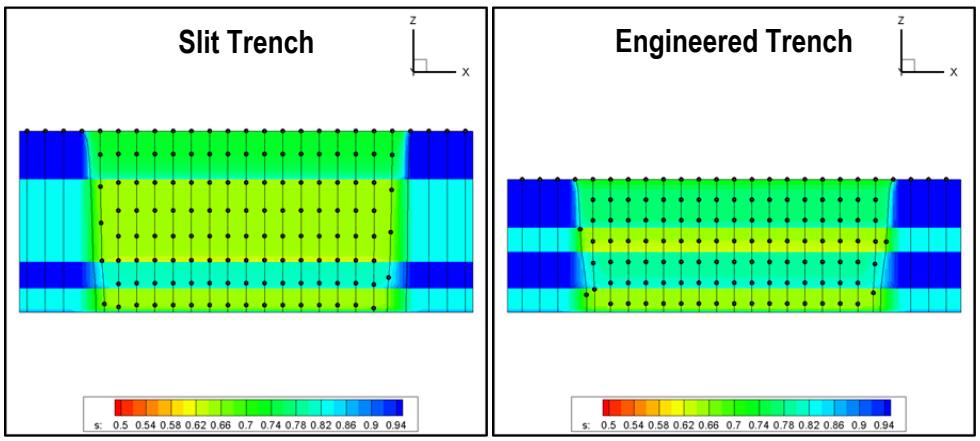

Figure 5-10. Centrally Located Slit Trench (left) and Engineered Trench (right) Saturation Profiles in XZ Plane During Interim Cover Period with Stream Traces Showing 1,000-Year Time Markers

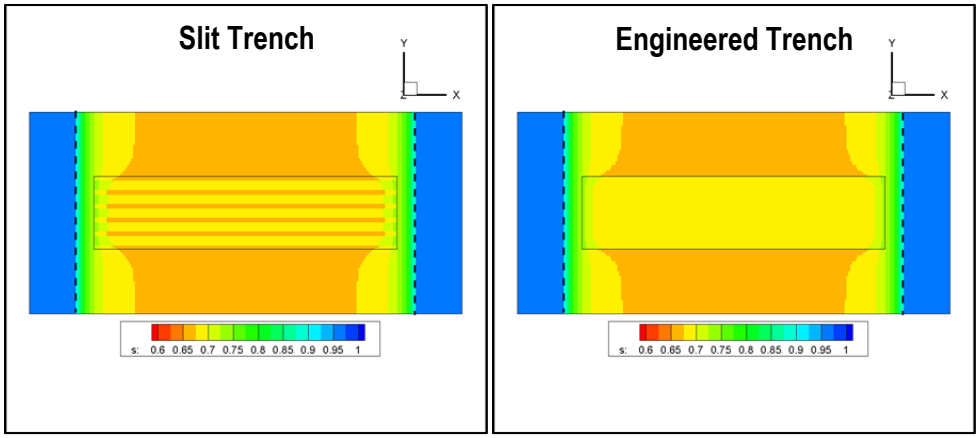

Figure 5-11. Slit Trench (left) and Engineered Trench (right) Overhead Saturation Profiles During First Period After Final Closure Cap Installation

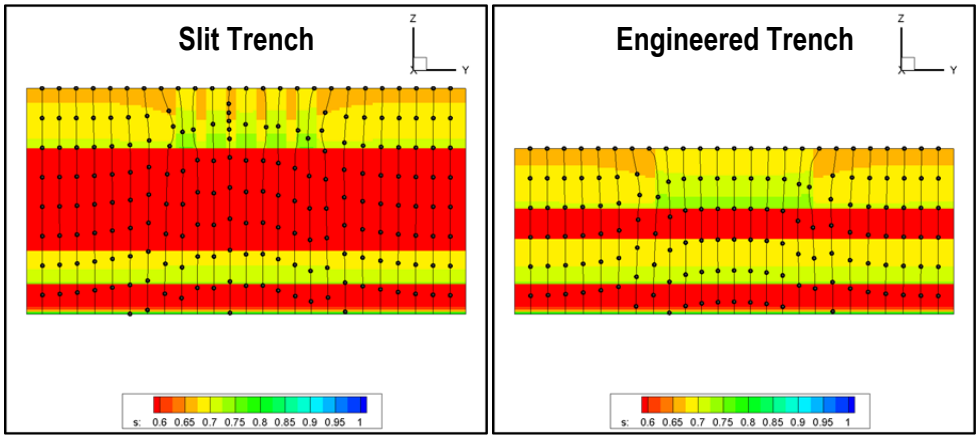

Figure 5-12. Centrally Located Slit Trench (left) and Engineered Trench (right) Saturation Profiles in YZ Plane During First Period After Final Closure Cap Installation with Stream Traces Showing 100,000-Year Time Markers

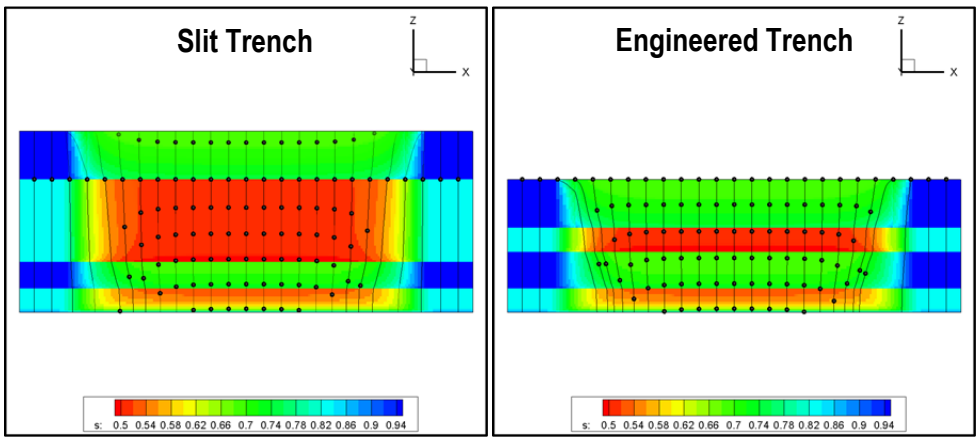

Figure 5-13. Centrally Located Slit Trench (left) and Engineered Trench (right) Saturation Profiles in XZ Plane During First Period After Final Closure Cap Installation with Stream Traces Showing 100,000-Year Time Markers

The streamtraces in the saturation profiles presented in Figure 5-12 and Figure 5-13 demonstrate the comparative effectiveness of the final closure cap, where the travel time from ground surface to the water table is on the order of 50,000 to 80,000 years depending on the depth to the water table. Time markers are placed along the streamlines to show the distance that flow travels during the time indicated in each figure caption. In comparison, the travel time is less than 15,000 years when the interim cover is present (Figure 5-9 and Figure 5-10). The final closure cap is not maintained after installation; therefore, the progressive degradation of the soil-geomembrane multilayer cover (as described in Section 3.4.1) causes the infiltration rate to progressively increase over time, eventually plateauing at approximately 11 in yr^{-1} at ~Year 2,700.

While the centrally located cover geometry is applicable for most STs and ETs in the ELLWF, a handful of DUs require an edge or corner cap geometry for the boundary conditions. Figure 5-14 shows overhead saturation profiles for the corner and edge configurations highlighting the impacts of the different geometries. Because of the suction along the exposed edges, these configurations display a higher overall water content impacting the waste zone when compared to the centrally located STs and ETs. The edge configuration (Figure 5-14, right side) is the most impacted.

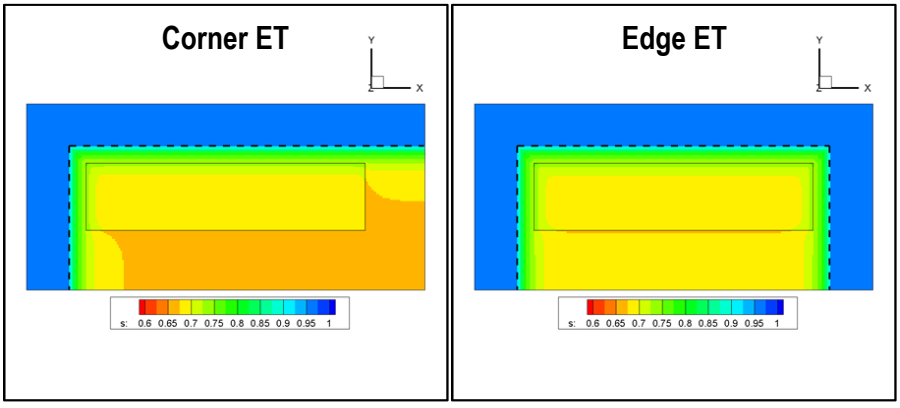

Figure 5-14. Corner (left) and Edge (right) Overhead Saturation Profiles for an Engineered Trench During First Period After Final Closure Cap Installation

5.1.1.1.2. Subsidence Boundary Condition

Figure 5-15 shows saturation profiles during the period at the end of IC for the four subsidence "hole sizes" to highlight the impact of percent subsidence. Note that water saturation is dimensionless (vol/vol). The subsidence area (i.e., hole) is represented in Figure 5-15 by a blue rectangle of individual trench width (20 feet) and varying length in the upper left portion of the ST footprint. Notably, as hole size decreases (from lower right panel to upper left panel in Figure 5-15), the water infiltration rate increases because of the combined surface runoff and lateral drainage emptying into the hole from the upslope, intact portion of the cap. Therefore, an inverse relationship exists between the areal footprint of the waste zone that is impacted by the subsidence region and water *velocity* through the waste zone.

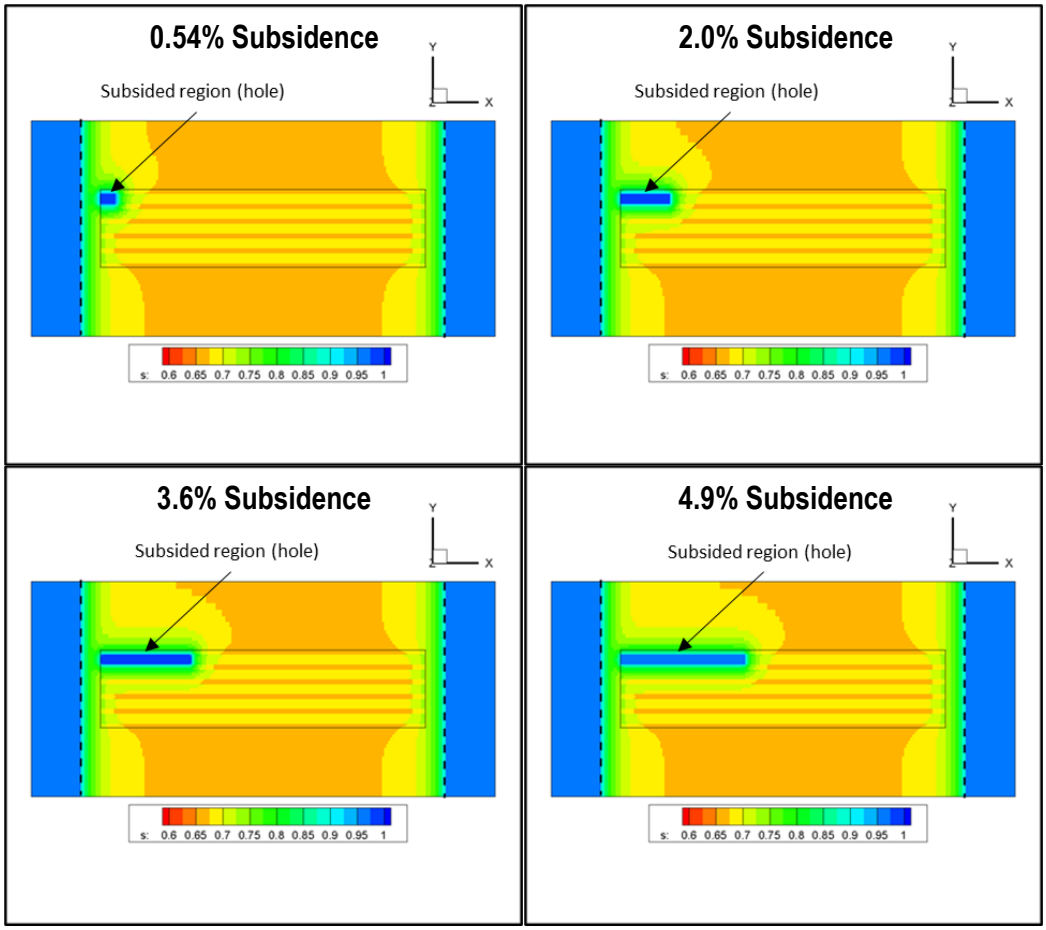

Figure 5-15. Saturation Profiles in XY Plane Demonstrating Differences Due to Subsidence Hole Size in STs: (Top Left) 0.54% Subsidence; (Top Right) 2.0% Subsidence; (Bottom Left) 3.6% Subsidence; (Bottom Right) 4.9% Subsidence

5.1.1.2. Transport Model for Nominal PA Cases

Radionuclide contaminant transport for each DU is simulated according to the operational timeline. Steady-state flow fields are input to PORFLOW to solve the transport equations for the 27 radionuclide species identified in the GW screening analysis. From this, flux to the water table is computed for up to a 10,471-year simulation period. This calculation is used as the source term

at the water table for contaminant transport in the aquifer zone. For future STs and ETs in the same hydrostratigraphic grouping and with the same cover geometry (e.g., ST17 through ST20 in ST Group 5), the same timeline is used; therefore, only one model is required. The following sections show a subset of results to demonstrate the differences in the flux to the water table for mobile versus immobile and short-lived versus longer-lived radionuclides.

5.1.1.2.1. Intact Closure Cap Boundary Condition

Figure 5-16 through Figure 5-18 present flux-to-the-water-table profiles for selected radionuclides emanating from the ST and ET waste zones corresponding to centrally located DUs, ST14 and ET01 (Figure 2-32). While both ST14 and ET01 are in Hydrostratigraphic Group 4 (Table 5-2), a direct comparison that explains the impacts of differing ST and ET geometries and waste zone hydraulic properties cannot be made. The timing of waste placement and stormwater runoff cover installation differs between these units by about 10 and 15 years, respectively. These differences are most notable in mobile radionuclide cases. In general, the lesser thickness of the boxed waste form at dynamic compaction (2.5 feet versus 11.1 feet for ET boxed waste and ST hybrid waste, respectively) decreases the travel time of radionuclide species to the water table.

The selected subset of radionuclides included in Figure 5-16 through Figure 5-18 demonstrates the variety of behaviors that arises from different combinations of mobile versus immobile and short-lived versus long-lived radionuclide species. For example, H-3 is both short lived and mobile, with a half-life of 12.32 years and a K_d equal to 0.0 mL g^{-1}. Notably, the vast majority of H-3 in both trench DUs is largely flushed out by the time the final closure cap is installed in September 2165 (Figure 5-16). Because ET01 will be uncovered until September 2065 (interim cover placed) while ST14 is assumed in this PA to have an operational stormwater runoff cover in place by September 2025, the release rate from ST14 is slightly lower.

Sr-90 represents a radionuclide that is short lived (28.79-year half-life) with a moderate to low K_d (5 and 17 mL g^{-1} in sand and clay, respectively). This combination of properties causes Sr-90 to peak later than H-3 at approximately Year 1,500 (Figure 5-16) for both types of trench DUs. The retarded radionuclide decays while in transit to the water table, and the plume center of mass does not reach the water table until after placement of the final closure cap.

Tc-99, on the other is hand, is longer lived (211,100-year half-life) and exhibits a low K_d (0.6 and 1.8 mL g^{-1} in sand and clay, respectively). Because of its mobility, an early peak is noted before installation of the final closure cap when water infiltration remains high (Figure 5-17). Once the final cover is placed and the water infiltration rate significantly decreases, a secondary, absolute peak occurs at about Year 750 when only marginal decay has occurred.

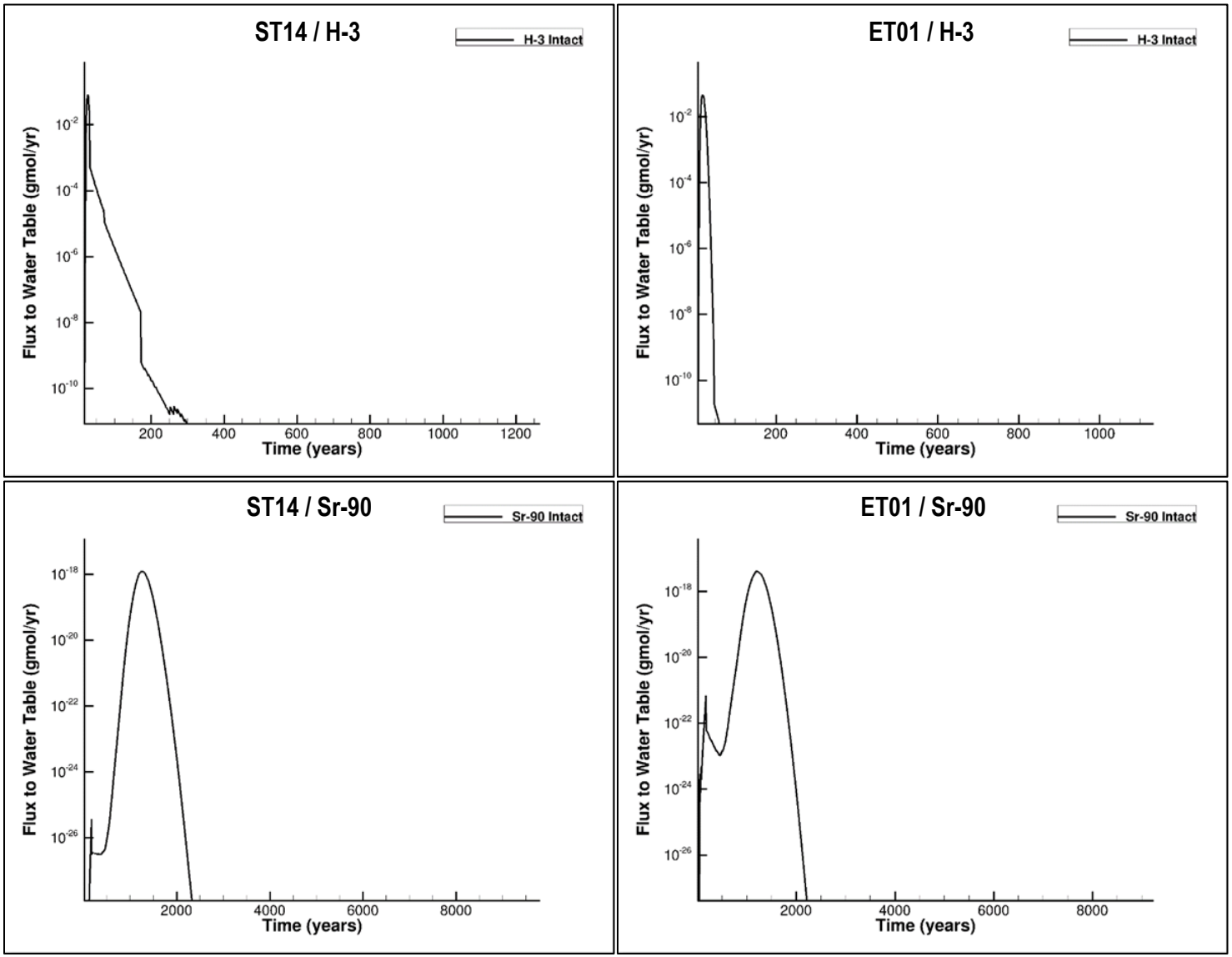

Figure 5-16. Flux-to-the-Water-Table Profiles of H-3 and Sr-90 for ST14 (Left) and ET01 (Right) Geometries

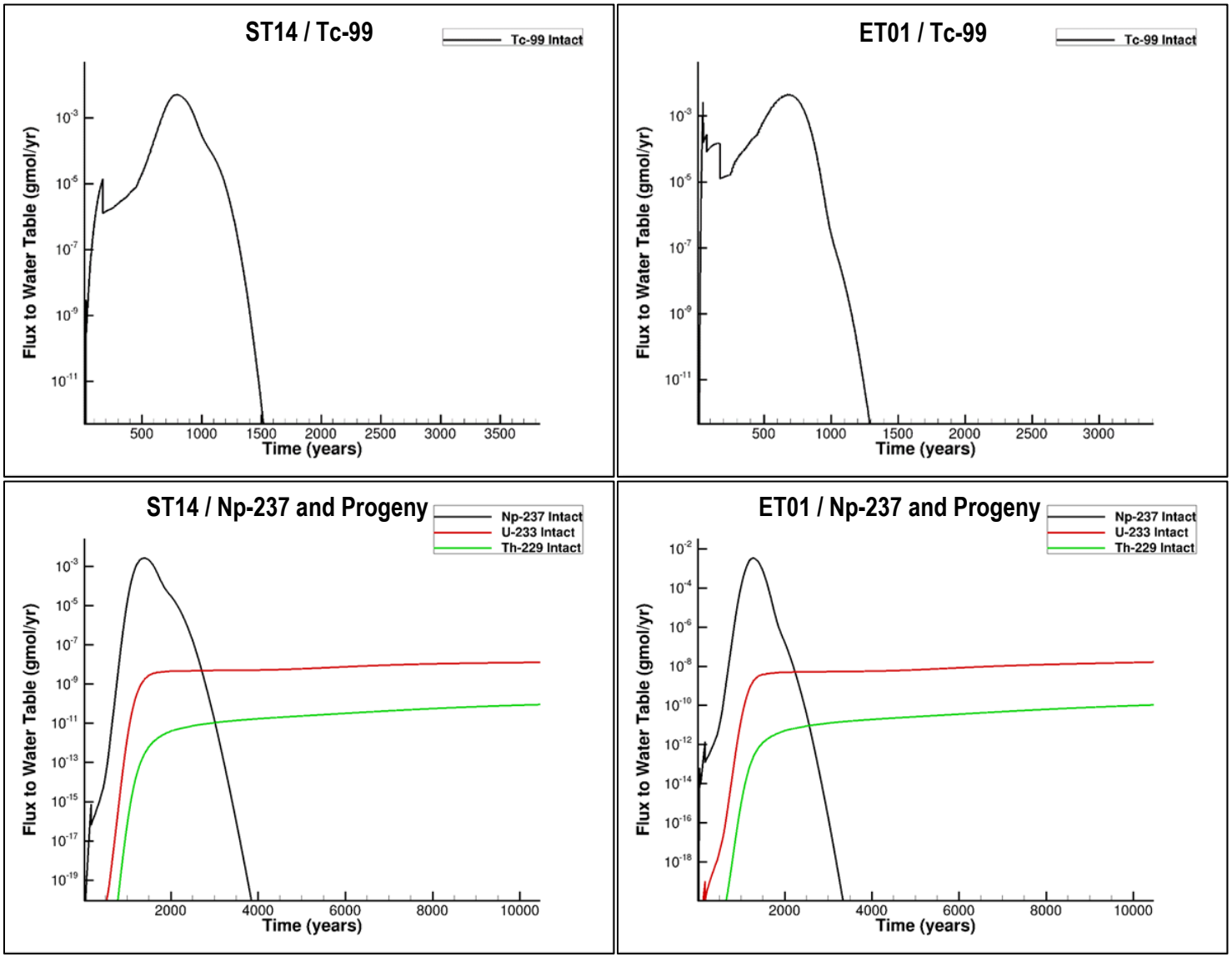

Figure 5-17. Flux-to-the-Water-Table Profiles of Tc-99 and Np-237 and Progeny for ST14 (Left) and ET01 (Right) Geometries

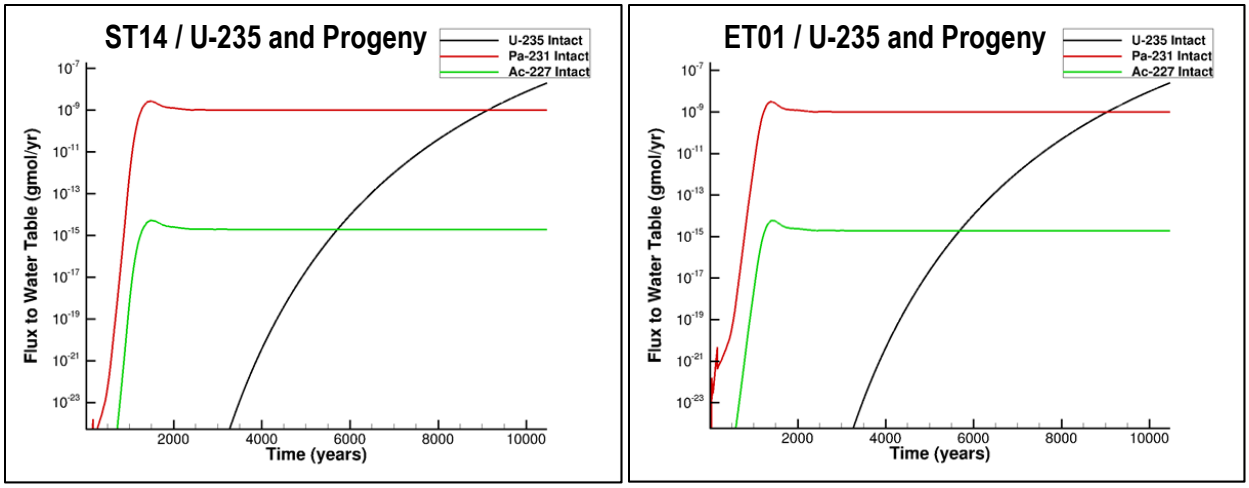

Figure 5-18. Flux-to-the-Water-Table Profiles of U-235 and Progeny for ST14 (Left) and ET01 (Right) Geometries

The final examples are decay chains Np-237 and U-235. Both parent radionuclides are long lived; however, Np-237 has a low K_d (3 and 9 mL g^{-1} in sand and clay, respectively) while U-235 has a moderate to high K_d (300 and 400 mL g^{-1} in sand and clay, respectively). Additionally, the daughters of Np-237 (U-233 and Th-229) exhibit moderate to high K_d values whereas the first daughter product of U-235 (Pa-231) has a low K_d and the second daughter (Ac-227) has a high K_d. Because of its low K_d and long half-life, Np-237 peaks at about Year 2,000 before appreciable decay occurs (Figure 5-17). Meanwhile, the two progeny are slowly transported to the water table at a near steady state as water infiltration plateaus at about Year 2,000. In contrast, U-235 takes much longer to reach the water table (Figure 5-18). While only marginal decay occurs, its daughter product, Pa-231, is readily mobile and has a half-life of 32,760 years. As a result, Pa-231 and Ac-227 arrive at the water table and peak much earlier than their parent, U-235.

5.1.1.2.2. Subsidence Boundary Condition

Contaminant transport simulations are performed to compute the flux-to-the-water-table profiles for the three subsidence hole locations (Holes 1, 2, and 3 in Figure 4-25 and Figure 4-26). Subsequently, the individual flux-to-the-water-table profiles for the three hole locations are blended uniformly, which becomes the source term at the aquifer zone boundary. Figure 5-19 displays the flux-to-the-water-table profiles for Sr-90 and Np-237 for the three subsidence hole locations and the post-processed blended case. The “end hole” (Hole 1 in Figure 4-25 and Figure 4-26) configuration has the highest infiltration rate because it has the largest upslope intact area relative to the subsidence area. As a result, this case typically displays the highest peak in the early time periods, such as seen for Sr-90 in Figure 5-19.

Conversely, the “crest hole” (Hole 3 in Figure 4-25 and Figure 4-26) has the lowest infiltration rate and often results in a broader flux profile over time. For radionuclides that peak later in time, such as Np-237, the crest hole often displays the largest absolute peak (Figure 5-19). More of the contaminant species is leached from the waste zone in the earlier time periods by the end hole and

the "midpoint hole" (Hole 2 in Figure 4-25 and Figure 4-26), which leaves less contaminant to leach during the later time periods when infiltration rates converge.

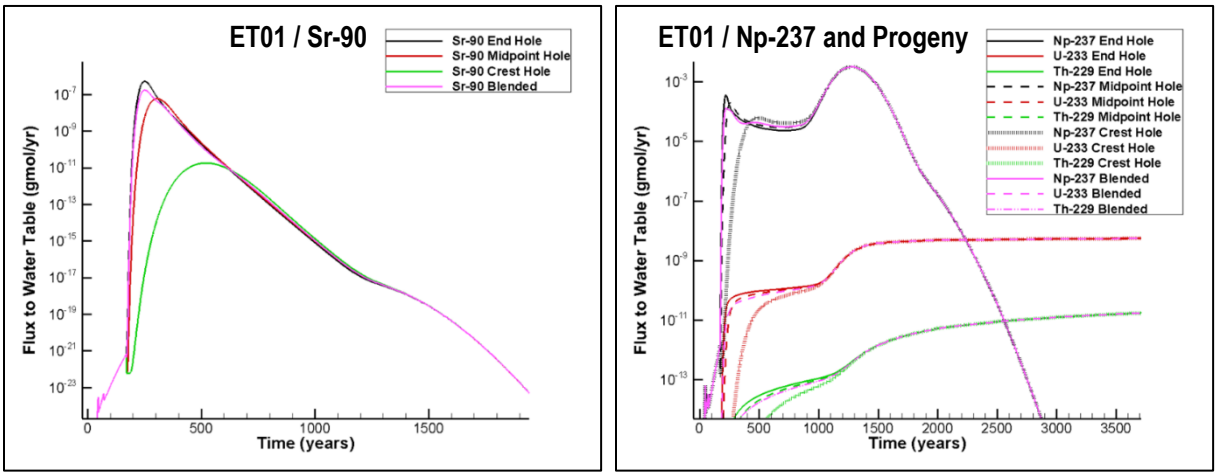

Figure 5-19. Flux-to-the-Water-Table Profiles of Sr-90 (left) and Np-237 and Progeny (right) at ET01 for Subsidence Cases

Subsidence hole locations are selected to include bounding cases and capture uncertainty in where the subsidence hole will occur. The probabilistic scheme implemented by Danielson (2019a; 2019b) shows that the three subsidence hole locations have approximately equal probability of occurring based on historical disposal actions. To capture the behavior of each subsidence hole possibility and avoid overly pessimistic assumptions, the three flux profiles are blended with equal weighting. Using this blending scheme, both the early and later peaks for some radionuclide species are better represented through time, as exhibited by Np-237 (Figure 5-19). However, for species with only one peak, such as Sr-90, the blending scheme tends toward conservatism because the higher peaks resulting from higher infiltration rates dominate (Figure 5-19).

5.1.1.3. Transport Model for Sensitivity Cases

Section 5.1.1.2 presents results for the nominal PA cases for the ST and ET vadose zone, which are based on the nominal PA (and best estimate) chemical, physical, infiltration, and timing parameterizations across the various data packages and databases. To perform sensitivity analysis of and quantify uncertainty in these parameters, seven sensitivity cases are implemented as listed in Table 5-3. For each sensitivity case, a specific input parameter is changed so that the impact can be quantified after progressing through the entire PA deterministic modeling framework (i.e., from infiltration through limits and doses). Simulations for the seven sensitivity cases assume an intact final closure cap and are conducted for three DUs only (ST06, ST09, and ET06). These DUs represent substantially different hydrostratigraphic regions within the ELLWF as well as substantially different flow paths in the GSA flow model. Only radionuclides known to be significant contributors to the SOF are modeled. These include H-3, I-129, Np-237, Sr-90, Tc-99, and C-14. Except for Sensitivity Case 6 (K_d) and Sensitivity Case 7 (timeline), new flow fields are computed and subsequently used as input to solve the radionuclide contaminant transport equations and to obtain the flux-to-the-water-table profile.

Table 5-3. Parameterization for Vadose Zone Model Sensitivity Cases for Slit and Engineered Trenches

Sensitivity Case Number	Topic	Best Estimate (and Nominal PA) Values	Sensitivity Values	Number of Sensitivity Cases	Flow Runs
1	Waste Zone Hydraulic Conductivity (cm s^{-1})	2.2E-05 [b] 8.7E-06 [c] 9.4E-05 [d] 1.5E-05 [e]	4.08E-05 [b] (+1σ) 1.57E-05 [c] (+1σ) 1.71E-04 [d] (+1σ) 2.79E-05 [e] (+1σ)	3 [a]	Yes
2	LVZ Porosity	0.380	0.420 (+1σ)	3 [a]	Yes
3	TCCZ (Tan Clay) Thickness	DU-Specific	0.5*Best Estimate Thickness	3 [a]	Yes
4	Waste Zone Porosity	0.889 [b]/0.303 [c] 0.600 [d]/0.277 [e]	0.939 [b] (+1σ) 0.615 [c] (+1σ) 0.617 [d] (+1σ) 0.307 [e] (+1σ)	3 [a]	Yes
5	Infiltration	2019 HELP Modeling	Table 5-4	3 [a]	Yes
6	Distribution Coefficient	Geochemical Data Package K_d Values (Kaplan, 2016b)	0.5*K_d	3 [a]	No
7	Timeline	DU-Specific	First Waste at Interim Closure	3	No

Notes:

[a] Intact only for ST09, ST06, ET06

[b] ET boxes before dynamic compaction (STETboxesBC)

[c] ET boxes after dynamic compaction (STETboxesAC)

[d] ST hybrid waste before dynamic compaction (SThybridBC)

[e] ST hybrid waste after dynamic compaction (SThybridAC)

Table 5-4. Infiltration Transient for Slit and Engineered Trench Sensitivity Cases

Cover Condition	Year	Intact Infiltration Rate (in yr^{-1})
Uncovered	DU-Specific	25.0
Operational Cover	DU-Specific	0.1
Interim Cover	71	0.1
Final Closure Cap	171	0.00217
	251	0.01955
	361	0.4521
	371	0.4863
	411	0.6363
	451	0.7947
	551	2.7983
	731	5.6695
	1,171	9.1754
	1,971	11.5645
	2,794	11.952
	3,371	11.9981
	5,771	12.0647
	10,171	12.0812

The flux-to-the-water-table profiles for the VZ for each radionuclide and DU are displayed in Figure 5-20 through Figure 5-22. Note that the flux-to-the-water-table profile for the best estimate case (same as nominal PA case) is shown on each plot as a dashed red line to benchmark the impact of each sensitivity parameter. The time-dependent flux is consistently observed to not be very sensitive to a 1-sigma change in waste zone porosity, waste zone conductivity, and LVZ porosity. In contrast, the flux-to-the-water-table profile is quite sensitive to changes in infiltration rate, model timeline, and K_d. The response to a change in the thickness of the TCCZ is somewhat mixed among the radionuclides and DUs. For example, H-3 displays essentially no change in flux to the water table (Figure 5-20) because its K_d is zero and the perturbations in the physical property values are not significant enough to cause a noteworthy change in the transport dynamics. C-14, on the other hand, displays a significantly higher flux in ET06 and ST09 during the first 1,000 years (Figure 5-21), but less so in ST06 where the clay thickness beneath the waste zone is much less. In ET06 and ST09, the peak flux occurs approximately 300 to 400 years earlier but with nearly the same flux as the best estimate (nominal PA) case. Adjusting the model timeline generally results in a similar peak flux but the profile is shifted in time. In addition, a much lower flux to the water table is seen at early times because the waste is emplaced when the interim cover is applied.

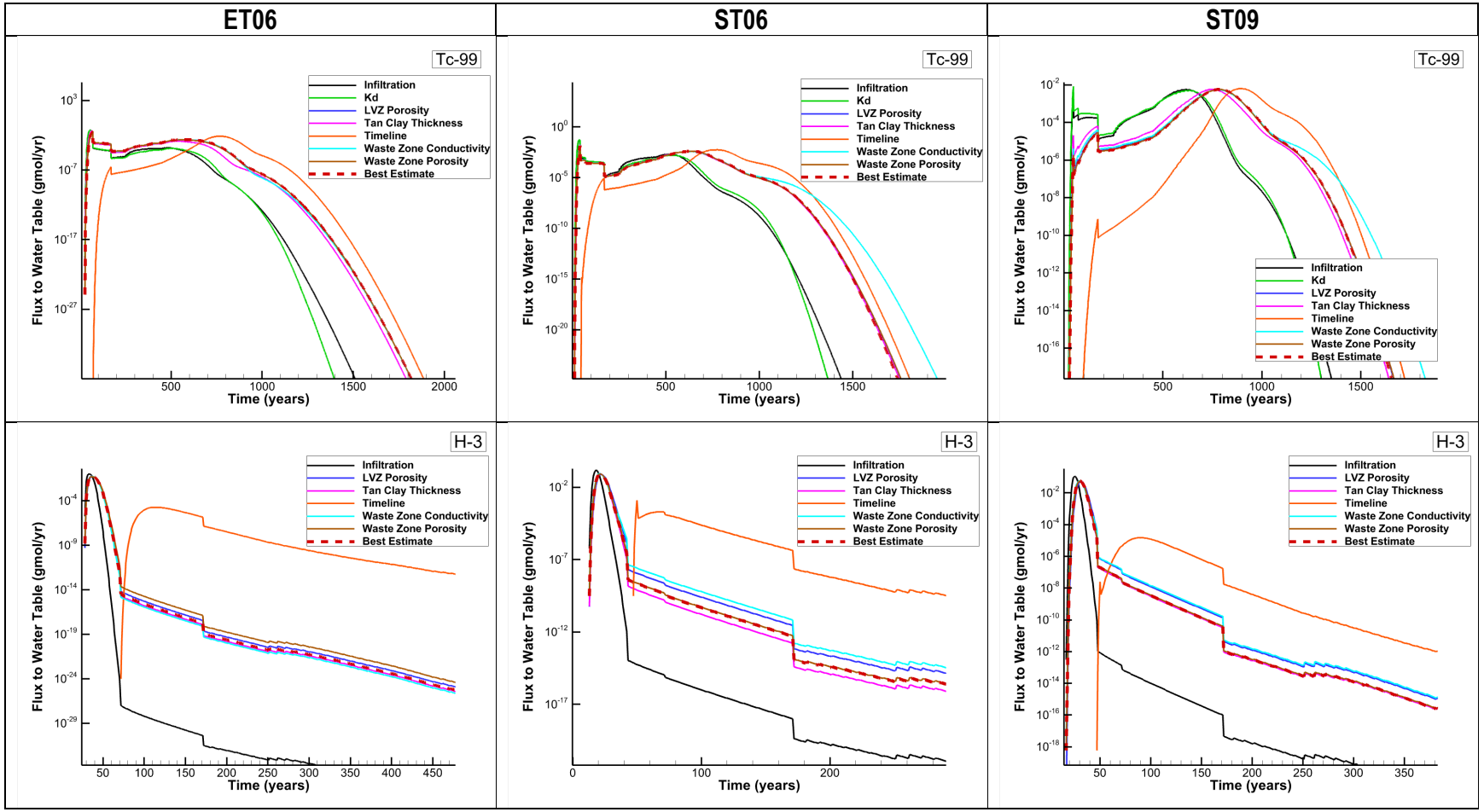

Figure 5-20. Tc-99 and H-3 Flux-to-the-Water-Table Profiles for ET06, ST06, and ST09 Comparing the Best Estimate (Nominal PA) and Sensitivity Cases

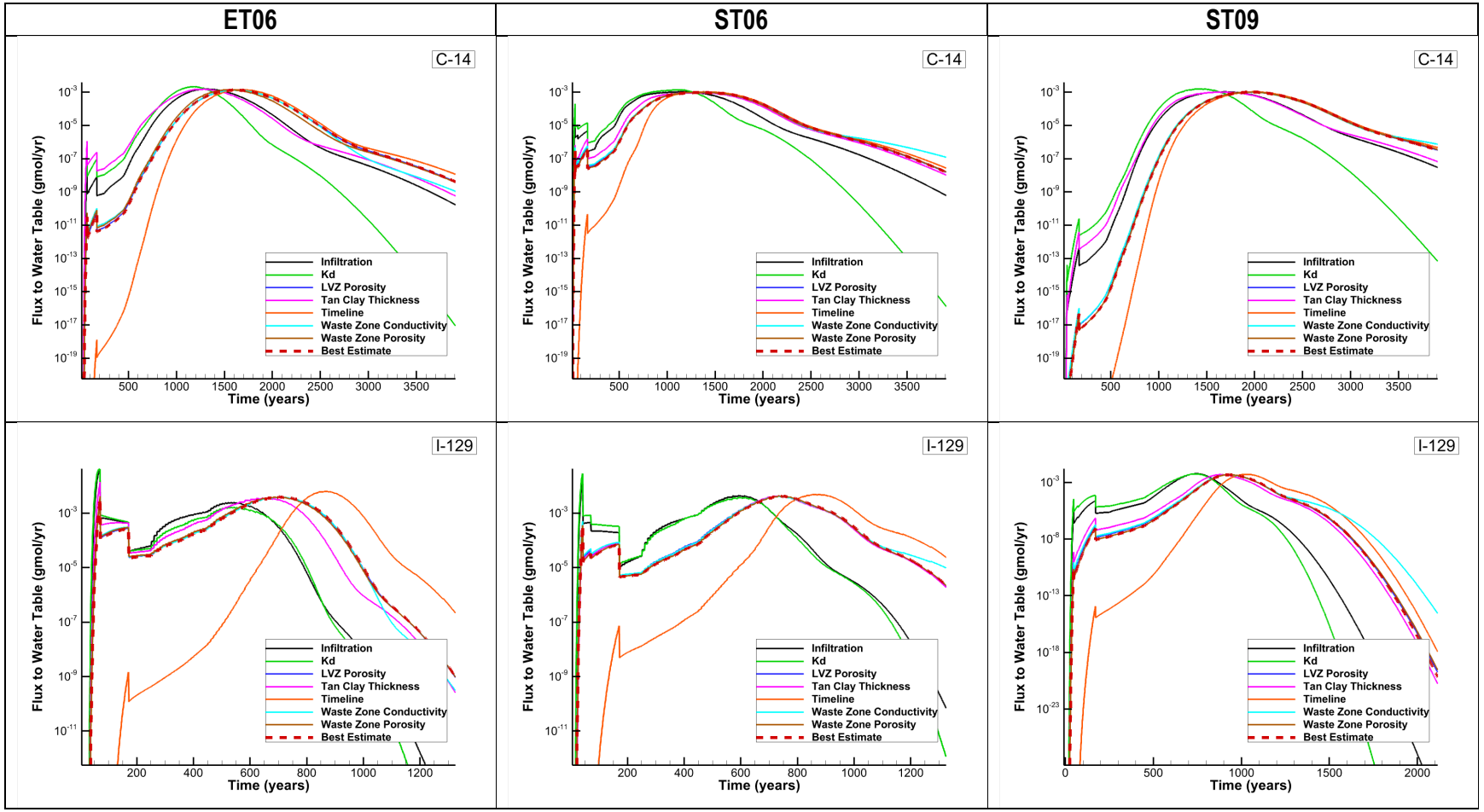

Figure 5-21. C-14 and I-129 Flux-to-the-Water-Table Profiles for ET06, ST06, and ST09 Comparing the Best Estimate (Nominal PA) and Sensitivity Cases

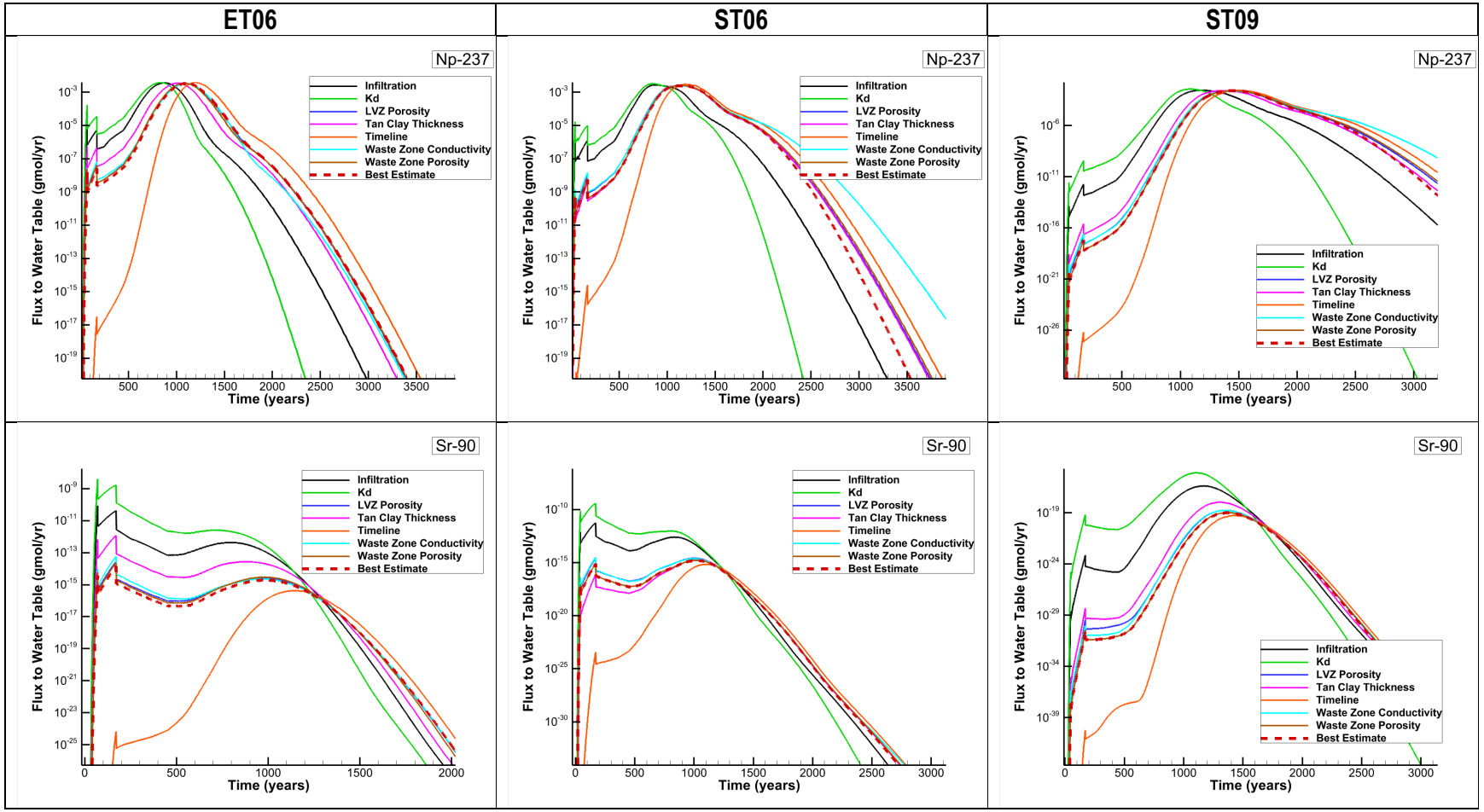

Figure 5-22. Np-237 and Sr-90 Flux-to-the-Water-Table Profiles for ET06, ST06, and ST09 Comparing the Best Estimate (Nominal PA) and Sensitivity Cases

5.1.2. Vadose Zone Models for Special Waste Forms

The implementation of SWFs in STs and ETs is documented by Danielson (2021). Figure 5-23 summarizes all SWFs modeled in STs and ETs, along with the release mechanism from the waste zone (e.g., effective K_d, delayed release, solubility controlled), the K_d assumed for the waste zone, and the timing of placement (e.g., existing or future). "Existing inventory" SWFs disposed in STs and ETs before this PA revision use the same timeline as STs and ETs with generic waste, which assumes all waste is placed on the date the DU is opened. Future SWF inventory is assumed to be placed on September 30, 2021. For DUs containing both future and existing inventory, the SWF is assumed to be placed on the date the DU is opened.

New VZ models for three simple SWFs have been developed for this PA revision as follows:

- CIG trench segments (Section 5.1.2.1)
- Tall boxes (Section 5.1.2.2)
- Other SWFs (Section 5.1.2.3)

New VZ models have not been developed for three complex SWFs (Danielson, 2021): HWCTR, HXs, and 232-F concrete rubble. Instead, HWCTR and HXs have applied the existing flux-to-the-water-table profiles from previous ELLWF SAs and UDQEs as a source term at the water table to simulate transport through the updated GSA flow model (more detail provided in Section 5.1.4.2). Previous analyses of the 232-F concrete rubble (Flach et al., 2005) did not account for the later placement of an operational stormwater runoff cover over ST01, which reduces infiltration rates substantially versus a soil-only cover scenario. Because of this substantial difference, the source term from the original SA cannot be applied. Rather than redeveloping this complex VZ model, generic waste form limits for H-3, which are pessimistically bounding, will be employed for SWF radionuclide H-3F instead.

Waste Form	CWTS Nuc Name	Source Release Type	Waste Zone Kd	1 ET07 future	2 ET08 future	3 ET09 future	4 ET03 open	5 ET04 future	6 ST08 open	7 ST09 open	8 ST10 future	9 ST11 future	10 ST01 closed	11 ST02 closed	12 ST03 closed	13 ST04 closed	14 ST23 open	15 ST24 future	16 ST05 closed	17 ST06 open	18 ST07 open	19 ET02 open	20 ET01 closed	21 ST14 open	22 ET05 future	23 ET06 future	24 ST17 future	25 ST18 future	26 ST19 future	27 ST20 future	28 ST21 future	29 ST22 future
F-WTU Dowex 21K	I-129D	Effective Kd	6800																													
H-WTU Dowex 21K	I-129E	Effective Kd	15600																													
H-WTU Filtercake	I-129F	Effective Kd	650																													
F-WTU CG-8	I-129G	Effective Kd	50																													
H-WTU CG-8	I-129H	Effective Kd	380																													
ETF GT-73	I-129I	Effective Kd	10000																													
F-WTU Filtercake	I-129J	Effective Kd	56.7																													
K and L Basin Resin	C-14K	Effective Kd	140																													
K and L Basin Resin	I-129K	Effective Kd	3700																													
K and L Basin Resin	Tc-99K	Effective Kd	810																													
Effluent Treatment Facility Carbon Column	H-3C	Delayed Release	0																													
Naval Reactors Pump	C-14N	Delayed Release	30																													
Effluent Treatment Facilities Carbon Columns	I-129C	Delayed Release	7400																													
Mark 50A Targets	I-129R	Solubility Controlled	3																													
Mark 50A Targets	Sr-90R	Solubility Controlled	17																													
Mark 50A Targets	Tc-99R	Solubility Controlled	1.8																													
M-Area Glass	U-234G	Solubility Controlled	400																													
HWCTR	Ag-108mH	Aquifer Source Only	NA																													
HWCTR	C-14H	Aquifer Source Only	NA																													
HWCTR	Ni-59H	Aquifer Source Only	NA																													
HWCTR	Ni-63H	Aquifer Source Only	NA																													
HWCTR	Tc-99H	Aquifer Source Only	NA																													
HX	C-14X	Aquifer Source Only	NA																													
HX	H-3X	Aquifer Source Only	NA																													
232-F Concrete	H-3F	Aquifer Source Only	NA																													
Tall Boxes	All	Standard	BE																													

Note: At the time SWF conceptual models were finalized for this PA in early 2021, ST08 was assumed to receive future generic waste forms only; no future SWFs. However, based on the modeling results for ST09, there will be no impact on the calculations if Tall Boxes are also disposed in ST08 in the future.

	Existing Inventory
	Existing+Future Inventory
	Future Inventory

Figure 5-23. Special Waste Forms as Modeled in Each Disposal Unit

5.1.2.1. Components-in-Grout Trench Segments

The implementation of the VZ flow and radionuclide transport conceptual model in PORFLOW is presented in Section 4.2.1. As part of the implementation, 98 steady-state flow fields are computed to serve as input for the transport of radionuclide species from the CIG waste zone to the water table and account for the specific timeline and material properties of each specific CIG unit. Section 4.2.1.4 provides a limited set of preliminary results for CIG-4, CIG-8, and CIG-9 for the intact closure cap case to demonstrate differences in the flux-to-the-water-table profiles arising from different CIG implementations. This section shares additional results that explore both the intact and subsidence closure cap cases, including the sensitivity case for CIG-4 through CIG-7.

5.1.2.1.1. Flow Model

Figure 4-52, Figure 4-53, and Figure 4-54 display the steady-state flow fields representing intact closure cap conditions for CIG-4, CIG-8, and CIG-9, respectively, to highlight changes during the following key periods: operational (i.e., uncovered), operational closure (i.e., closure of CIG unit), interim closure (i.e., start of IC), and final closure (i.e., end of IC). Flow fields for units with identical material geometries (i.e., CIG-1 through CIG-7; Figure 4-52) are the same except that the time periods represented by the different steady-state flow fields change. Figure 4-55 presents the steady-state flow field for the CIG-4 bounding subsidence case to demonstrate the impact of a high infiltration rate through the CIG waste zone while the closure cap surrounding the subsided region remains intact. The bounding subsidence case flow field for CIG-4 shown in Figure 4-55 is qualitatively representative of CIG-4 through CIG-7 at the end of IC. However, because the area of the intact closure cap upslope of the subsidence region (i.e., hole) differs among CIG units, substantial differences exist in infiltration rates through the hole (see Table 4-25 and Table 4-26). Figure 5-24 presents flow fields at the end of IC for the bounding subsidence case for CIG-4 through CIG-7 with streamtraces and 10-year time markers through the waste zone. Notably, the travel time from the ground surface to the water table decreases with increasing infiltration (and greater upslope intact area). Note that water saturation is dimensionless (vol/vol).

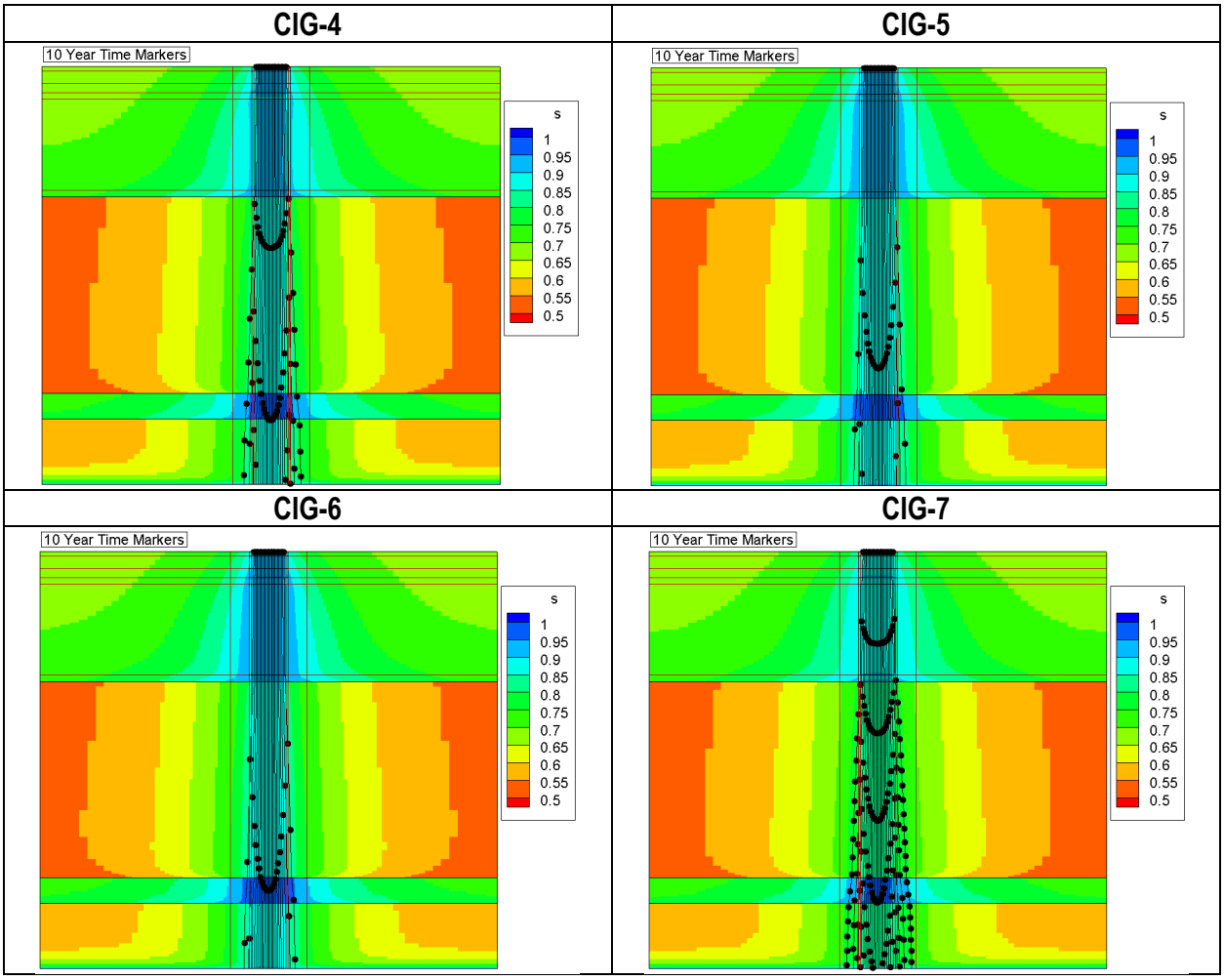

Figure 5-24. Saturation Profiles for Bounding Subsidence Case at End of IC: (Top Left) CIG-4; (Top Right) CIG-5; (Bottom Left) CIG-6; (Bottom Right) CIG-7

For CIG-8 and CIG-9, which have a reinforced concrete mat, subsidence is delayed until Year 371 (i.e., 200 years after the end of IC). To explore the impact and need for placement of a reinforced concrete mat above CIG-4 through CIG-7, a sensitivity case with the CIG-8 material setup is applied to CIG-4 through CIG-7. With placement of the reinforced mat, subsidence is also delayed to Year 371 for CIG-4 through CIG-7. Figure 5-25 shows the first period when subsidence occurs for CIG-4 through CIG-9, demonstrating the difference in travel time for the various CIG locations in the best estimate subsidence case. Notably, the travel times for each CIG unit are nearly the same as the bounding subsidence case (Figure 5-24) because the subsidence infiltration rate does not change significantly (i.e., by less than 1 in yr^{-1}) over the course of the 200-year period. Therefore, the primary impact of the reinforced mat is to delay release an additional 200 years to allow for greater decay of the shorter-lived radionuclide species.

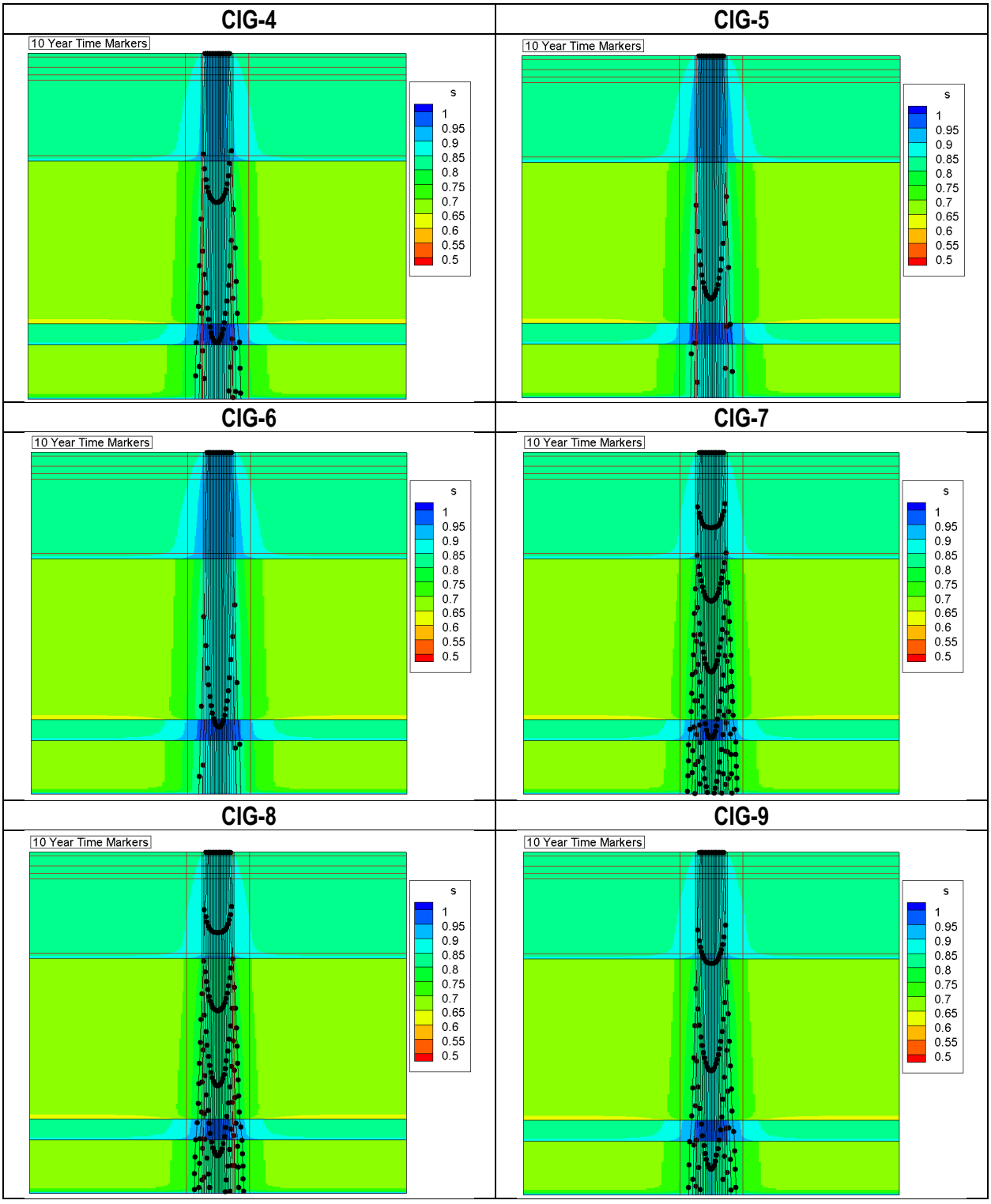

Figure 5-25. Saturation Profiles of Subsidence at Year 371 (Best Estimate Subsidence Case): (Top Left) CIG-4; (Top Right) CIG-5; (Middle Left) CIG-6; (Middle Right) CIG-7; (Bottom Left) CIG-8; (Bottom Right) CIG-9

5.1.2.1.2. Transport Model

PORFLOW VZ radionuclide transport simulations are available for 27 parent radionuclides and their progeny with a one-year half-life cutoff. Table 5-5 lists the half-lives for each radionuclide species as well as the K_d values for each material zone, including aging cementitious materials.

Table 5-5. Radionuclide Half-Lives and K_d Values from Components-in-Grout Vadose Zone Transport Model Simulations

Species[1]	Half-Life (yr)	K_d Value				Cementitious Leachate Factor	K_d Value	
		Stage I (mL g^{-1})	Stage II (mL g^{-1})	Stage III (mL g^{-1})	Gone (mL g^{-1})		Sandy (mL g^{-1})	Clayey (mL g^{-1})
C-14	5.70E+03	2,000	5,000	50	30	5	1	30
H-3	1.23E+01	0	0	0	0	1	0	0
I-129	1.57E+07	8	10	4	3	0.1	1	3
Np-237	2.14E+06	10,000	10,000	5,000	9	1.5	3	9
U-233	1.59E+05	1,000	5,000	5,000	400	3	300	400
Th-229	7.34E+03	10,000	10,000	2,000	2,000	2	900	2,000
Sr-90	2.88E+01	90	15	90	17	3	5	17
Tc-99	2.11E+05	0.8	0.8	0.5	1.8	0.1	0.6	1.8
Ag-108m	4.18E+02	4,000	4,000	400	30	3.2	10	30
Am-241	4.32E+02	6,000	6,000	600	8,500	1.5	1,100	8,500
Be-10	1.51E+06	90	15	90	17	3	5	17
Cf-249	3.51E+02	6,000	6,000	600	8,500	1.5	1,100	8,500
Cm-245	8.50E+03	6,000	6,000	600	8,500	1.5	1,100	8,500
Pu-241	1.44E+01	10,000	10,000	2,000	6,000	2	650	6,000
Cl-36	3.01E+05	0	10	1	8	0.1	1	8
Cs-135	2.30E+06	2	20	10	50	1	10	50
Cs-137	3.02E+01	2	20	10	50	1	10	50
K-40	1.25E+09	2	20	10	25	1	5	25
Ni-59	1.01E+05	65	400	400	30	3.2	7	30
Ni-63	1.00E+02	65	400	400	30	3.2	7	30
Pa-231	3.28E+04	10,000	10,000	5,000	9	1.5	3	9
Ac-227	2.18E+01	6,000	6,000	600	8,500	1.5	1,100	8,500
Pd-107	6.50E+06	4,000	4,000	400	30	3.2	7	30
Pu-239	2.41E+04	10,000	10,000	2,000	6,000	2	650	6,000
U-235	7.04E+08	1,000	5,000	5,000	400	3	300	400
Ra-226	1.60E+03	200	100	200	180	3	25	180
Pb-210	2.22E+01	300	300	100	5,000	3.2	2,000	5,000
Rb-87	4.92E+10	2	20	10	50	1	10	50
Th-230	7.54E+04	10,000	10,000	2,000	2,000	2	900	2,000
Th-231	2.91E-03	10,000	10,000	2,000	2,000	2	900	2,000
U-234	2.46E+05	1,000	5,000	5,000	400	3	300	400

Notes:

[1] Parent radionuclides appear in bold; progeny appear unbolded. (Note: some species appear as both parents and progeny.)

As presented in Section 4.2.1.4.1, the steady-state flow fields for each CIG unit are post-processed to compute the number of pore volumes per period passing through each cementitious material waste zone. From these calculations, the transition time to each chemical aging stage is obtained. The cementitious aging times for all CIG units for both intact and subsidence cases are summarized in Table 5-6.

Table 5-6. Chemical Degradation Transition Times of Cementitious Materials in Components-in-Grout Vadose Zone Transport Model Simulations

Unit	Case	Transition	Enclosure (yr)	CIG (yr)	Reinforced Mat (yr)	CLSM (yr)
CIG-1	Intact	Stage I to Stage II	613	1,158	-	-
		Stage II to Stage III	1,284	3,697	-	-
		Stage III to Stage IV	5,885	36,734	-	-
CIG-2	Intact	Stage I to Stage II	618	1,157	-	-
		Stage II to Stage III	1,285	3,698	-	-
		Stage III to Stage IV	5,886	36,735	-	-
CIG-3	Intact	Stage I to Stage II	618	1,157	-	-
		Stage II to Stage III	1,285	3,698	-	-
		Stage III to Stage IV	5,886	36,735	-	-
CIG-4	Intact	Stage I to Stage II	622	1,157	-	-
		Stage II to Stage III	1,286	3,698	-	-
		Stage III to Stage IV	5,887	36,735	-	-
CIG-4	Bounding Subsidence	Stage I to Stage II	177	297	-	-
		Stage II to Stage III	251	1,555	-	-
		Stage III to Stage IV	2,550	22,150	-	-
CIG-4	Best Estimate Subsidence (Reinforced Mat, Year 371)	Stage I to Stage II	384	502	386	380
		Stage II to Stage III	535	1793	554	492
		Stage III to Stage IV	3,048	22,399	3,495	2,358
CIG-5	Intact	Stage I to Stage II	622	1,157	-	-
		Stage II to Stage III	1,286	3,698	-	-
		Stage III to Stage IV	5,887	36,735	-	-
CIG-5	Bounding Subsidence	Stage I to Stage II	175	246	-	-
		Stage II to Stage III	219	1,002	-	-
		Stage III to Stage IV	1,546	17,279	-	-
CIG-5	Best Estimate Subsidence (Reinforced Mat, Year 371)	Stage I to Stage II	379	449	380	377
		Stage II to Stage III	469	1,265	481	444
		Stage III to Stage IV	2,155	17,615	2,455	1,632
CIG-6	Intact	Stage I to Stage II	627	1,157	-	-
		Stage II to Stage III	1,288	3,698	-	-
		Stage III to Stage IV	5,888	36,735	-	-
CIG-6	Bounding Subsidence	Stage I to Stage II	174	237	-	-
		Stage II to Stage III	213	896	-	-
		Stage III to Stage IV	1,339	16,078	-	-
CIG-6	Best Estimate Subsidence (Reinforced Mat, Year 371)	Stage I to Stage II	378	440	379	376
		Stage II to Stage III	458	1,157	468	436
		Stage III to Stage IV	1,946	16,435	2,217	1,481

Table 5-6 (cont'd). Chemical Degradation Transition Times of Cementitious Materials in Components-in-Grout Vadose Zone Transport Model Simulations

Unit	Case	Transition	Enclosure (yr)	CIG (yr)	Reinforced Mat (yr)	CLSM (yr)
CIG-7	Intact	Stage I to Stage II	627	1,157	-	-
		Stage II to Stage III	1,288	3,698	-	-
		Stage III to Stage IV	5,888	36,735	-	-
CIG-7	Bounding Subsidence	Stage I to Stage II	184	428	-	-
		Stage II to Stage III	333	2,358	-	-
		Stage III to Stage IV	3,812	27,760	-	-
CIG-7	Best Estimate Subsidence (Reinforced Mat, Year 371)	Stage I to Stage II	397	624	402	390
		Stage II to Stage III	686	2,511	721	606
		Stage III to Stage IV	4,120	27,910	4,769	3,296
CIG-8	Intact	Stage I to Stage II	636	1,157	678	612
		Stage II to Stage III	1,291	3,698	1,412	1,189
		Stage III to Stage IV	5,890	36,735	6,980	4,916
CIG-8	Subsided (Year 371)	Stage I to Stage II	395	608	400	389
		Stage II to Stage III	667	2,446	701	592
		Stage III to Stage IV	4,024	27,421	4,653	3,211
CIG-9	Intact	Stage I to Stage II	646	1,158	680	621
		Stage II to Stage III	1,294	3,697	1,413	1,191
		Stage III to Stage IV	5,892	36,734	6,980	4,917
CIG-9	Subsided (Year 371)	Stage I to Stage II	390	546	392	385
		Stage II to Stage III	592	2,118	616	534
		Stage III to Stage IV	3,538	24,930	4,071	2,782

As expected, intact closure cap conditions lead to the longest cementitious aging times because of the low water velocity through the cementitious material waste zones. Conversely, the bounding subsidence case for CIG-6 exhibits the shortest aging time, highest water infiltration rate, and earliest increase in infiltration.

Figure 4-56 presents a limited set of flux-to-the-water-table profiles for CIG-4, CIG-8, and CIG-9 under intact closure cap conditions. This limited set of radionuclides was selected to demonstrate the release behavior from the cementitious waste form across a spectrum of radionuclide mobilities and half-lives (e.g., to demonstrate the differences among highly mobile and short-lived radionuclides and highly immobile and long-lived radionuclides). The profiles highlight the differences in radionuclide flux to the water table with (CIG-8 and CIG-9) and without (CIG-4) a reinforced concrete mat and with the old (CIG-4 and CIG-8; CIGgrout1to8) versus new (CIG-9; CIGgrout9on) grout formulation. Figure 5-26 through Figure 5-31 provide flux-to-the-water-table profiles for a limited subset of radionuclides disposed of in CIG-6 and CIG-7 for the intact case and the bounding and best estimate (i.e., sensitivity) subsidence cases at the highest and lowest infiltration rates, respectively.

Note that the sensitivity case for CIG-6 and CIG-7 is also qualitatively representative of CIG-8 and CIG-9 for which a reinforced concrete mat is installed. In general, a lower infiltration rate results in a delay of the peak flux to the water table due to a lower water velocity and a longer

aging time for the cementitious materials. For shorter-lived radionuclides, this delay can lead to a substantially lower peak flux to the water table. For example, Sr-90 peak flux to the water table for CIG-6 and CIG-7 (Figure 5-30) is approximately two to three orders of magnitude lower for the sensitivity case than the bounding subsidence case because the combination of the lower infiltration rate and temporal delay allows more decay to occur.

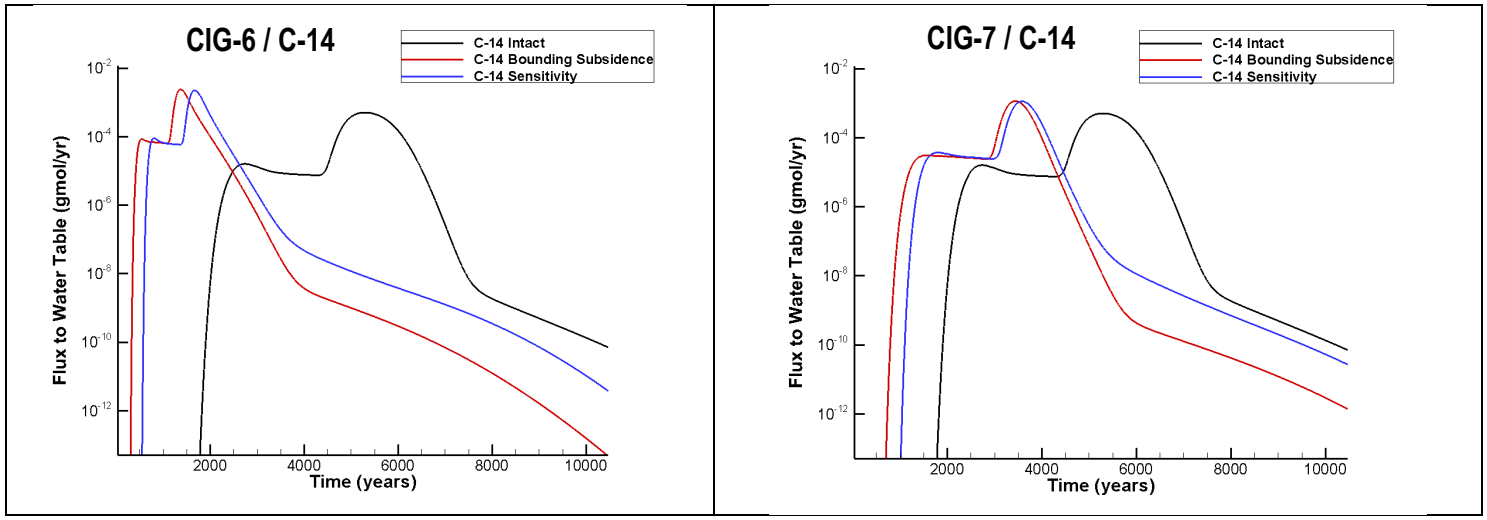

Figure 5-26. Flux-to-the-Water-Table Profiles of C-14 for Intact, Bounding Subsidence, and Best Estimate Subsidence (Sensitivity) Cases for CIG-6 (left) and CIG-7 (right)

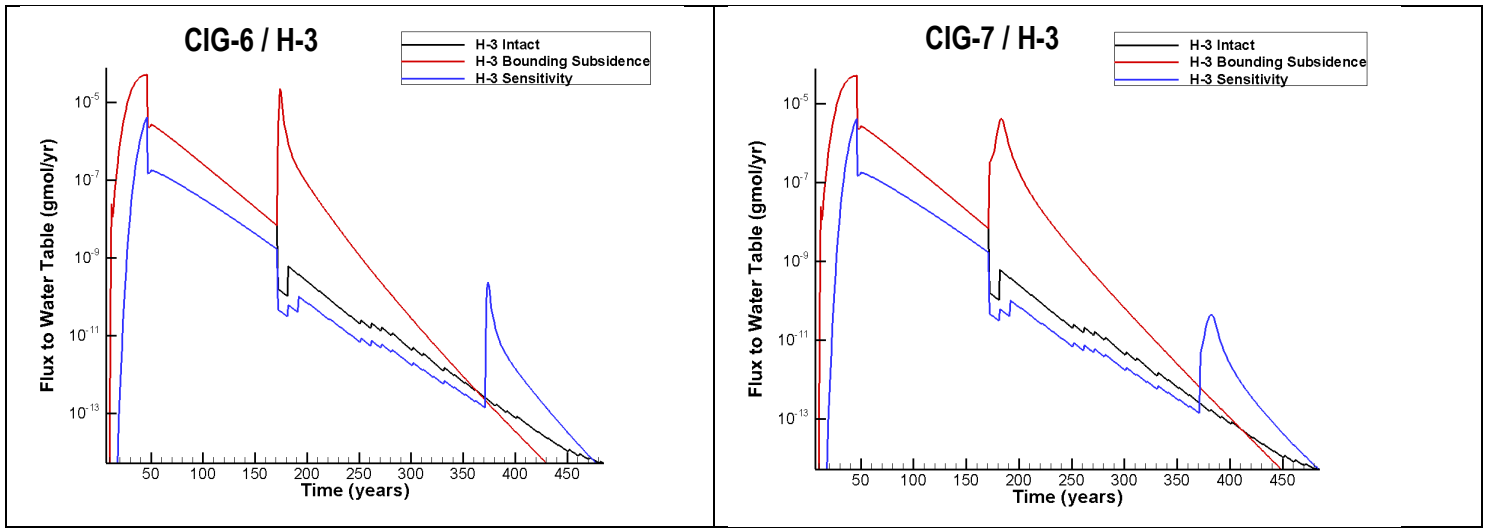

Figure 5-27. Flux-to-the-Water-Table Profiles of H-3 for Intact, Bounding Subsidence, and Best Estimate Subsidence (Sensitivity) Cases for CIG-6 (left) and CIG-7 (right)

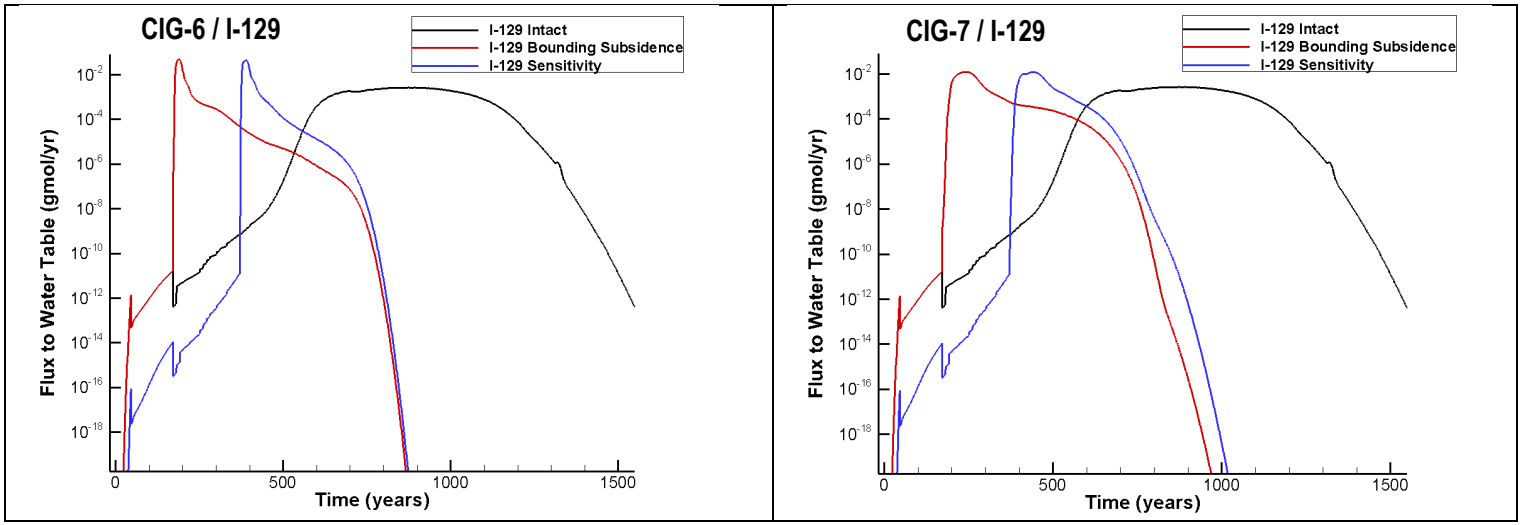

Figure 5-28. Flux-to-the-Water-Table Profiles of I-129 for Intact, Bounding Subsidence, and Best Estimate Subsidence (Sensitivity) Cases for CIG-6 (left) and CIG-7 (right)

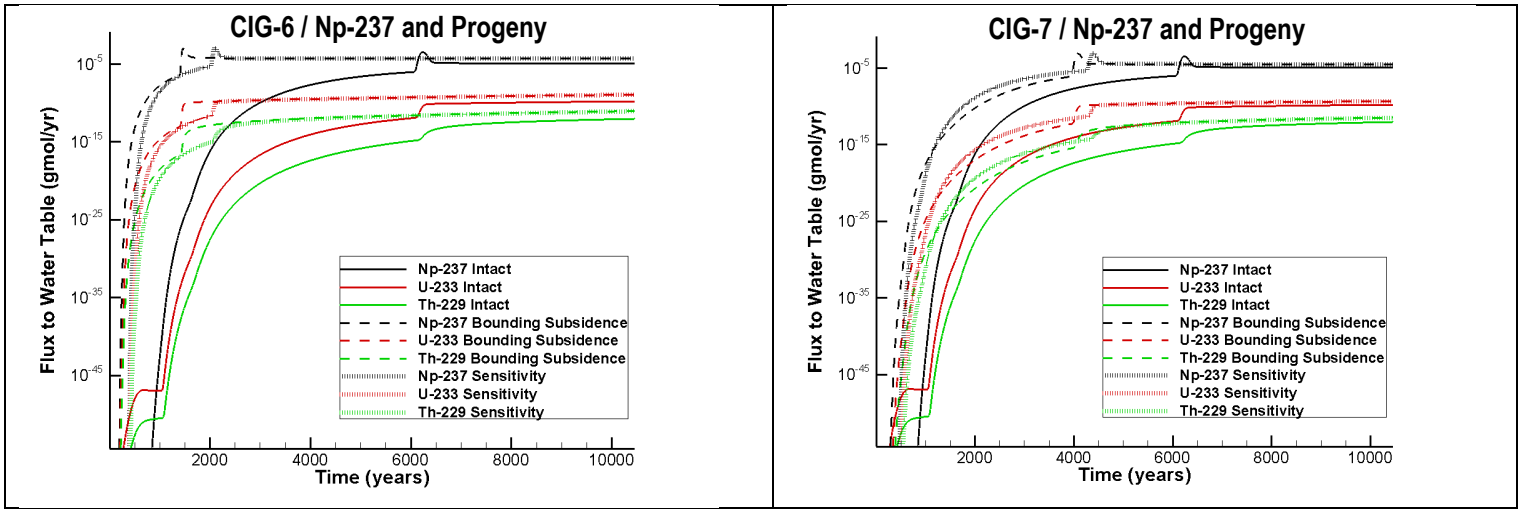

Figure 5-29. Flux-to-the-Water-Table Profiles of Np-237 and Progeny for Intact, Bounding Subsidence, and Best Estimate Subsidence (Sensitivity) Cases for CIG-6 (left) and CIG-7 (right)

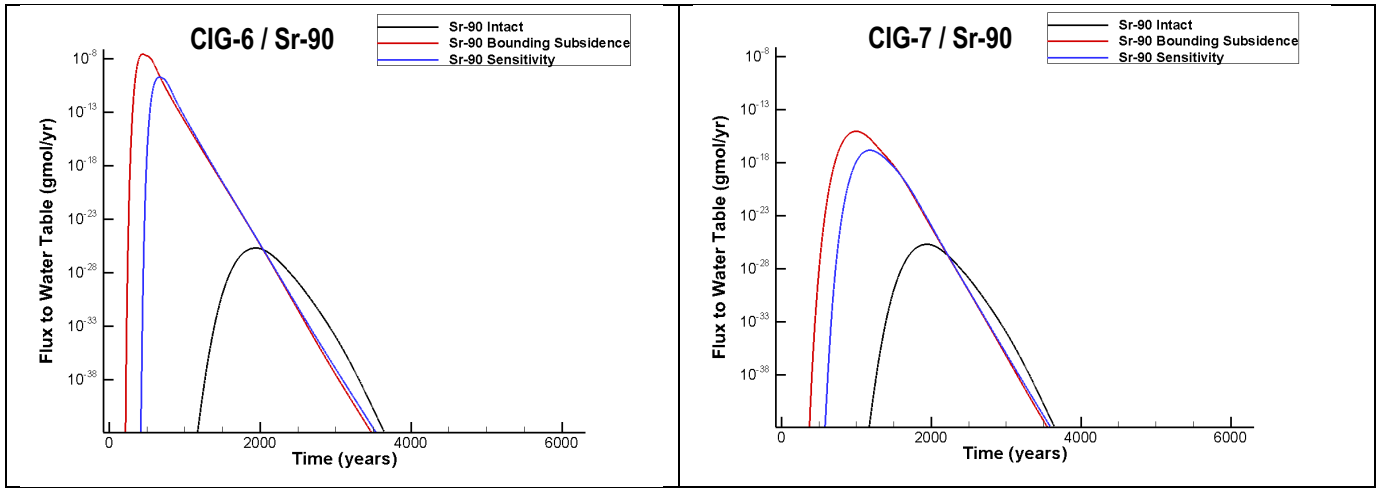

Figure 5-30. Flux-to-the-Water-Table Profiles of Sr-90 for Intact, Bounding Subsidence, and Best Estimate Subsidence (Sensitivity) Cases for CIG-6 (left) and CIG-7 (right)

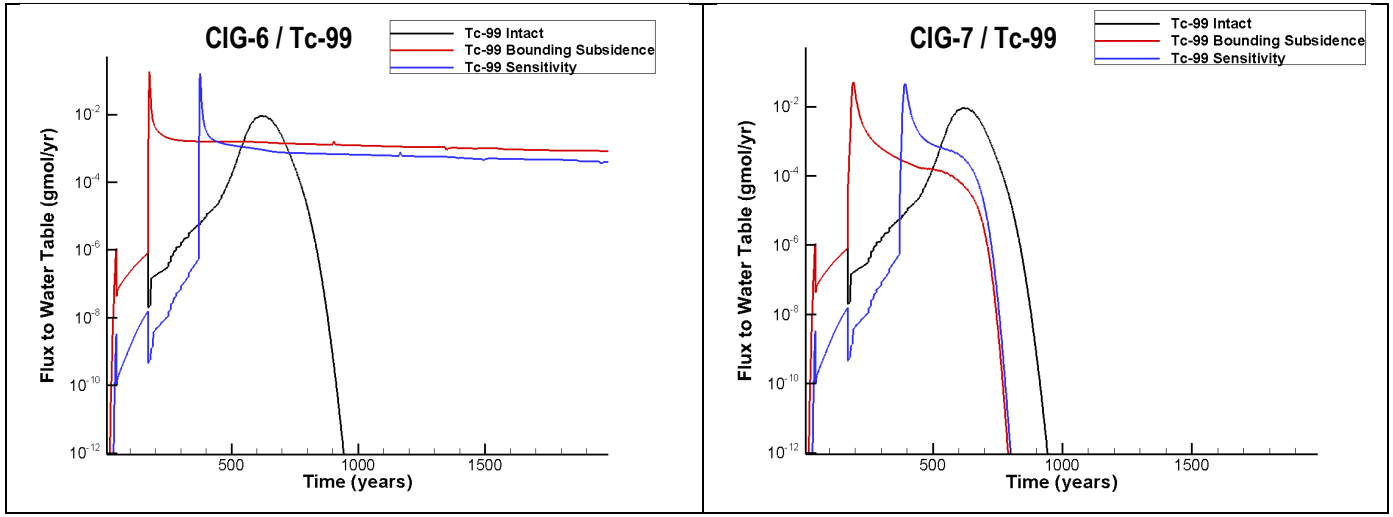

Figure 5-31. Flux-to-the-Water-Table Profiles of Tc-99 for Intact, Bounding Subsidence, and Best Estimate Subsidence (Sensitivity) Cases for CIG-6 (left) and CIG-7 (right)

Figure 5-32 highlights several key events in the I-129 flux-to-the-water-table profile for CIG-6. At interim closure (Year 46), the flux of I-129 to the water table notably decreases for the three cases shown. At final closure (Year 171), the flux of I-129 to the water table drops again for the intact case (black line) and sensitivity case (blue line) because the final closure cap remains intact. On the other hand, I-129 flux to the water table increases dramatically at Year 171 for the bounding subsidence case (red line) because the highest subsidence-induced infiltration rate is applied at final closure. A similar peak occurs for the best estimate subsidence case (blue line) at Year 371 when subsidence occurs and the decay of I-129 has been negligible. Because I-129 has a low to moderate K_d (even for cementitious materials), the high infiltration rate quickly leaches the contaminant from the waste zone in the direction of the water table. However, a slight increase in I-129 flux caused by cementitious aging of the enclosure and CIG waste form is evident at Year 260 and Year 450, respectively, for the bounding (red line) and sensitivity (blue line) cases. While the K_d for I-129 increases from Stage I to Stage II, it decreases by a factor of 2.5 from Stage II to Stage III, allowing rapid leaching from the waste zone as the enclosure transitions. The increase in K_d from Stage I to Stage II manifests itself for the intact case (black line) as a slight decrease in I-129 flux around Year 700 (labeled as "Enclosure, Stage I to Stage II" in Figure 5-32) after the enclosure has transitioned to Stage II. When the enclosure transitions from Stage II to Stage III for the intact case, a slight increase in I-129 flux is seen around Year 1,300 (labeled as "Enclosure, Stage II to Stage III" in Figure 5-32).

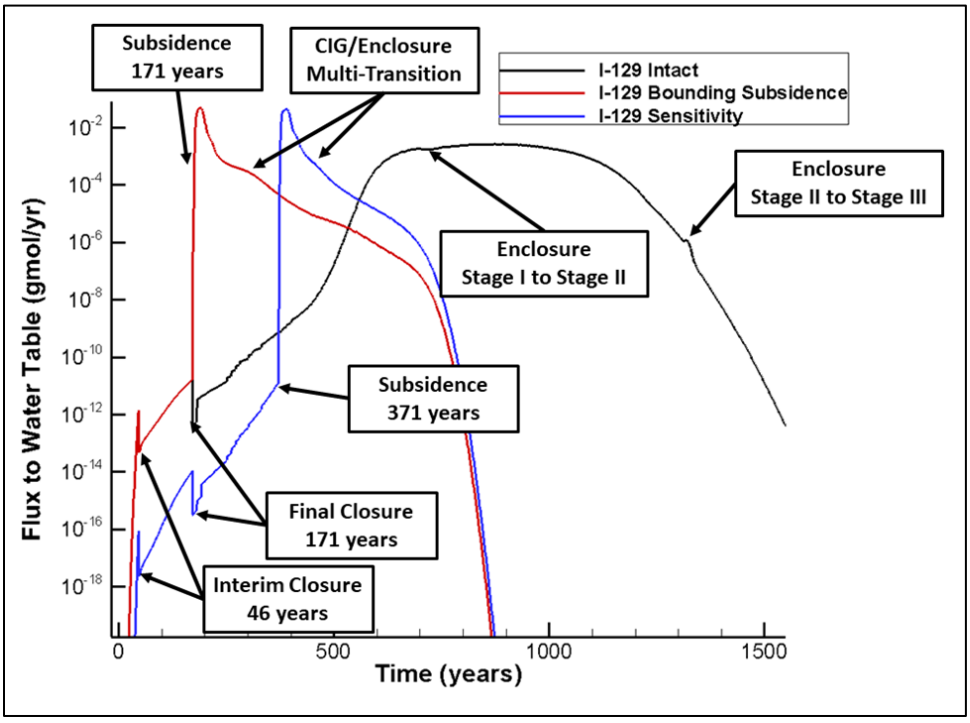

Figure 5-32. Flux-to-the-Water-Table Profile of I-129 from CIG-6 with Cover Degradation and Cementitious Aging Key Events

5.1.2.2. Tall Boxes

The tall box SWF is modeled with the same set of 27 radionuclides used for the ST and ET generic waste form. In addition, the tall boxes require simulating both flow and transport to capture the impact of the increased depth of the trench segments in ST08, ST09, and ST10 where tall boxes are placed. Because the tall box inventory is allowed only in the southern one-third of these three STs, only a single subsidence case is modeled using infiltration rates based on the short slope of the bounding infiltration model. Consequently, because each of the three STs has a 2% subsidence potential (giving a hole size of 200 feet parallel with the trench), the subsided region intersects with the cap crest, yielding a constant subsidence infiltration rate of 16.5 in yr^{-1}. All SWF inventory is uniformly distributed throughout the 3-D VZ model for the specific DU.

Figure 5-33 shows the material layout and mesh used for PORFLOW simulations containing the tall boxes. Note that the depth to the water table is reduced by 15 feet (from the generic waste form), the non-dynamically compacted waste zone is 31-foot tall, and the dynamically compacted waste zone is 4.8-foot tall. Figure 5-34, Figure 5-35, Figure 5-36, Figure 5-37, and Figure 5-38 show the saturation profiles for the tall box model for the uncovered, operational cover, interim cover, final cover, and subsidence periods, respectively. Note that water saturation is dimensionless (vol/vol) and the cover geometries for ST08, ST09, and ST10 are applied in the same way as the generic waste form. Similarly, the material properties for the tall box waste form are the same as those assumed for ET boxed waste in the generic waste models.

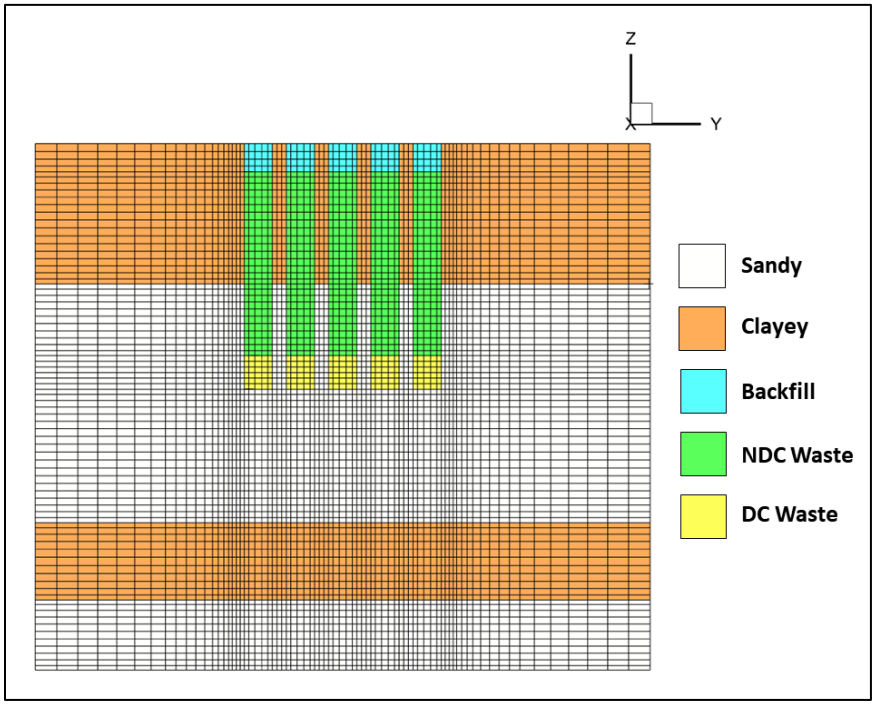

Figure 5-33. Material Layout for the Tall Box Special Waste Form

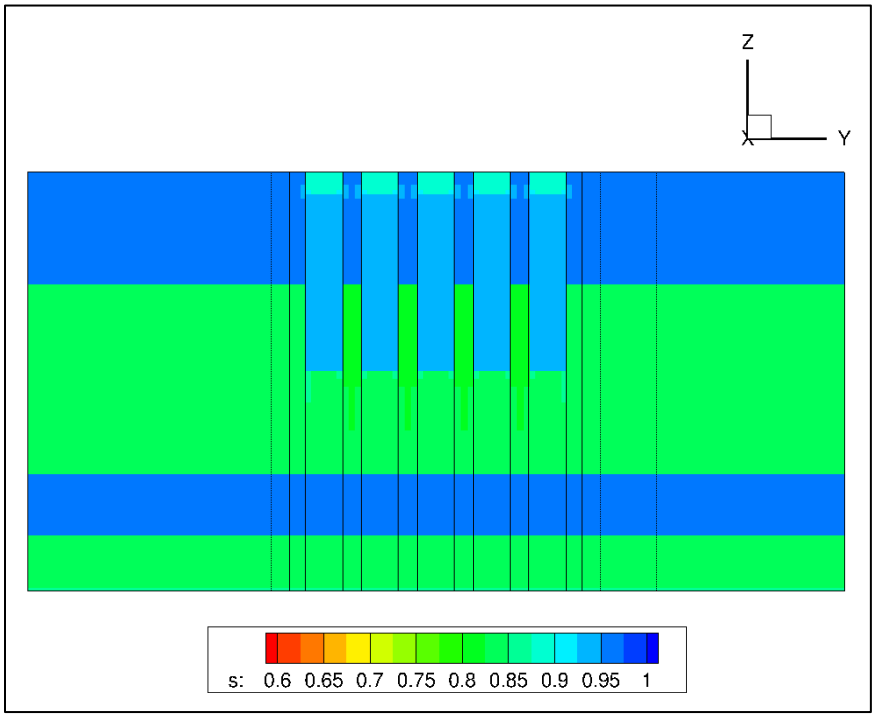

Figure 5-34. Saturation Profile for ST09 during the Uncovered Period

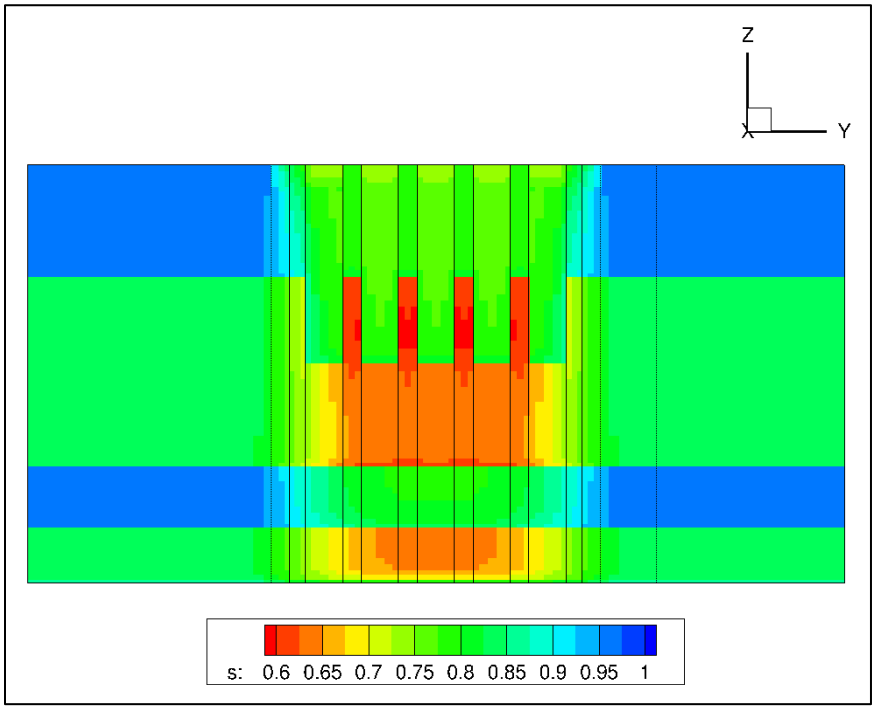

Figure 5-35. Saturation Profile for ST09 during the Operational Cover Period

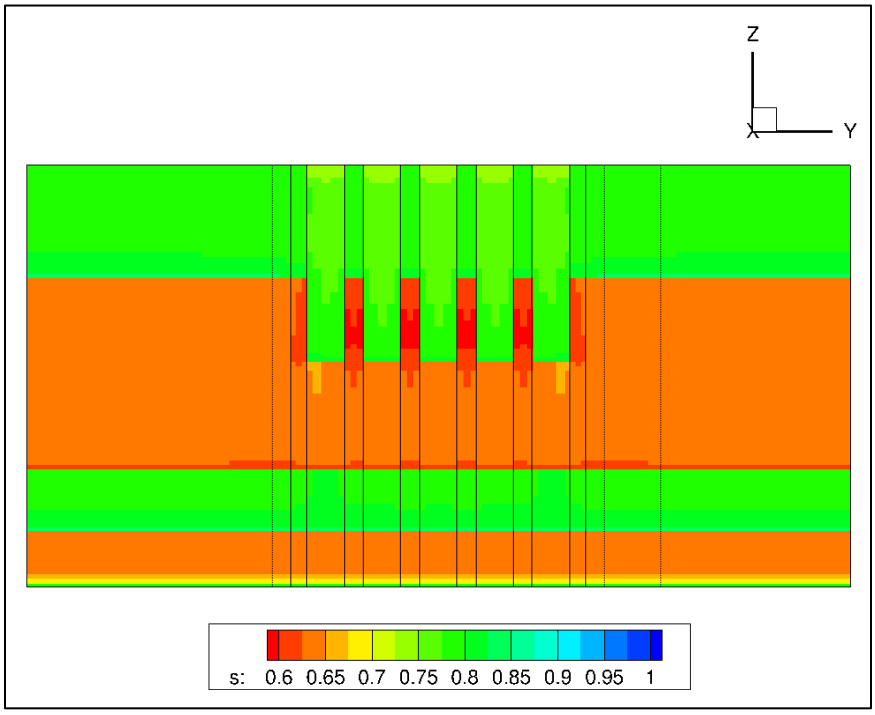

Figure 5-36. Saturation Profile for ST09 during the Interim Cover Period

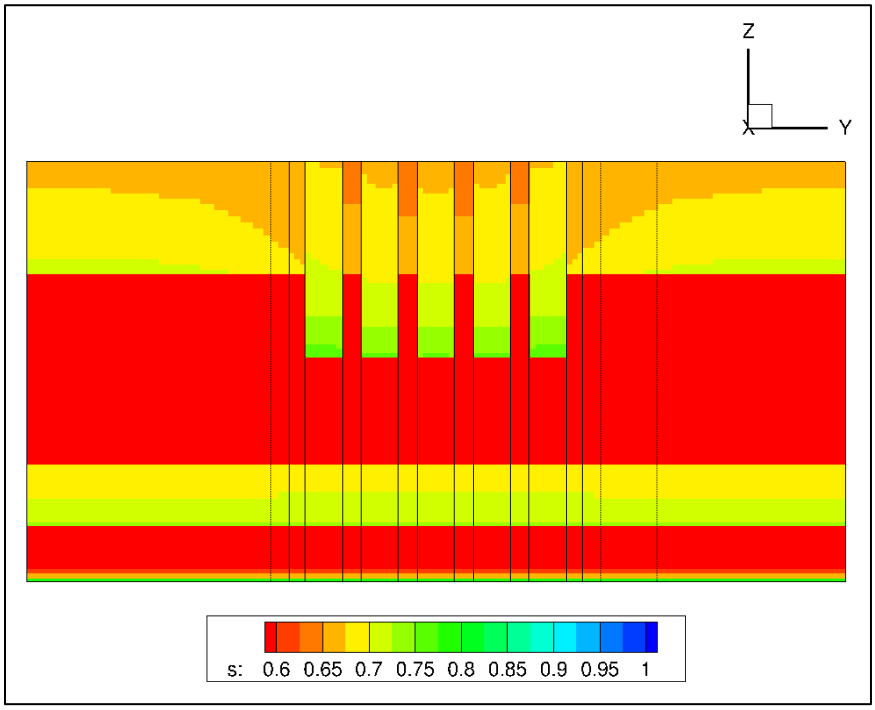

Figure 5-37. Saturation Profile for ST09 during the Final Cover Period

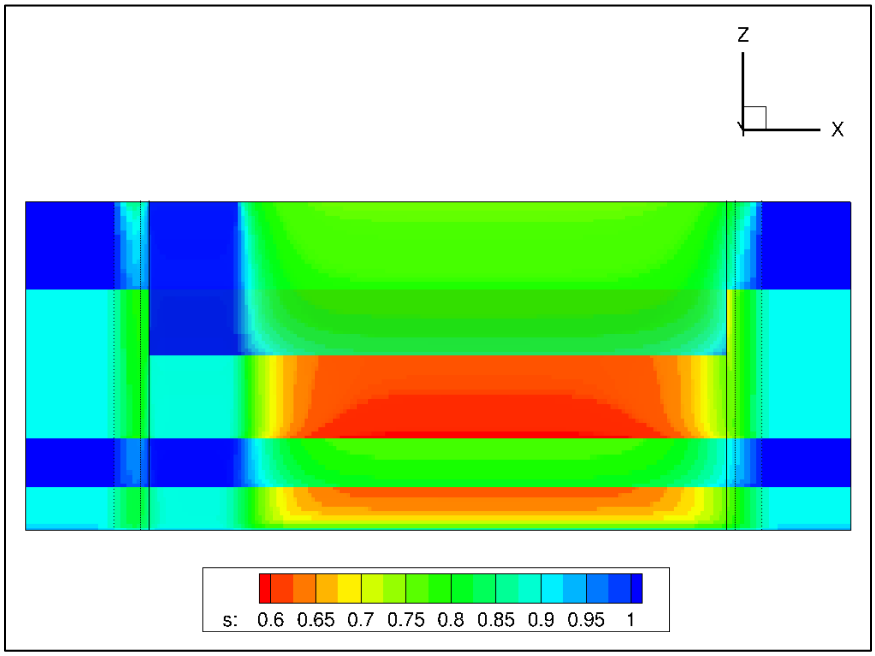

Figure 5-38. Saturation Profile for ST09 during the Subsidence Period

The flux-to-the-water-table profiles of a limited set of radionuclides for the tall box SWF in ST08, ST09, and ST10 are shown in Figure 5-39 for the intact and subsided cases. Additionally, a subsidence case for ST09 generic waste (where the subsided area is located at the cap crest and the infiltration rate is 16.5 in yr^{-1} as assumed in the tall box subsidence case) and an intact case for ST09 generic waste are shown as benchmarks for the tall box SWF.

Notably for H-3, the generic waste form has a sharper and higher peak flux than the tall box SWF for two reasons. First, the generic waste form is more highly concentrated in the waste zone. Second, transport of H-3 from the waste zone is not retarded. Sr-90, on the other hand, displays a higher peak flux for the tall box SWF, where the shallower depth to the water table allows for more Sr-90 to reach the water table before decay. For longer-lived, moderately mobile radionuclides, the increased travel time to the water table for the generic waste form results in a peak that occurs close to or later than the ST10 tall box SWF peak (which has the latest disposal timing because it contains future waste only).

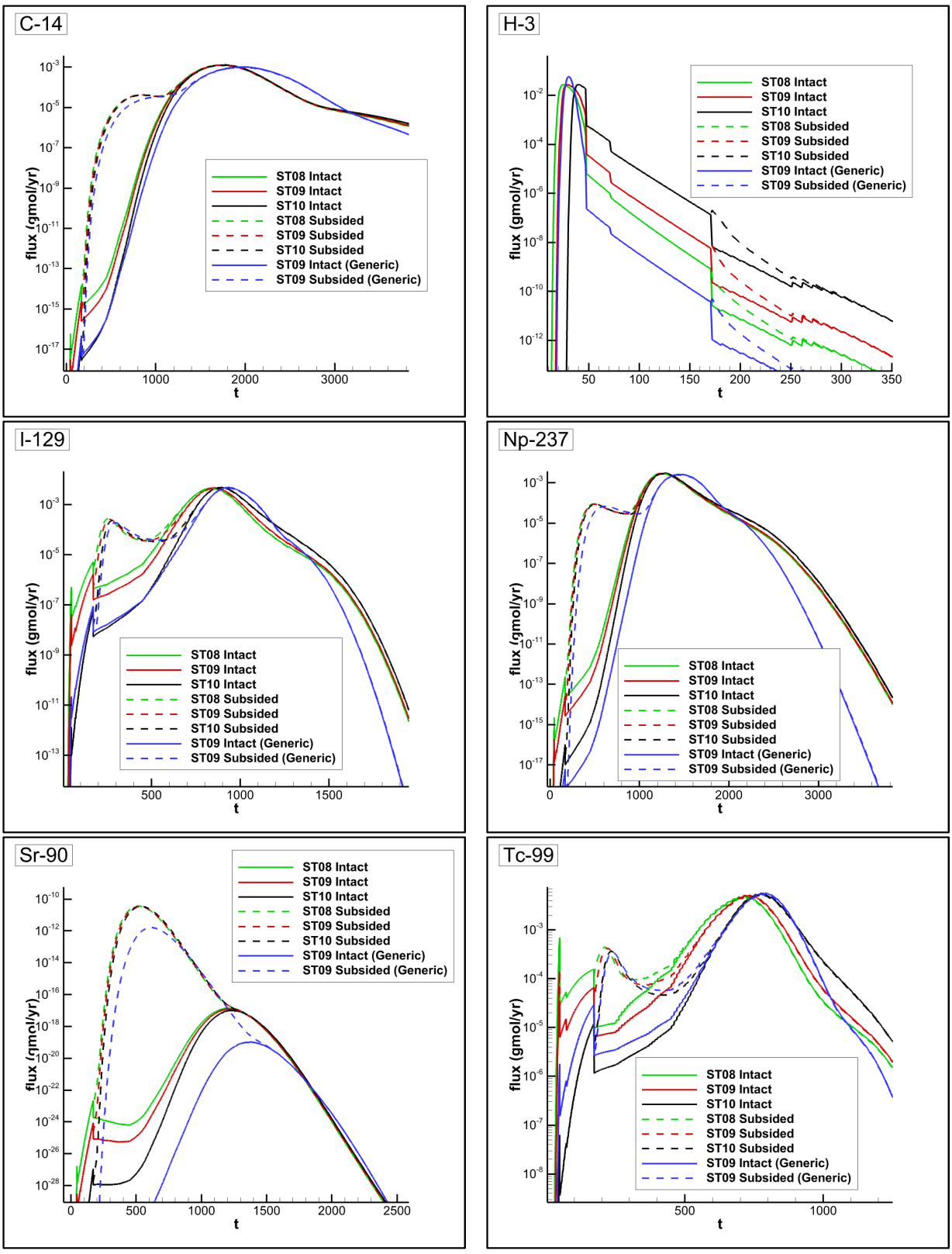

Figure 5-39. Flux-to-the-Water-Table Profiles of C-14, H-3, I-129, Np-237, Sr-90, and Tc-99 for Intact and Subsided Tall Box Models

5.1.2.3. Other Simple Special Waste Forms

For all other SWFs, no additional flow fields need to be recomputed. Rather, the inventory is placed in the waste zone of the trench model for generic waste forms with adjusted disposal timelines (i.e., for existing versus future inventory) and transport parameters (i.e., K_ds or solubility-controlled release curves). In all cases, radionuclide transport is slowed, resulting in a decrease and/or delay in the peak time. In particular, the effective-K_d implementation results in simply a slower release of radionuclides from the waste zone. This allows for greater decay of the shorter-lived radionuclides as well as the potential for a broader (and therefore lower) peak flux. The delayed-release mechanism results in a later actual release of the radionuclides because the contaminant is assumed to be immobile until dynamic compaction occurs; therefore, for short-lived radionuclides such as H-3, much of the contaminant decays before the cover is placed. In some cases, such as for I-129, the delayed-release implementation also assumes a greater K_d than for generic waste. This results in a slower release and a potentially broader peak, coupled with the fact that no waste is released until the final closure cap has been placed. Finally, the solubility-controlled-release implementation imposes a gradual release over time by assuming the same K_d values as for generic waste. This results in a lower, and more constant, release rate. Examples of these behaviors are illustrated by the following flux-to-the-water-table profiles:

- Figure 5-40 Effective-K_d (I-129D, E, G, H, I, and J) SWFs containing I-129 in ET01
- Figure 5-41 Solubility-controlled-release (I-129R) and effective-K_d (I-129J) SWFs containing I-129 in ST05
- Figure 5-42 Delayed-release (I-129C) and effective-K_d (I-129I and I-129J) SWFs containing I-129 in ST03

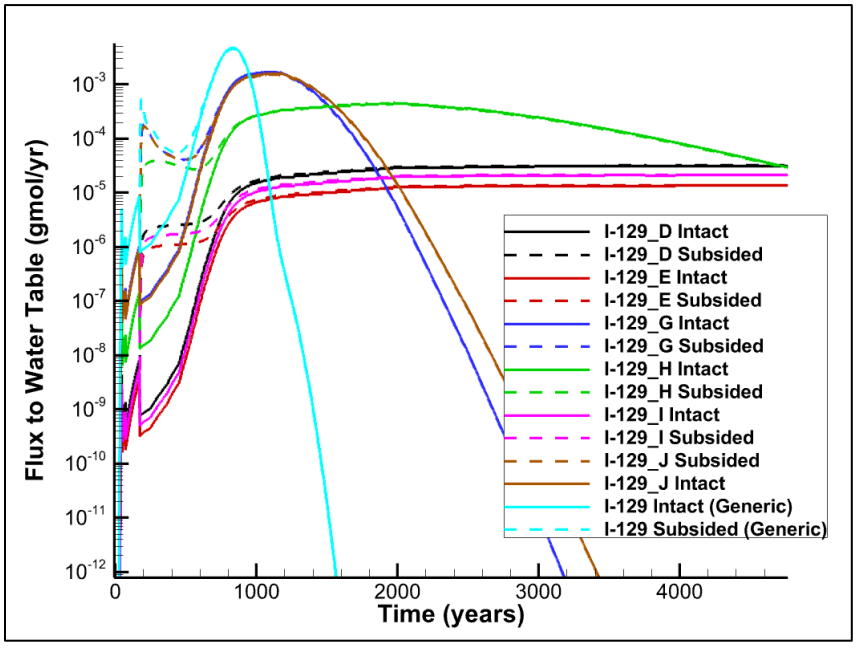

Figure 5-40. Flux-to-the-Water-Table Profiles of I-129 from Intact and Subsided ET01 Special Waste Forms

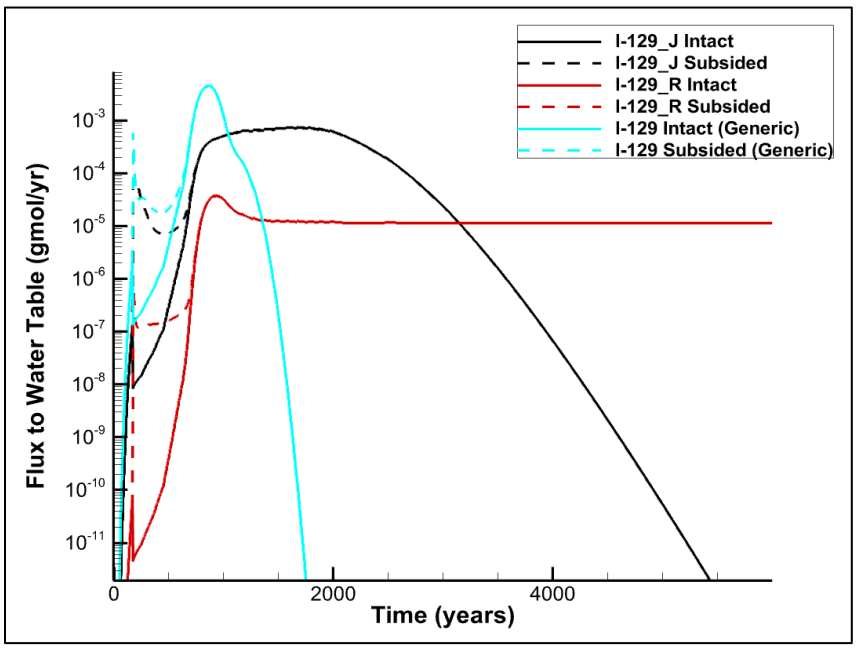

Figure 5-41. Flux-to-the-Water-Table Profiles for I-129 from Intact and Subsided ST05 Special Waste Forms

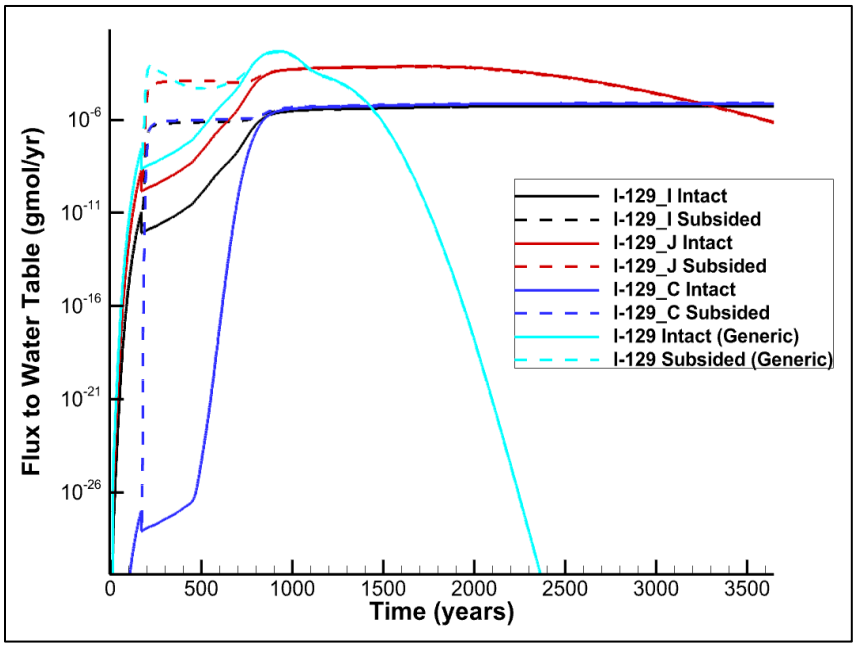

Figure 5-42. Flux-to-the-Water-Table Profiles for I-129 from Intact and Subsided ST03 Special Waste Forms

Refer to Figure 5-23 for a definition of the CWTS radionuclide name for the different I-129 SWF species (I-129D, I-129G, etc.). Appendix D contains supplemental concentration profiles of SWF radionuclides that contribute to at least 0.1% of the sum-of-fractions.

5.1.3. Aquifer Zone Model for Generic Waste Forms

Radionuclide contaminant transport through the aquifer is simulated for the intact and subsidence cases for each ST and ET. The source terms, obtained from the VZ flux-to-the-water-table profiles, are applied at the water table surface directly under the footprint of each DU in the GSA flow model(s). Three subsidence cases, representing three subsidence hole locations along the surface of the final closure cap, are modeled at the VZ level. To obtain a source term that is representative of subsidence, the flux-to-the-water-table profile for each subsidence case is blended by taking a weighted average of the radionuclide flux at each point in time. Because each hole location is deemed equally likely, all fluxes are weighted equally through time. This method of blending captures all possible hole locations while avoiding overly conservative assumptions.

5.1.3.1. Flow Model

As presented in Section 3.5.3, a steady-state aquifer flow field is computed at several points in time, representing the various stages of change that occur from the installation and degradation of the low-permeability caps (e.g., interim and final closure caps) placed over the ELLWF. Like the workflow for the VZ radionuclide transport models, the steady-state GSA flow fields are introduced on the following timeline:

- Year 0 (uncovered conditions)
- Year 71 (area-wide cover conditions)
- Year 451 (partially degraded conditions)
- Year 731 (partially degraded conditions)
- Year 1,171 (partially degraded conditions)
- Year 10,171 (completely degraded conditions)

These time markers coincide with key points in the closure cap infiltration rate time profile when significant increases or decreases in water flow occur through the ELLWF. At each time marker, the representative steady-state flow field is provided as input for solving the radionuclide transport equations within the specific GSA cutout flow model for each DU.

Additional details on the implementation of the aquifer flow model for STs and ETs are provided in Section 3.5.3.

5.1.3.2. Transport Model for Nominal PA Cases

The concentration profile at the 100-meter POA depends on several DU-specific features, such as the source location (i.e., impact of the flow field and travel distance at/from that location), ST or ET geometry, cover geometries (i.e., central versus edge versus corner DUs), disposal timing, and final closure cap degradation (i.e., time-dependent aquifer flow field and infiltration rates applied at the surface), as well as the physical and geochemical parameters for the radionuclides of interest. This section presents several time-dependent concentration profiles that demonstrate the interplay of the above physical and chemical characteristics. In addition to the impacts of DU-specific features, Figure 5-43 demonstrates how the node along the 100-meter POA can change over time, creating the appearance of discontinuities in the concentration profile. These discontinuities are a

simulation artifact caused by how the concentrations are collected from PORFLOW over time (i.e., the concentration is recorded at the node with the peak concentration of the contaminant). However, and more importantly, this collection technique ensures that the peak concentration is captured to compute inventory limits and project doses. In some cases, such as when the node shifts slightly along the POA because of plume migration, the discontinuity is less severe. In other cases, sudden changes are attributed to changes in the aquifer flow field and/or occurrences at the ground surface that substantially change the source term. For example, the node change at Year 73 corresponds with the timing of final closure cap placement at Year 71 when reduced water infiltration passes through the VZ and results in a lower flux to the water table. Along with the reduced flux to the water table (and corresponding source term), the aquifer flow field changes at Year 71 because of the placement of the low-permeability interim cover. The aquifer flow field similarly changes at Years 451, 731, and 1,171, which results in subsequent changes in the peak concentration node at Years 624, 736, and 1,171, respectively (see Figure 5-43).

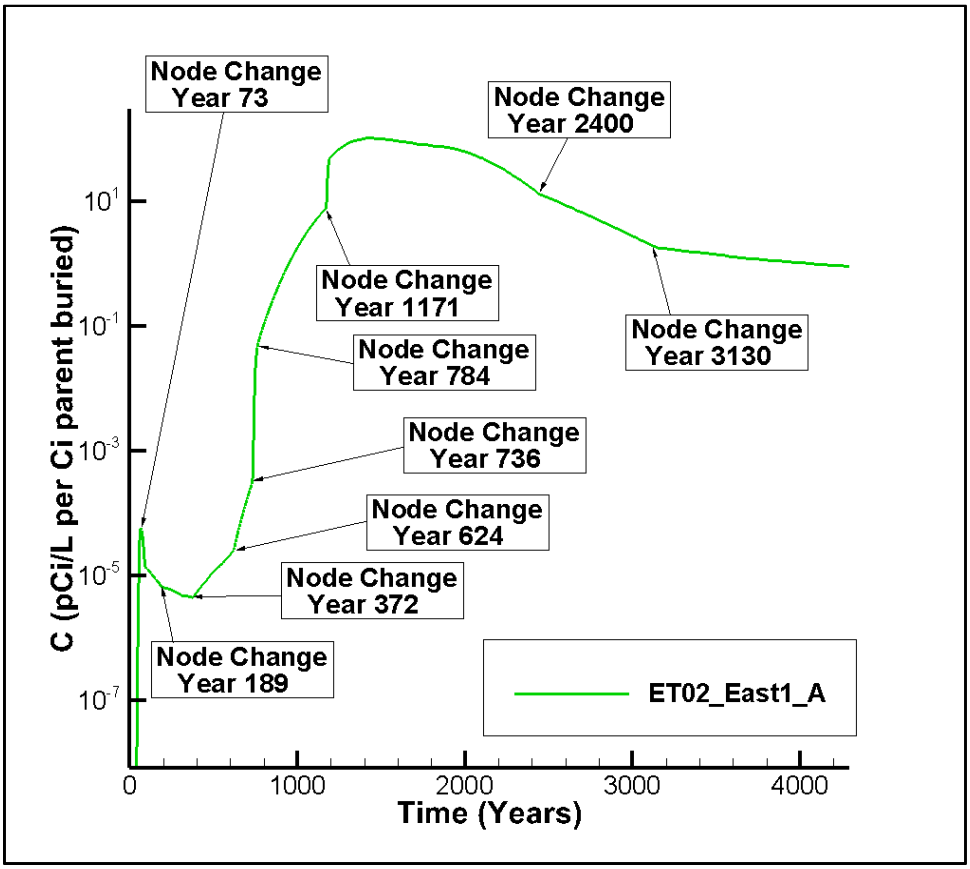

Figure 5-43. Peak Concentration Node Changes Over Time Along the 100-meter Boundary Based on Concentration Profile of Tc-99 Emanating from ET02

Figure 5-44 shows a 2-D projection of the maximum concentration of Tc-99 emanating from the source zone at ET02 and illustrates how GSA flow model changes can cause the peak concentration to shift along the nodes of the 100-meter POA.

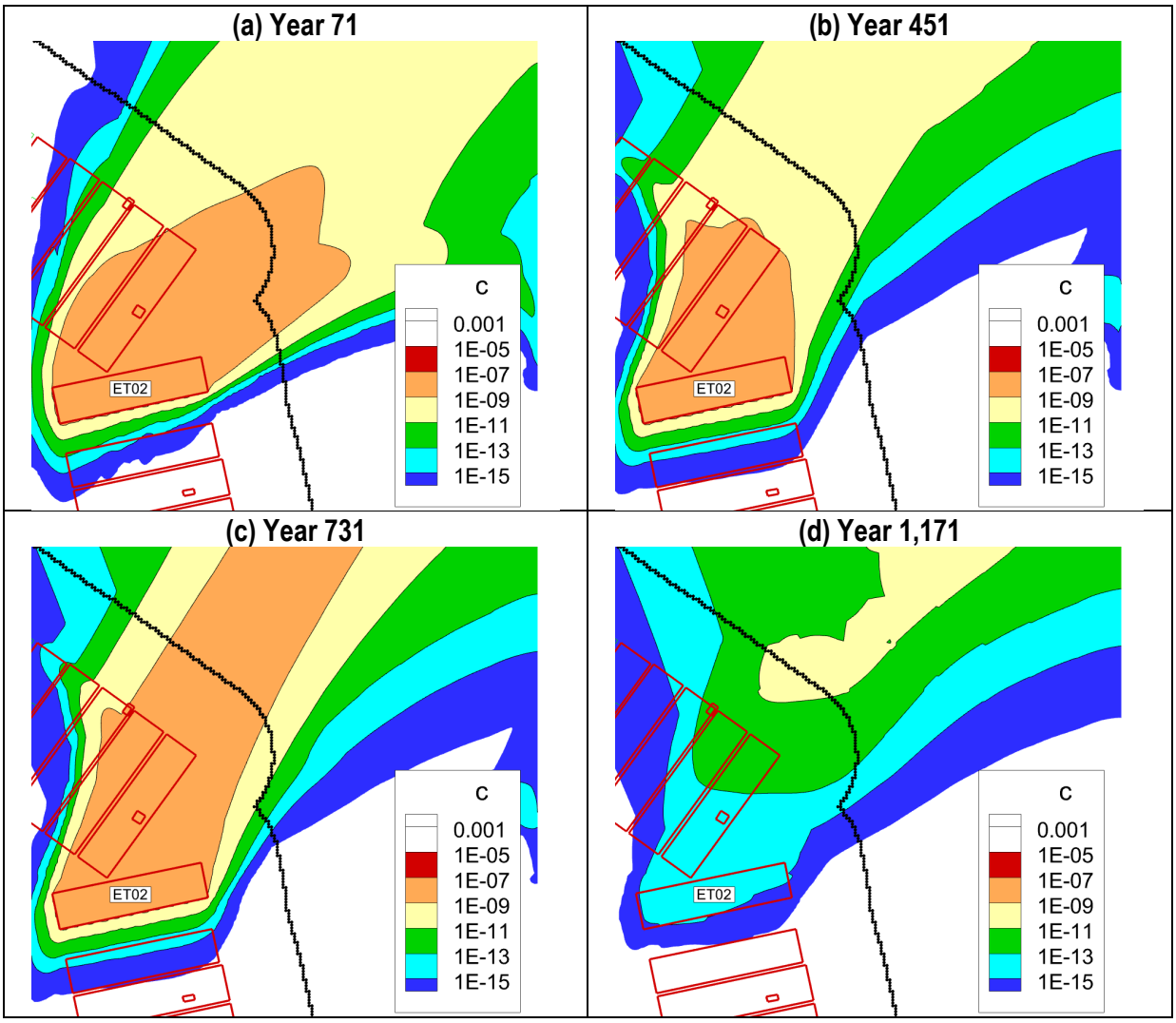

Figure 5-44. Projection of Maximum Concentration Profile of Tc-99 (gmol ft^{-3} per gmole parent buried) for ET02 at (a) Year 71; (b) Year 451;(c) Year 731; and (d) Year 1,171

The impact of disposal timing on the concentration at the 100-meter POA varies by radionuclide. The most noticeable impact is seen in more mobile radionuclides (e.g., H-3) that peak early in time (i.e., prior to the placement of any cover). Figure 5-45 shows the impact of disposal timing for a limited set of radionuclides in the same VZ hydrostratigraphic grouping (i.e., same depth to the water table and same subsurface features) and with similar length (i.e., nearly straight-line travel paths to the 100-meter POA). In Figure 5-45, the "g" suffix (e.g., ST03g) denotes that the concentration profile represents generic waste only, not SWFs.

While ST03 and ST04 operations began within six months of each other, ST23 began disposing of waste approximately 17 years later. Notably, the H-3 peak for ST23 occurs 17 years later than ST03 and ST04. The higher peak concentration of H-3 from ST23 is attributed to the cementitious CIG trench segments (modeled as SWF) occupying a portion of the ST23 waste footprint. The area occupied by the CIG trench segments is not considered in the aquifer model results displayed in Figure 5-45 (note "g" suffix for ST23 in legend). Compared to ST03 and ST04, the H-3 inventory

in ST23 is distributed across a smaller trench footprint and is concentrated at the source nodes nearest the 100-meter POA.

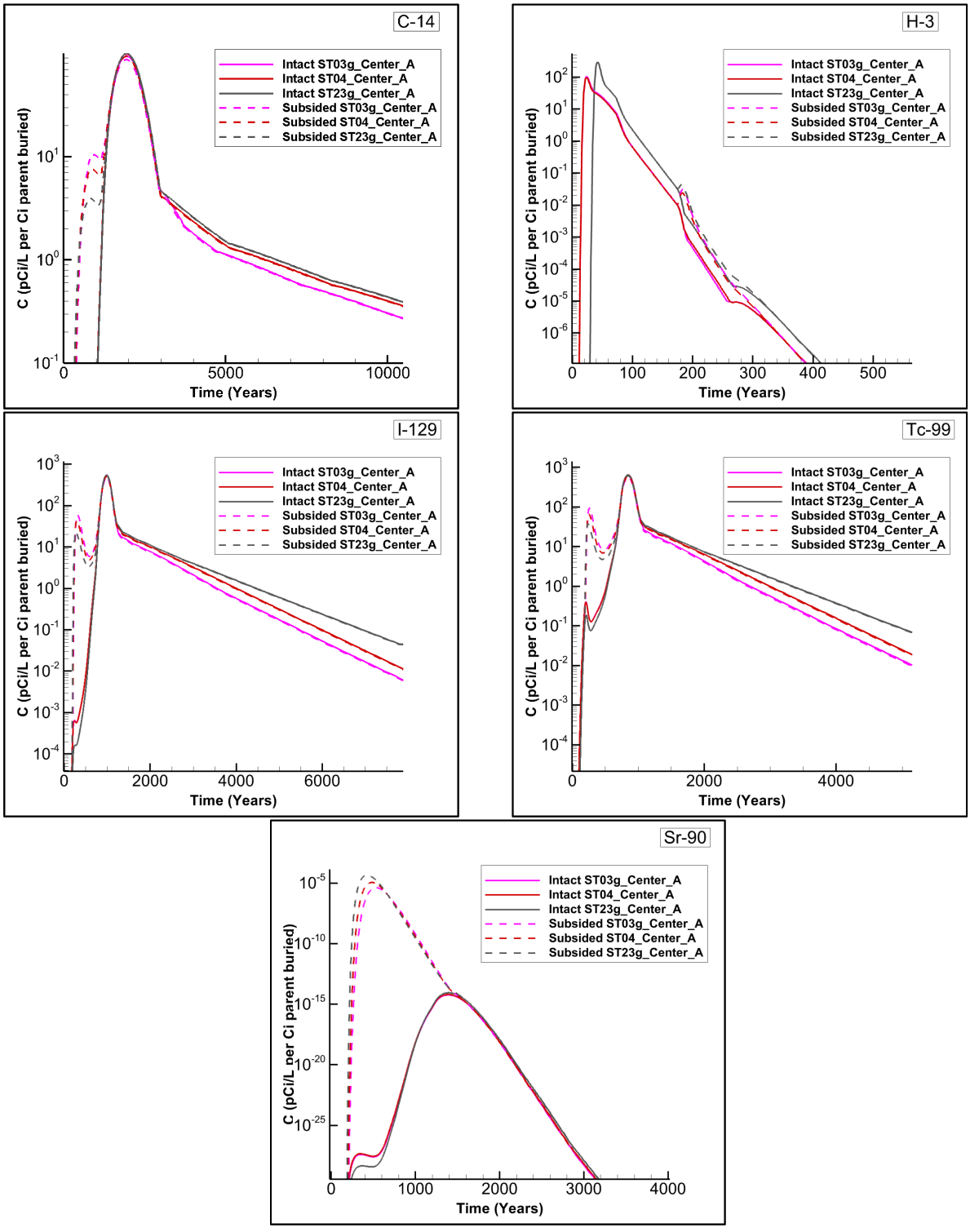

Figure 5-45. Concentration Profiles of C-14, H-3, I-129, Tc-99, and Sr-90 for Intact and Subsidence Cases at ST03, ST04, and ST23

In all other cases shown, the peak concentration occurs after low-permeability covers have been placed when water velocities are lower. Therefore, a shift along the temporal axis is less noticeable and, ultimately, attributable to a combination of half-life, K_d values, and the timing of disposal. Note that when considering subsidence cases, each DU shown has a different subsidence infiltration rate that is based on the percentage of non-crushable inventory (i.e., 4.9% for ST03, 3.6% for ST04, and 2% for ST23). Figure 5-46 shows a comparison of the Tc-99 plume emanating from ST22 and ST23, where the travel distance from ST22 is significantly longer than from ST23 and a different GSA flow model cutout is used for each ST.

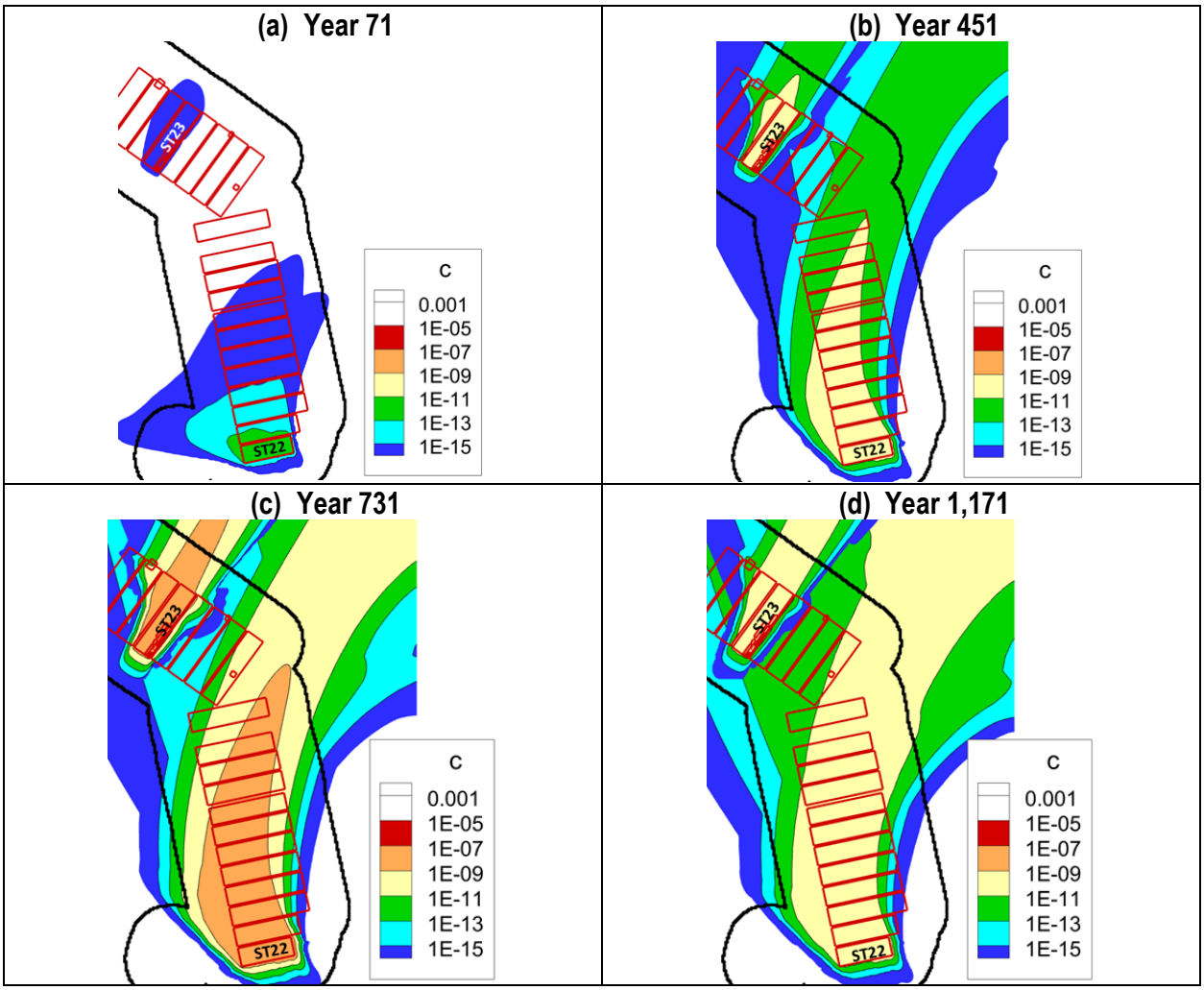

Figure 5-46. 2-D Projection of Maximum Concentration Profile (gmol ft^{-3} per gmole parent buried) of Tc-99 Emanating from ST23 and ST22 at (a) Year 71; (b) Year 451; (c) Year 731; and (d) Year 1,171

The plume travel path from ST22 is along longitudinal and transverse directions with respect to the orientation of nearby DUs. In contrast, the travel path from ST23 is parallel to the orientation of DUs and perpendicular to the 100-meter POA. Consequently, the ST23 concentration profiles along the 100-meter POA for the six radionuclides shown in Figure 5-47 have a narrower, higher, and earlier peak compared to the profiles for ST22.

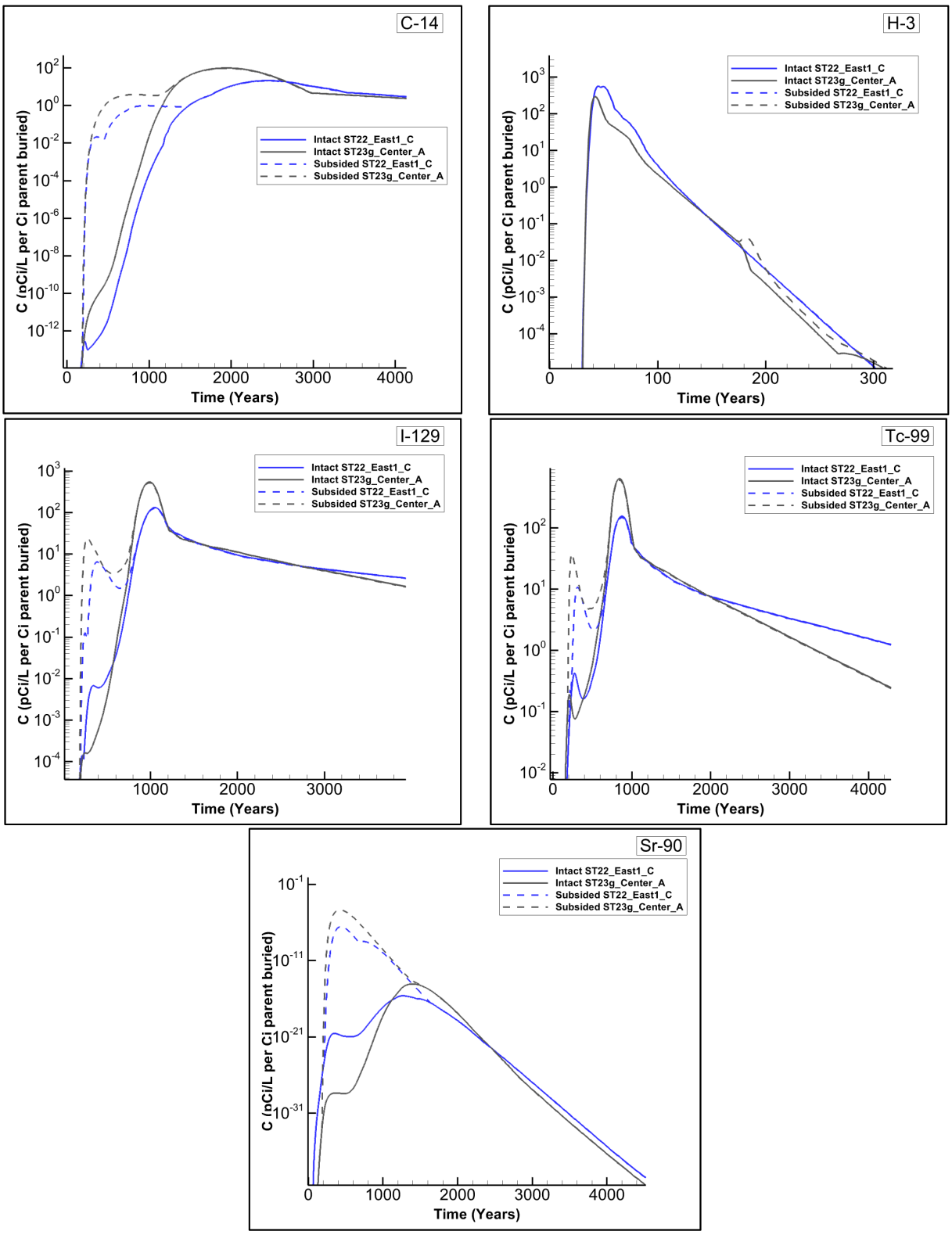

Figure 5-47. Concentration Profiles of C-14, H-3, I-129, Tc-99, and Sr-90 for Intact and Subsidence Cases at ST22 and ST23

Notably, the H-3 peak concentration from ST22 is higher and occurs slightly later than the H-3 peak from ST23. Figure 5-48 shows the 2-D projection of the maximum H-3 concentration emanating from ST22 and ST23 at the time the interim cover is installed. In both cases, the H-3 concentration migrates beyond the 100-meter POA during the uncovered period. More specifically, the bulk of the H-3 mass emanating from ST23 has moved beyond the 100-meter POA during the uncovered period. The remaining mass is isolated to the ST23 footprint once the interim cover is applied. Similarly, much of the H-3 mass emanating from ST22 has migrated beyond the 100-meter POA at the time the interim cover is installed in Year 71. However, the longer travel path between ST22 and the 100-meter POA results in some remaining H-3 mass inside the 100-meter POA at the time the interim cover is placed, which results in a higher peak at a later time.

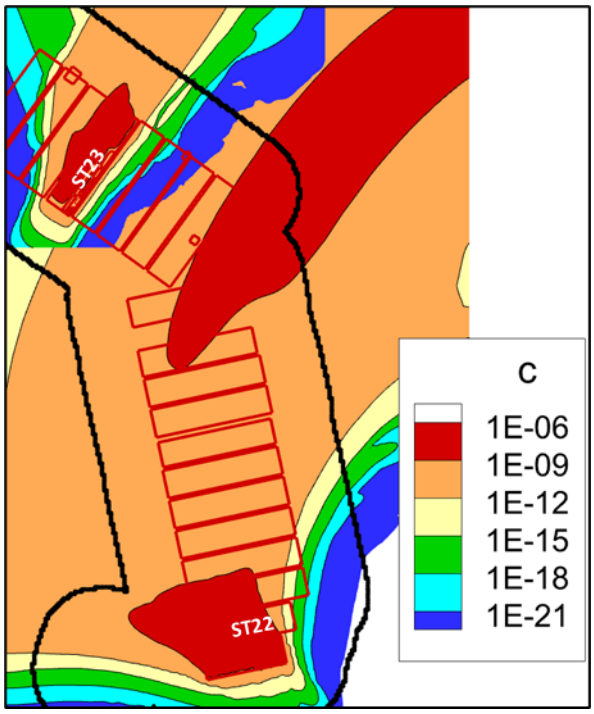

Figure 5-48. 2-D Projection of Maximum Concentration Profile (gmol ft^{-3} per gmole parent buried) of H-3 emanating from ST23 and ST22 at Year 71

Figure 5-49 through Figure 5-52 show the concentration time profiles at the 100-meter POA for all radionuclides (except for Th-231, which decays quickly) from one DU for each of the GSA flow model cutouts. These concentration profiles further demonstrate the complexity of behaviors manifested by the combination of features that are built into the models from the ground surface through the aquifer zone.

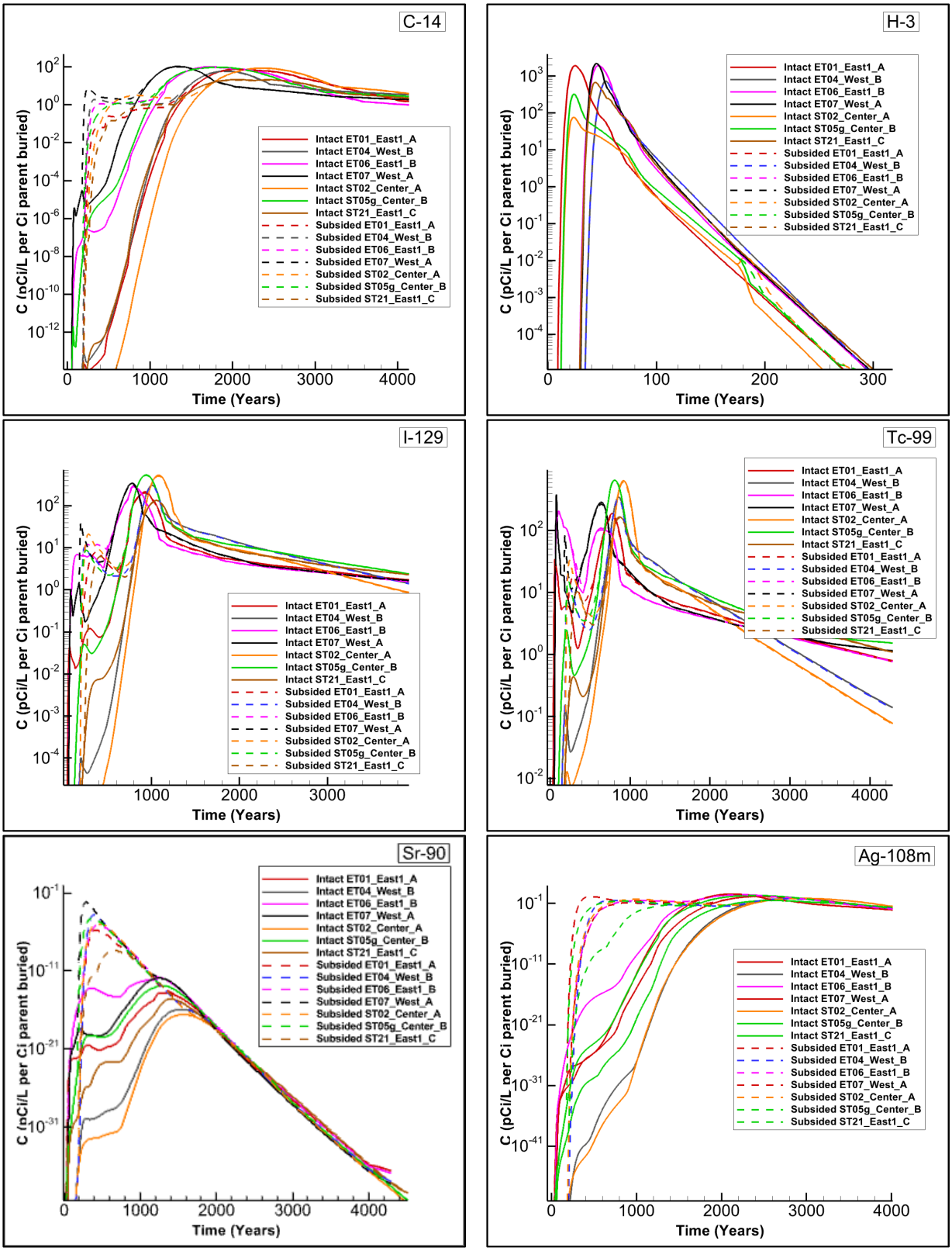

Figure 5-49. Concentration Profiles of C-14, H-3, I-129, Tc-99, Sr-90, and Ag-108m for Intact and Subsidence Cases at a Selected Disposal Unit for Each General Separations Area Flow Model Cutout

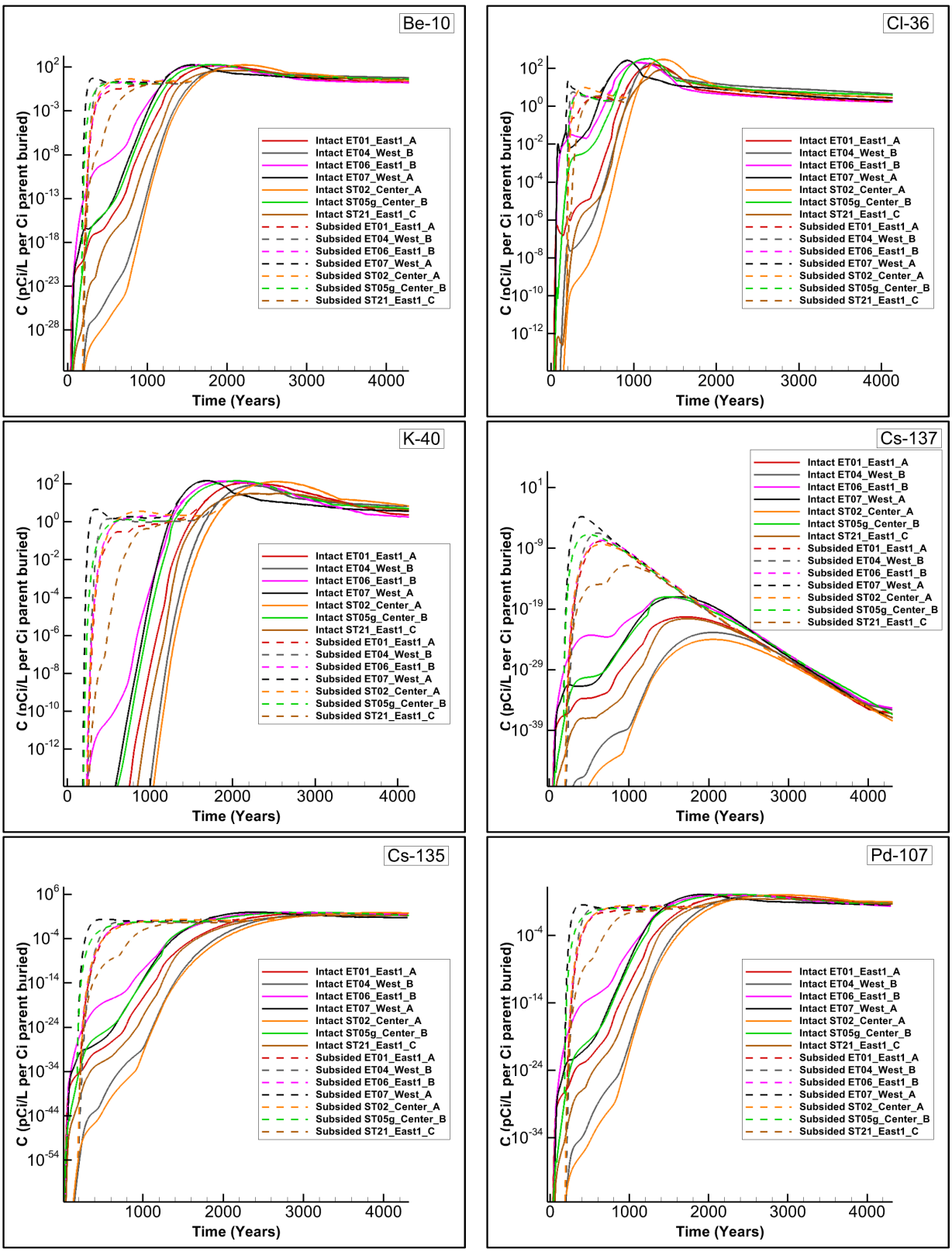

Figure 5-50. Concentration Profiles of Be-10, Cl-36, K-40, Cs-137, Cs-135, and Pd-107 for Intact and Subsidence Cases at a Selected Disposal Unit for Each General Separations Area Flow Model Cutout

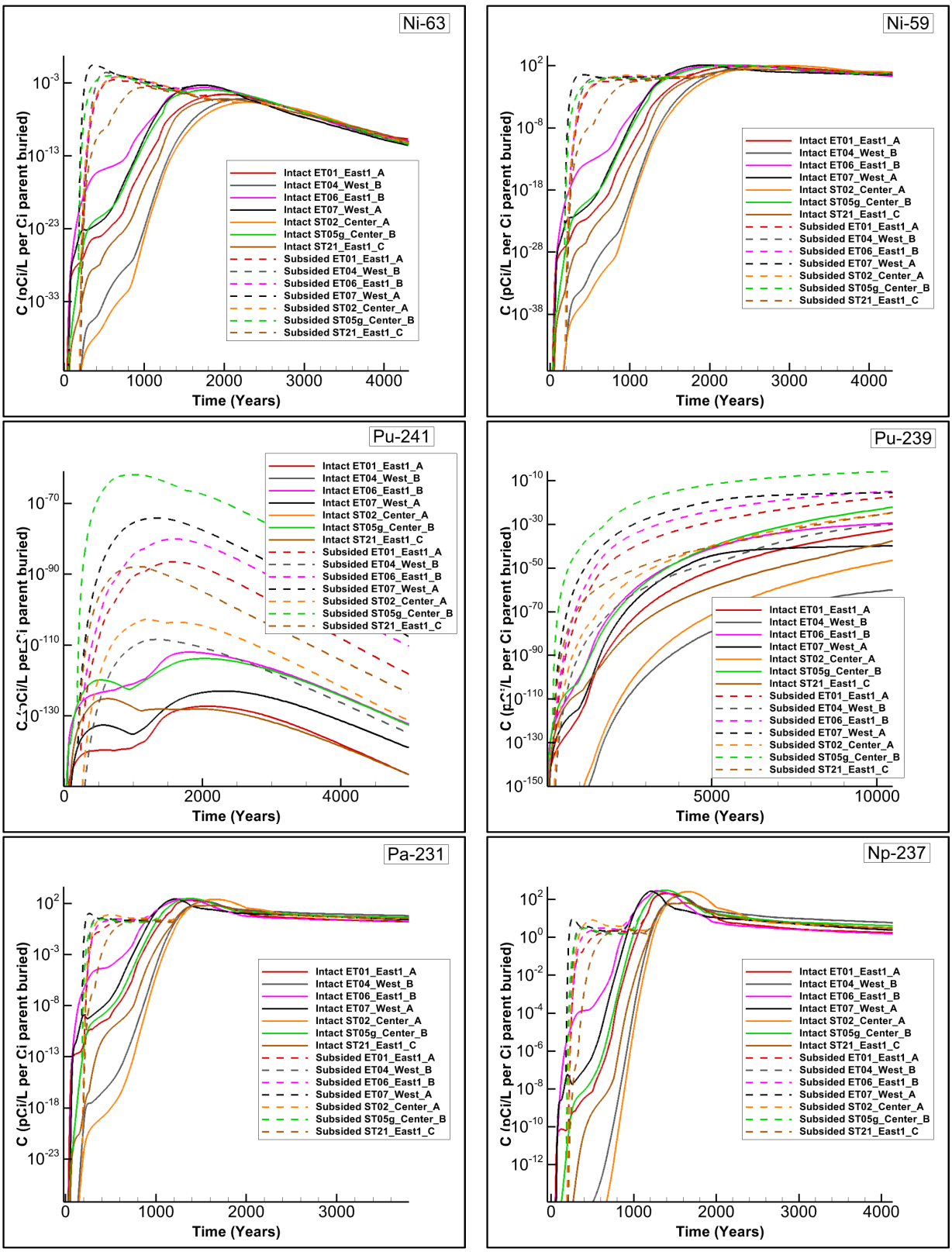

Figure 5-51. Concentration Profiles of Ni-63, Ni-59, Pu-241, Pu-239, Pa-231, and Np-237 for Intact and Subsidence Cases at a Selected Disposal Unit for Each General Separations Area Flow Model Cutout

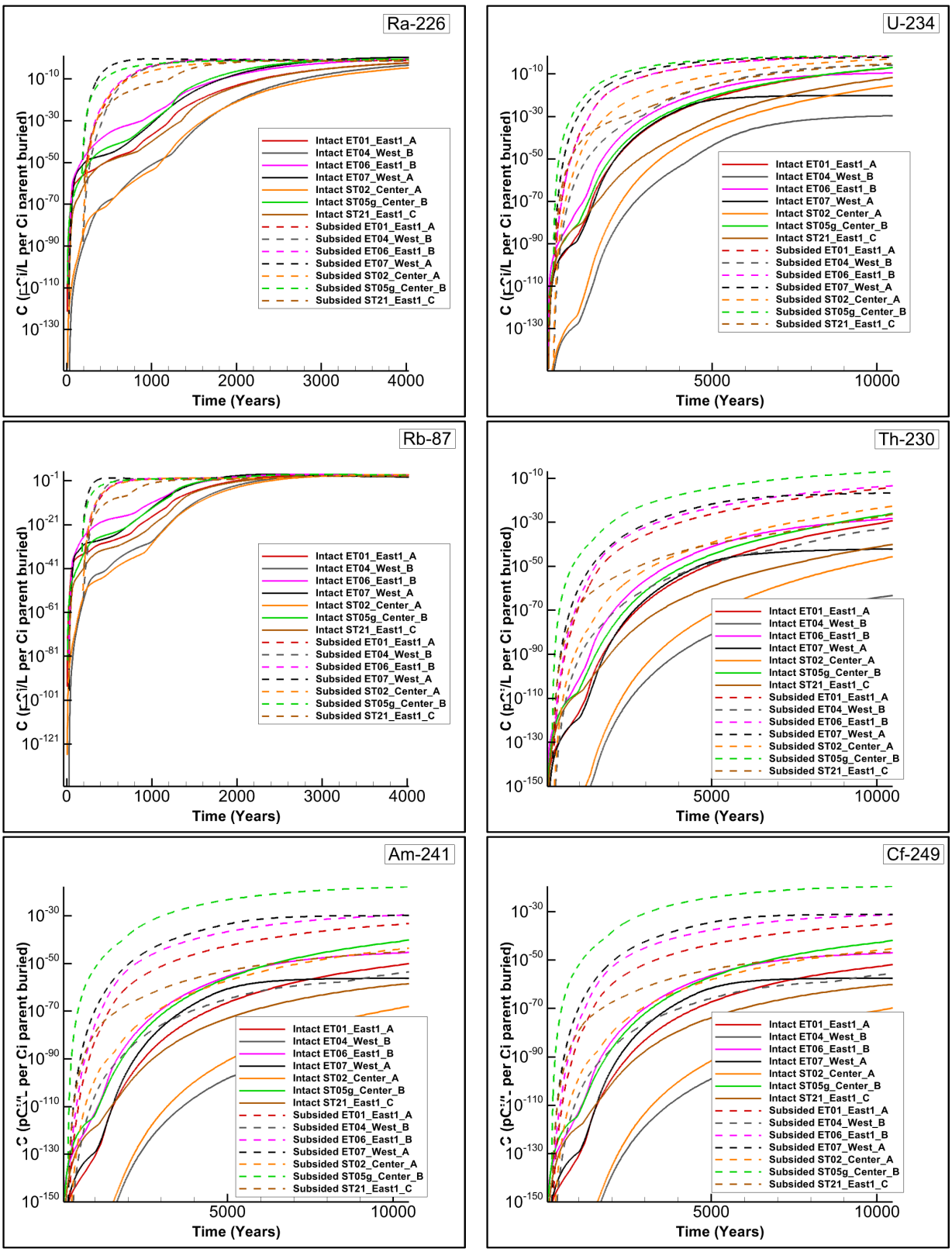

Figure 5-52. Concentration Profiles of Ra-226, U-234, Rb-87, Th-230, Am-241, and Cf-249 for Intact and Subsidence Cases at a Selected Disposal Unit for Each General Separations Area Flow Model Cutout

5.1.3.3. Transport Model for Sensitivity Cases

The flux-to-the-water-table profiles for the VZ sensitivity cases (Table 5-3) for STs and ETs serve as the source terms for radionuclide transport simulations through the aquifer. Parameters are unchanged in the aquifer model except for K_d values for the sandy and clayey aquifer zone materials in the K_d sensitivity case. Figure 5-53 through Figure 5-55 highlight the concentration profiles of six radionuclides at the 100-meter POA for each sensitivity case and DU. The same general trends observed at the water table are also seen at the 100-meter POA, where changes in K_d, infiltration rate, and model timeline have the greatest impact on concentration at the POA.

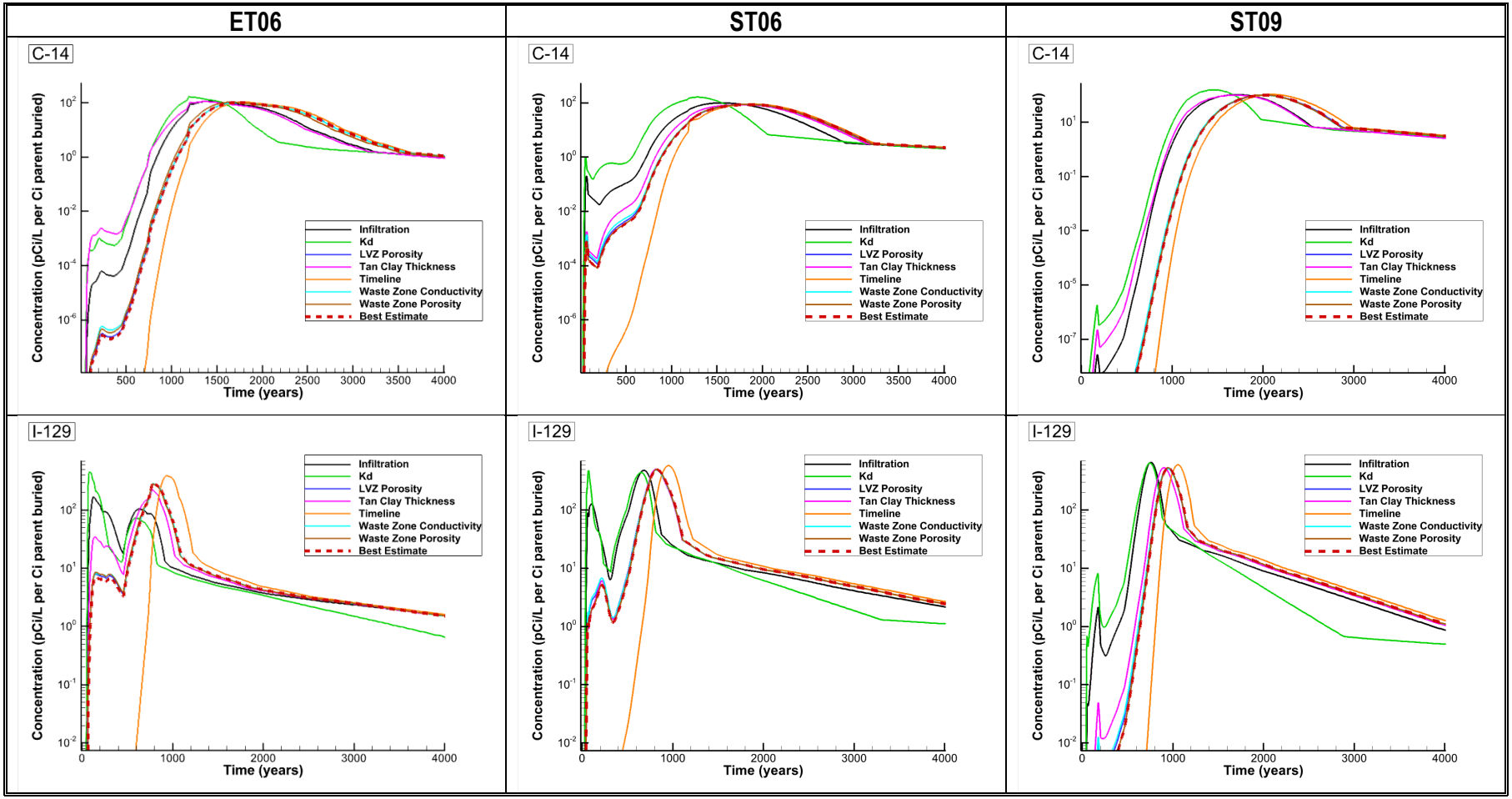

Figure 5-53. C-14 and I-129 Concentration Profiles at 100-meter POA for ET06, ST06, and ST09 Comparing Best Estimate (Nominal PA) and Sensitivity Cases

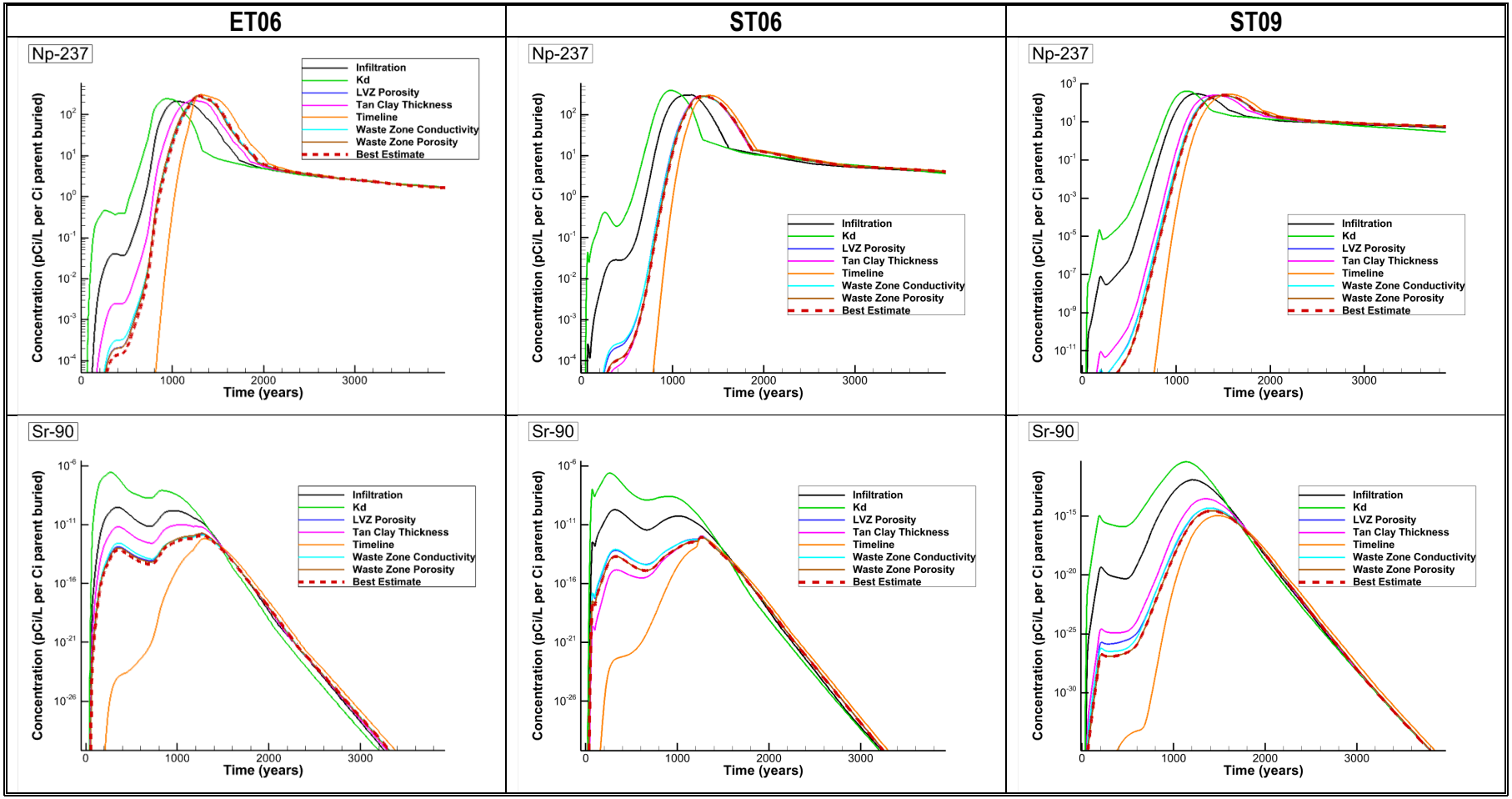

Figure 5-54. Np-237 and Sr-90 Concentration Profiles at 100-meter POA for ET06, ST06, and ST09 Comparing Best Estimate (Nominal PA) and Sensitivity Cases

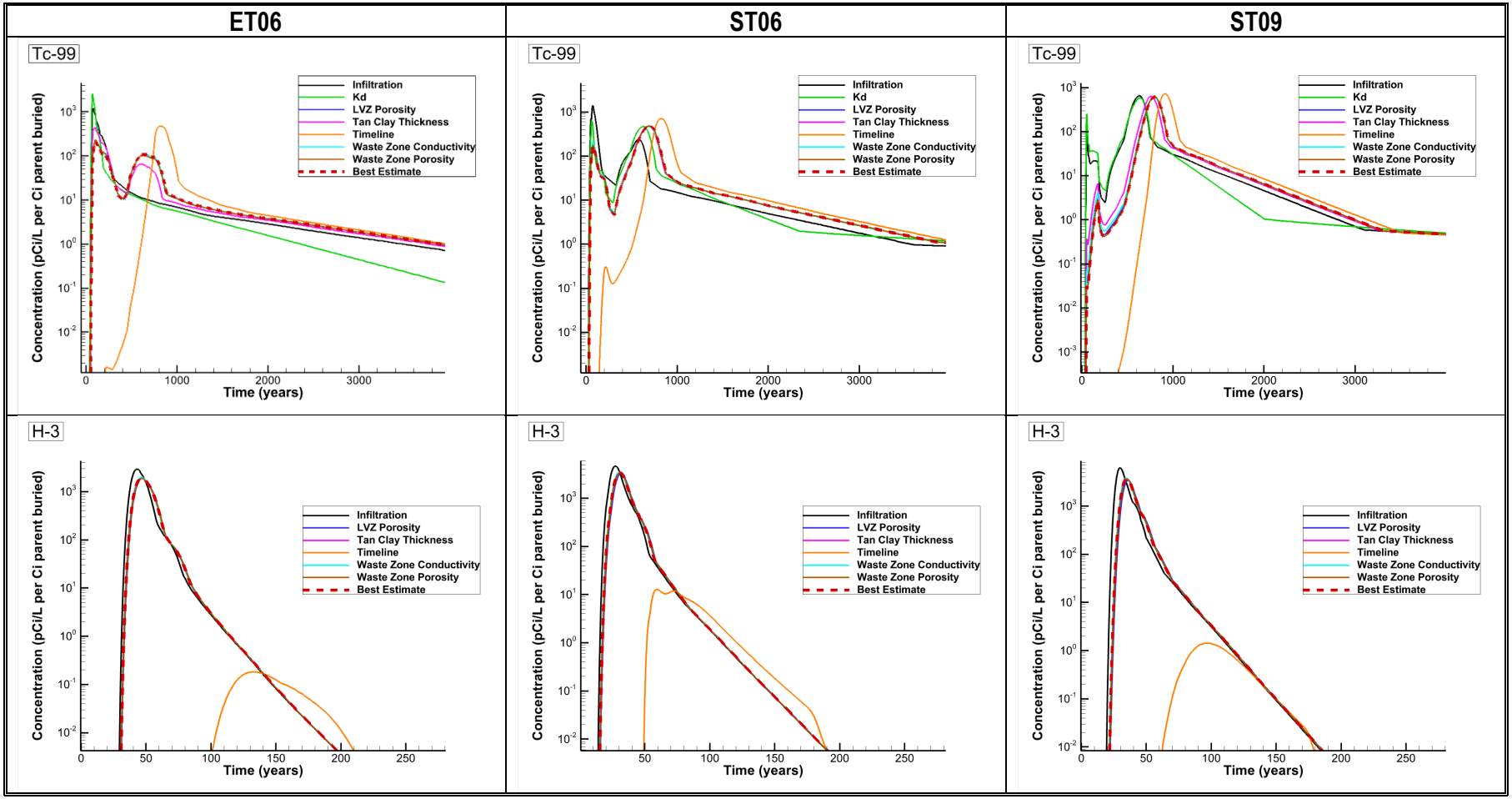

Figure 5-55. Tc-99 and H-3 Concentration Profiles at 100-meter POA for ET06, ST06, and ST09 Comparing the Best Estimate (Nominal PA) and Sensitivity Cases

5.1.4. Aquifer Zone Model for Special Waste Forms

This section presents aquifer model results for simple and complex SWFs in slit and engineered trenches. Section 5.1.4.1 addresses CIG trench segments, while Section 5.1.4.2 presents results for all other simple and complex SWFs.

5.1.4.1. Components-in-Grout Trench Segments

The fate and transport of radionuclide species emanating from CIG-1 through CIG-9 within the aquifer is governed by the CIG trench segment's location. The location determines the infiltration rate (i.e., for subsidence cases), modeling timeline, and material properties (e.g., reinforced concrete mat versus no reinforced concrete mat, cementitious aging times, etc.). Figure 5-56 through Figure 5-58 display a 2-D projection of the maximum concentration within the Tc-99 plume emanating from each CIG trench segment. Note that CIG-1 through CIG-8 opened within a 4-year time window spanning August 29, 2000, through August 18, 2004, yet all segments were fitted with their operational cover on the same date (April 1, 2006). As a result, CIG-1 went six years while CIG-8 went only two years without a cover. The impact of cover placement timing is highlighted in the concentration profile at Year 731 for CIG-1 (Figure 5-56; right-hand plot) where two distinct high-concentration regions (orange in color) are evident. The larger, high-concentration region closest to the 100-meter POA (black zig-zag line to upper right) is a remnant of Tc-99 release during the no-cover period, whereas the smaller, high-concentration region near the CIG-1 footprint represents the remaining inventory after the operational cover is placed. Furthermore, the concentration at the 100-meter POA in Year 71 is lower for each subsequent CIG trench segment due to its progressively later opening date (Note that the concentration scale changes from CIG-1 through CIG-7 to CIG-8 to CIG-9 to account for the lower concentrations emanating from CIG-8 and CIG-9.)

The peak concentration time profiles are presented in Figure 5-59 and Figure 5-60 with both log-linear and linear-linear scaling. The log-linear scaling highlights differences in concentration at the 100-meter POA at earlier times for more mobile radionuclides (H-3, I-129, Tc-99) whose K_d values remain the same (H-3), slightly increase (I-129), or decrease (Tc-99) in the cementitious environment. In comparison, K_d values for the three other radionuclides (C-14, Np-237, Sr-90) increase (in many cases by several orders of magnitude) during the early period, thereby resulting in less meaningful (i.e., the absolute value is many orders of magnitude below the peak) differences in concentration early in time. With a linear-linear scale, however, their peak concentrations are more clearly shown and demonstrate that, in most cases, the higher peaks are for CIG trench segments located nearer to the 100-meter POA. The peak concentration of H-3 essentially follows the sequential opening of the CIG trench segments.

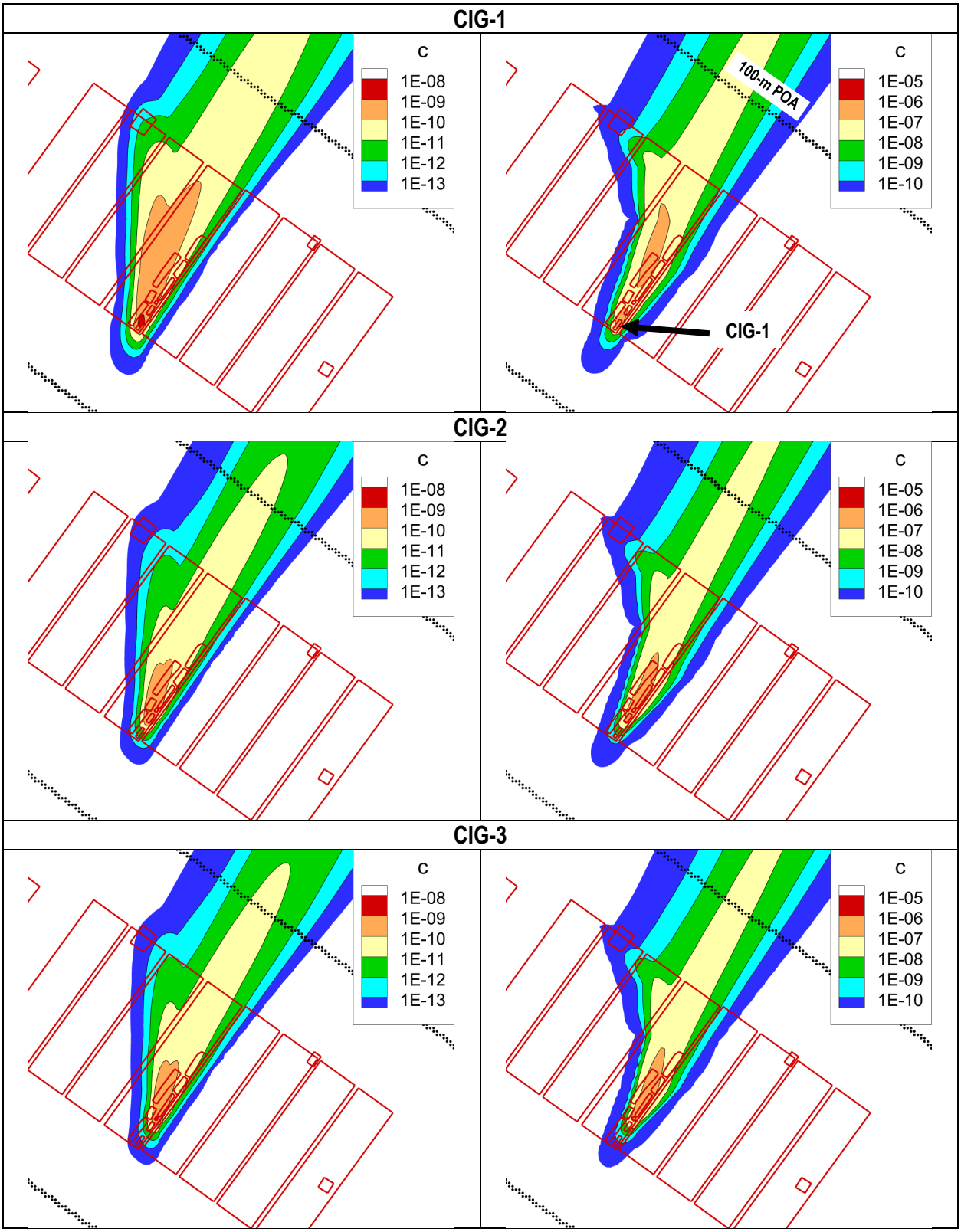

Figure 5-56. 2-D Projection of the Maximum Tc-99 Concentration (gmol ft^{-3} per gmole parent buried) Emanating from CIG-1 through CIG-3 for the Intact Case at Year 71 (left) and Year 731 (right)

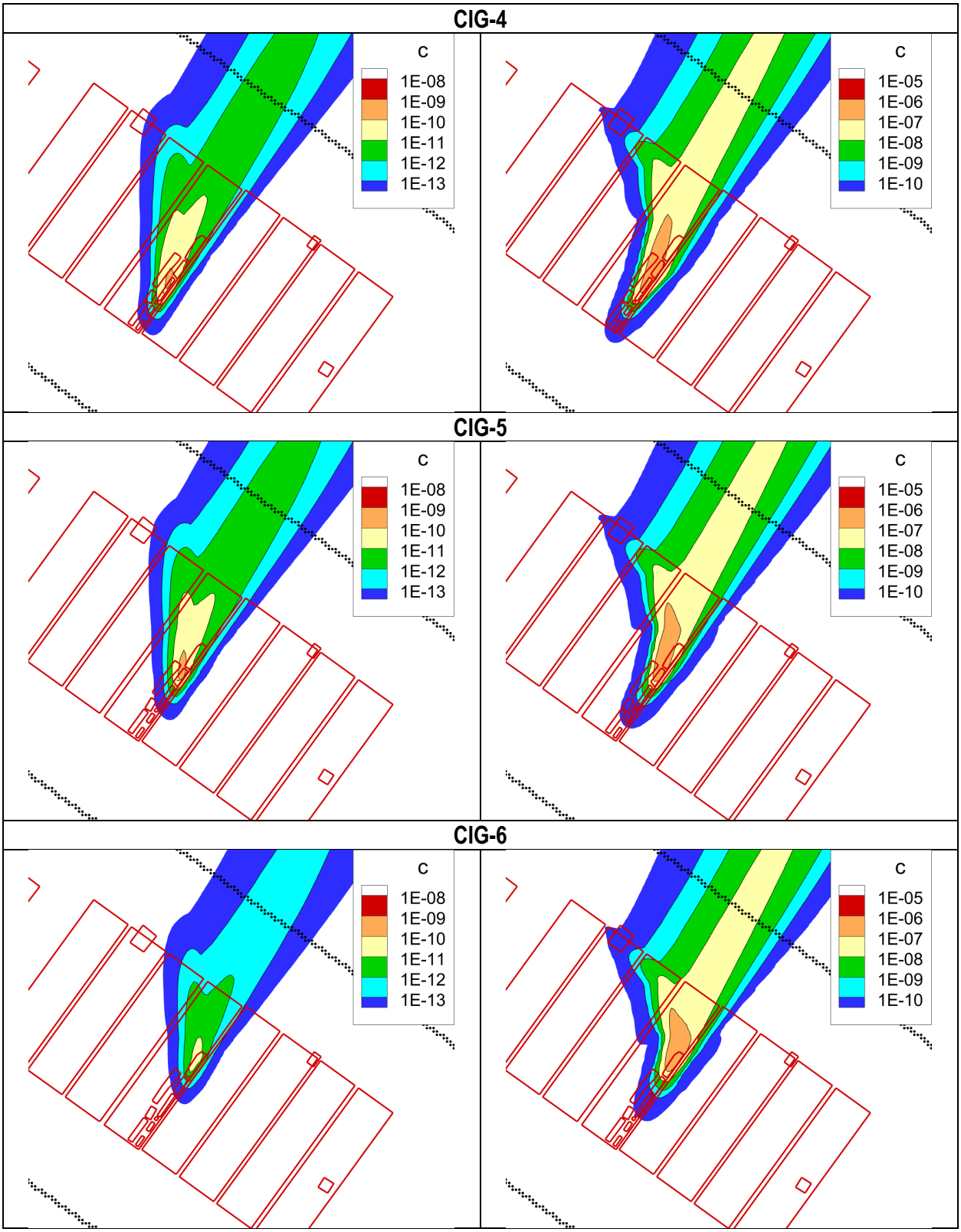

Figure 5-57. 2-D Projection of the Maximum Tc-99 Concentration (gmol ft^{-3} per gmole parent buried) Emanating from CIG-4 through CIG-6 for the Intact Case at Year 71 (left) and Year 731 (right)

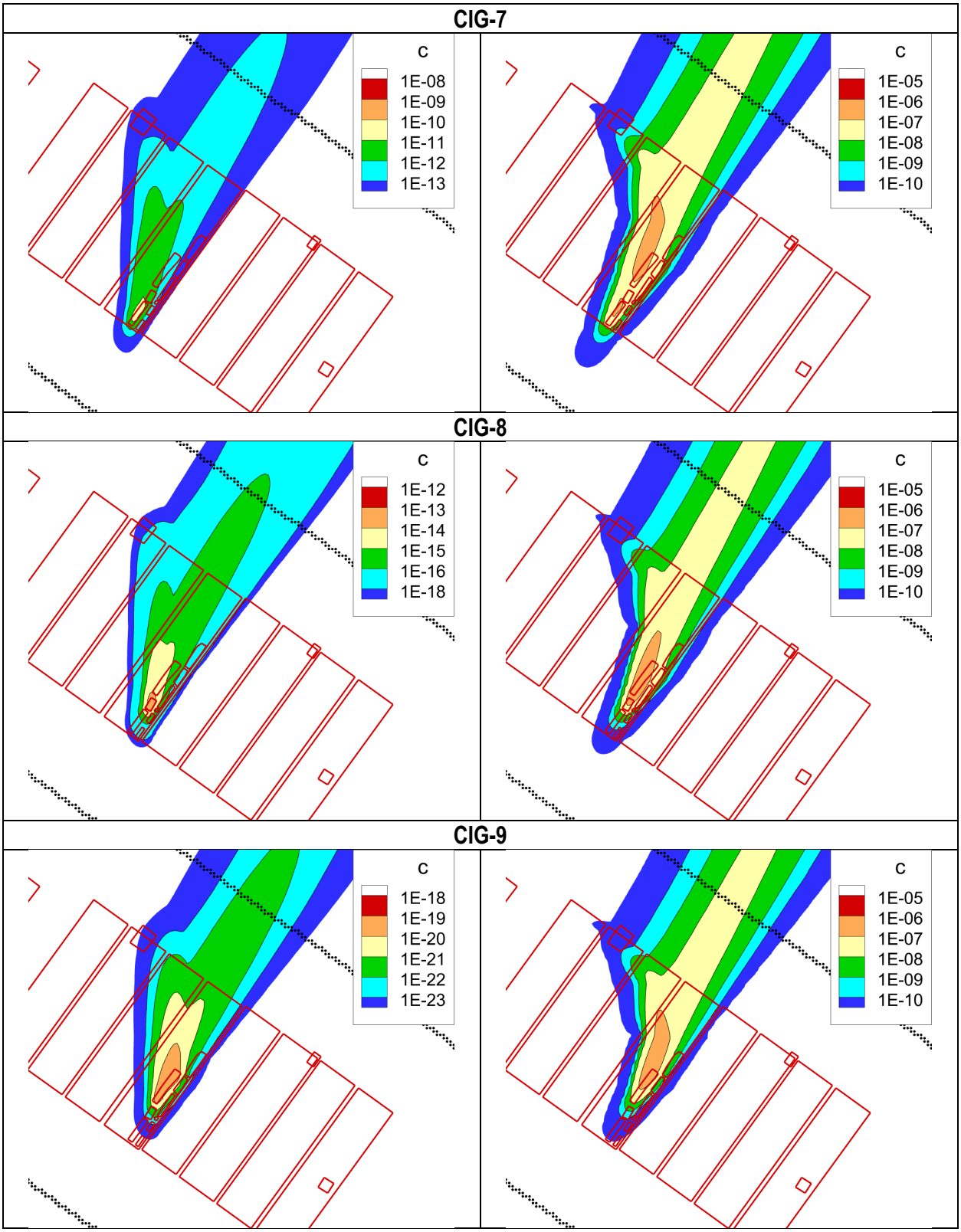

Figure 5-58. 2-D Projection of the Maximum Tc-99 Concentration (gmol ft^{-3} per gmole parent buried) Emanating from CIG-7 through CIG-9 for the Intact Case at Year 71 (left) and Year 731 (right)

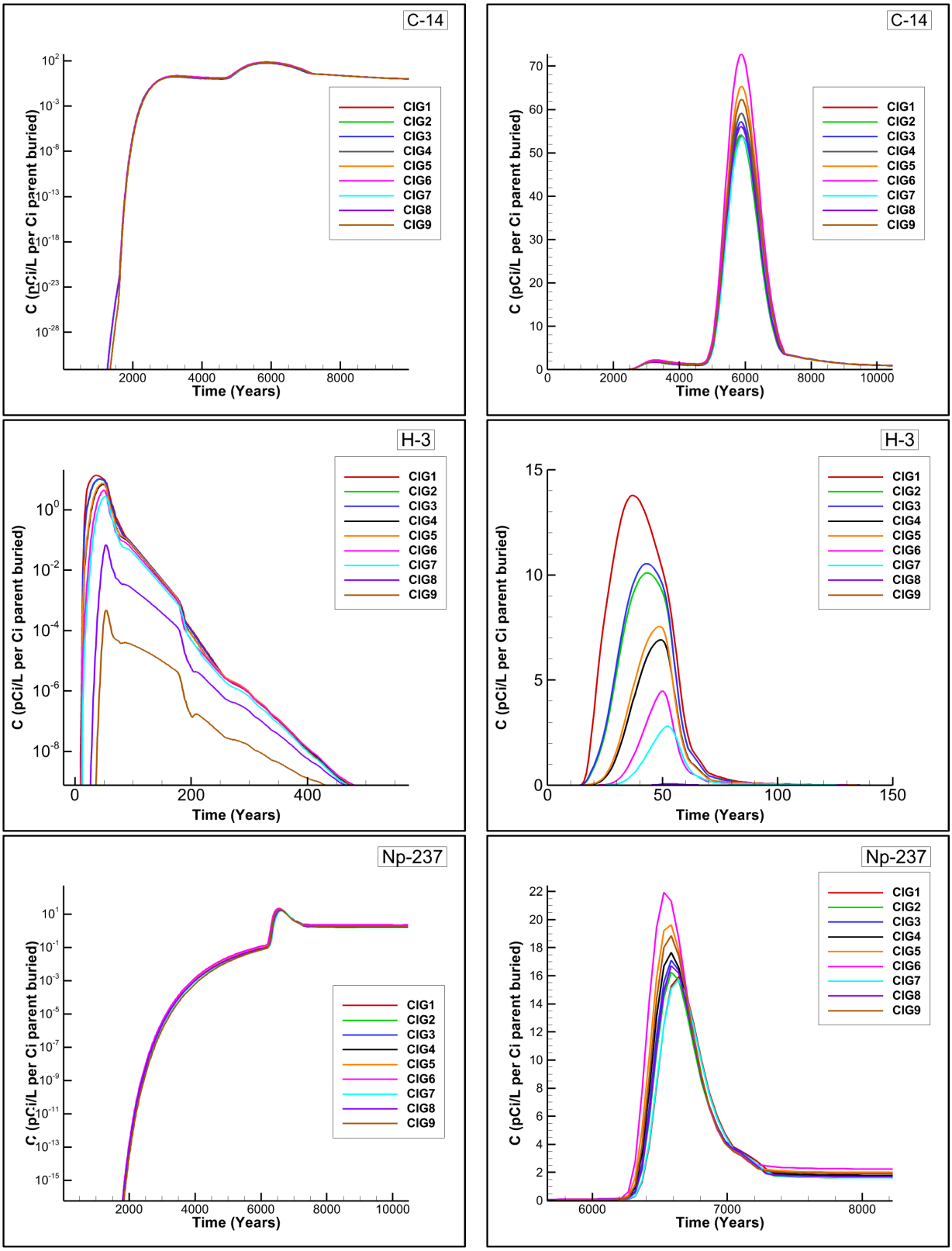

Figure 5-59. C-14, H-3, and Np-237 Concentration Profiles for CIG-1 through CIG-9 with Log-Linear (left) and Linear-Linear (right) Scales

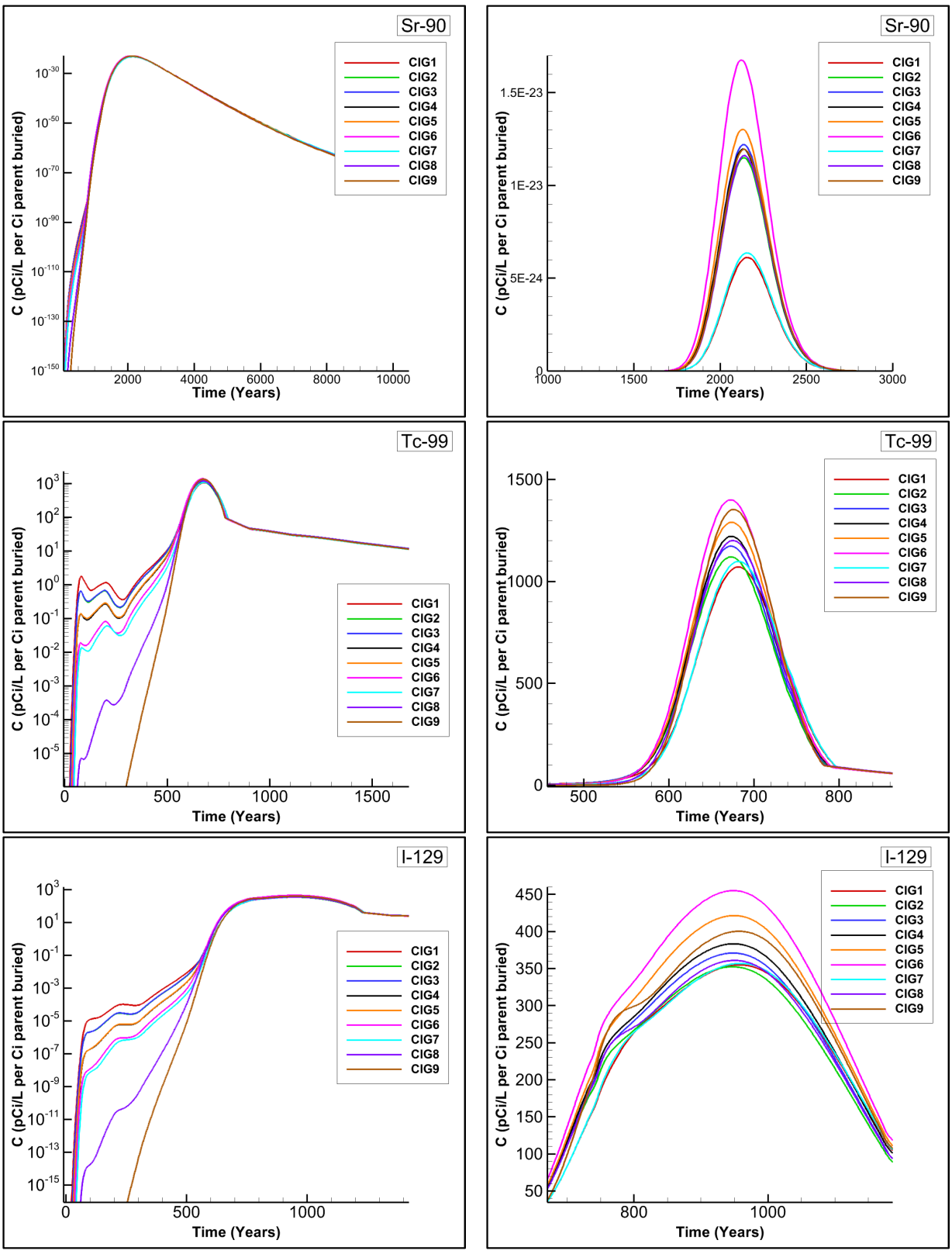

Figure 5-60. Sr-90, Tc-99, and I-129 Concentration Profiles for CIG-1 through CIG-9 with Log-Linear (left) and Linear-Linear (right) Scales

Two subsidence cases are modeled at the VZ level: (1) subsidence occurring at the end of IC when no reinforced concrete mat is present; (2) subsidence occurring 200 years after the end of IC when a reinforced concrete mat is present. These two different boundary conditions alter both infiltration rates and cementitious chemical aging times. The impact of a reinforced concrete mat placed over CIG-4 through CIG-7 during the uncovered periods is displayed for H-3 in Figure 5-61, where the concentration at the 100-meter POA is several orders of magnitude lower with a reinforced mat installed. The effect of delaying subsidence by 200 years is clearly evidenced by a shift along the temporal axis and, for shorter-lived radionuclides, a notable decrease in the peak concentration at the 100-meter POA. Subsidence infiltration rates for each CIG trench segment (Table 4-26) are calculated based on the segment's position relative to the crest of the final closure cap (Table 4-27). Consequently, CIG trench segments with higher infiltration rates (e.g., CIG-5 and CIG-6) age faster and release radionuclides at a higher rate. This leads to both earlier and higher peak concentrations as seen for CIG-6 and CIG-5 in Figure 5-61, which have the two highest infiltration rates (followed in decreasing order by CIG-4, CIG-9, CIG-8, and CIG-7).

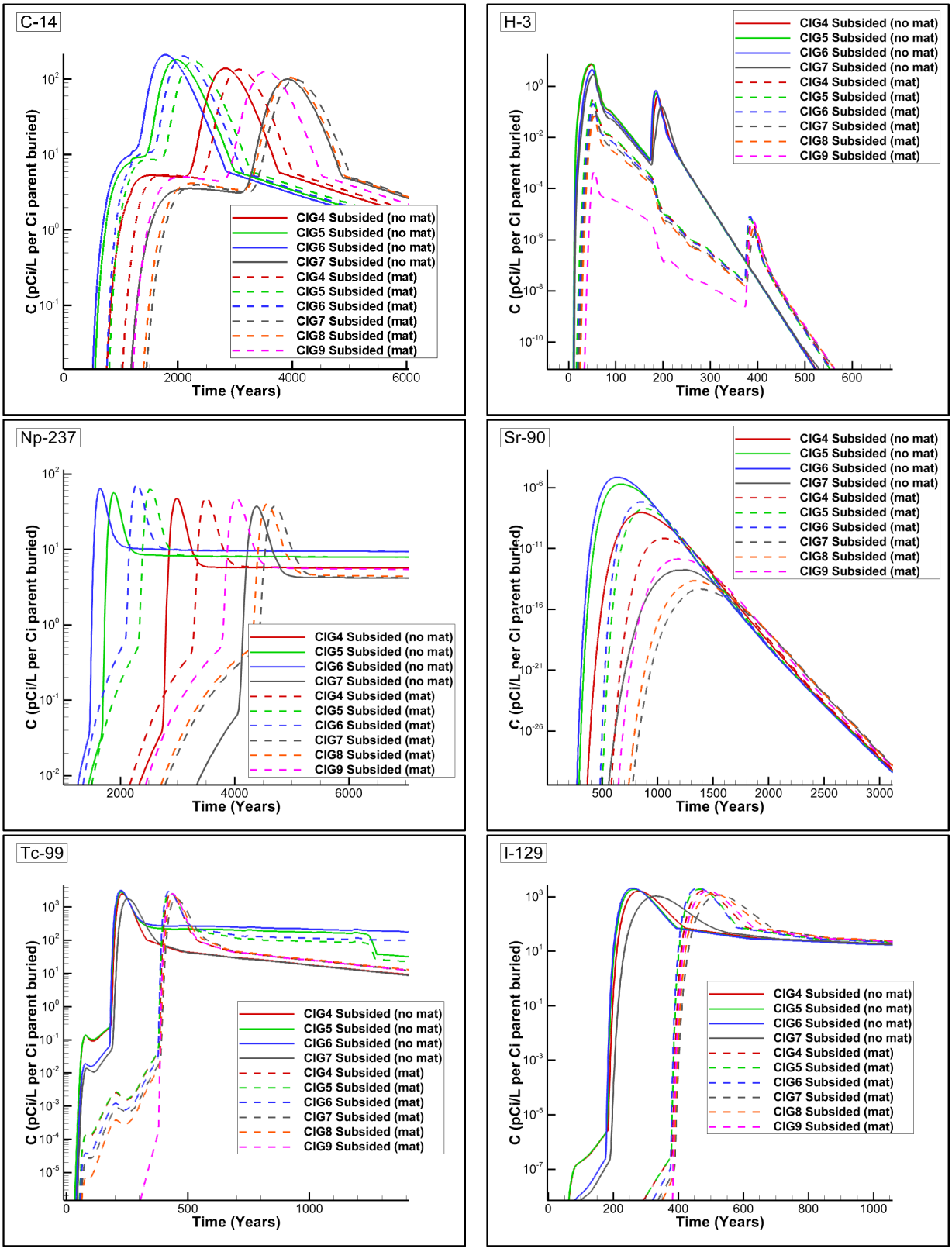

Figure 5-61. Concentration Profiles for CIG-4 through CIG-9 Subsidence Cases

5.1.4.2. All Other Simple and Complex Special Waste Forms

The flux-to-the-water-table profiles for radionuclides present in each simple and complex SWF (Figure 5-23) are applied as source terms at the water table to model contaminant transport through the aquifer and to obtain concentrations at the 100-m POA. For each SWF where a known disposal location exists, the corresponding nodes within the DU footprint are selected as the source nodes. In some cases (e.g., HWCTR, ETF Carbon Columns, and Mk50A targets), no additional generic waste is placed within the footprint of the SWF. K_d values for the sandy and clayey aquifer materials are set as the nominal PA K_d values in the simulations (as opposed to K_d values listed in Figure 5-23 which apply to the waste zone only).

Figure 5-62 displays the concentration profile for all SWFs containing I-129 in ET01 compared to the generic waste form. As discussed in Section 5.1.2.3, the SWF implementation (e.g., effective K_d, delayed release, or solubility-controlled release) slows radionuclide transport from the waste zone, which results in a decreased and/or delayed concentration peak when compared to generic waste. Consequently, the concentration profiles for the aquifer reveal the same trends as the flux-to-the-water-table profiles for the VZ where the higher the waste zone K_d, the lower the peak concentration (with the peak for generic waste being the highest). The same is true for the other SWF release mechanisms.

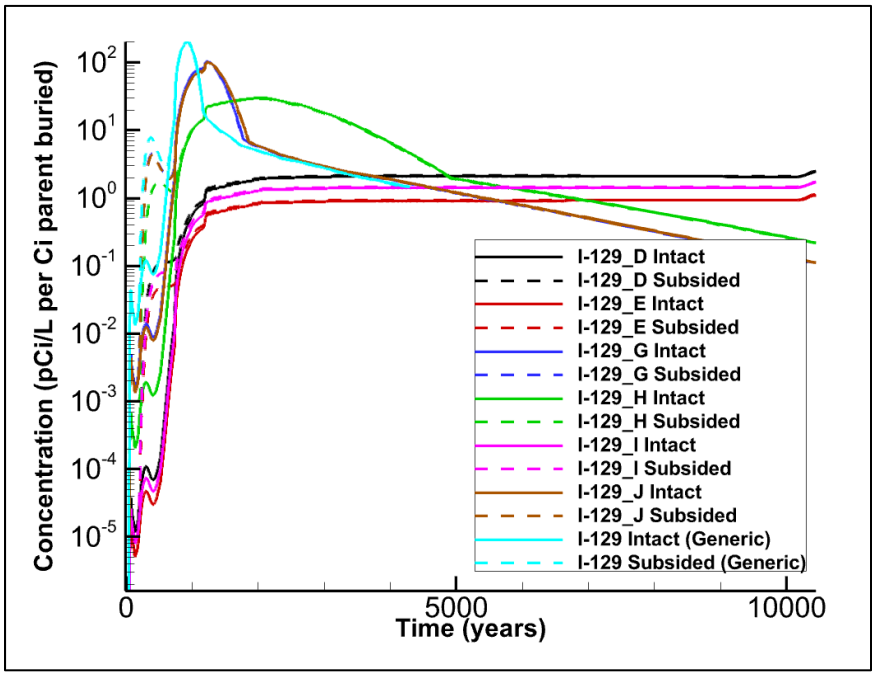

Note: Refer to Figure 5-23 for a definition of SWF radionuclides.

Figure 5-62. Intact and Subsidence Concentration Profiles for All ET01 Special Waste Forms Containing I-129 Compared to the Generic Waste Form

Two complex SWFs employ source terms from the VZ models created for prior ELLWF SAs and UDQEs as listed in Table 5-7 (Danielson, 2021): HWCTR and HXs. The complex SWF for H-3F in 232-F concrete rubble employs the generic waste form inventory limits for H-3, which are

bounding because no credit is taken for the lower release rates due to diffusion through the concrete.

Table 5-7. Summary of Source Terms for Complex Special Waste Forms

Waste Form	Radionuclides[1]	Comments
HWCTR	Ag-108mH C-14H Ni-59H Ni-63H Tc-99H	Case 1: Sources obtained from 16-foot-wide model by Hamm and Smith (2010; Section 4.3) Case 2: Sources obtained from 20-foot-wide model by Hamm and Smith (2010; Section 4.4)
Reactor Process HXs	H-3X C-14X	Case 1: Sources obtained by extracting the maximum flux to the water table through time across all cases as reported by Hamm et al. (2012; Section 3.3.4)
232-F	H-3F	Generic H-3 inventory limits employed to bound behavior.

Notes:

[1] Refer to Figure 5-23 for a definition of SWF radionuclides.

Appendix D contains supplemental concentration profiles of SWF radionuclides that contribute to at least 0.1% of the sum-of-fractions.

5.1.5. Air Pathway and Radon Flux Analyses

This section presents the air pathway and radon flux modeling results for STs, ETs, and CIG trench segments. Pertinent information regarding specific material zones, thicknesses, and properties for the ARM of STs and ETs is presented in Table 5-8; layer and material properties for the ARM of CIG trench segments are provided in Table 5-9. In both cases, waste is assumed to be equally distributed throughout the waste zone. Additional configuration information is provided below.

Table 5-8. Layer and Material Properties for Atmospheric Release Model of Slit and Engineered Trenches

Layer	Thickness (ft)	Number of Cells	Bulk Dry Density (g cm^{-3})	Porosity	Residual Water Saturation
Before Closure (Year 71 to Year 171)					
Clean Fill	4	10	1.44[a]	0.4561[a]	0.6718[b]
Waste Zone	16	20	0.82[c]	0.69[c]	0.00001[d]
After Closure (Year 171 to Year 1,171)					
Closure Cap	per Section 3.6.1.9				
Clean Fill	4	10	1.44[a]	0.4561[a]	0.6718[b]
Compaction Fill	13.5	10	1.44[a]	0.4561[a]	0.6718[b]
Waste Zone (compacted)	2.5	20	1.89[c]	0.29[c]	0.70[d]

Notes:

[a] From Nichols (2020)

[b] From Phifer et al. (2006)

[c] Weighted average of STs and ETs (by number of units) from material properties database.

[d] Waste is assumed to be lowest saturation value of trench for GW pathway analysis.

Table 5-9. Layer and Material Properties for Atmospheric Release Model of Components-in-Grout Trench Segments

Layer	Thickness (ft)	Number of Cells	Bulk Dry Density (g cm^{-3})	Porosity	Residual Water Saturation
Before Closure (Year 0 to Year 100)					
Clean Fill	4	10	1.44[a]	0.4561[a]	0.6718[b]
CIG Vault Top	1	1	1.441[c]	0.456[a]	0.00001[d]
Waste Zone	14	20	1.441[c]	0.456[a]	0.00001[d]
After Closure (Year 100 to Year 300)					
Closure Cap	per Section 3.6.1.9				
Clean Fill	4	10	1.44[a]	0.4561[a]	0.6718[b]
CIG Vault Top	1	1	1.441[c]	0.456[a]	0.00001[d]
Waste Zone	14	20	1.441[c]	0.456[a]	0.00001[d]
After Collapse (Year 300 to Year 1,100)					
Closure Cap (sandy soil)	per Section 3.6.1.9		1.44[a]	0.4561[a]	0.6718[b]
Clean Fill	4	10	1.44[a]	0.4561[a]	0.6718[b]
CIG Vault Top	1	1	1.44[a]	0.4561[a]	0.6718[b]
Waste Zone	7	20	1.44[a]	0.4561[a]	0.6718[b]

Notes:

[a] From Nichols (2020)

[b] From Phifer et al. (2006)

[c] Calculated from the particle density of CIG concrete from (Nichols, 2020).

[d] From Phifer et al. (2006) Table 7-1 "half filled with an air space;" therefore, the air content equals the porosity.

5.1.5.1. Slit and Engineered Trenches

The configuration of the ARM for a trench representing generic waste forms in STs and ETs consists of a 1-D vertical stack from the base of the waste zone to either the top of clean fill before closure at Year 171 or the top of the erosion barrier of the closure cap after Year 171. For the first 100 years (before closure), the top of the waste zone links to the clean fill layer and the top of the clean fill layer links to the atmosphere. Following closure at Year 171, the clean fill and waste zone layers are compacted. The compaction is represented by the consolidation of the contamination within the clean fill layer and the waste zone into a reduced size waste zone. The top of this waste zone links to a layer of clean compaction fill and a new layer of clean fill, which is linked to the closure cap.

5.1.5.2. Components-in-Grout Trench Segments

The configuration of the ARM of CIG trench segments consists of a 1-D vertical stack of cells from the base of the waste zone to a vault top constituting of clean CIG grout and a layer of clean fill. The top of the clean fill is considered the ground surface before closure. Following closure at Year 171, the clean fill is linked to the bottom of the closure cap (Section 3.6.1.9) and the top of the erosion barrier is considered the ground surface. In the ARM, CIG grout collapse and cap and waste degradation is implemented 300 years (Year 371) after the end of operations (200 years following cap application). At Year 371, the grout structure encapsulating the waste collapses, resulting in the settlement of the waste zone and destruction of the closure cap structure. The waste layer collapses from 14-foot to 7-foot thick at Year 300 per Phifer et al. (2006). This reduction in

waste layer thickness is achieved by conservatively reassigning the radionuclide inventory of the lower 7 feet of the waste zone to the upper 7 feet of the waste zone. Waste and grout material properties are changed at collapse to those for sandy soil. Due to the collapse, the closure cap structure is also destroyed. Therefore, the hydraulic properties of all closure cap layers convert to those of the sandy soil (Phifer et al., 2006).

5.1.5.3. Air Pathway

Surface flux time histories of screened-in air pathway radionuclides (C-14 and H-3; Section 2.3.8) generated by the ARMs of STs and ETs and CIG trench segments are converted to dose by multiplying by the DRFs of the corresponding time period (Section 3.6.2.2.5). The time histories of these doses are used to determine the grouping (immediate, delayed, or non-factor) of the radionuclide-DU pairs to account for temporal differences in dose impact (Section 8.5). The peak dose and grouping-specific effective PO are used to develop a disposal limit for each radionuclide (Section 8.5). Dose results for STs, ETs, and CIG trench segments are presented below.

5.1.5.3.1. Slit and Engineered Trenches

Surface flux and the resultant dose from 1 Ci of C-14 buried in STs and ETs have the greatest impact on the receptor following application of the final closure cap, while H-3 peaks before the end of IC (Figure 5-63 and Table 5-10). Doses from C-14 peak after the end of IC (Year 171) when the POA shifts from the site boundary to the 100-meter POA. This shift results in larger DRFs and, subsequently, higher doses. H-3, on the other hand, becomes trapped under the final closure cap after Year 171 before decaying and, therefore, is unaffected by the shift in the POA. Note that truncation of the H-3 curve in Year 171 is an artifact of the GoldSim® model, wherein the H-3 dose drops below the model quantification limit of 1.0E-26 mrem yr^{-1} when the final closure cap is installed.

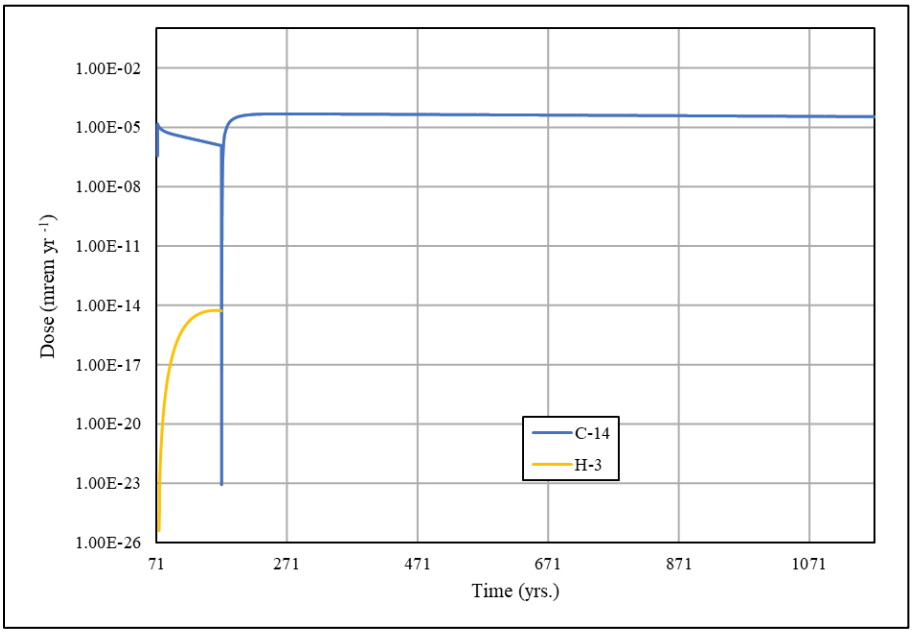

Figure 5-63. Air Pathway Dose Time Histories for 1 Curie of C-14 and H-3 Buried in Slit and Engineered Trenches

Table 5-10. Peak Doses from 1 Curie of C-14 and H-3 Buried for the Slit and Engineered Trench Air Pathway

Radionuclide	Peak Dose (mrem yr^{-1} Ci^{-1} parent buried)	Peak Time (Year)
C-14	4.79E-05	266
H-3	5.50E-15	162

5.1.5.3.2. Components-in-Grout Trench Segments

The surface flux and the resultant atmospheric dose of C-14 buried in CIG trench segments have the largest impact at Year 371 (Table 5-11 and Figure 5-64), primarily due to a spike in dose during collapse. Time histories of each radionuclide emanating from CIG trench segments are complex because of the presence and collapse of CIG concrete. The dose caused by H-3 peaks before Year 171 and then decays within the concrete matrix and closure cap. C-14 displays a large spike in dose at Year 371 as the contamination trapped within the CIG concrete and final closure cap sitting above the waste zone is released during cover collapse.

Table 5-11. Peak Doses from 1 Curie of C-14 and H-3 Buried for the Components-in-Grout Trench Segment Air Pathway

Radionuclide	Peak Dose (mrem yr^{-1} Ci^{-1} parent buried)	Peak Time (Year)
C-14	8.58E-08	371.04
H-3	4.82E-15	168.84

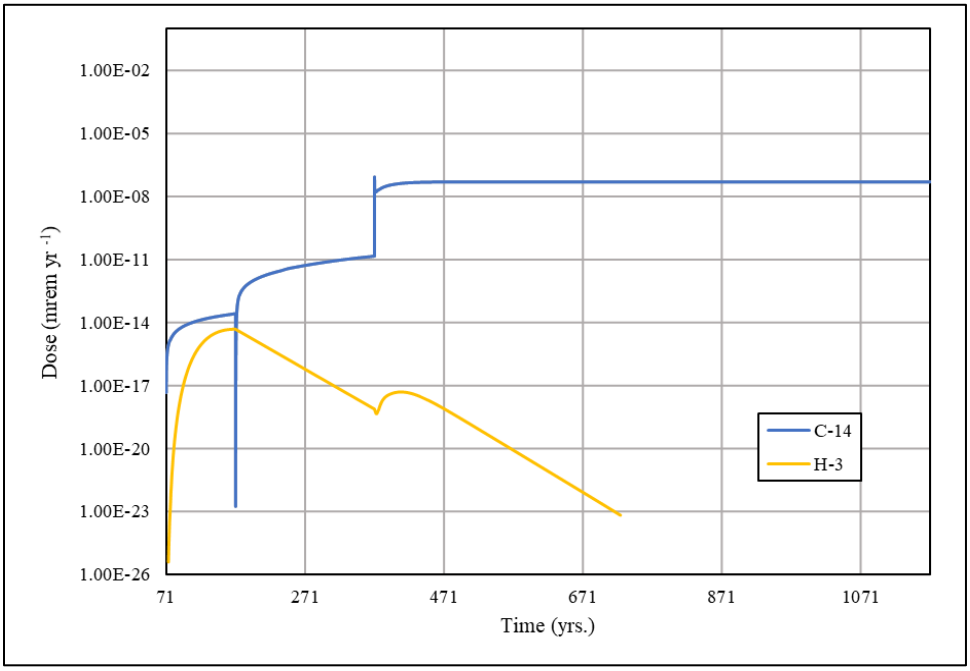

Figure 5-64. Air Pathway Dose Time Histories for 1 Curie of C-14 and H-3 Buried in Components-in-Grout Trench Segment

5.1.5.4. Radon Pathway

Surface-flux time histories are generated for Rn-222 from each of its 20 parent radionuclides for STs, ETs, and CIG trench segments. Peak flux on a 1-m^2 unit area basis is used for radon pathway screening. Example Rn-222 time histories are provided for the parents Ra-226, Th-230, and U-234. These three parents generate the largest flux of Rn-222 at the surface. Ra-226 is a required limit for most DUs based on screening performed in Section 2.3.8. U-234 and Th-230 are two other parent radionuclides requiring disposal limits or trigger values in any DU. U-234 represents the convergence point of all decay chains that generate Rn-222.

5.1.5.4.1. Slit and Engineered Trenches

Rn-222 flux time history characteristics for STs and ETs are largely the same for each of the parent radionuclides investigated (Figure 5-65). Rn-222 flux increases until, and peaks immediately before, the placement of the final closure cap in Year 171. After closure, Rn-222 diffuses through the cap, further degrading Rn-222 and decreasing flux. The relative difference in the magnitude of Rn-222 flux produced from parent radionuclides arises from a combination of parent radionuclide specific activity and the time until Rn-222 production occurs down the decay chain. Unsurprisingly, Ra-226 (the direct parent of Rn-222) provides the highest Rn-222 flux, followed by its parent Th-230. Short-lived parents produce the lowest Rn-222 fluxes at the surface. The high specific activity of theses radionuclides results in disequilibrium of the parents and progeny where secular or transient equilibrium is not reached. Rn-222 buried in the unit does not result in Rn-222 flux at the surface because it decays before the end of operations. Rn-222 peak fluxes from each parent are provided in Table 5-12. These fluxes are used for radionuclide screening in Section 2.3.8 and to determine disposal limits in Section 8.6. Radionuclides that are screened in and require further analysis and limits determination are denoted in Table 5-12 by “Limit” in the last column.

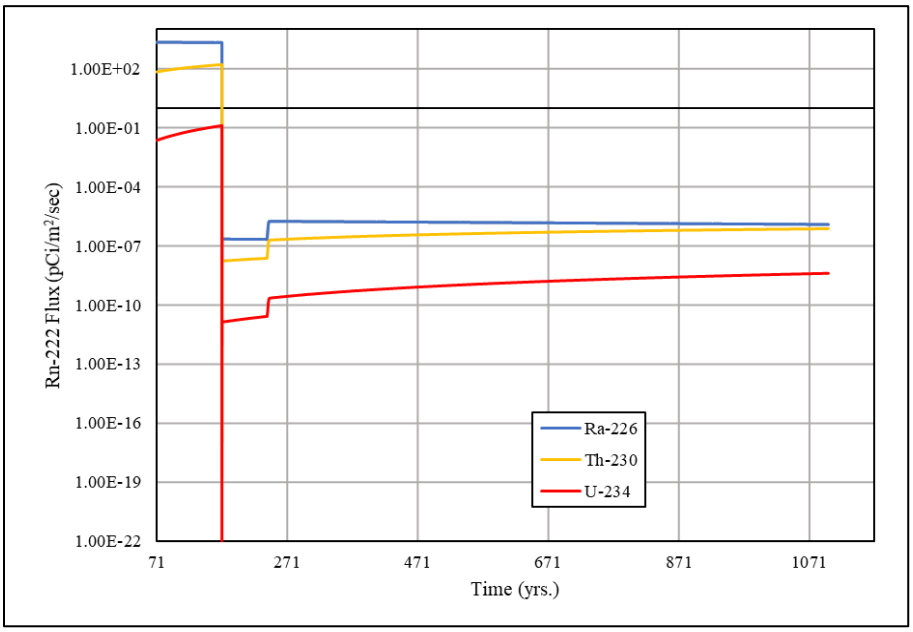

Figure 5-65. Rn-222 Flux Time Histories for 1 Curie of Ra-226, Th-230, and U-234 Buried in Slit and Engineered Trenches

Table 5-12. Peak Rn-222 Flux from 1 Curie of Rn-222 Parent Radionuclides and Rn-222 Buried for the Slit and Engineered Trench Radon Pathway

Radionuclide	Peak Rn-222 Flux (pCi $m^{-2}s^{-1}$)	Peak Time (Year)	Limit or Trigger Required? [a]
Am-242	2.61E-10	170.99	--
Am-242m	3.82E-06	170.99	--
Am-246m	0.00E+00	--	--
Bk-250	6.34E-11	170.99	--
Cf-250	1.52E-20	170.99	--
Cm-242	7.71E-08	170.99	--
Cm-246	8.81E-18	170.99	--
Cm-250	1.52E-20	170.99	--
Np-238	1.01E-09	170.99	--
Pa-234	4.00E-10	170.99	--
Pa-234m	1.16E-12	170.99	--
Pu-238	1.53E-05	170.99	--
Pu-242	1.39E-13	170.99	--
Pu-246	0.00E+00	--	--
Ra-226	2.19E+03	72	Limit
Rn-222	0.00E+00	--	--
Th-230	1.61E+02	170.99	Limit
Th-234	3.45E-08	170.99	--
U-234	1.28E-01	170.99	Limit
U-238	2.08E-05	170.99	--

Notes:

[a] Based on radionuclide screening in Section 2.3.8.

5.1.5.4.2. Components-in-Grout Trench Segments

Rn-222 flux time history characteristics for the CIG trench segments are also largely the same for each parent radionuclides investigated (Figure 5-66). Rn-222 flux increases until the placement of the final closure cap at Year 171. After final closure cap placement, Rn-222 diffuses through the cap, allowing for further Rn-222 degradation before it reaches the surface. Once the CIG grout collapses and cap and waste degradation occur, Rn-222 flux increases with the quicker transport to the surface. Fluxes continue to increase as parent radionuclides slowly decay. The relative difference in the magnitude of Rn-222 flux produced by parent radionuclides arises from a combination of parent radionuclide specific activity and time until Rn-222 production occurs down the decay chain. Ra-226, the direct parent of Rn-222, provides the highest Rn-222 flux, followed by its parent Th-230. Rn-222 buried in the unit does not result in Rn-222 flux at the surface as it decays before the end of operations. Rn-222 peak fluxes from each parent are provided in Table 5-13. These fluxes are used for radionuclide screening in Section 2.3.8 and to determine disposal limits in Section 8.6. Radionuclides that are screened in and require further analysis and limits determination are denoted in Table 5-13 by “Limit” in the last column.

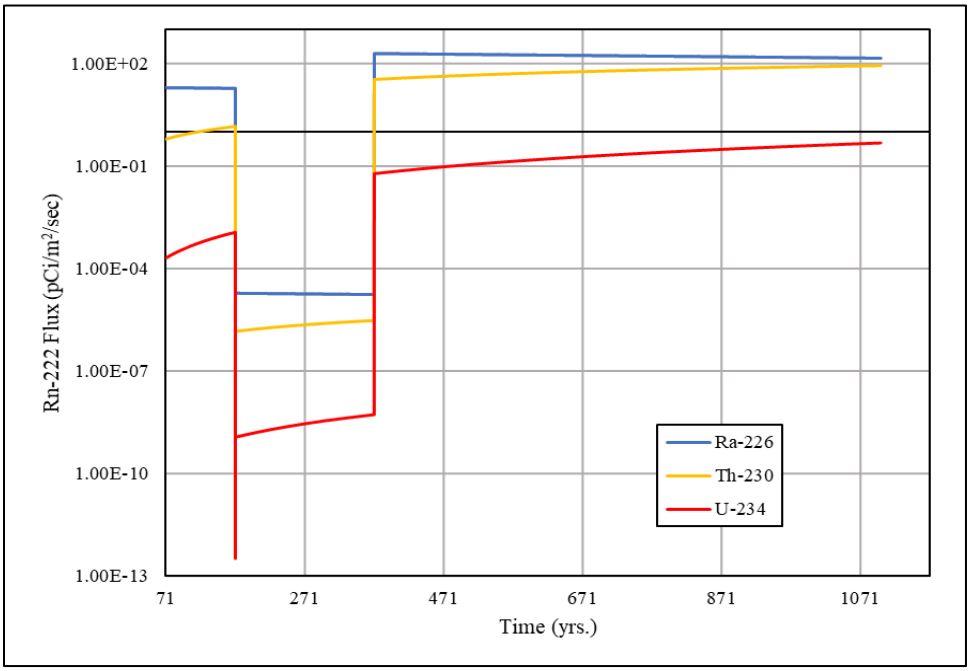

Figure 5-66. Rn-222 Flux Time Histories for 1 Curie of Ra-226, Th-230, and U-234 Buried in a Components-in-Grout Trench Segment

Table 5-13. Peak Rn-222 Flux from 1 Curie of Rn-222 Parent Radionuclides and Rn-222 Buried for Components-in-Grout Trench Segment Radon Pathway

Radionuclide	Peak Rn-222 Flux (pCi $m^{-2}s^{-1}$)	Peak Time (Year)	Limit or Trigger Required? [a]
Am-242	2.69E-09	1,171	--
Am-242m	1.46E-04	1,171	--
Am-246m	0.00E+00	--	--
Bk-250	6.53E-10	1,171	--
Cf-250	3.11E-17	1,171	--
Cm-242	7.94E-07	1,171	--
Cm-246	1.22E-14	1,171	--
Cm-250	3.11E-17	1,171	--
Np-238	1.03E-08	1,171	--
Pa-234	1.67E-09	1,171	--
Pa-234m	4.85E-12	1,171	--
Pu-238	1.56E-04	1,171	--
Pu-242	2.85E-11	1,171	--
Pu-246	7.61E-20	1,171	--
Ra-226	1.97E+02	371.21	--
Rn-222	0.00E+00	--	--
Th-230	9.18E+01	1,171	--
Th-234	1.44E-07	1,171	--
U-234	5.35E-01	1,171	Limit
U-238	6.14E-04	1,171	--

Notes:

[a] Based on radionuclide screening in Section 2.3.8.

5.2. LOW-ACTIVITY WASTE VAULT

5.2.1. Vadose Zone Model

Section 4.5.3 summarizes the PORFLOW implementation of the LAWV VZ flow and transport conceptual models for the purpose of evaluating dose impacts and producing disposal limits for the ELLWF. The VZ model is limited to a 2-D treatment because of the complexity of modeling the entire vault structure. A cross-sectional area is modeled along the short axes of the structure (i.e., a lateral slice through a typical waste storage cell is modeled including exterior walls exposed to water infiltration but neglecting the interface between adjacent cells). This section presents selected flow and radionuclide contaminant transport results of the PORFLOW VZ LAWV model. A more comprehensive set of transport model results is provided in Appendix E.

Modeling the VZ includes simulating infiltration flow above and around the LAWV to the top of the water table and radionuclide transport from the waste disposal region within the vault to the aquifer. The flux of radionuclides to the water table is calculated as gmoles of radionuclide entering the water table per year per 1.0 gmole of parent isotope deposited in the waste zone. The fluxes are used as a boundary condition in a separate PORFLOW transport model through the aquifer zone to calculate radionuclide concentrations at the 100-meter POA. Based on the results of the tiered radionuclide screening process implemented by Aleman and Hamm (2021) and summarized in Section 2.3.7, 19 generic radionuclides are selected for LAWV VZ modeling because they have a significant impact on dose after removing trigger-value radionuclides (Table 5-14).

Table 5-14. Generic Parent Radionuclides for Low-Activity Waste Vault Vadose Zone and Aquifer Zone Modeling

Radionuclides			
Ag-108m	Cm-245	Ni-59	Ra-226
Am-241	Cs-137	Ni-63	Sr-90
C-14	H-3	Np-237	Tc-99
Ca-41	I-129	Pu-239	U-235
Cl-36	K-40	Pu-241	--

PORFLOW modeling of the LAWV VZ includes the case studies listed in Table 5-15. In addition to the nominal (base case) model settings used for PA calculations, a best estimate case, and eight sensitivity cases were run. The best estimate case differs from the nominal PA case primarily in that it assumes LAWV concrete will maintain its integrity twice as long as the 500-year limit suggested by the PAWG in NUREG-1573 (U.S. NRC, 2000). The best estimate case also assumes a more tightly packed waste zone with a porosity of only one-third of the nominal PA case. (Because the actual porosity of LAWV waste cannot be accurately characterized, the nominal PA case assumes a conservative value. The waste porosity used in the best estimate case is that of clayey soil.) Sensitivity cases are all one-sided calculations designed to investigate model response to changes in what are deemed to be modeling parameters having the most significant impact on radionuclide transport. The eight sensitivity cases assess the individual effect of each variation and, therefore, perturb each of the eight parameters or parameter sets individually. Five of the eight sensitivity cases (1, 2, 4, 5, and 6) alter parameters that affect the water flow distribution, requiring

five separate PORFLOW flow calculations. The other three cases (3, 7, and 8) change transport parameters only; therefore, the nominal PA case water flow distribution still applies. As an example, Sensitivity Case 1 assumes nominal PA model parameters except for an increased gravel content in the initial concrete composition to simulate more extensive concrete cracking. Sensitivity Case 8 specifically addresses tritium diffusion in concrete. The other sensitivity cases are executed for all 19 generic parent radionuclides.

Table 5-15. Nominal PA, Best Estimate, and Sensitivity Cases Used to Model Low-Activity Waste Vault and Intermediate-Level Vault Performance in Vadose Zone

Model Parameters		Nominal PA	Best Estimate	Sensitivity Cases							
				1	2	3	4	5	6	7	8
Initial Concrete Gravel (wt%)	Roof	10	10	20[1]	10	10	10	10	10	10	10
	Walls	10	10	20[1]	10	10	10	10	10	10	10
	Floor	0	0	20[1]	0	0	0	0	0	0	0
Concrete Degradation Period (years)		500	1,000[2]	500	1,000[2]	500	500	500	500	500	500
Pore Volume Exchanges for Concrete Aging	Stage I to Stage II	50	50	50	50	25	50	50	50	50	50
	Stage II to Stage III	500	500	500	500	250	500	500	500	500	500
	Stage III to soil	4,000	4,000	4,000	4,000	1,500	4,000	4,000	4,000	4,000	4,000
LVZ Porosity (unitless)		0.380	0.380	0.380	0.380	0.380	0.420 (+1σ)[3]	0.380	0.380	0.380	0.380
Waste Zone Porosity (unitless)		0.900	0.300	0.900	0.900	0.900	0.900	0.300	0.900	0.900	0.900
Infiltration (in yr^{-1})		2019 HELP[4]	2019 HELP[4]	2019 HELP[4]	2019 HELP[4]	2019 HELP[4]	2019 HELP[4]	2019 HELP[4]	+½σ[5]	2019 HELP[4]	2019 HELP[4]
Solid-Liquid Distribution Coefficients		2016 Chem[6]	2016 Chem[6]	2016 Chem[6]	2016 Chem[6]	2016 Chem[6]	2016 Chem[6]	2016 Chem[6]	2016 Chem[6]	½K_d values[7]	2016 Chem[6]
H-3 Diffusivity Coefficient in Concrete[8] (cm^2 yr^{-1})		2.02	2.02	2.02	2.02	2.02	2.02	2.02	2.02	2.02	2.15 (+1σ)[9]

Notes:

Gold-highlighted cells indicate the nominal PA case model parameters adjusted in each sensitivity case.

1 Ten concrete/soil mixture properties are developed specifically for this analysis.

2 Twenty additional concrete/soil mixture properties are developed for these analyses.

3 The porosity value of 0.420 represents a one-standard-deviation increase from the mean value used in the nominal PA case.

4 Infiltration rates are calculated using the HELP model (Dyer, 2019b) and SRS historical rainfall data (49.14 in yr^{-1} annual average).

5 Infiltration rates are based on annual average rainfall of 61.68 in yr^{-1} (+½σ based on SRS historical mean monthly rainfall or +1.6σ on annual average basis).

6 Solid-liquid distribution coefficients (K_d) obtained from the 2016 Geochemical Data Package (Kaplan, 2016b; SRNL, 2018).

7 All solid-liquid distribution coefficients are one-half the values reported in the 2016 Geochemical Data Package (Kaplan, 2016b; SRNL, 2018).

8 Tritium effective diffusivity in concrete is from the 2019 Hydraulic Properties Data Package (Nichols and Butcher, 2020).

9 The H-3 diffusivity coefficient value of 2.15 cm^2 yr^{-1} represents a 1σ increase in the value reported in the 2019 Hydraulic Properties Data Package (Nichols and Butcher, 2020).

5.2.1.1. Flow Model Results

Figure 5-67 through Figure 5-69 display infiltration flow over the entire computational mesh at selected time steps for the nominal PA case, best estimate case, and Sensitivity Case 6, respectively. As noted in Table 5-15, the nominal PA case degrades LAWV concrete hydraulic performance over 500 years, the best estimate case degrades the concrete over 1,000 years, and Sensitivity Case 6 increases the infiltration flow. These three are expected to have the greatest impact on VZ flow. In each figure, the material zones are illustrated by various color-coded shading.

In all three figures, the first plot (Year 0 to Year 171) shows flow before final closure cap installation. The PORFLOW model simulations during this period include the backfill soil around the LAWV even though the soil will not be placed until Year 171 when the final closure cap is installed. In addition, a negligible but non-zero infiltration rate through the LAWV roof is imposed to facilitate model convergence.[2] Nevertheless, water flow directly over the LAWV during this period is low and model-calculated flow lines display the expected behavior (i.e., relatively uniform flow on either side of the LAWV, negligible flow through the vault, little flow directly under the LAWV, and water encroachment under the LAWV caused by the elevated suction created by the presence of dry soil beneath and moist, uncovered soil surrounding the LAWV).

Degradation of vault concrete hydraulic properties occurs between Year 171 and Year 671 for the nominal PA case and Sensitivity Case 6 and between Year 171 and Year 1,171 for the best estimate case. From Year 171 to Year 2,976, when the LAWV roof is predicted to collapse (Carey, 2005), the HDPE geomembrane and GCL composite barrier within the final closure cap progressively deteriorates and allows more water flow directly above and beside the LAWV. The nominal PA and best estimate simulations continue to show little flow under the LAWV up to Year 471. In Sensitivity Case 6, greater flow occurs through the LAWV from Year 421 to Year 471 because of higher rainfall. Because the LAWV concrete hydraulic properties are still not fully degraded from Year 721 to Year 771, lower flow through the LAWV is seen in the best estimate case compared to the nominal PA case. Otherwise, the flow patterns from Years 721 to 771 are quite similar. Examining Figure 5-69 during these years shows higher flow rates for Sensitivity Case 6 than the nominal PA and best estimate cases. From Year 721 to Year 2,976, flow through the LAWV and the final closure cap steadily increases in all three cases as the performance of the HDPE geomembrane and GCL composite barrier declines. At Year 2,976 and beyond, flow through the LAWV region is higher than background flow. The collapse of the LAWV roof is assumed to open a hole in the final closure cap, allowing runoff from the intact upslope portion of the cap to drain into the LAWV region (Dyer, 2019b). After roof collapse (Year 2,976 and beyond), flow is nearly identical for the nominal PA and best estimate cases and clearly higher for Sensitivity Case 6.

[2] When PORFLOW simulates drainage off the roof, model convergence is difficult with either zero flow through the roof or full background flow over the LAWV. Therefore, the model includes a small inflow (0.001 in yr^{-1}) representing an insignificant leak through the rain cover and concrete. The basis for including this parameter is that the gutter or drain system catches the water and is maintained until final closure.

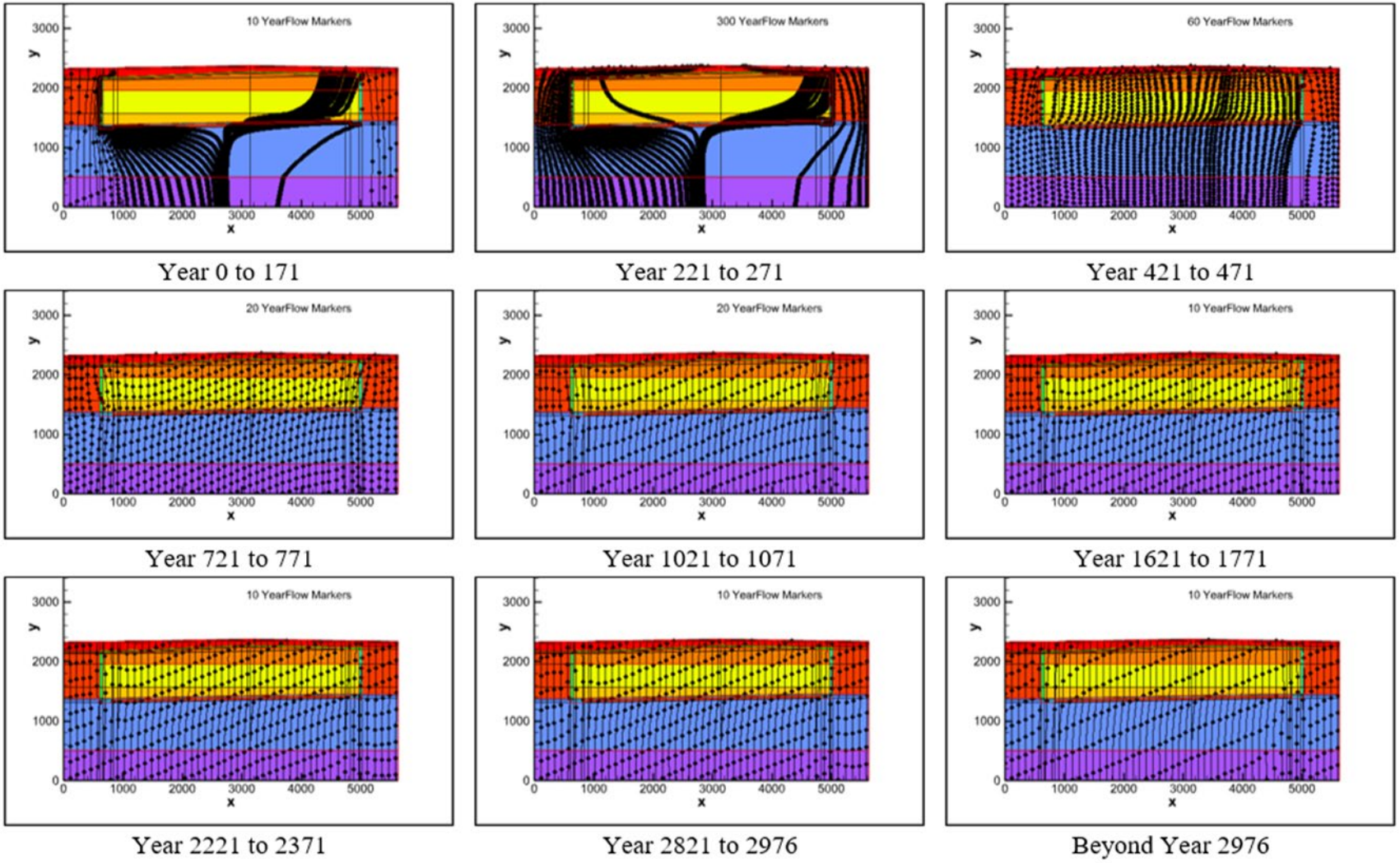

Figure 5-67. Flow through Low-Activity Waste Vault Vadose Zone for Nominal PA Case

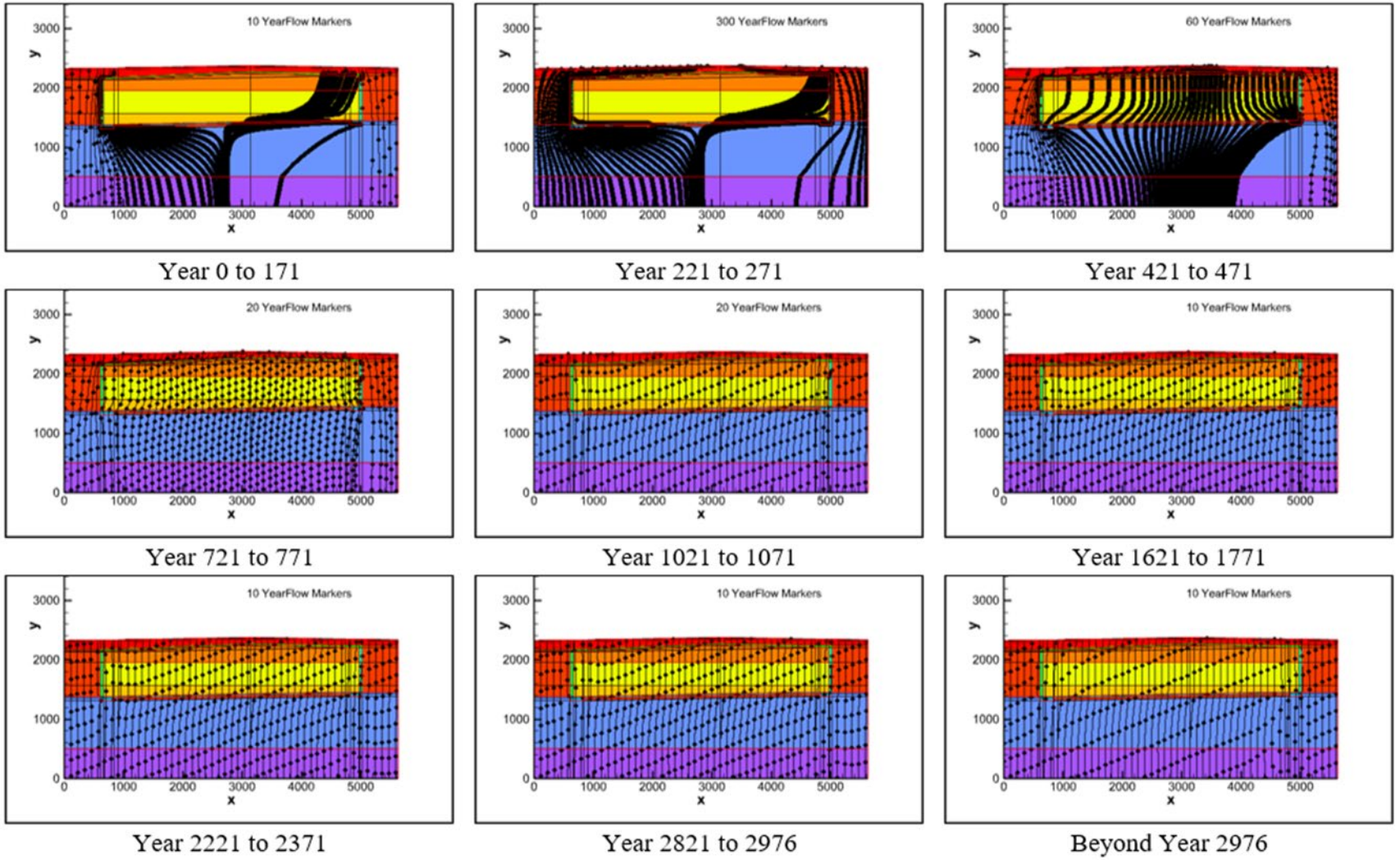

Figure 5-68. Flow through Low-Activity Waste Vault Vadose Zone for Best Estimate Case

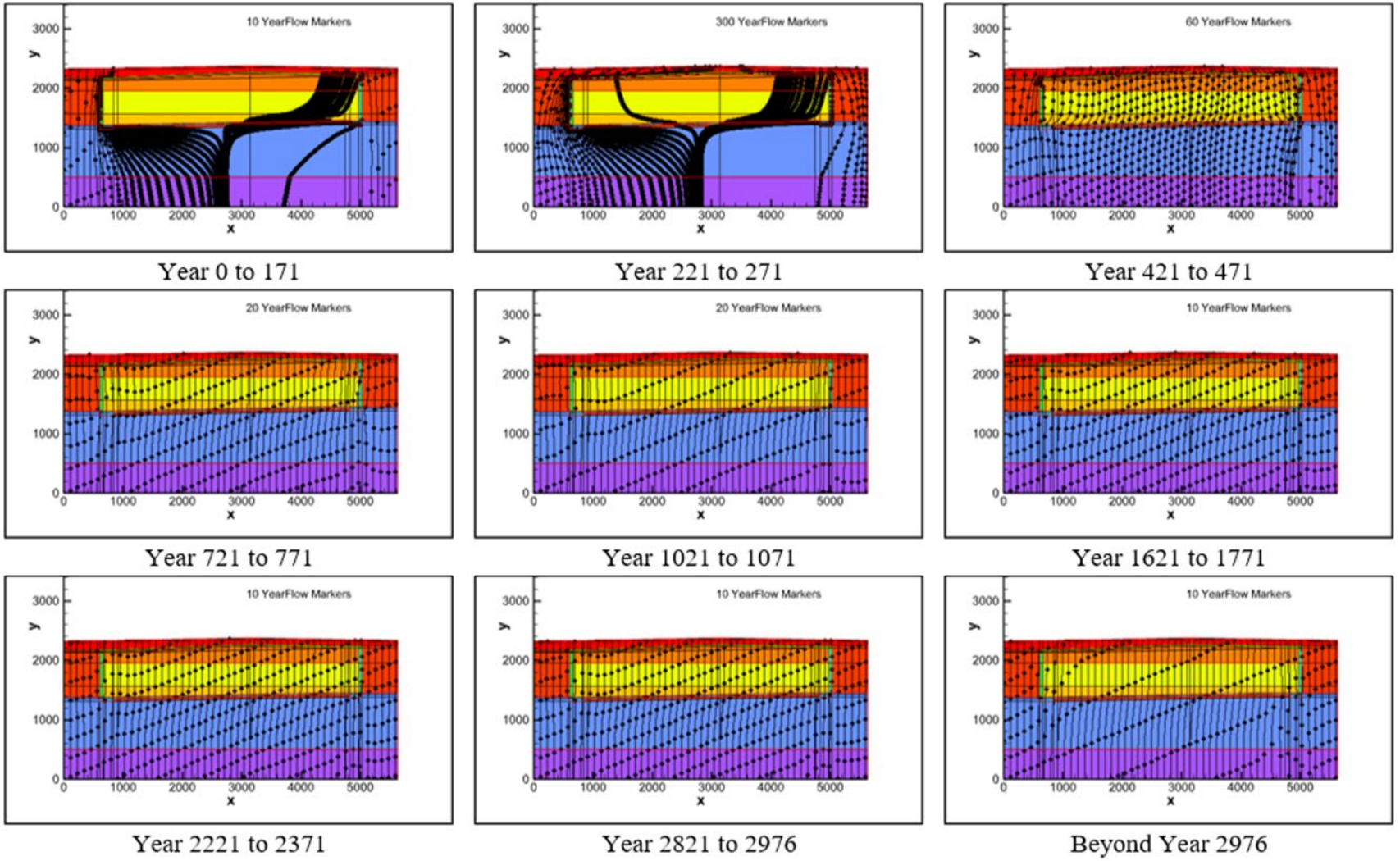

Figure 5-69. Flow through Low-Activity Waste Vault Vadose Zone for Sensitivity Case 6

Figure 5-70 and Figure 5-71 provide expanded views of water flow through the LAWV region and associated VZ from Year 571 to Year 621 for all seven simulated flow cases: nominal PA; best estimate; and Sensitivity Cases 1, 2, 4, 5, and 6. This time interval is selected because the LAWV concrete remains somewhat intact, and the flux to the water table occurs early enough to impact the aquifer concentration during the 1,000-year compliance period. Flow profiles for the best estimate case and Sensitivity Case 2 are similar to each other yet different from the other cases. The best estimate case and Sensitivity Case 2 assume slower degradation of the LAWV concrete (1,000 years versus 500 years in the nominal PA case) (Table 5-15). Flow patterns in the other five cases are similar to each other.

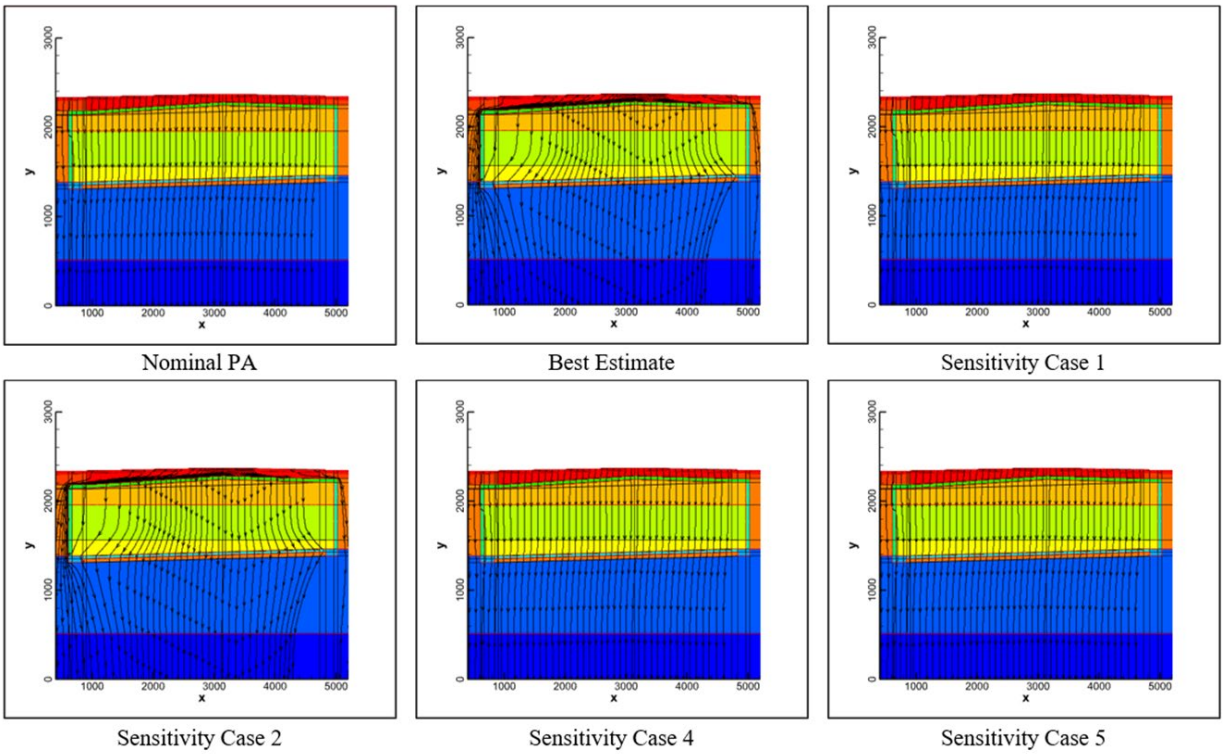

Figure 5-70. Year 571 to Year 621 Flow Lines for Low-Activity Waste Vault Vadose Zone Model Nominal PA Case; Best Estimate Case; Sensitivity Cases 1, 2, 4, and 5

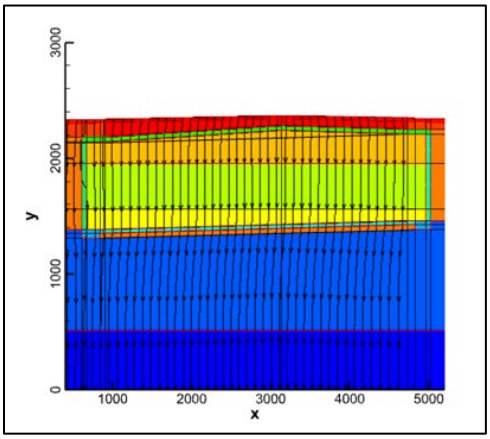

Figure 5-71. Year 571 to Year 621 Flow Lines for Low-Activity Waste Vault Vadose Zone Model Sensitivity Case 6

5.2.1.2. Transport Model Results for Generic Waste

This section summarizes PORFLOW modeling results for the transport of generic waste radionuclides through the LAWV VZ. For comparison purposes and to analyze the vast quantity of data, this section includes transport model results used to establish PA limits, results for the best estimate case representing the expected behavior of the LAWV, and results for the sensitivity cases listed in Table 5-15. The decay and transport of 28 total isotopes through the VZ are modeled over a 50,000-year period. The isotopes include 19 generic LAWV parent radionuclides listed in Table 5-14 as well as nine progeny isotopes in the parent decay chains with half-lives equal to or greater than one year.

Table 5-16 and Table 5-17 compare peak flux to the water table and the time when the peak flux occurs for each radionuclide and each case. To further reduce the size of the dataset, radionuclides are screened out if they do not peak within 50,000 years for the nominal PA case or if the peak flux is less than 1.0E-20 gmol yr^{-1} per gmole buried. Using this criterion, Am-241 (1.98E-35 gmol yr^{-1} peak flux), Cm-245 (3.62E-34 gmol yr^{-1} peak flux), Cs-137(3.19E-32 gmol yr^{-1} peak flux), Pu-239 (2.15E-24 gmol yr^{-1} peak flux), Pu-241 (2.41E-204 gmol yr^{-1} peak flux), and Sr-90 (2.69E-26 gmol yr^{-1} peak flux) are eliminated from consideration. Peak flux and time of occurrence for the remaining 18 parent and daughter radionuclides are listed in Table 5-16 and Table 5-17 for the nine cases that include these radionuclides. Except for H-3 and I-129, all radionuclides peak beyond the compliance period; however, the leading release curve may still impact limit calculations.

Table 5-16. Peak Flux to Water Table and Time of Occurrence for Low-Activity Waste Vault Vadose Zone Nominal PA Case, Best Estimate Case, and Sensitivity Cases 1 to 3

Radionuclide		Nominal PA Case		Best Estimate Case		Sensitivity Case 1 Concrete Cracking		Sensitivity Case 2 Degraded Concrete		Sensitivity Case 3 Concrete Aging	
Parent	Progeny	Maximum (gmol yr^{-1})	Time (Year)	Maximum (gmol yr^{-1})	Time (Year)	Maximum (gmol yr^{-1})	Time (Year)	Maximum (gmol yr^{-1})	Time (Year)	Maximum (gmol yr^{-1})	Time (Year)
Ag-108m	-	2.68E-06	3,596	2.67E-06	4,006	2.68E-06	3,596	2.61E-06	3,596	1.14E-05	3,356
Am-241	Np-237	4.40E-03	3,366	4.40E-03	3,366	4.40E-03	3,366	4.29E-03	3,366	4.45E-03	2,380
Am-241	U-233	1.22E-07	20,216	1.11E-07	20,406	1.22E-07	20,206	1.18E-07	20,236	6.66E-08	19,496
Am-241	Th-229	8.67E-10	23,086	8.22E-10	23,536	8.66E-10	23,076	8.45E-10	23,136	5.12E-10	22,206
C-14	-	1.76E-03	2,986	1.08E-03	3,126	1.75E-03	2,986	1.69E-03	2,986	1.58E-03	2,986
Ca-41	-	2.47E-03	2,222	1.43E-03	2,589	2.45E-03	2,222	2.35E-03	2,239	2.37E-03	2,222
Cl-36	-	4.12E-03	1,488	3.17E-03	1,673	4.05E-03	1,484	3.94E-03	1,562	4.06E-03	1,490
Cm-245	Np-237	7.85E-04	3,366	7.77E-04	3,366	7.85E-04	3,366	7.81E-04	3,366	4.52E-04	2,386
Cm-245	U-233	1.59E-08	20,226	1.52E-08	20,346	1.58E-08	20,206	1.57E-08	20,216	8.49E-09	19,336
Cm-245	Th-229	1.30E-10	23,306	1.27E-10	23,506	1.29E-10	23,226	1.28E-10	23,236	8.12E-11	22,406
H-3	-	1.04E-10	94	2.23E-10	91	7.89E-11	92	7.82E-11	92	1.04E-10	94
I-129	-	6.98E-03	1,099	5.66E-03	1,223	6.70E-03	1,094	7.50E-03	1,172	6.97E-03	1,099
K-40	-	1.79E-03	2,610	1.84E-03	2,986	1.78E-03	2,607	1.82E-03	2,672	1.80E-03	2,611
Ni-59	-	1.48E-03	3,226	1.20E-03	3,556	1.43E-03	3,216	1.55E-03	3,316	1.89E-03	3,246
Ni-63	-	1.45E-12	2,591	1.58E-13	3,126	2.03E-12	2,540	4.93E-13	3,056	1.02E-12	2,672
Np-237	-	4.38E-03	3,366	4.41E-03	3,366	4.36E-03	3,366	4.23E-03	3,366	4.64E-03	2,380
Np-237	U-233	1.50E-07	20,236	1.32E-07	20,536	1.50E-07	20,226	1.45E-07	20,256	9.38E-08	19,596
Np-237	Th-229	8.60E-10	23,136	8.17E-10	23,836	8.59E-10	23,116	8.39E-10	23,196	5.06E-10	22,406
Pu-239	U-235	2.21E-05	28,516	2.95E-05	24,486	2.60E-05	23,346	2.61E-05	23,356	2.54E-05	23,706
Pu-239	Pa-231	5.64E-10	3,366	5.43E-10	3,376	5.64E-10	3,366	5.62E-10	3,366	3.97E-10	19,646
Pu-239	Ac-227	1.02E-15	3,396	9.84E-16	3,406	1.02E-15	3,396	1.02E-15	3,396	7.75E-16	19,666
Pu-241	Np-237	4.40E-03	3,366	4.40E-03	3,366	4.40E-03	3,366	4.29E-03	3,366	4.44E-03	2,380
Pu-241	U-233	1.21E-07	20,216	1.11E-07	20,406	1.21E-07	20,206	1.18E-07	20,226	6.57E-08	19,496

Notes:

Reference point for time is start of LAWV operations in late 1994; the compliance period is from Year 171 to Year 1,171.

Table 5-16 (cont'd). Peak Flux to Water Table and Time of Occurrence for Low-Activity Waste Vault Vadose Zone Nominal PA Case, Best Estimate Case, and Sensitivity Cases 1 to 3

Radionuclide		Nominal PA Case		Best Estimate Case		Sensitivity Case 1 Concrete Cracking		Sensitivity Case 2 Degraded Concrete		Sensitivity Case 3 Concrete Aging	
Parent	Progeny	Maximum (gmol yr^{-1})	Time (Year)	Maximum (gmol yr^{-1})	Time (Year)	Maximum (gmol yr^{-1})	Time (Year)	Maximum (gmol yr^{-1})	Time (Year)	Maximum (gmol yr^{-1})	Time (Year)
Pu-241	Th-229	8.60E-10	23,086	8.17E-10	23,526	8.59E-10	23,076	8.39E-10	23,136	5.06E-10	22,196
Ra-226	-	1.11E-05	8,186	7.50E-06	8,846	1.11E-05	8,186	1.09E-05	8,206	1.28E-05	7,966
Ra-226	Pb-210	1.93E-09	8,226	1.31E-09	8,876	1.94E-09	8,216	1.91E-09	8,236	2.24E-09	7,996
Tc-99	-	2.47E-03	3,106	2.95E-03	3,106	2.38E-03	3,106	2.92E-03	3,106	1.68E-02	1,914
U-235	-	1.68E-04	20,366	1.60E-04	21,156	1.68E-04	20,356	1.68E-04	20,376	1.68E-04	19,916
U-235	Pa-231	1.31E-08	3,366	1.29E-08	3,366	1.31E-08	3,366	1.29E-08	3,366	8.44E-09	2,384
U-235	Ac-227	2.36E-14	3,396	2.33E-14	3,396	2.36E-14	3,396	2.33E-14	3,396	1.55E-14	2,413

Notes:

Reference point for time is start of LAWV operations in late 1994; the compliance period is from Year 171 to Year 1,171.

Table 5-17. Peak Flux to the Water Table and Time of Occurrence for Low-Activity Waste Vault Vadose Zone Nominal PA Case, Best Estimate Case, and Sensitivity Cases 4 to 7

Radionuclide		Nominal PA Case		Sensitivity Case 4 LVZ Porosity		Sensitivity Case 5 Waste Porosity		Sensitivity Case 6 Infiltration		Sensitivity Case 7 K_d	
Parent	Progeny	Maximum (gmol yr^{-1})	Time (Year)	Maximum (gmol yr^{-1})	Time (Year)	Maximum (gmol yr^{-1})	Time (Year)	Maximum (gmol yr^{-1})	Time (Year)	Maximum (gmol yr^{-1})	Time (Year)
Ag-108m	-	2.68E-06	3,596	2.72E-06	3,586	2.66E-06	3,996	7.31E-06	3,256	1.46E-05	2,672
Am-241	Np-237	4.40E-03	3,366	4.40E-03	3,366	4.45E-03	3,366	5.49E-03	3,236	5.66E-03	3,206
Am-241	U-233	1.22E-07	20,216	1.24E-07	19,896	1.14E-07	20,386	1.79E-07	14,226	2.40E-07	11,566
Am-241	Th-229	8.67E-10	23,086	8.71E-10	22,736	8.36E-10	23,466	9.61E-10	16,466	1.06E-09	13,426
C-14	-	1.76E-03	2,986	1.76E-03	2,986	1.15E-03	3,106	1.28E-03	2,615	2.23E-03	2,146
Ca-41	-	2.47E-03	2,222	2.46E-03	2,195	1.24E-03	2,550	2.89E-03	1,802	4.20E-03	1,622
Cl-36	-	4.12E-03	1,488	4.13E-03	1,486	2.83E-03	1,633	5.47E-03	1,153	6.43E-03	1,172

Notes:

Reference point for time is start of LAWV operations in late 1994; the compliance period is from Year 171 to Year 1,171.

Table 5-17 (cont'd). Peak Flux to Water Table and Time of Occurrence for Low-Activity Waste Vault Vadose Zone Nominal PA Case and Sensitivity Cases 4 to 7

Radionuclide		Nominal PA Case		Sensitivity Case 4 LVZ Porosity		Sensitivity Case 5 Waste Porosity		Sensitivity Case 6 Infiltration		Sensitivity Case 7 K_d	
Parent	Progeny	Maximum (gmol yr^{-1})	Time (Year)	Maximum (gmol yr^{-1})	Time (Year)	Maximum (gmol yr^{-1})	Time (Year)	Maximum (gmol yr^{-1})	Time (Year)	Maximum (gmol yr^{-1})	Time (Year)
Cm-245	Np-237	7.85E-04	3,366	7.85E-04	3,366	7.78E-04	3,366	9.81E-04	3,236	1.05E-03	3,206
Cm-245	U-233	1.59E-08	20,226	1.60E-08	19,896	1.53E-08	20,346	2.04E-08	14,246	2.58E-08	11,586
Cm-245	Th-229	1.30E-10	23,306	1.29E-10	22,866	1.27E-10	23,486	1.21E-10	16,596	1.23E-10	13,526
H-3	-	1.04E-10	94	7.30E-11	93	2.10E-10	91	9.38E-11	86	1.04E-10	94
I-129	-	6.98E-03	1,099	7.00E-03	1,097	5.41E-03	1,172	9.77E-03	858	9.24E-03	922
K-40	-	1.79E-03	2,610	1.79E-03	2,602	1.80E-03	2,986	2.06E-03	2,098	3.12E-03	1,833
Ni-59	-	1.48E-03	3,226	1.48E-03	3,216	1.18E-03	3,536	1.26E-03	2,986	1.66E-03	2,139
Ni-63	-	1.45E-12	2,591	1.56E-12	2,581	2.62E-13	2,621	1.23E-10	2,138	1.49E-09	1,922
Np-237	-	4.38E-03	3,366	4.38E-03	3,366	4.47E-03	3,366	5.46E-03	3,236	5.59E-03	3,206
Np-237	U-233	1.50E-07	20,236	1.52E-07	19,916	1.36E-07	20,496	2.22E-07	14,236	2.98E-07	1,1576
Np-237	Th-229	8.60E-10	23,136	8.64E-10	22,786	8.30E-10	23,716	9.54E-10	16,486	1.05E-09	1,3446
Pu-239	U-235	2.21E-05	28,516	2.61E-05	22,976	2.95E-05	24,486	2.96E-05	15,496	3.62E-05	12,186
Pu-239	Pa-231	5.64E-10	3,366	5.64E-10	3,366	5.43E-10	3,376	7.02E-10	3,246	7.56E-10	3,206
Pu-239	Ac-227	1.02E-15	3,396	1.03E-15	3,396	9.85E-16	3,396	1.22E-15	3,266	1.39E-15	3,236
Pu-241	Np-237	4.40E-03	3,366	4.40E-03	3,366	4.44E-03	3,366	5.49E-03	3,236	5.66E-03	3,206
Pu-241	U-233	1.21E-07	20,216	1.23E-07	19,896	1.13E-07	20,386	1.78E-07	14,226	2.38E-07	11,566
Pu-241	Th-229	8.60E-10	23,086	8.64E-10	22,736	8.30E-10	23,456	9.54E-10	16,466	1.05E-09	13,426
Ra-226	-	1.11E-05	8,186	1.12E-05	8,166	7.51E-06	8,836	3.87E-05	6,246	8.50E-05	5,146
Ra-226	Pb-210	1.93E-09	8,226	1.96E-09	8,196	1.31E-09	8,866	6.77E-09	6,286	1.50E-08	5,176
Tc-99	-	2.47E-03	3,106	2.46E-03	3,106	2.50E-03	3,106	1.37E-03	3,076	9.41E-04	1,772
U-235	-	1.68E-04	20,366	1.71E-04	20,036	1.60E-04	21,156	2.46E-04	14,276	3.32E-04	11,606
U-235	Pa-231	1.31E-08	3,366	1.31E-08	3,366	1.29E-08	3,366	1.62E-08	3,236	1.71E-08	3,206
U-235	Ac-227	2.36E-14	3,396	2.39E-14	3,396	2.34E-14	3,396	2.82E-14	3,266	3.13E-14	3,226

Notes:

Reference point for time is start of LAWV operations in late 1994; the compliance period is from Year 171 to Year 1,171.

Table 5-18 further simplifies the results by normalizing peak flux values to the nominal PA case. A condensed summary of the results in Table 5-18 is provided in Table 5-19. The impact of the sensitivity cases on peak flux to the water table can be generalized as follows:

Significant Impact

Sensitivity Case 6 – Raising the mean monthly infiltration rates by 0.5 standard deviation significantly increases peak flux for all radionuclides except C-14, Ni-59, and Tc-99.

Sensitivity Case 7 – Lowering K_d values by a factor of two significantly increases peak flux for all radionuclides but Tc-99.

Limited Impact

Sensitivity Case 3 – Decreasing the number of pore volume exchanges required for concrete aging lowers the maximum flux for most radionuclides. However, peak flux increases for Ag-108m, Ni-59, Pu-239, Ra-226, Pb-210 (daughter of Ra-226), and Tc-99.

Sensitivity Case 5 – Lowering waste porosity relative to soil increases peak flux by a factor of approximately 2.0 for H-3 and 1.3 for Pu-239.

Minimal Impact

Sensitivity Case 1 – Doubling the gravel content to simulate an increase in concrete cracking of the vault roof and side walls when the final closure cap is installed increases concrete hydraulic conductivity and porosity without representing through-cracking of the concrete. This change has a minimal impact on peak flux for all radionuclides except H-3, Ni-63, and Pu-239.

Sensitivity Case 2 – Extending concrete hydraulic degradation over 1,000 years instead of the 500-year limit suggested by the PAWG in NUREG-1573 (U.S. NRC, 2000) has a minimal impact on peak flux for all radionuclides except H-3, Ni-63, Tc-99, and Pu-239.

Sensitivity Case 4 – Increasing soil porosity in the LVZ by one standard deviation has a minimal impact on peak flux for all radionuclides except H-3, Ni-63, and Pu-239.

The best estimate case combines Sensitivity Cases 2 and 5; therefore, the results for this case closely match those of the two sensitivity cases.

Ni-63 flux to the water table is strongly impacted in Sensitivity Cases 5 and 6. Ni-63 has a relatively short half-life of 101 years. As a result, parameters that affect the timing of flux to the water table, such as a higher water flow rate or a lower K_d, have a substantial impact on Ni-63 transport. Based on 1.0 gmol of each isotope buried in the LAWV for the nominal PA case, the maximum flux to the water table for Ni-59 (half-life 76,000 years) is 5.0E-04 gmol yr^{-1}. The maximum flux for Ni-63 is only 5.7E-14 gmol yr^{-1} because of the greater decay rate.

Table 5-18. Maximum Flux to Water Table for Low-Activity Waste Vault Vadose Zone Best Estimate and Sensitivity Cases 1 through 7 Normalized to Nominal PA Case

Radionuclide		Best Estimate	Sensitivity Cases						
Parent	Progeny	Case	1	2	3	4	5	6	7
Ag-108m	-	1.00	1.00	0.98	4.25	1.02	0.99	2.73	5.45
Am-241	Np-237	1.00	1.00	0.97	1.01	1.00	1.01	1.25	1.29
Am-241	U-233	0.91	1.00	0.97	0.55	1.01	0.93	1.47	1.96
Am-241	Th-229	0.95	1.00	0.97	0.59	1.00	0.96	1.11	1.22
C-14	-	0.62	1.00	0.96	0.90	1.00	0.66	0.73	1.27
Ca-41	-	0.58	0.99	0.95	0.96	1.00	0.50	1.17	1.70
Cl-36	-	0.77	0.98	0.96	0.99	1.00	0.69	1.33	1.56
Cm-245	Np-237	0.99	1.00	1.00	0.58	1.00	0.99	1.25	1.34
Cm-245	U-233	0.96	1.00	0.99	0.53	1.01	0.96	1.29	1.62
Cm-245	Th-229	0.98	0.99	0.99	0.63	0.99	0.98	0.94	0.95
H-3	-	2.16	0.76	0.76	1.00	0.71	2.03	0.91	1.00
I-129	-	0.81	0.96	1.07	1.00	1.00	0.77	1.40	1.32
K-40	-	1.03	0.99	1.02	1.01	1.00	1.01	1.15	1.74
Ni-59	-	0.81	0.96	1.04	1.27	1.00	0.79	0.85	1.12
Ni-63	-	0.11	1.40	0.34	0.71	1.08	0.18	85.18	1,032.77
Np-237	-	1.01	1.00	0.97	1.06	1.00	1.02	1.25	1.28
Np-237	U-233	0.88	1.00	0.97	0.62	1.01	0.90	1.48	1.99
Np-237	Th-229	0.95	1.00	0.98	0.59	1.00	0.96	1.11	1.22
Pu-239	U-235	1.33	1.18	1.18	1.15	1.18	1.33	1.34	1.63
Pu-239	Pa-231	0.96	1.00	1.00	0.70	1.00	0.96	1.25	1.34
Pu-239	Ac-227	0.96	1.00	1.00	0.76	1.01	0.96	1.20	1.36

Notes:

Fluxes greater than 10% above the nominal PA case (i.e., an exceedance) are shaded in light green.

Fluxes greater than 10% below the nominal PA case are shaded in light gold.

Radionuclides with flux ratios greater than 50 are highlighted in yellow.

Table 5-18 (cont'd). Maximum Flux to Water Table for Low-Activity Waste Vault Vadose Zone Best Estimate and Sensitivity Cases 1 through 7 Normalized to Nominal PA Case

Radionuclide		Best Estimate Case	Sensitivity Cases						
Parent	Progeny		1	2	3	4	5	6	7
Pu-241	Np-237	1.00	1.00	0.97	1.01	1.00	1.01	1.25	1.29
Pu-241	U-233	0.91	1.00	0.97	0.54	1.01	0.94	1.47	1.96
Pu-241	Th-229	0.95	1.00	0.98	0.59	1.00	0.96	1.11	1.22
Ra-226	-	0.68	1.00	0.99	1.16	1.01	0.68	3.50	7.68
Ra-226	Pb-210	0.68	1.00	0.99	1.16	1.01	0.68	3.50	7.74
Tc-99	-	1.19	0.96	1.18	6.79	0.99	1.01	0.55	0.38
U-235	-	0.95	1.00	1.00	1.00	1.01	0.95	1.46	1.97
U-235	Pa-231	0.99	1.00	0.99	0.65	1.00	0.99	1.24	1.31
U-235	Ac-227	0.99	1.00	0.99	0.66	1.01	0.99	1.20	1.33

Notes:

Fluxes greater than 10% above the nominal PA case (i.e., an exceedance) are shaded in light green.

Fluxes greater than 10% below the nominal PA case are shaded in light gold.

Radionuclides with flux ratios greater than 50 are highlighted in yellow.

Table 5-19. Summary of Maximum Flux to Water Table Ratios and Number of Flux Ratios Greater or Less than 1 for Low-Activity Waste Vault Vadose Zone

Parameter		Best Estimate	Sensitivity Cases						
			1	2	3	4	5	6	7
Maximum Conc. Ratios	Maximum Value	2.16	1.40	1.18	6.79	1.18	2.03	85.18	1,032.77
	Minimum Value	0.11	0.76	0.34	0.53	0.71	0.18	0.55	0.38
No. of Conc. Ratios < 1	Conc. Ratios < 0.5	1	0	1	0	0	1	0	1
	Conc. Ratios < 0.9	9	1	2	14	1	8	3	1
No. of Conc. Ratios > 1	Conc. Ratios > 1.1	3	2	2	6	1	2	25	27
	Conc. Ratios > 1.5	1	0	0	2	0	1	4	13

Figure 5-72 through Figure 5-74 compare flux to the water table for the nominal PA case, best estimate case, and Sensitivity Cases 6 and 7.

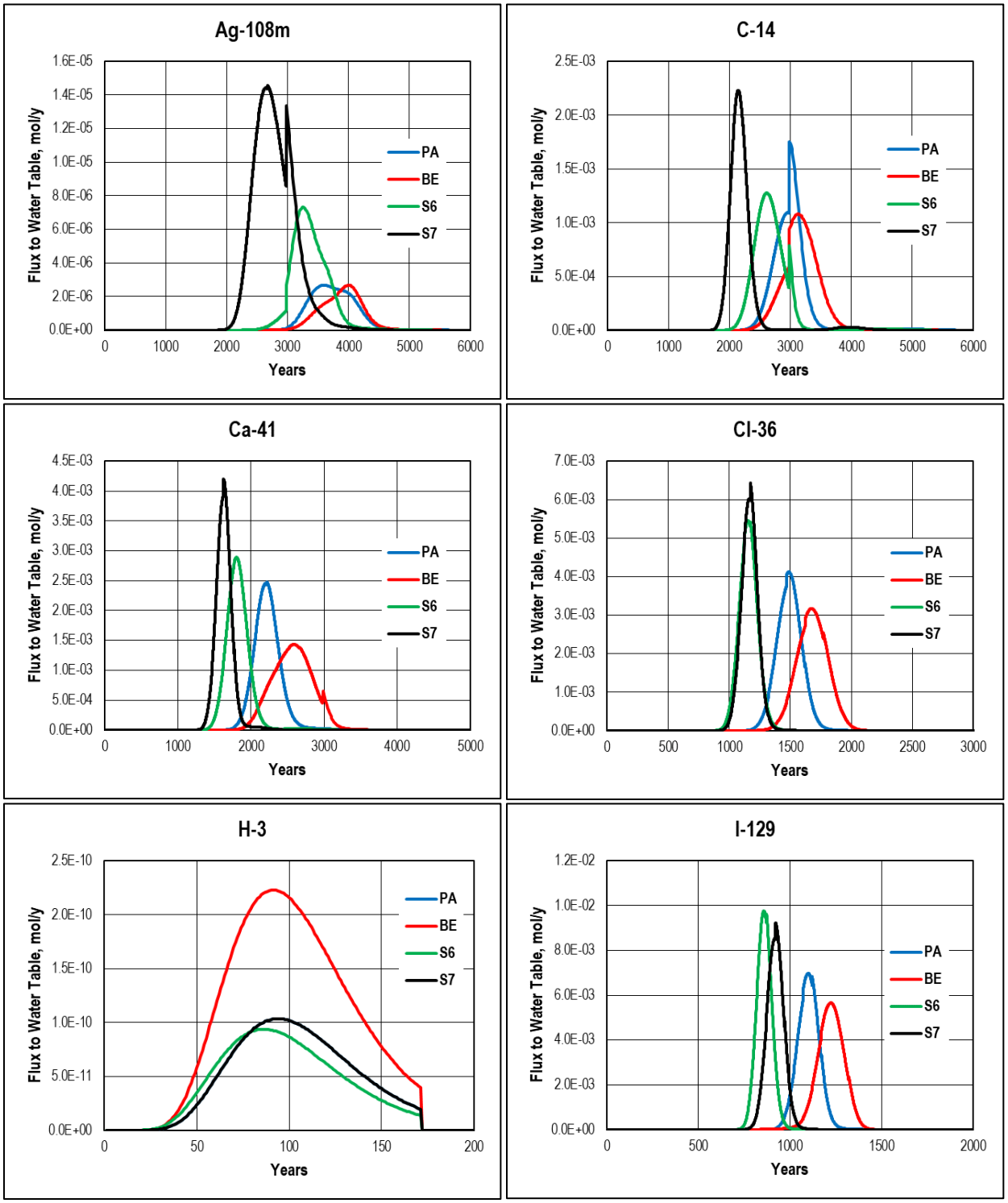

Figure 5-72. Comparison of Nominal PA Case (PA), Best Estimate (BE) Case, Sensitivity Case 6 (S6), and Sensitivity Case 7 (S7) Flux to Water Table for Parent Radionuclides Ag-108m through I-129 in Low-Activity Waste Vault Vadose Zone

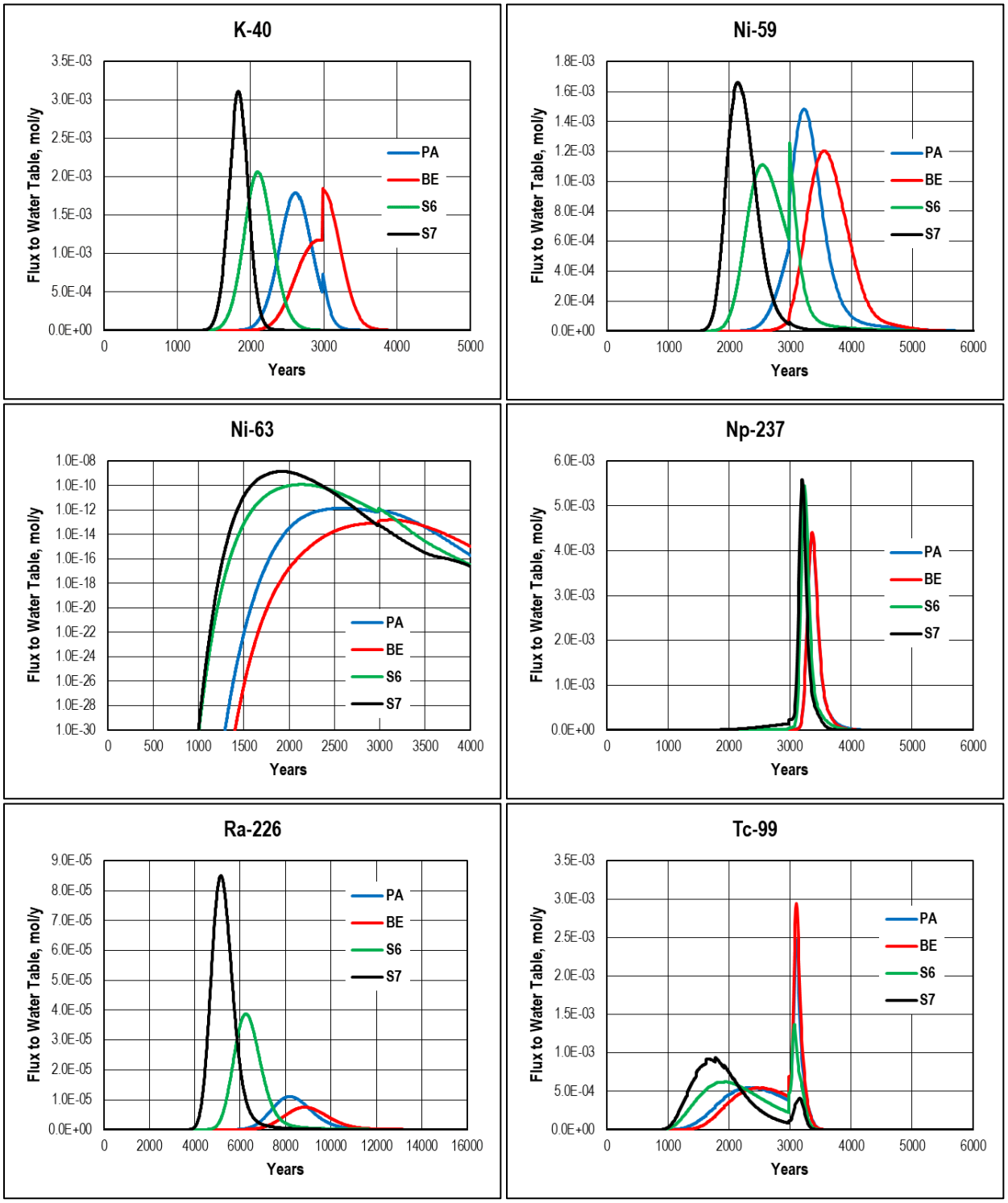

Figure 5-73. Comparison of Nominal PA Case (PA), Best Estimate (BE) Case, Sensitivity Case 6 (S6), and Sensitivity Case 7 (S7) Flux to Water Table for Parent Radionuclides K-40 through Tc-99 in Low-Activity Waste Vault Vadose Zone

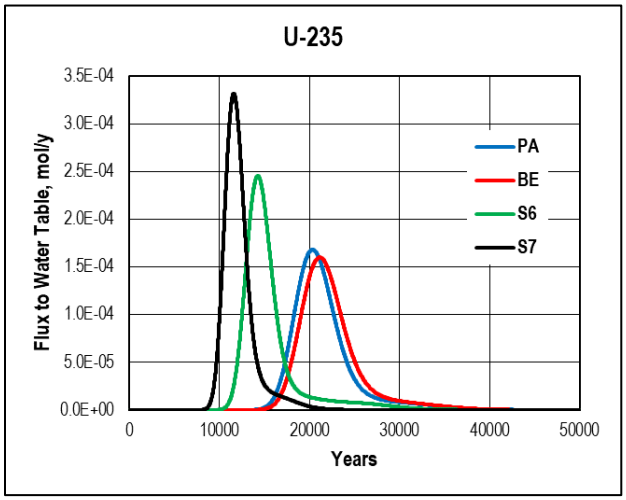

Figure 5-74. Comparison of Nominal PA Case (PA), Best Estimate (BE) Case, Sensitivity Case 6 (S6), and Sensitivity Case 7 (S7) Flux to Water Table for Parent Radionuclide U-235 in Low-Activity Waste Vault Vadose Zone

For most of the radionuclides evaluated, the nominal PA case and best estimate case are in close agreement while the sensitivity cases display fluxes that peak higher and earlier than the nominal PA case. Exceptions are H-3, where the maximum best estimate flux is approximately twice the nominal PA flux (obscured by the Sensitivity Case 7 curve, which overlaps it), and Ni-59 where the maximum best estimate flux peaks lower and later than the nominal PA case flux. In Figure 5-73, Ni-63 is plotted on a semi-log graph to clearly show all cases.

The impact of increasing the diffusivity of tritium in concrete by one standard deviation (from 2.02 to 2.15 $cm^2\ yr^{-1}$) for Sensitivity Case 8 is shown in Figure 5-75. A greater diffusion rate through the concrete increases the maximum H-3 flux to the water table by 30% from 1.04E-10 gmol yr^{-1} per gmole buried to 1.36E-10 gmol yr^{-1} per gmole buried.

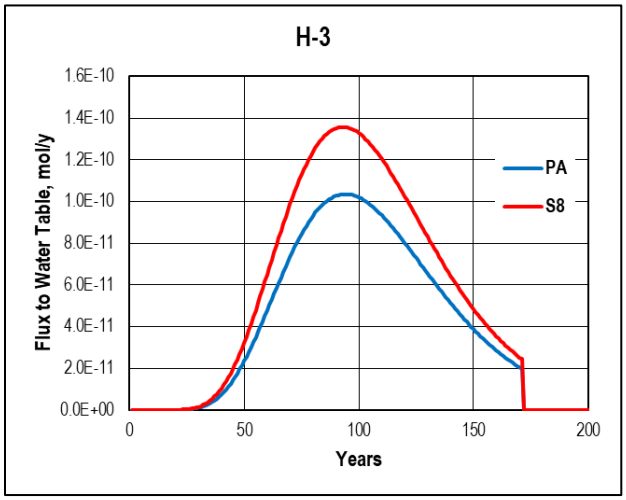

Figure 5-75. Comparison of Nominal PA Case and Sensitivity Case 8 (S8) Flux to Water Table for H-3 in Low-Activity Waste Vault Vadose Zone

Figure 5-76 and Figure 5-77 present the flux to the water table for all decay chains. Except for Pu-239 and Ra-226, all decay chains shown in Figure 5-76 include Np-237, which is likely the leading contributor to dose from these parent radionuclides.

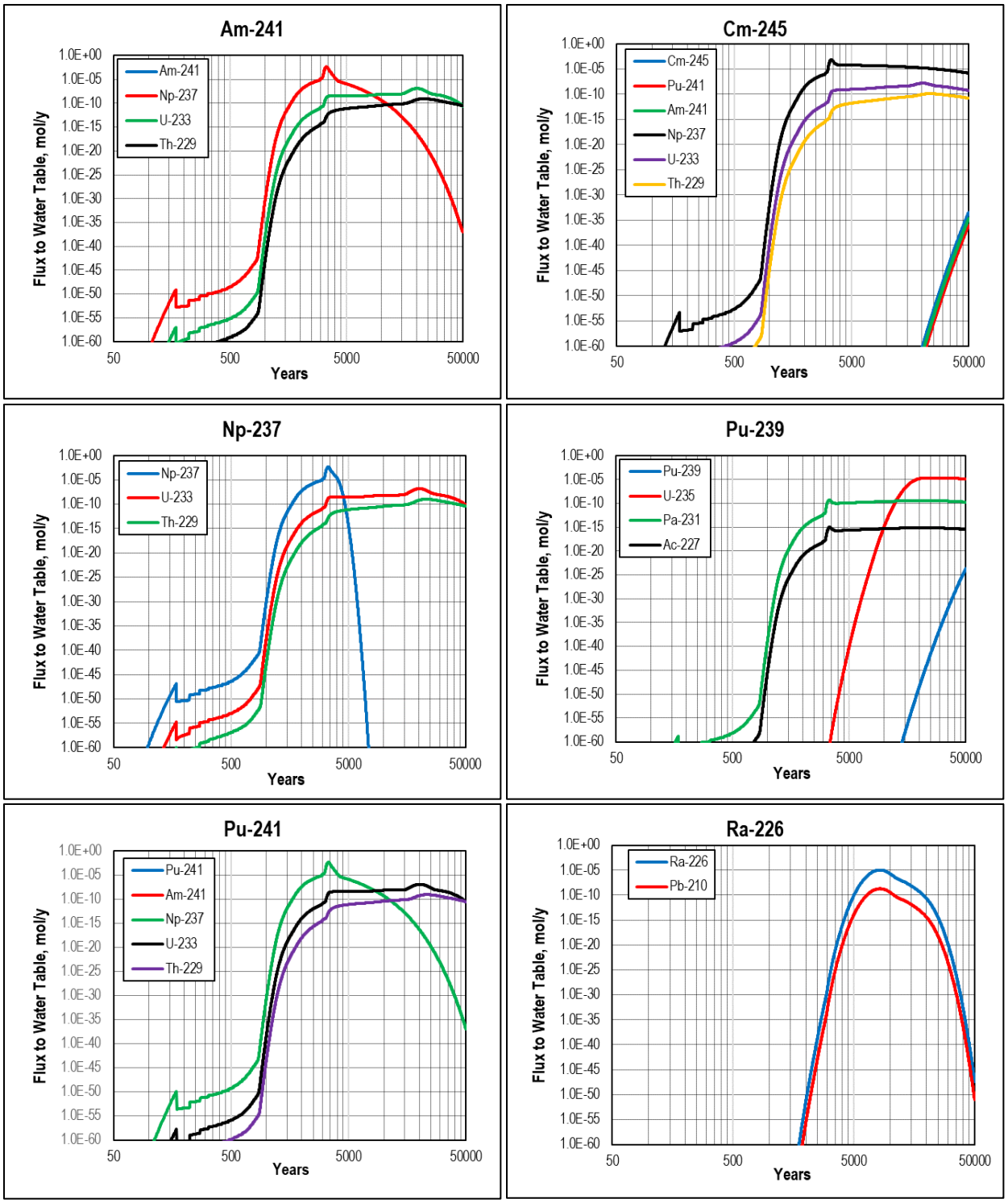

Figure 5-76. Flux to Water Table for Decay Chain Parents Am-241 through Ra-226 and Daughter Radionuclides of Nominal PA Case in Low-Activity Waste Vault Vadose Zone

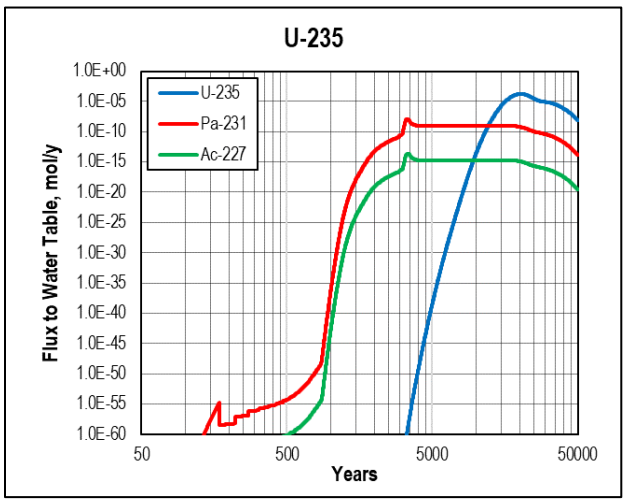

Figure 5-77. Flux to Water Table for Decay Chain Parent U-235 and Daughter Radionuclides of Nominal PA Case in Low-Activity Waste Vault Vadose Zone

5.2.2. Aquifer Zone Model

LAWV aquifer transport modeling includes all case studies previously described for the LAWV VZ transport calculations in Section 5.2.1. In addition to the nominal model settings used for PA calculations, a best estimate and eight sensitivity cases are simulated with the PORFLOW aquifer transport model. Aquifer transport calculations are made for all radionuclides for which flux to the water table is calculated by the LAWV VZ model. That is, even though some radionuclides with small fluxes to the water table are not included in the VZ model discussion, all LAWV VZ results are processed in the aquifer model. In the same way, some radionuclides with low concentrations in the aquifer are not discussed in this section, but all results from the aquifer model are processed with the dose model.

Sensitivity cases were developed for all 19 generic parent radionuclides listed in Table 5-14. These cases are all one-sided calculations designed to investigate model response to changes in what are deemed to be model parameters having the most significant impact on radionuclide transport. Performing one-at-a-time sensitivity studies does not capture non-linear effects in the model; however, the parameters used in this sensitivity study are largely independent. The only parameter variation considered in the aquifer modeling is the reduction of K_d values by 50% for Sensitivity Case 7.

Due to the large size of the full 3-D PORFLOW aquifer flow model for the GSA, the performance of individual waste DUs is modeled using only a "cutout" portion of the full model. The LAWV is in the East1_A cutout. Additional details on the implementation of the aquifer flow model for the LAWV are provided in Section 3.5.3.

5.2.2.1. Transport Model Results for Generic Waste

For comparison purposes and to analyze the vast quantity of data, this section includes the aquifer transport model results used to establish PA limits, the best estimate case representing the expected behavior of the LAWV, and the sensitivity results for the aquifer model based on the VZ sensitivity

cases outlined in Table 5-15. The 19 generic LAWV parent radionuclides and nine progeny isotopes in parent decay chains with half-lives equal to or greater than one year yield a total of 28 isotopes whose transport and decay through the aquifer are modeled over a 50,000-year simulation time.

The simplest way to analyze the large simulation dataset is to compare peak concentrations at the 100-meter POA and the time when the peak occurs for each radionuclide and each case (see Table 5-20 and Table 5-21).

To further reduce the dataset, radionuclides that do not peak within 50,000 years for the nominal PA case (Cm-245, and its daughters Pu-241 and Am-241, as well as Pu-239) and those with peak concentrations less than 1.0E-28 pCi L^{-1} per Ci buried (Am-241 at 4.43E-69 pCi L^{-1} as well as Pu-241 at 1.39E-232 pCi L^{-1} and its daughter, Am-241, at 1.52E-70 pCi L^{-1}) are not included in the comparison. Peak concentrations and the time of occurrence for the 24 parent and daughter radionuclides remaining after this screening are listed in Table 5-20 and Table 5-21 for the nine cases that included all these radionuclides. Except for H-3 and I-129, all radionuclide concentrations peak beyond the compliance period. However, the leading release curve impacts limit calculations.

Table 5-22 further simplifies the results by ratioing peak concentrations to the values obtained for the nominal PA case. Ratios greater than 1.0 in Table 5-22 indicate that a case exceeds the nominal PA value. Note that all concentrations are in pCi L^{-1} per Ci of parent buried. In table headers and plot axis labels, this has been shortened to simply pCi L^{-1} or pCi L^{-1} Ci^{-1}.

A summary of the ratios of the peak concentrations at the 100-meter POA for the cases in Table 5-22 to the nominal PA case is presented in Table 5-23. The impact of the sensitivity cases on peak concentrations at the 100-meter POA can be generalized as follows:

Significant Impact

Sensitivity Case 6 – Raising the mean monthly infiltration rates by 0.5 standard deviation increases peak concentration at the 100-meter POA for most radionuclides. Notable radionuclides experiencing a decrease include C-14, Ni-59, Pu-239, and Tc-99.

Sensitivity Case 7 – Lowering K_d values by a factor of two, which represents a change of more than two standard deviations (95% confidence limit), significantly increases peak flux for all but four radionuclides. Tc-99 is the only radionuclide that experiences a substantial decrease in peak concentration. Lowering K_d values has the most significant impact on peak concentrations at the 100-meter POA.

Table 5-20. Peak Concentration at 100-meter POA and Time of Occurrence for Nominal PA, Best Estimate, and Sensitivity Cases for Low-Activity Waste Vault

Radionuclide		Nominal PA Case		Best Estimate Case		Sensitivity Case 1 Concrete Cracking		Sensitivity Case 2 Degraded Concrete		Sensitivity Case 3 Concrete Aging	
Parent	Progeny	Maximum (pCi L^{-1})	Time (year)	Maximum (pCi L^{-1})	Time (year)	Maximum (pCi L^{-1})	Time (year)	Maximum (pCi L^{-1})	Time (year)	Maximum (pCi L^{-1})	Time (year)
Ag-108m	-	1.21E-01	4,006	1.15E-01	4,296	1.21E-01	3,996	1.18E-01	4,006	4.23E-01	3,656
Am-241	Np-237	6.34E-02	3,496	6.36E-02	3,496	6.34E-02	3,496	6.20E-02	3,496	6.63E-02	2,500
Am-241	U-233	1.75E-05	28,400	1.68E-05	28,800	1.75E-05	28,300	1.71E-05	28,400	1.02E-05	27,400
Am-241	Th-229	3.49E-06	32,100	3.41E-06	32,600	3.48E-06	32,000	3.43E-06	32,200	2.17E-06	30,900
C-14	-	1.23E+02	3,106	8.66E+01	3,256	1.22E+02	3,106	1.16E+02	3,096	1.08E+02	3,076
Ca-41	-	1.91E+02	2,396	1.20E+02	2,793	1.89E+02	2,391	1.81E+02	2,432	1.85E+02	2,391
Cl-36	-	3.43E+02	1,546	2.71E+02	1,730	3.36E+02	1,543	3.33E+02	1,616	3.39E+02	1,548
Cm-245	Np-237	2.24E-01	3,496	2.22E-01	3,496	2.24E-01	3,496	2.23E-01	3,496	1.34E-01	2,506
Cm-245	U-233	5.51E-05	28,600	5.37E-05	28,700	5.46E-05	28,500	5.43E-05	28,500	3.59E-05	27,600
Cm-245	Th-229	1.22E-05	32,400	1.19E-05	32,500	1.20E-05	32,200	1.20E-05	32,200	8.56E-06	31,800
Cs-137	-	1.51E-29	2,443	3.54E-31	2,530	1.62E-29	2,437	2.20E-30	2,530	1.41E-29	2,443
H-3	-	3.02E-06	71	7.16E-06	71	2.48E-06	71	2.46E-06	71	3.02E-06	71
I-129	-	4.60E+02	1,204	4.86E+02	1,272	4.27E+02	1,202	6.77E+02	1,219	4.60E+02	1,204
K-40	-	1.42E+02	2,820	1.32E+02	3,246	1.42E+02	2,820	1.44E+02	2,876	1.43E+02	2,820
Ni-59	-	1.14E+02	3,516	9.70E+01	3,856	1.10E+02	3,506	1.17E+02	3,596	1.39E+02	3,516
Ni-63	-	2.57E-08	2,793	2.70E-09	3,326	3.59E-08	2,741	8.16E-09	3,266	1.82E-08	2,857
Np-237	-	3.13E+02	3,496	3.16E+02	3,496	3.12E+02	3,496	3.03E+02	3,496	3.42E+02	2,500
Np-237	U-233	1.07E-01	28,400	1.01E-01	29,000	1.06E-01	28,400	1.04E-01	28,500	6.96E-02	27,600
Np-237	Th-229	1.15E-07	32,200	1.12E-07	32,900	1.15E-07	32,100	1.13E-07	32,300	7.11E-08	31,200
Pu-239	U-235	7.01E-05	39,000	8.10E-05	35,800	7.60E-05	35,600	7.60E-05	35,600	7.54E-05	35,800
Pu-239	Pa-231	3.89E-05	33,300	3.92E-05	32,800	3.85E-05	32,200	3.85E-05	32,200	3.84E-05	32,100
Pu-239	Ac-227	1.06E-07	29,300	1.07E-07	28,800	1.04E-07	28,200	1.04E-07	28,200	1.04E-07	28,200
Pu-241	Np-237	2.11E-03	3,496	2.11E-03	3,496	2.10E-03	3,496	2.06E-03	3,496	2.20E-03	2,500
Pu-241	U-233	5.76E-07	28,400	5.53E-07	28,700	5.75E-07	28,300	5.63E-07	28,400	3.33E-07	27,400
Pu-241	Th-229	1.15E-07	32,100	1.12E-07	32,600	1.15E-07	32,000	1.13E-07	32,200	7.11E-08	30,900
Ra-226	-	5.61E-01	9,000	3.86E-01	9,650	5.61E-01	9,000	5.54E-01	9,010	6.46E-01	8,770
Ra-226	Pb-210	1.69E-02	9,390	1.18E-02	10,138	1.69E-02	9,380	1.67E-02	9,400	1.94E-02	9,160

Notes:

Reference point for time is start of LAWV operations in late 1994; the compliance period is from Year 171 to Year 1,171.

Table 5-20 (cont'd). Peak Concentration at 100-meter POA and Time of Occurrence for Nominal PA, Best Estimate, and Sensitivity Cases for Low-Activity Waste Vault

Radionuclide		Nominal PA Case		Best Estimate Case		Sensitivity Case 1 Concrete Cracking		Sensitivity Case 2 Degraded Concrete		Sensitivity Case 3 Concrete Aging	
Parent	Progeny	Maximum (pCi L^{-1})	Time (year)	Maximum (pCi L^{-1})	Time (year)	Maximum (pCi L^{-1})	Time (year)	Maximum (pCi L^{-1})	Time (year)	Maximum (pCi L^{-1})	Time (year)
Sr-90	-	8.42E-23	2,097	5.63E-23	2,080	8.90E-23	2,091	1.62E-22	2,071	1.05E-21	1,987
Tc-99	-	1.93E+02	3,166	2.31E+02	3,166	1.86E+02	3,156	2.29E+02	3,166	1.26E+03	1,945
U-235	-	8.99E+00	28,700	8.86E+00	29,500	8.99E+00	28,700	8.97E+00	28,700	9.01E+00	28,200
U-235	Pa-231	2.02E+01	3,496	2.00E+01	3,496	2.01E+01	3,496	2.00E+01	3,496	1.35E+01	2,506
U-235	Ac-227	5.60E-02	3,526	5.54E-02	3,526	5.59E-02	3,526	5.54E-02	3,526	3.76E-02	2,536

Notes:

Reference point for time is start of LAWV operations in late 1994; the compliance period is from Year 171 to Year 1,171.

Table 5-21. Peak Concentration at 100-meter POA and Time of Occurrence for Nominal PA and Sensitivity Cases 4 to 7 for Low-Activity Waste Vault

Radionuclide		Nominal PA Case		Sensitivity Case 4 LVZ Porosity		Sensitivity Case 5 Waste Porosity		Sensitivity Case 6 Infiltration		Sensitivity Case 7 K_d Values	
Parent	Progeny	Maximum (pCi L^{-1})	Time (year)	Maximum (pCi L^{-1})	Time (year)	Maximum (pCi L^{-1})	Time (year)	Maximum (pCi L^{-1})	Time (year)	Maximum (pCi L^{-1})	Time (year)
Ag-108m	-	1.21E-01	4,006	1.23E-01	3,996	1.16E-01	4,286	3.00E-01	3,586	8.93E-01	2,857
Am-241	Np-237	6.34E-02	3,496	6.34E-02	3,496	6.41E-02	3,496	7.22E-02	3,366	8.50E-02	3,286
Am-241	U-233	1.75E-05	28,400	1.76E-05	28,000	1.70E-05	28,700	1.93E-05	22,300	3.53E-05	15,689
Am-241	Th-229	3.49E-06	32,100	3.51E-06	31,700	3.44E-06	32,500	3.65E-06	25,900	4.77E-06	18,382
C-14	-	1.23E+02	3,106	1.23E+02	3,106	9.09E+01	3,226	1.02E+02	2,716	1.83E+02	2,199
Ca-41	-	1.91E+02	2,396	1.91E+02	2,387	1.07E+02	2,741	2.17E+02	1,991	3.27E+02	1,730
Cl-36	-	3.43E+02	1,546	3.43E+02	1,545	2.42E+02	1,699	4.87E+02	1,216	5.80E+02	1,201
Cm-245	Np-237	2.24E-01	3,496	2.24E-01	3,496	2.23E-01	3,496	2.56E-01	3,366	3.11E-01	3,286
Cm-245	U-233	5.51E-05	28,600	5.48E-05	28,200	5.39E-05	28,700	5.47E-05	22,500	8.35E-05	15,756
Cm-245	Th-229	1.22E-05	32,400	1.20E-05	31,900	1.20E-05	32,500	1.10E-05	26,200	1.22E-05	19,159
Cs-137	-	1.51E-29	2,443	2.04E-29	2,432	2.42E-30	2,443	6.16E-25	2,061	2.76E-21	1,936
H-3	-	3.02E-06	71	2.23E-06	71	6.78E-06	71	3.64E-06	71	3.02E-06	71
I-129	-	4.60E+02	1,204	4.50E+02	1,202	5.31E+02	1,215	5.71E+02	921	5.75E+02	960

Notes:

Reference point for time is start of LAWV operations in late 1994; the compliance period is from Year 171 to Year 1,171.

Table 5-21 (cont'd). Peak Concentration at 100-meter POA and Time of Occurrence for Nominal PA and Sensitivity Cases 4 to 7 for Low-Activity Waste Vault

Radionuclide		Nominal PA Case		Sensitivity Case 4 LVZ Porosity		Sensitivity Case 5 Waste Porosity		Sensitivity Case 6 Infiltration		Sensitivity Case 7 K_d Values	
Parent	Progeny	Maximum (pCi L^{-1})	Time (year)	Maximum (pCi L^{-1})	Time (year)	Maximum (pCi L^{-1})	Time (year)	Maximum (pCi L^{-1})	Time (year)	Maximum (pCi L^{-1})	Time (year)
K-40	-	1.42E+02	2,820	1.42E+02	2,811	1.27E+02	3,236	1.61E+02	2,299	2.54E+02	1,943
Ni-59	-	1.14E+02	3,516	1.14E+02	3,506	9.50E+01	3,826	8.94E+01	2,848	1.40E+02	2,303
Ni-63	-	2.57E-08	2,793	2.77E-08	2,784	4.70E-09	2,829	2.16E-06	2,327	5.12E-05	2,032
Np-237	-	3.13E+02	3,496	3.13E+02	3,496	3.20E+02	3,496	3.56E+02	3,366	4.16E+02	3,286
Np-237	U-233	1.07E-01	28,400	1.07E-01	28,100	1.02E-01	28,900	1.18E-01	22,300	2.18E-01	15,689
Np-237	Th-229	1.15E-07	32,200	1.16E-07	31,800	1.14E-07	32,800	1.20E-07	25,900	1.57E-07	18,476
Pu-239	U-235	7.01E-05	39,000	7.61E-05	35,300	8.09E-05	35,800	7.64E-05	28,600	9.36E-05	18,197
Pu-239	Pa-231	3.89E-05	33,300	3.82E-05	31,900	3.92E-05	32,800	3.42E-05	3,376	4.16E-05	3,286
Pu-239	Ac-227	1.06E-07	29,300	1.03E-07	27,900	1.07E-07	28,800	9.36E-08	3,406	1.18E-07	3,316
Pu-241	Np-237	2.11E-03	3,496	2.10E-03	3,496	2.13E-03	3,496	2.40E-03	3,366	2.82E-03	3,286
Pu-241	U-233	5.76E-07	28,400	5.80E-07	28,000	5.60E-07	28,700	6.35E-07	22,300	1.16E-06	15,689
Pu-241	Th-229	1.15E-07	32,100	1.16E-07	31,700	1.14E-07	32,500	1.20E-07	25,900	1.57E-07	18,382
Ra-226	-	5.61E-01	9,000	5.68E-01	8,970	3.87E-01	9,650	1.82E+00	7,040	5.13E+00	5,580
Ra-226	Pb-210	1.69E-02	9,390	1.71E-02	9,360	1.18E-02	10,127	5.22E-02	7,390	1.67E-01	5,800
Sr-90	-	8.42E-23	2,097	1.00E-22	2,091	3.84E-23	2,109	5.58E-20	1,647	1.82E-17	1,724
Tc-99	-	1.93E+02	3,166	1.92E+02	3,166	1.95E+02	3,156	1.07E+02	3,126	8.19E+01	1,808
U-235	-	8.99E+00	28,700	9.04E+00	28,400	8.86E+00	29,500	9.72E+00	22,500	1.80E+01	15,756
U-235	Pa-231	2.02E+01	3,496	2.01E+01	3,496	2.00E+01	3,496	2.29E+01	3,366	2.74E+01	3,286
U-235	Ac-227	5.60E-02	3,526	5.59E-02	3,526	5.56E-02	3,526	6.26E-02	3,396	7.76E-02	3,316

Notes:

Reference point for time is start of LAWV operations in late 1994; the compliance period is from Year 171 to Year 1,171.

Table 5-22. Ratios of Peak Concentrations for Low-Activity Waste Vault at 100-meter POA for Best Estimate and Sensitivity Cases to Nominal PA Case

Radionuclide		Best	Sensitivity Cases						
Parent	Progeny	Estimate	1	2	3	4	5	6	7
Ag-108m	-	0.95	1.00	0.98	3.49	1.02	0.96	2.48	7.38
Am-241	Np-237	1.00	1.00	0.98	1.04	1.00	1.01	1.14	1.34
Am-241	U-233	0.96	1.00	0.98	0.58	1.01	0.97	1.10	2.02
Am-241	Th-229	0.98	1.00	0.98	0.62	1.00	0.99	1.04	1.37
C-14	-	0.71	1.00	0.95	0.88	1.00	0.74	0.83	1.50
Ca-41	-	0.63	0.99	0.95	0.97	1.00	0.56	1.14	1.71
Cl-36	-	0.79	0.98	0.97	0.99	1.00	0.71	1.42	1.69
Cm-245	Np-237	0.99	1.00	1.00	0.60	1.00	0.99	1.14	1.39
Cm-245	U-233	0.98	0.99	0.99	0.65	1.00	0.98	0.99	1.52
Cm-245	Th-229	0.98	0.99	0.98	0.70	0.99	0.98	0.91	1.00
Cs-137	-	0.02	1.07	0.15	0.93	1.35	0.16	4.07E+04	1.82E+08
H-3	-	2.37	0.82	0.82	1.00	0.74	2.25	1.21	1.00
I-129	-	1.06	0.93	1.47	1.00	0.98	1.15	1.24	1.25
K-40	-	0.93	0.99	1.01	1.01	1.00	0.89	1.13	1.78
Ni-59	-	0.85	0.97	1.03	1.22	1.00	0.83	0.79	1.23
Ni-63	-	0.11	1.40	0.32	0.71	1.08	0.18	83.8	1991
Np-237	-	1.01	0.99	0.97	1.09	1.00	1.02	1.14	1.33
Np-237	U-233	0.95	0.99	0.97	0.65	1.01	0.96	1.11	2.04
Np-237	Th-229	0.98	1.00	0.98	0.62	1.00	0.99	1.04	1.37
Pu-239	U-235	1.16	1.08	1.08	1.08	1.09	1.15	1.09	1.34
Pu-239	Pa-231	1.01	0.99	0.99	0.99	0.98	1.01	0.88	1.07
Pu-239	Ac-227	1.01	0.99	0.99	0.98	0.98	1.01	0.89	1.12
Pu-241	Np-237	1.00	1.00	0.98	1.04	1.00	1.01	1.14	1.34
Pu-241	U-233	0.96	1.00	0.98	0.58	1.01	0.97	1.10	2.02
Pu-241	Th-229	0.98	1.00	0.98	0.62	1.00	0.99	1.04	1.37

Notes:

Concentrations greater than 10% above the nominal PA case (i.e., an exceedance) are shaded in light green.

Concentrations greater than 10% below the nominal PA case are shaded in light gold.

Radionuclides with concentration ratios greater than 50 are highlighted in yellow.

Table 5-22 (cont'd). Ratios of Peak Concentrations for Low-Activity Waste Vault at 100-meter POA for Best Estimate and Sensitivity Cases to Nominal PA Case

Radionuclide		Best	Sensitivity Cases						
Parent	Progeny	Estimate	1	2	3	4	5	6	7
Ra-226	-	0.69	1.00	0.99	1.15	1.01	0.69	3.24	9.14
Ra-226	Pb-210	0.70	1.00	0.99	1.15	1.01	0.70	3.09	9.90
Sr-90	-	0.67	1.06	1.93	12.48	1.19	0.46	662	2.17E+05
Tc-99	-	1.20	0.96	1.19	6.54	0.99	1.01	0.55	0.42
U-235	-	0.99	1.00	1.00	1.00	1.01	0.99	1.08	2.00
U-235	Pa-231	0.99	1.00	0.99	0.67	1.00	0.99	1.14	1.36
U-235	Ac-227	0.99	1.00	0.99	0.67	1.00	0.99	1.12	1.39

Notes:

Concentrations greater than 10% above the nominal PA case (i.e., an exceedance) are shaded in light green.

Concentrations greater than 10% below the nominal PA case are shaded in light gold.

Radionuclides with concentration ratios greater than 50 are highlighted in yellow.

Table 5-23. Summary of Maximum Concentration Ratios and Number of Concentration Ratios Greater or Less than 1 for Low-Activity Waste Vault Aquifer Zone

Parameter		Best Estimate	Sensitivity Cases						
			1	2	3	4	5	6	7
Maximum Conc. Ratios	Maximum Value	2.37	1.40	1.93	12.48	1.35	2.25	4.07E+04	1.82E+08
	Minimum Value	0.02	0.82	0.15	0.58	0.74	0.16	0.55	0.42
No. of Conc. Ratios < 1	Conc. Ratios < 0.5	2	0	2	0	0	3	0	1
	Conc. Ratios < 0.9	9	1	3	13	1	10	5	1
No. of Conc. Ratios > 1	Conc. Ratios > 1.1	3	1	3	6	2	3	18	28
	Conc. Ratios > 1.5	1	0	1	3	0	1	6	14

Limited Impact

Sensitivity Case 3 – Decreasing the number of pore volume exchanges required for concrete aging lowers the peak concentrations for more than half of the radionuclides. On the other hand, peak concentrations of Ag-108m, Ni-59, Sr-90, Ra-226, and Tc-99 at the 100-meter POA increase.

Sensitivity Case 5 – Lowering waste porosity relative to soil from 0.90 to 0.30 increases peak concentrations at the 100-meter POA by a factor of approximately 2.2 for H-3 and 1.15 for I-129 and Pu-239. Concentrations for most other radionuclides decrease.

Minimal Impact

Sensitivity Case 1 – Doubling the gravel content to simulate an increase in concrete cracking of the vault roof and side walls when the final closure cap is installed increases concrete hydraulic conductivity and porosity without representing through-cracking of the concrete. This change has a minimal impact on peak flux for all radionuclides except H-3 and Ni-63.

Sensitivity Case 2 – Extending concrete hydraulic degradation over 1,000 years instead of the 500-year limit suggested by the PAWG in NUREG-1573 (U.S. NRC, 2000) has a minimal impact on peak flux for all radionuclides except Cs-137, H-3, I-129, Ni-63, Sr-90, and Tc-99.

Sensitivity Case 4 – Increasing soil porosity in the LVZ by one standard deviation has a minimal impact on peak flux for all radionuclides except Cs-137, H-3, and Sr-90.

The best estimate case combines Sensitivity Cases 2 and 5; therefore, the results for this case closely match those of the two sensitivity cases.

The peak concentrations at the 100-meter POA for Cs-137, Ni-63, and Sr-90 are strongly impacted in Sensitivity Cases 6 and 7, as emphasized by the yellow highlighting of the entries in Table 5-22. Cs 137, Ni 63, and Sr 90 have relatively short half-lives of 30.17 years, 101 years, and 28.79 years, respectively. Consequently, any effect that speeds up transport of these isotopes to the 100-meter POA, such as higher flow or lower K_d, significantly impacts concentration because of the difference in decay.

Figure 5-78 through Figure 5-80 show concentration comparisons at the 100-meter POA for the nominal PA case, best estimate case, Sensitivity Case 6, and Sensitivity Case 7 for 15 of the parent radionuclides. In most instances, the nominal PA and best estimate case curves are similar, with the former leading the latter. The sensitivity cases show concentrations at the 100-meter POA peaking both higher and earlier than the nominal PA case. The exceptions are H-3, where the peak best estimate concentration is approximately twice the nominal PA value (obscured by the Sensitivity Case 7 curve, which overlaps it) and Tc-99 where all four cases exhibit a second peak following the collapse of the vault roof in Year 2,976. All four H-3 cases exhibit a sharp, well-defined peak at Year 71 and a broad, lower maximum at around Year 100. These results are consistent with the VZ model results for H-3 where flux at the water table peaks at Year 94 and a

step change in aquifer transport occurs at Year 71 because of placement of an interim cover on adjacent trench DUs. The second peak for Tc-99 is higher than the first for all cases but Sensitivity Case 7. The best estimate case has the highest peak concentration value. In the figures, Cs-137, Ni-63, and Sr-90 are plotted on a semi-log graph to clearly show all four cases.

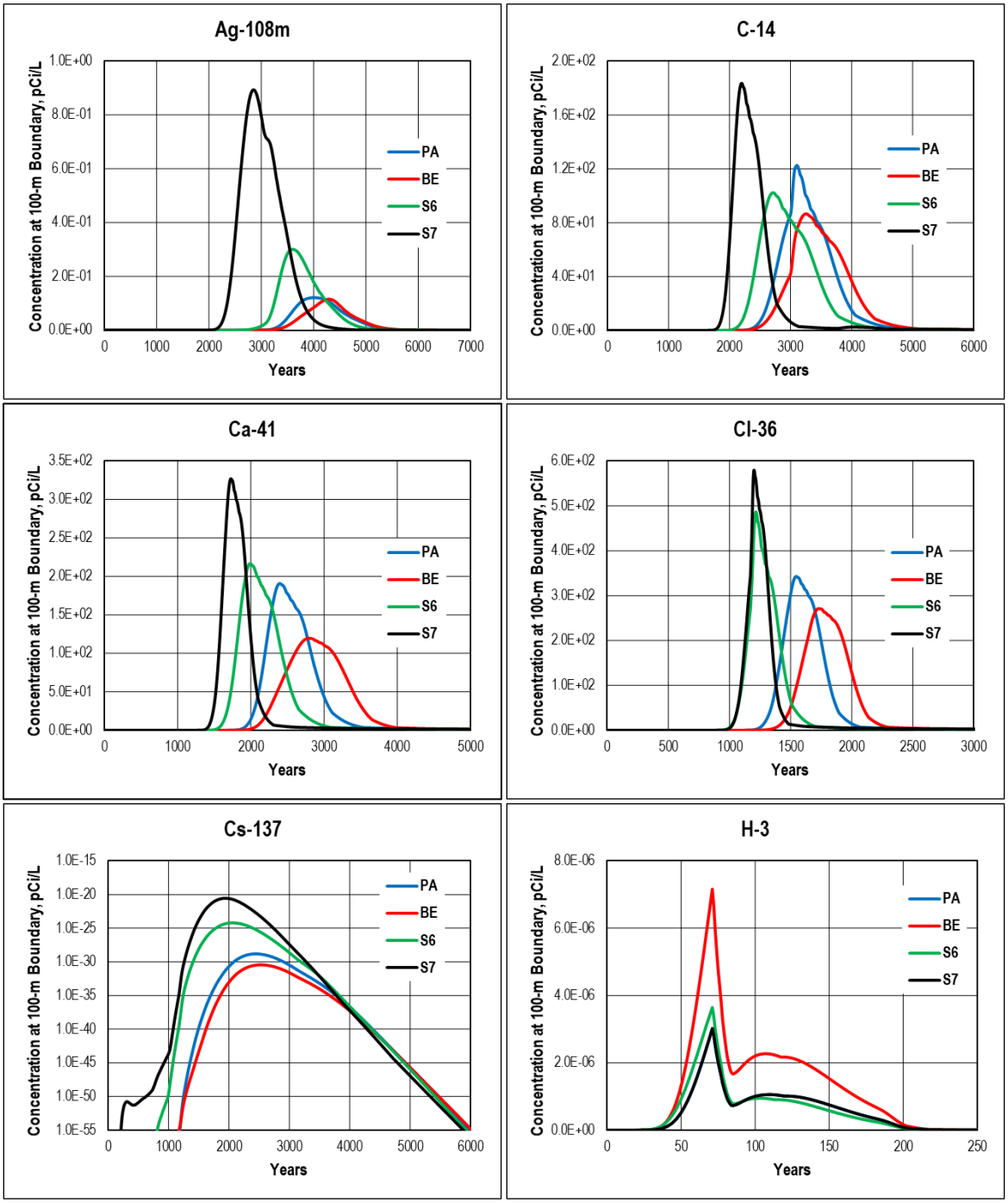

Figure 5-78. Comparison of Nominal PA Case, Best Estimate (BE) Case, Sensitivity Case 6 (S6), and Sensitivity Case 7 (S7) Concentrations for Low-Activity Waste Vault at 100-meter POA for Parent Radionuclides Ag-108m through H-3

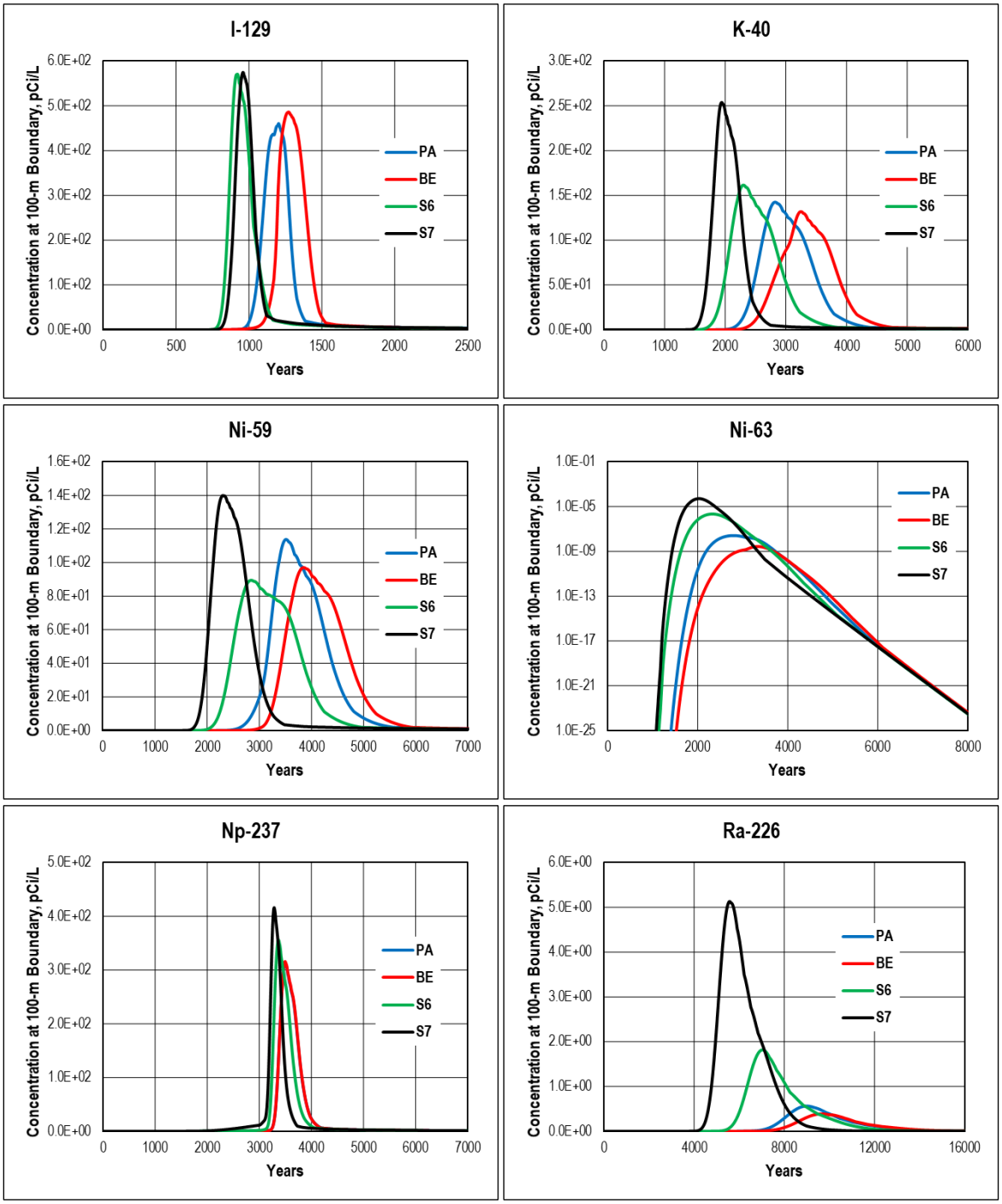

Figure 5-79. Comparison of Nominal PA Case, Best Estimate (BE) Case, Sensitivity Case 6 (S6), and Sensitivity Case 7 (S7) Concentrations for Low-Activity Waste Vault at 100-meter POA for Parent Radionuclides I-129 through Ra-226

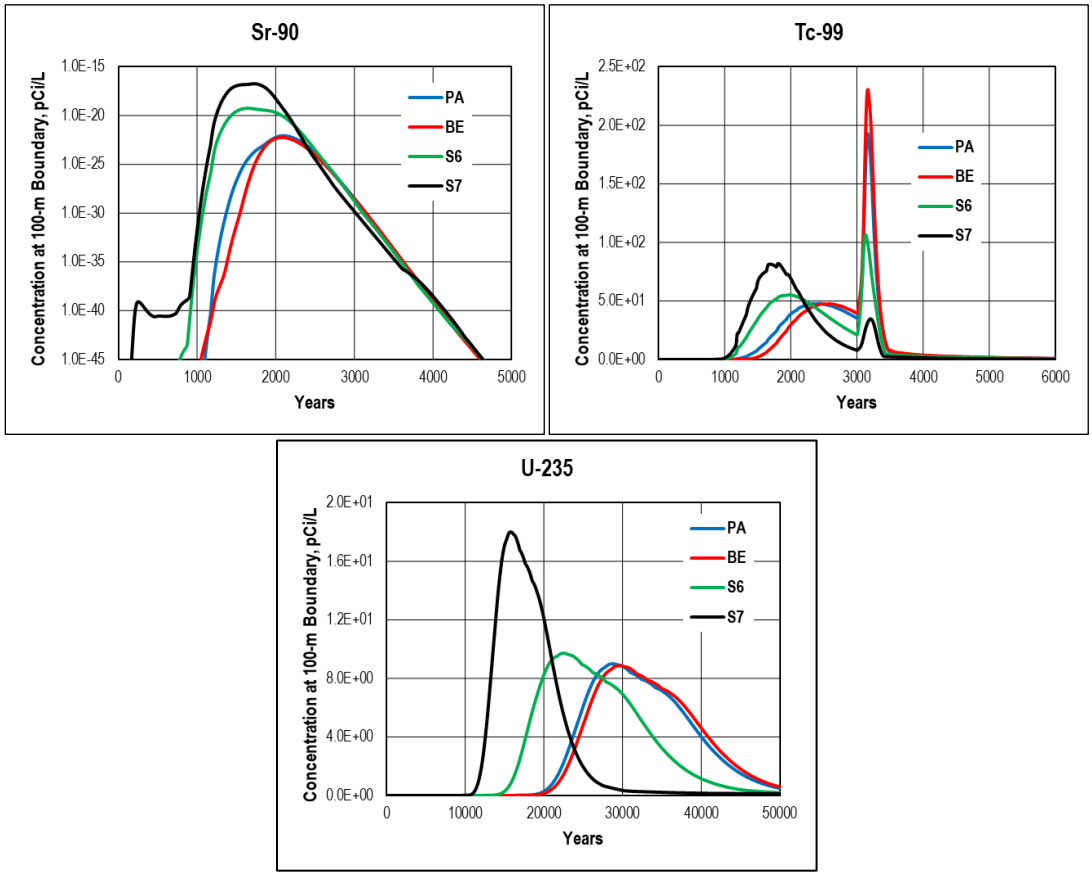

Figure 5-80. Comparison of Nominal PA Case, Best Estimate (BE) Case, Sensitivity Case 6 (S6), and Sensitivity Case 7 (S7) Concentrations for Low-Activity Waste Vault at 100-meter POA for Parent Radionuclides Sr-90 through U-235

The last sensitivity case investigates the impact of increasing the diffusivity of tritium in concrete by one standard deviation (from 2.02 to 2.15 $cm^2\ yr^{-1}$). Results are shown in Figure 5-81. Higher diffusion through the concrete increases the maximum H-3 concentration by 36% at the 100-meter POA (from 3.02E-06 to 4.09E-06 pCi L^{-1} per Ci buried).

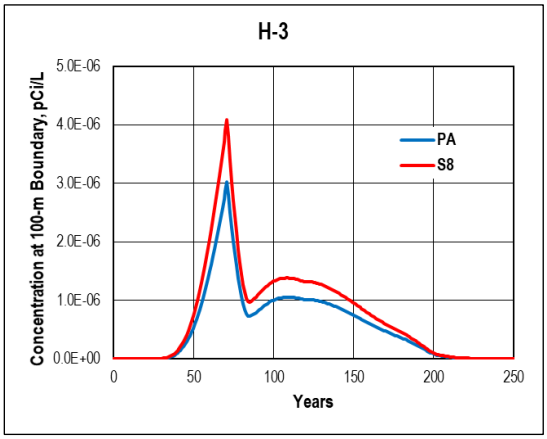

Figure 5-81. Comparison of Nominal PA and Sensitivity Case 8 (S8) Concentrations for Low-Activity Waste Vault at 100-meter POA for Parent Radionuclide H-3

Figure 5-82 through Figure 5-84 show a comparison of 100-meter POA concentrations for the same radionuclides as in Figure 5-78 through Figure 5-80 during the 1,000-year compliance period from Year 171 to Year 1,171.

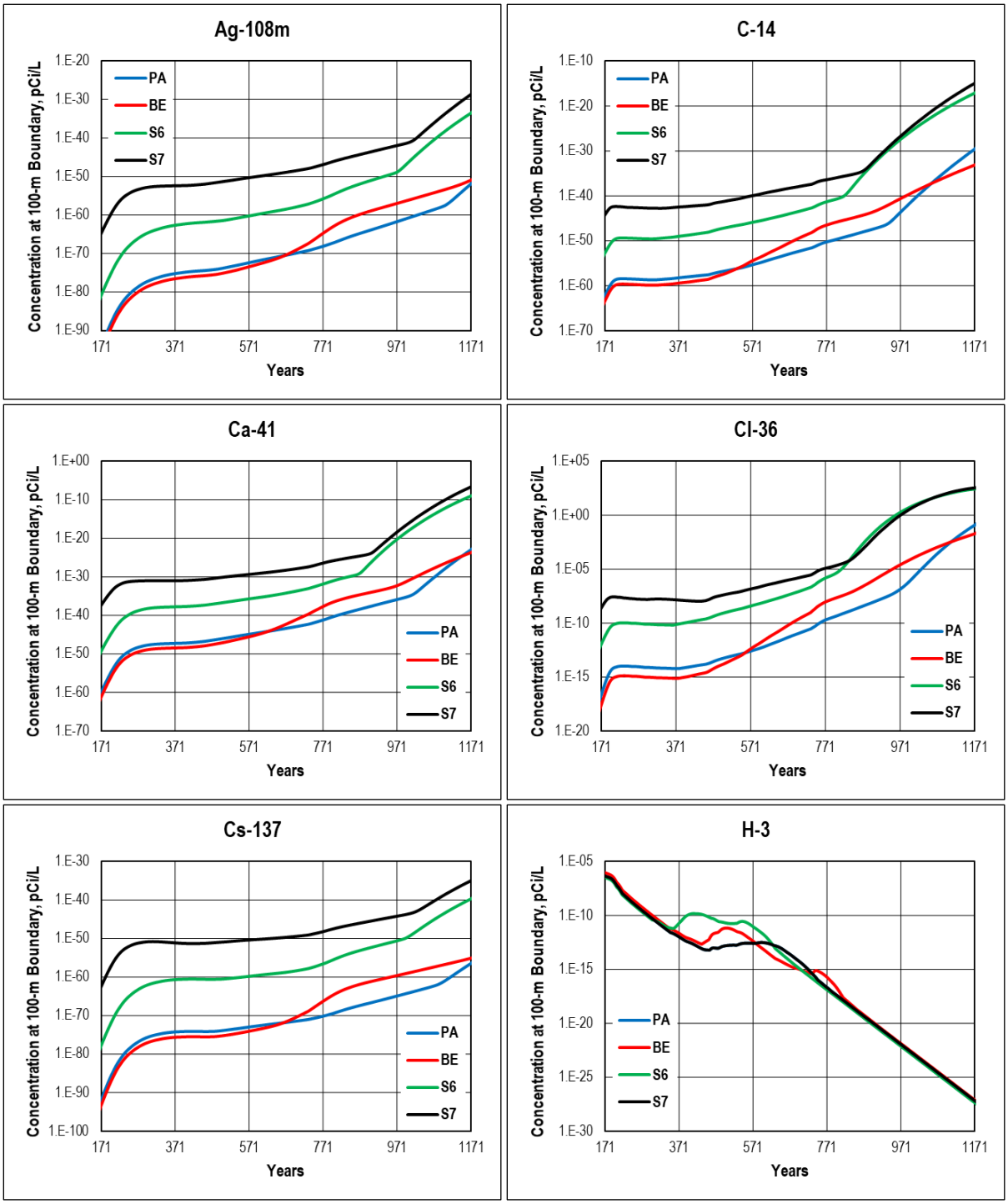

Figure 5-82. Comparison of Nominal PA Case, Best Estimate (BE) Case, Sensitivity Case 6 (S6), and Sensitivity Case 7 (S7) Concentrations for Low-Activity Waste Vault at 100-meter POA for Parent Radionuclides Ag-108m through H-3 During the Compliance Period

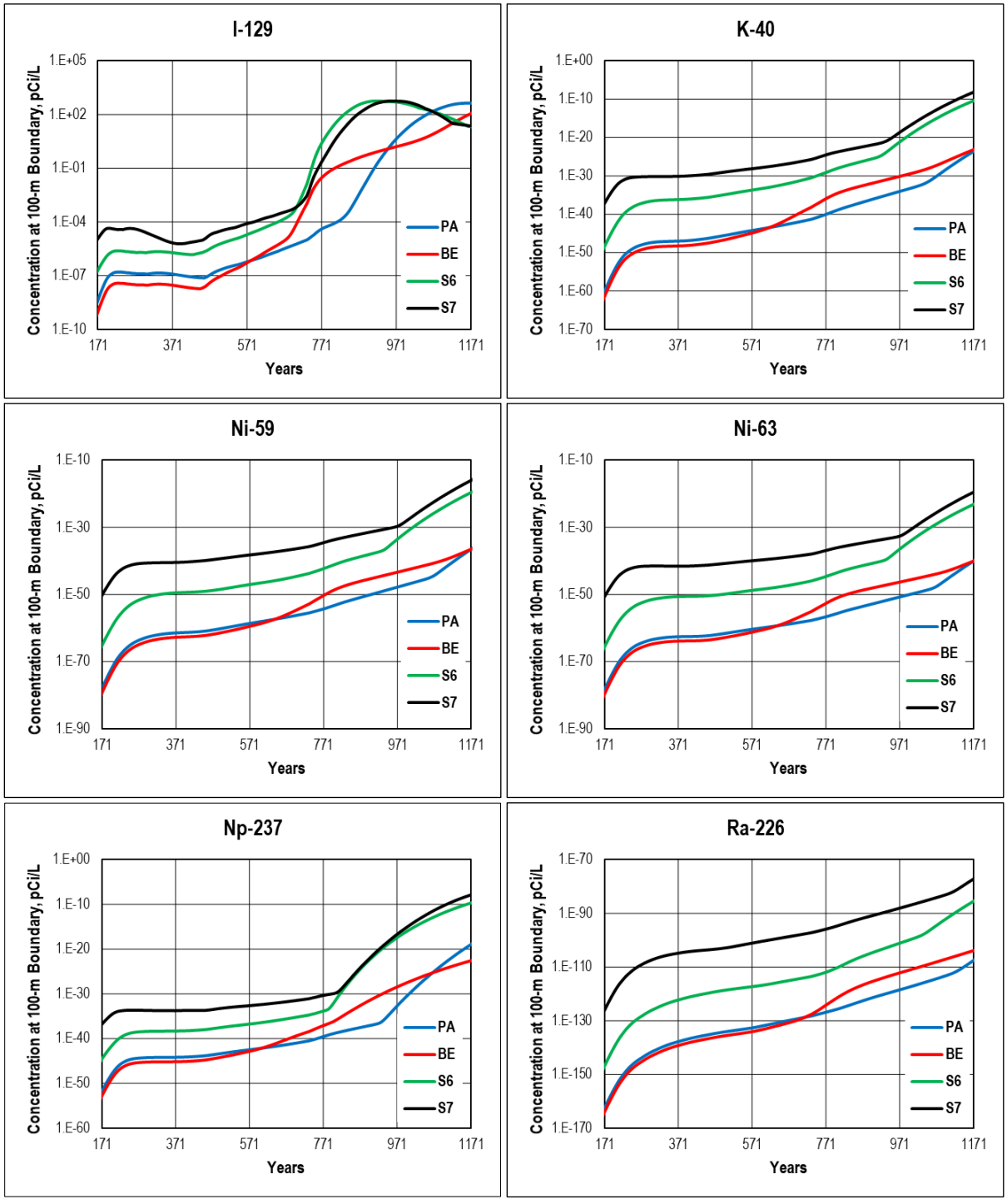

Figure 5-83. Comparison of Nominal PA Case, Best Estimate (BE) Case, Sensitivity Case 6 (S6), and Sensitivity Case 7 (S7) Concentrations for Low-Activity Waste Vault at 100-meter POA for Parent Radionuclides I-129 through Ra-226 During the Compliance Period

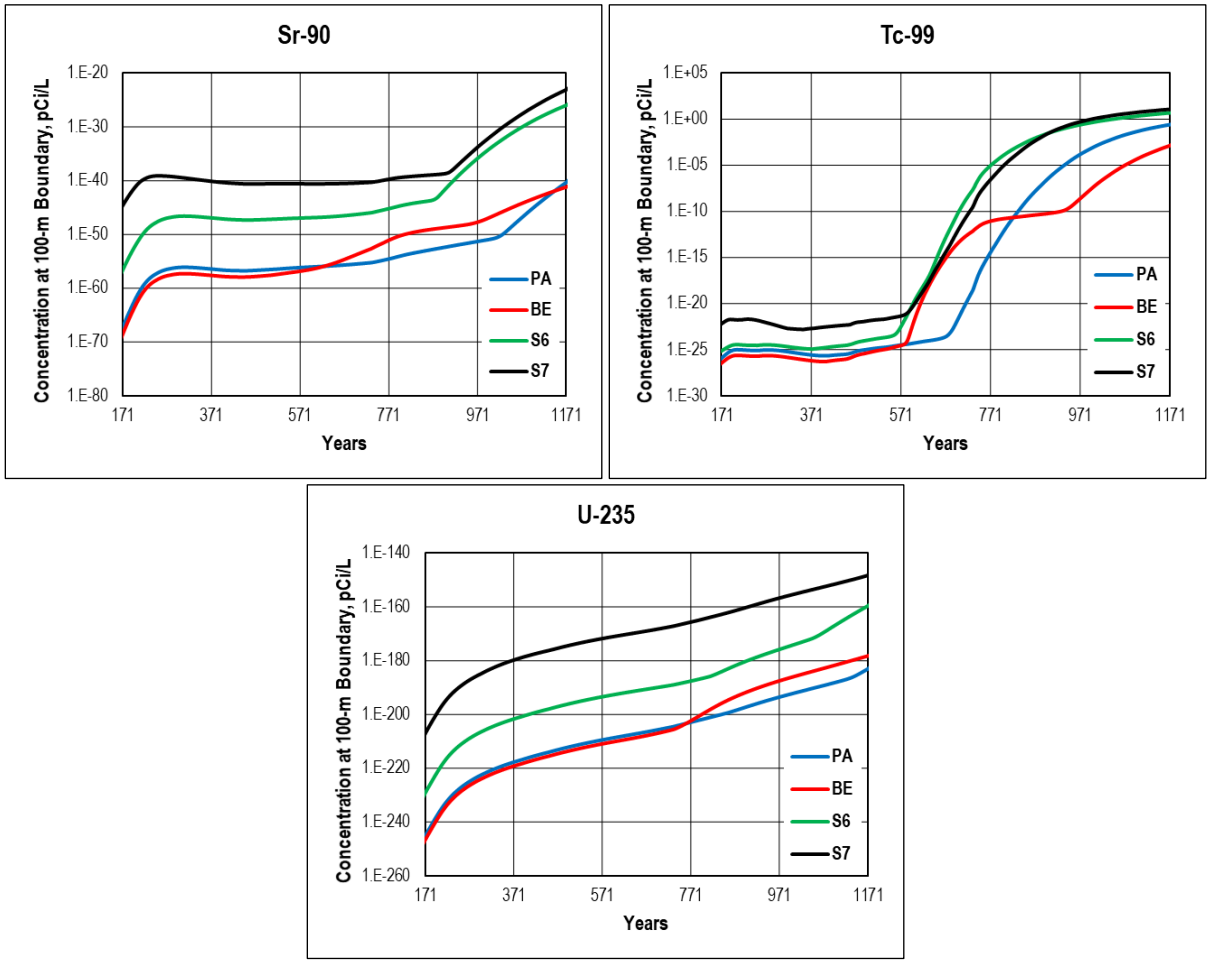

Figure 5-84. Comparison of Nominal PA Case, Best Estimate (BE) Case, Sensitivity Case 6 (S6), and Sensitivity Case 7 (S7) Concentrations for Low-Activity Waste Vault at 100-meter POA for Parent Radionuclides Sr-90 through U-235 During the Compliance Period

In general, the nominal PA and best estimate cases are in close agreement. The exception is H-3 where Sensitivity Case 7 overlaps the nominal PA case. In addition, Sensitivity Cases 6 and 7 have the greatest impact on peak concentrations and generally show significantly higher concentrations at the 100-meter POA during the compliance period. Sensitivity Case 7, which decreases K_d in the VZ and aquifer zone by approximately two standard deviations, has the highest 100-meter POA concentrations. Sensitivity Case 7 is a rough approximation of a 95% confidence bound on radionuclide concentrations. One interesting observation is that the best estimate case curve for most parent radionuclides exceeds the nominal PA case curve for several hundred years from about Year 600 forward. There is no obvious reason for this trend.

The peak concentrations at the 100-meter POA for all decay chains are presented in Figure 5-85 and Figure 5-86. Except for Pu-239 and Ra-226, all decay chains in Figure 5-85 include Np-237, which is likely the leading contributor to the calculated dose from these parent radionuclides.

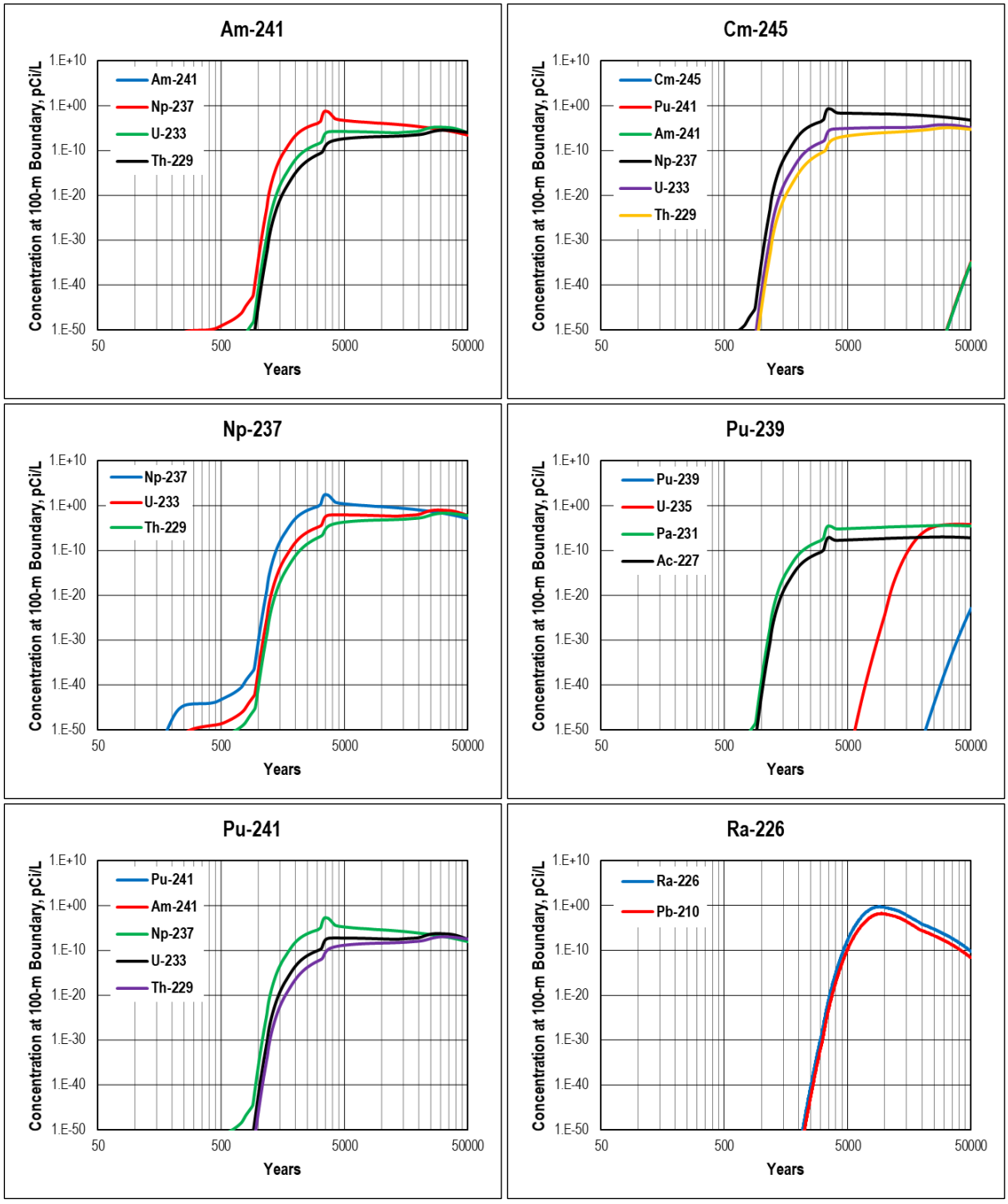

Figure 5-85. Nominal PA Case Concentrations for Low-Activity Waste Vault at 100-meter POA for Decay Chain Parents Am-241 through Ra-226 and Daughter Radionuclides

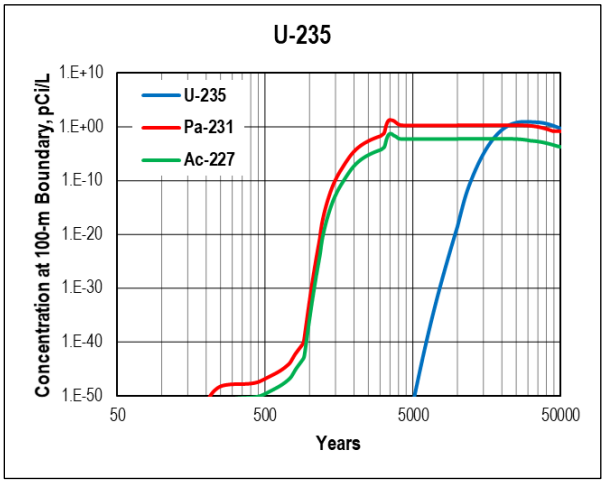

Figure 5-86. Nominal PA Case Concentrations for Low-Activity Waste Vault at 100-meter POA for Decay Chain Parent U-235 and Daughter Radionuclides

5.2.2.2. Concentration Contour Plots

The PORFLOW aquifer model for the LAWV uses a 3-D mesh with 178, 322, and 42 nodes in the x, y, and z coordinate directions, respectively. The x-y grid used by the model is outlined in blue in Figure 5-87 below. A map of the portion of E-Area included in the aquifer cutout is overlain the grid showing the ELLWF DUs outlined in red, the 100-meter POA around the ELLWF, and a stream nearby.

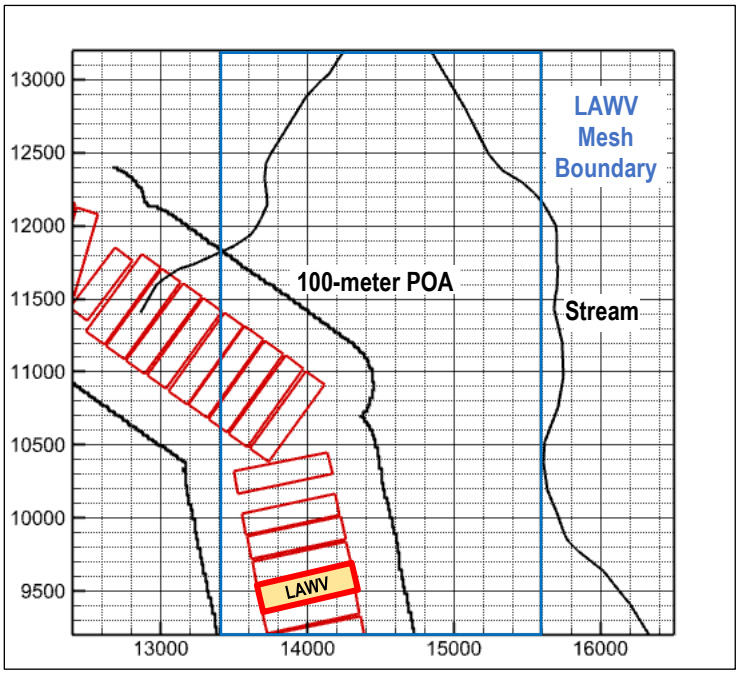

Figure 5-87. Low-Activity Waste Vault Aquifer PORFLOW Model X-Y Grid Overlaid with E-Area Low-Level Waste Facility Features

The movement of radionuclides through the aquifer is best described through contour plots using the ELLWF map scheme in Figure 5-87 to create x-y contours of the maximum concentration (pCi L^{-1} Ci^{-1} parent buried) in the vertical z direction. The PORFLOW aquifer model simulates 50,000 years, starting in 1994 when ELLWF and LAWV operations began. LAWV plume concentrations are saved at only nine discrete times to limit model output to a manageable size: Years 71 (end of operations); 451; 731; 1,171 (end of compliance period); 2,000; 5,000; 10,000; 20,000; and 50,000. Snapshots of the maximum concentration in the z-direction are subsequently plotted. Figure 5-88 through Figure 5-97 illustrate the evolution of plumes of select radionuclides.

Concentration contours for 10 different parent radionuclides are plotted at three different times for both the nominal PA case and one sensitivity case. Figure 5-88 through Figure 5-90 and Figure 5-92 through Figure 5-97 compare the nominal PA case with Sensitivity Case 7 to contrast nominal and worst-case results. Figure 5-91 compares the nominal PA case with the best estimate case for H-3 because worst-case and nominal PA case results for this radionuclide are identical. Three of the four radionuclides omitted from the parent contour plots (Am-241, Cm-245, and Pu-241) have Np-237 as a daughter. In one case, the concentration of Np-237 from decay of these parents is greater than the concentration of Np-237 as a parent itself. Concentration contours for Cs-137 and Sr-90 are not shown because of relatively lower and variable concentrations (Table 5-22). A concentration contour for Ni-63 is omitted because of its extreme variability (Table 5-22).

As seen on these figures, plumes evolve toward the northeast. With distance, some turn toward the northwest after crossing the 100-meter POA and before reaching the stream in the upper right-hand corner of the LAWV mesh boundary. These results are consistent with GW flow direction, which is toward the northeast at shallower depths and the northwest at deeper levels. As the plumes spread, they sink deeper and encounter a change in flow direction.

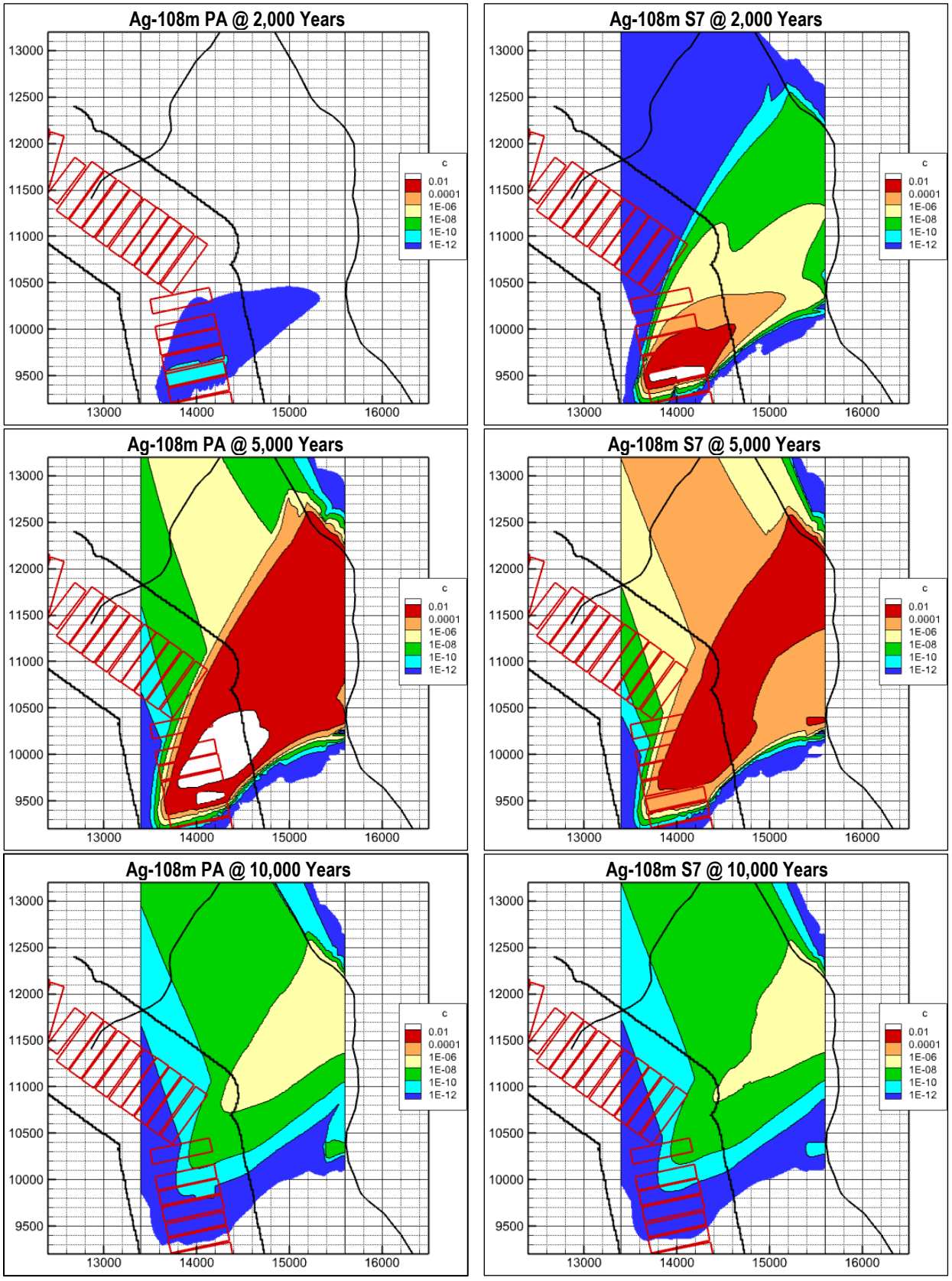

Figure 5-88. Maximum Concentration (pCi L^{-1} Ci^{-1} parent buried) Contours of Ag-108m for Nominal PA Case (left) and Sensitivity Case 7 (right) for Low-Activity Waste Vault

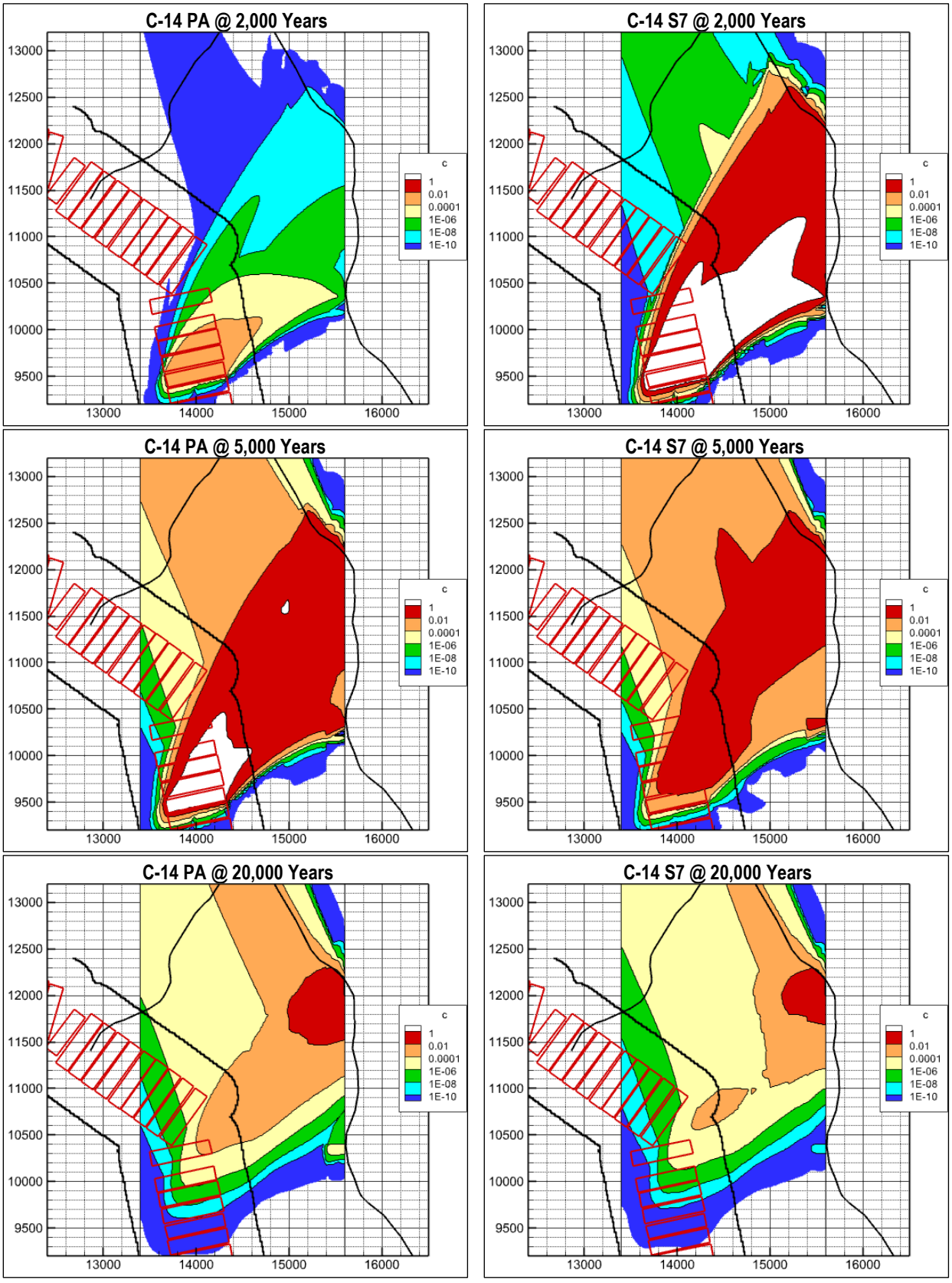

Figure 5-89. Maximum Concentration (pCi L^{-1} Ci^{-1} parent buried) Contours of C-14 for Nominal PA Case (left) and Sensitivity Case 7 (right) for Low-Activity Waste Vault

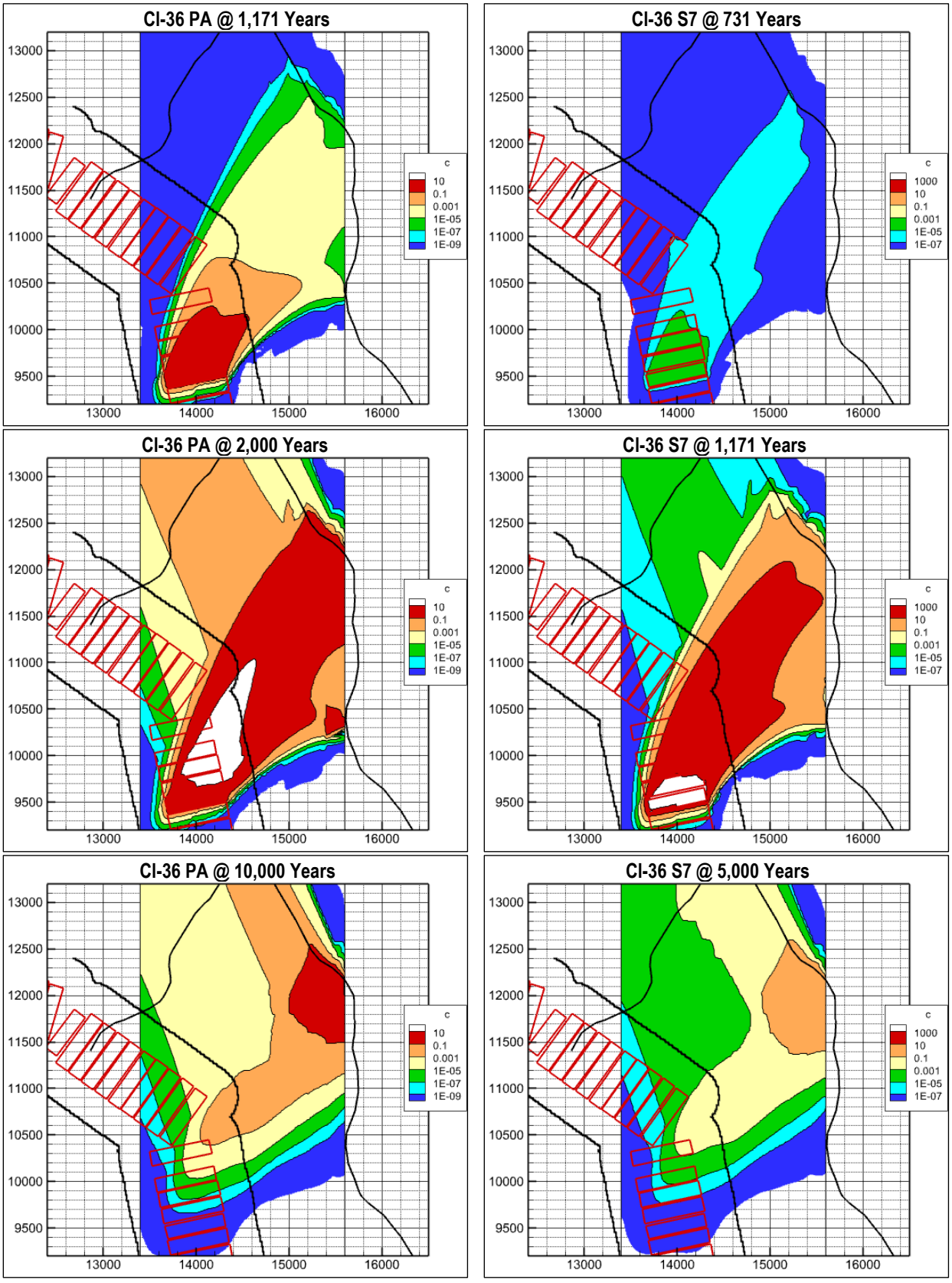

Figure 5-90. Maximum Concentration (pCi L^{-1} Ci^{-1} parent buried) Contours of Cl-36 for Nominal PA Case (left) and Sensitivity Case 7 (right) for Low-Activity Waste Vault

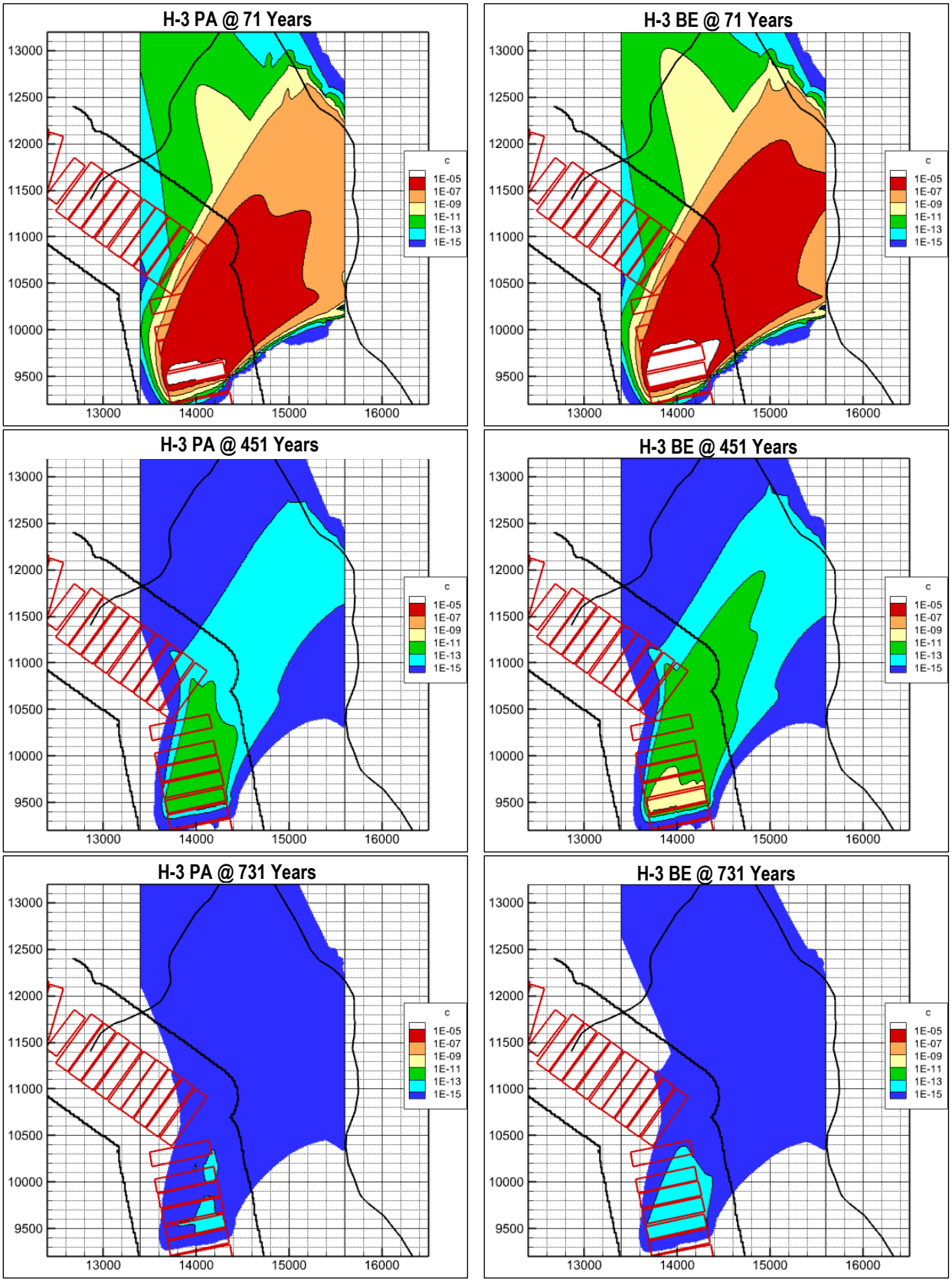

Figure 5-91. Maximum Concentration (pCi L^{-1} Ci^{-1} parent buried) Contours of H-3 for Nominal PA Case (left) and Best Estimate Case (right) for Low-Activity Waste Vault

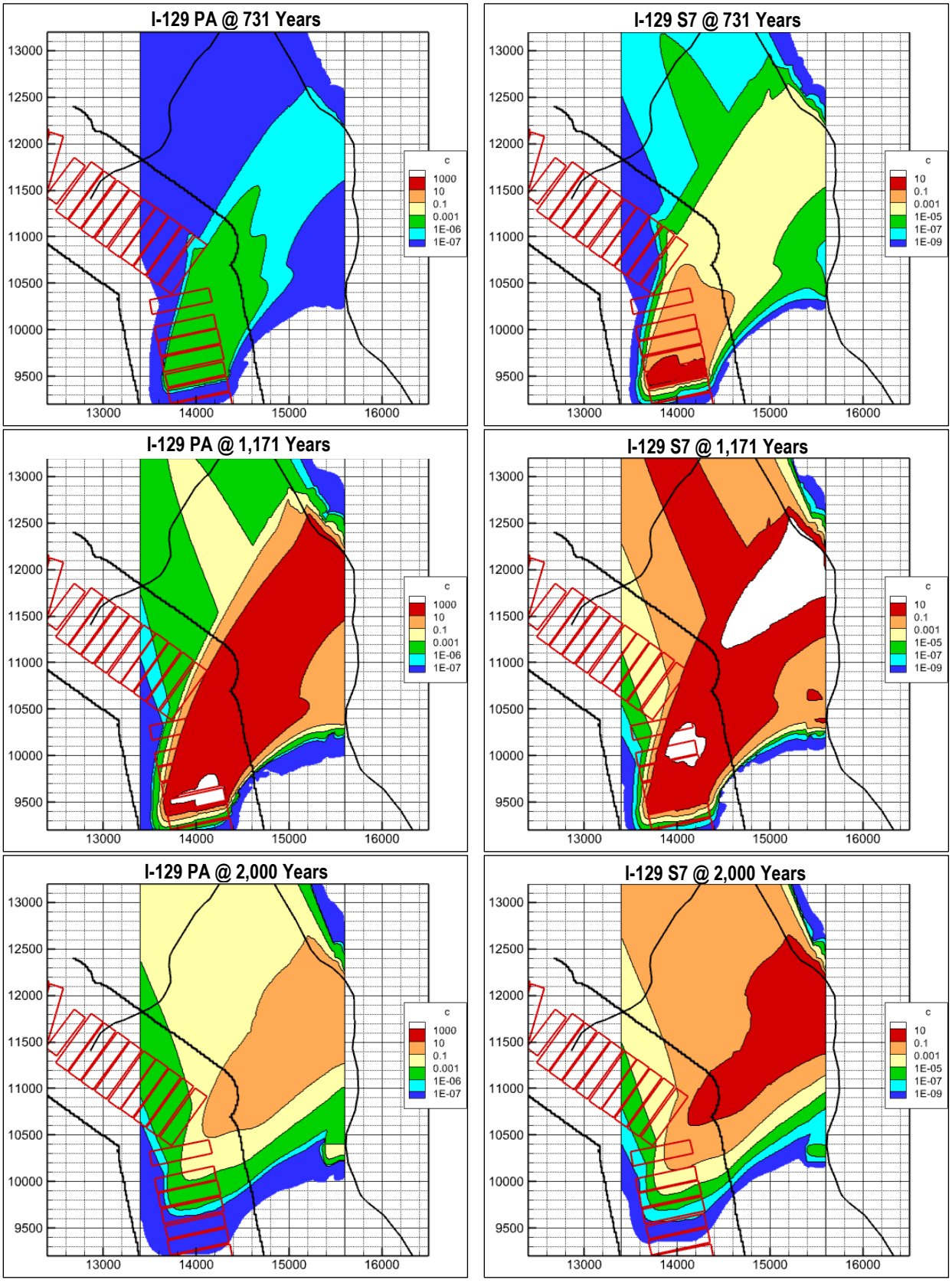

Figure 5-92. Maximum Concentration (pCi L^{-1} Ci^{-1} parent buried) Contours of I-129 for Nominal PA Case (left) and Sensitivity Case 7 (right) for Low-Activity Waste Vault

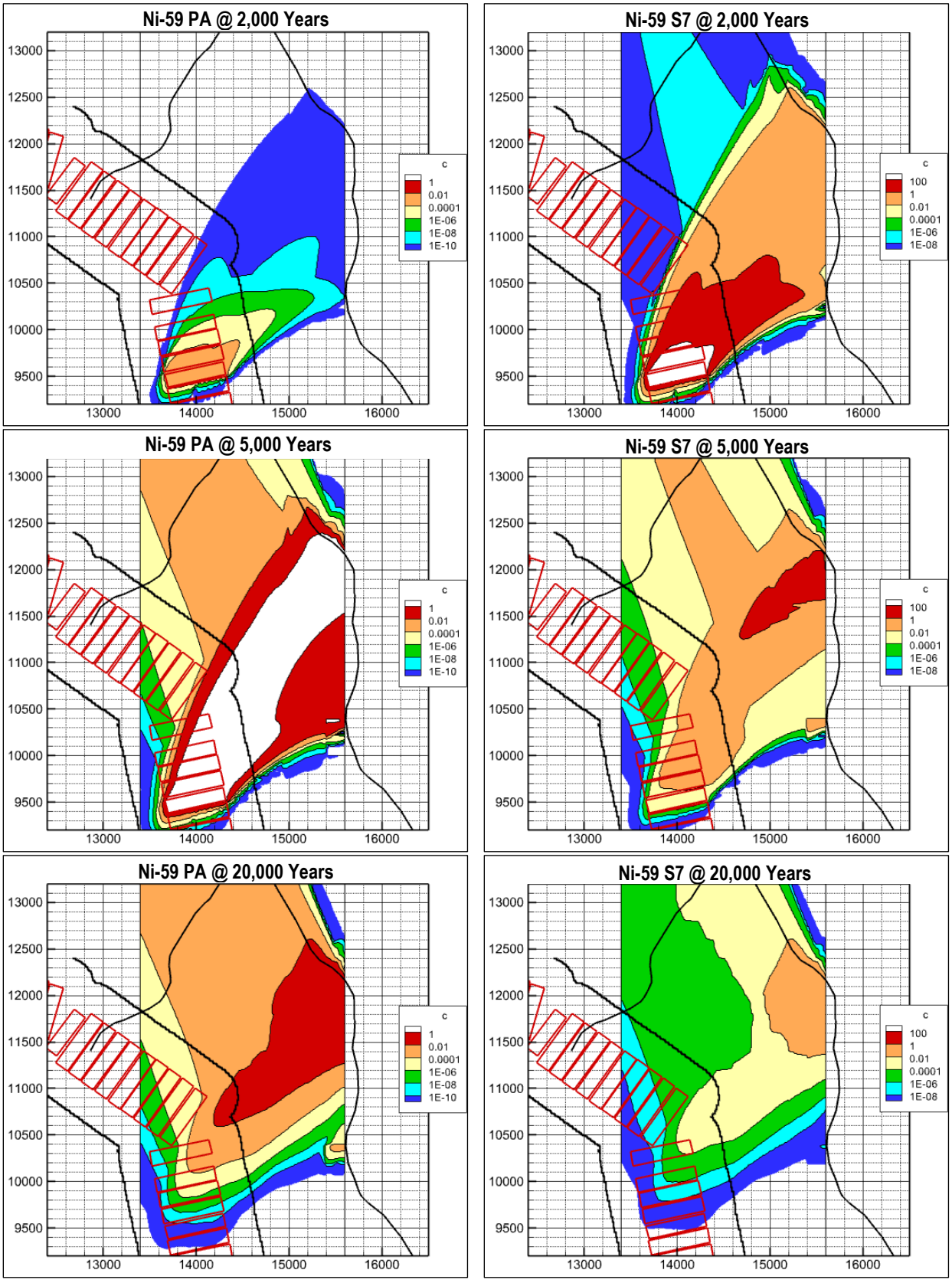

Figure 5-93. Maximum Concentration (pCi L^{-1} Ci^{-1} parent buried) Contours of Ni-59 for Nominal PA Case (left) and Sensitivity Case 7 (right) for Low-Activity Waste Vault

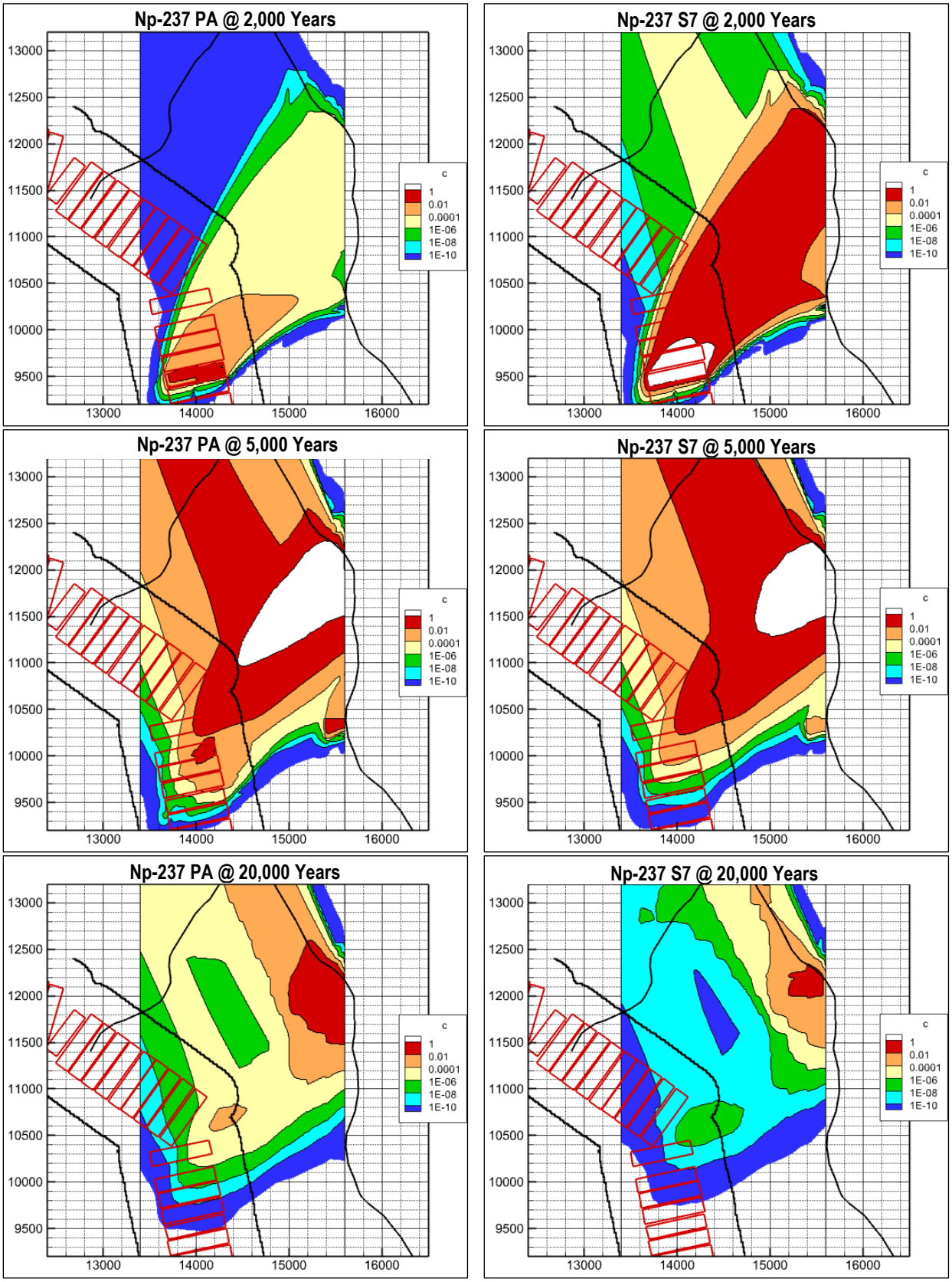

Figure 5-94. Contours of Maximum Concentration (pCi L^{-1} Ci^{-1} parent buried) of Np-237 for Nominal PA Case (left) and Sensitivity Case 7 (right) for Low-Activity Waste Vault

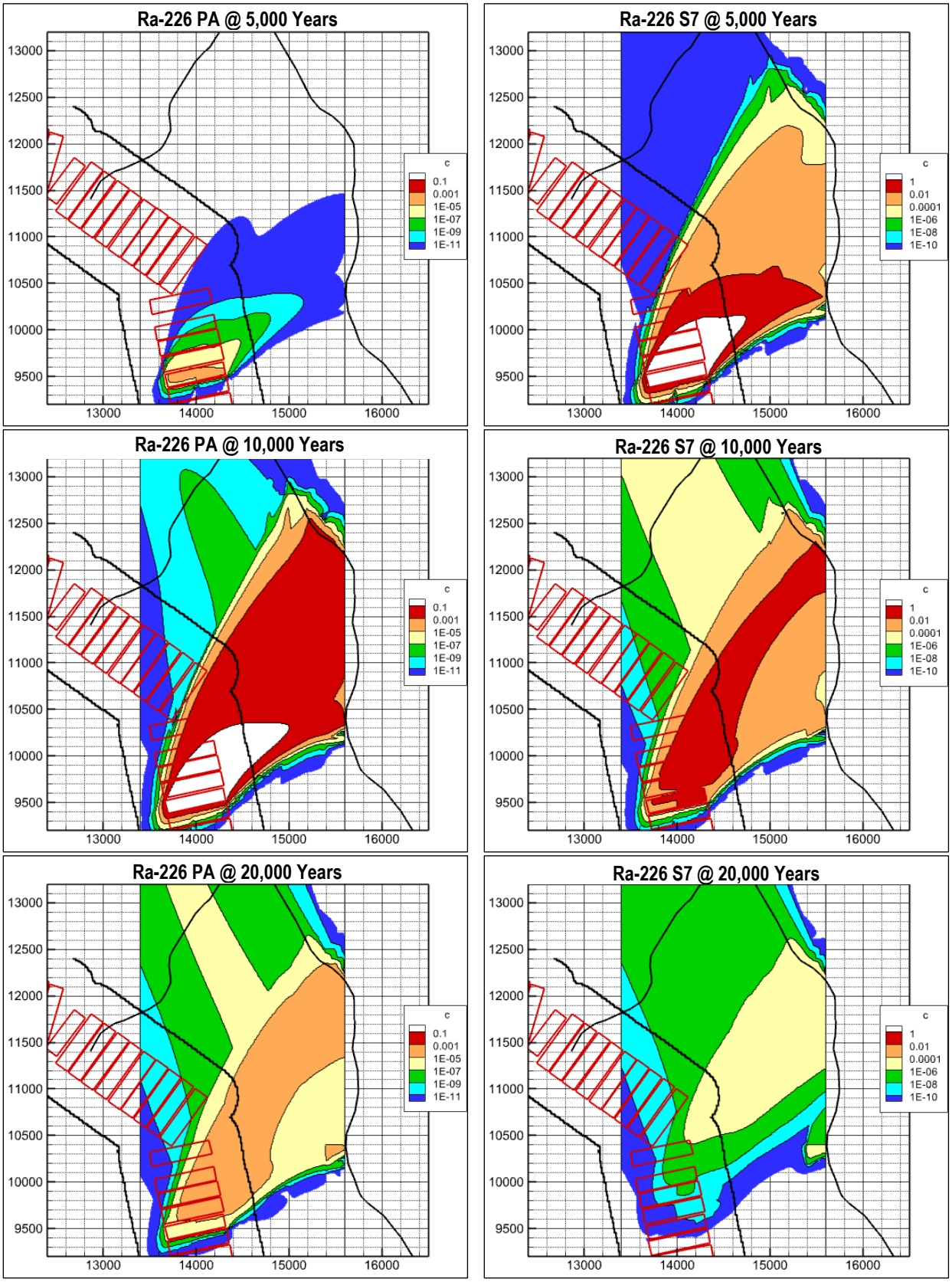

Figure 5-95. Contours of Maximum Concentration (pCi L^{-1} Ci^{-1} parent buried) of Ra-226 for Nominal PA Case (left) and Sensitivity Case 7 (right) for Low-Activity Waste Vault

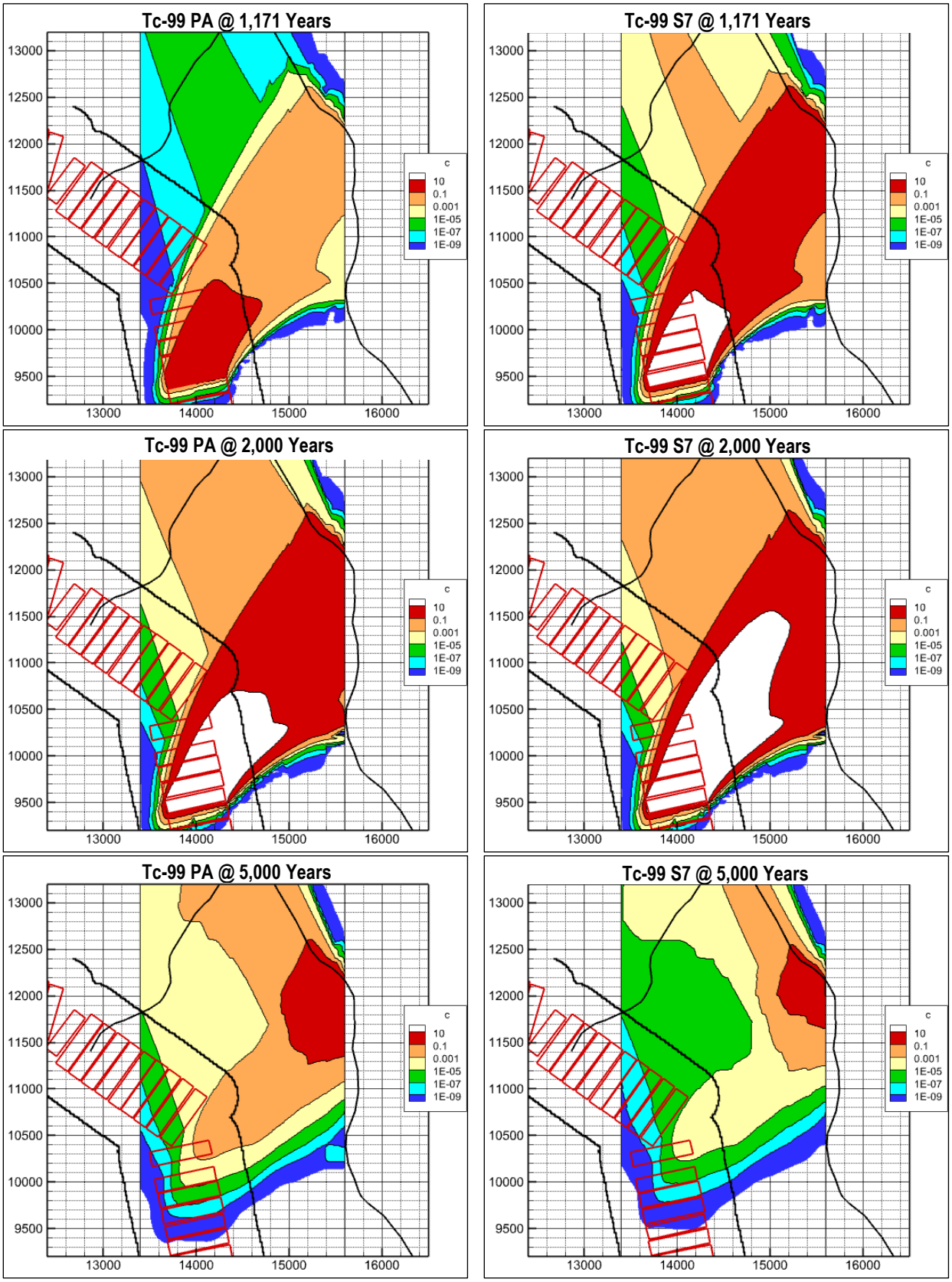

Figure 5-96. Contours of Maximum Concentration (pCi L^{-1} Ci^{-1} parent buried) of Tc-99 for Nominal PA Case (left) and Sensitivity Case 7 (right) for Low-Activity Waste Vault

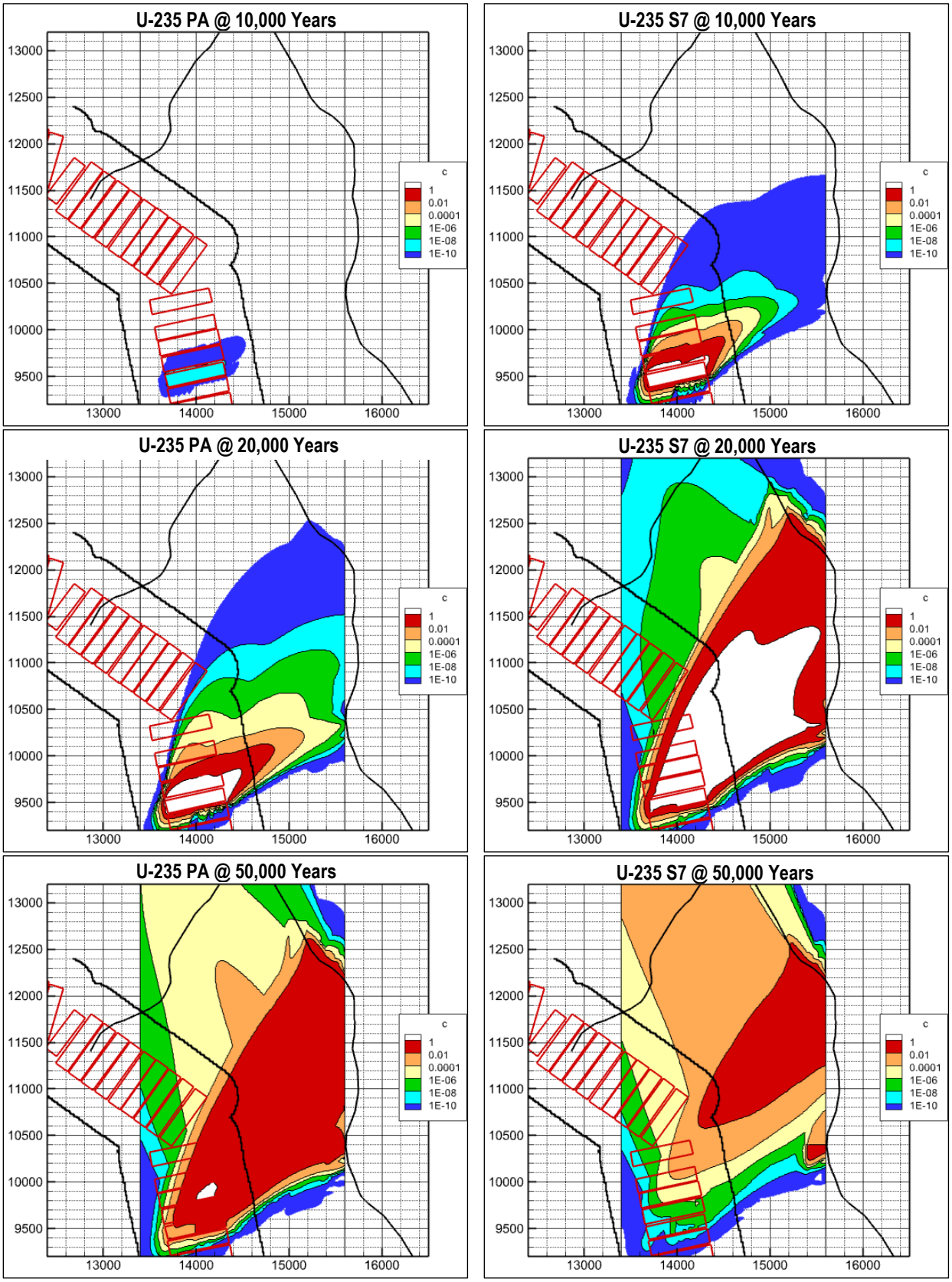

Figure 5-97. Contours of Maximum Concentration (pCi L^{-1} Ci^{-1} parent buried) of U-235 for Nominal PA Case (left) and Sensitivity Case 7 (right) for Low-Activity Waste Vault

5.2.3. Air Pathway and Radon Flux Analyses

This section presents the air pathway and radon flux modeling results for the LAWV. The configuration of the ARM for the LAWV consists of a 1-D vertical stack of cells from the base of the waste zone to a concrete roof. The top of the concrete roof is considered the ground surface before closure. Following closure at Year 171, the roof is linked to the bottom of the closure cap (Section 3.6.1.9) with the top of the erosion barrier considered the ground surface. The pertinent information regarding specific material zones, thicknesses, and properties for the LAWV ARM is provided in Table 5-24. The waste is assumed to be equally distributed throughout the waste zone.

Table 5-24. Layer and Material Properties for Low-Activity Waste Vault Atmospheric Release Model

Layer	Thickness (ft)	Number of Cells	Bulk Dry Density (g cm^{-3})	Porosity	Residual Water Saturation
Before Closure (Year 71 to Year 171)					
LAWV Roof	1.33	8	2.54[a]	0.158[a]	0.823[a]
Waste Zone	24.5	18	0.245[a]	0.9[a]	0.00001[b]
After Closure (Year 171 to Year 1,171)					
Closure Cap	Per Section 3.6.1.9				
LAWV Roof	1.33	8	2.54[a]	0.158[a]	0.823[a]
Waste Zone	24.5	18	0.245[a]	0.9[a]	0.00001[b]

Notes:

[a] From Nichols (2020).

[b] Waste is assumed to be dry resulting in the air-filled porosity equaling the total porosity (WSRC, 2008)

5.2.3.1. Air Pathway

The surface flux time histories of screened-in air pathway radionuclides (C-14 and H-3; Section 2.3.8) generated by the ARM for the LAWV are converted to dose by multiplying by the DRFs of the corresponding time period (Section 3.6.2.2.5). The time histories of these doses are used to determine the grouping (immediate, delayed, or non-factor) of the radionuclide-DU pairs to account for temporal differences in dose impact (Section 8.5). The peak dose and grouping-specific effective PO are used to develop a disposal limit for each radionuclide (Section 8.5). Dose results for the LAWV are presented below.

The surface flux and the resultant dose from 1 Ci of C-14 buried in the LAWV have the greatest impact on the receptor following application of the final closure cap, while H-3 peaks before the end of IC (Table 5-25 and Figure 5-98). C-14, which is solubility limited as it diffuses through the concrete roof, reaches a maximum at the end of the period of performance (Year 1,171). H-3, on the other hand, peaks before the end of IC because it becomes trapped and decays away under the final closure cap beyond Year 171. Note that truncation of the H-3 curve in Year 171 is an artifact of the GoldSim® model, wherein the H-3 dose drops below the model quantification limit of 1.0E-26 mrem yr^{-1} when the final closure cap is installed.

Table 5-25. Peak Doses from 1 Curie of C-14 and H-3 Buried for the Low-Activity Waste Vault Air Pathway

Radionuclide	Peak Dose (mrem yr^{-1} Ci^{-1})	Peak Time (Year)
C-14	8.27E-14	1,171
H-3	2.95E-19	170.99

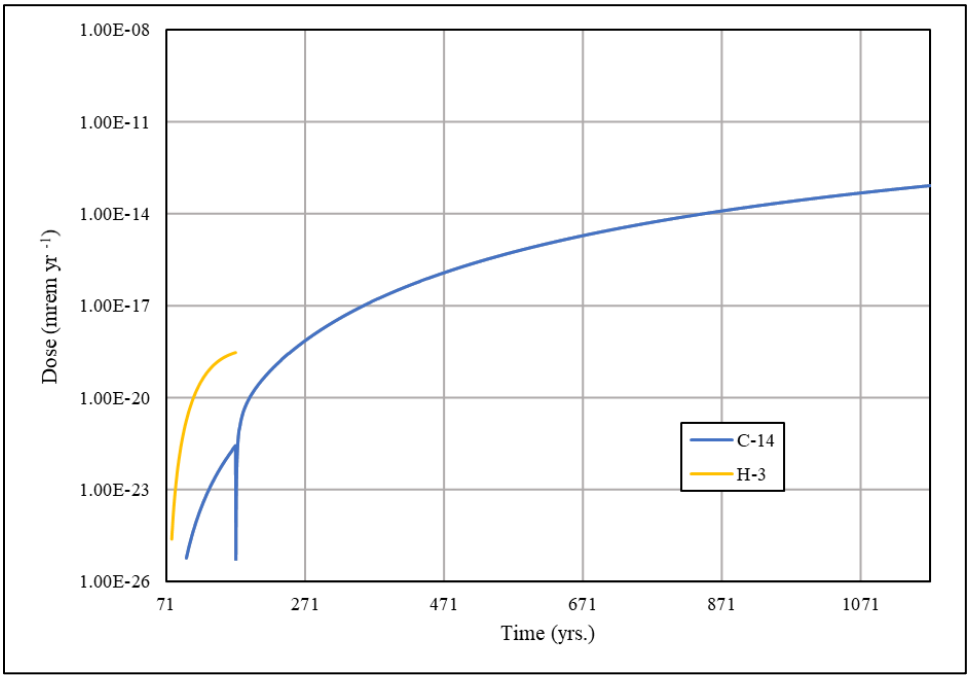

Figure 5-98. Air Pathway Dose Time Histories for 1 Curie of C-14 and H-3 Buried in the Low-Activity Waste Vault

5.2.3.2. Radon Pathway

Surface-flux time histories are generated for Rn-222 from each of its 20 parent radionuclides for the LAWV as explained in Section 5.1.5.3. Rn-222 flux time history characteristics for the LAWV are largely the same for each of the parent radionuclides investigated (Figure 5-99) and as detailed for STs and ETs in Section 5.1.5.3. Rn-222 peak fluxes from each parent are provided in Table 5-26. These fluxes are used for radionuclide screening in Section 2.3.8 and to determine disposal limits in Section 8.6. Radionuclides that are screened in and require further analysis and limits determination are denoted in Table 5-26 by "Limit" in the last column.

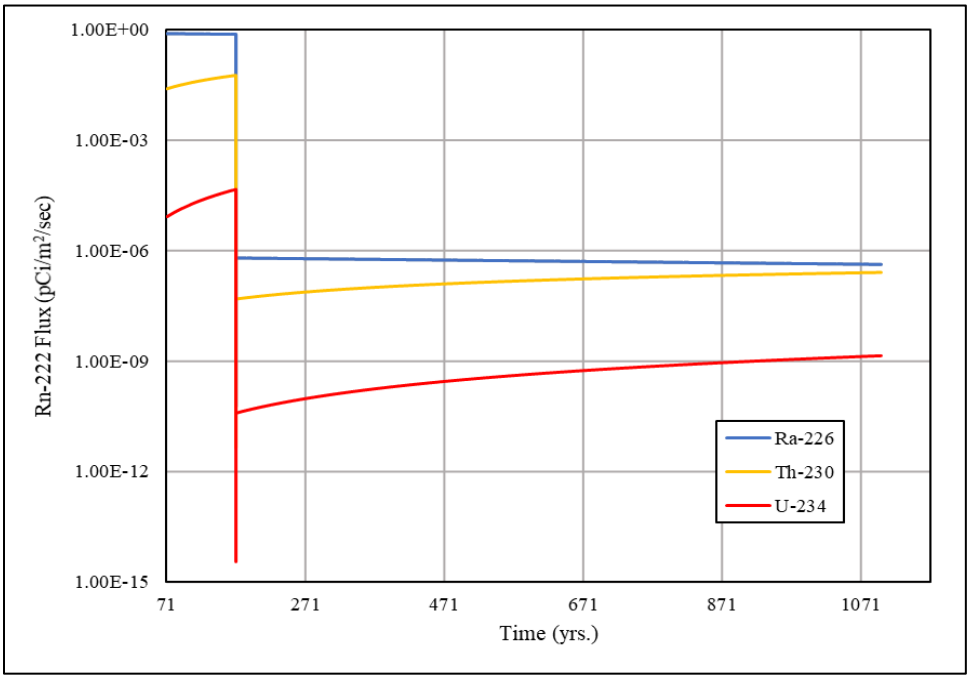

Figure 5-99. Rn-222 Flux Time Histories for 1 Curie of Ra-226, Th-230, and U-234 Buried in the Low-Activity Waste Vault

Table 5-26. Peak Rn-222 Flux from 1 Curie of Rn-222 Parent Radionuclides and Rn-222 Buried for the Low-Activity Waste Vault Radon Pathway

Radionuclide	Peak Rn-222 Flux (pCi $m^{-2}s^{-1}$)	Peak Time (Year)	Limit or Trigger Required? [a]
Am-242	9.34E-14	170.99	--
Am-242m	1.37E-09	170.99	--
Am-246m	0.00E+00	--	--
Bk-250	2.27E-14	170.99	--
Cf-250	0.00E+00	--	--
Cm-242	2.76E-11	170.99	--
Cm-246	3.15E-21	170.99	--
Cm-250	0.00E+00	--	--
Np-238	3.62E-13	170.99	--
Pa-234	1.43E-13	170.99	--
Pa-234m	4.16E-16	170.99	--
Pu-238	5.48E-09	170.99	--
Pu-242	4.97E-17	170.99	--
Pu-246	0.00E+00	--	--
Ra-226	7.89E-01	72	Limit
Rn-222	0.00E+00	--	--
Th-230	5.76E-02	170.99	--
Th-234	1.23E-11	170.99	--
U-234	4.59E-05	170.99	--
U-238	7.44E-09	170.99	--

Notes:

[a] Based on radionuclide screening in Section 2.3.8.

5.3. INTERMEDIATE-LEVEL VAULT

5.3.1. Vadose Zone Model

Section 4.6.3 summarizes the PORFLOW implementation of the flow and transport conceptual models of the ILV VZ to evaluate dose impacts and produce disposal limits for the ELLWF. This section presents selected flow and radionuclide contaminant transport results for the final PA implementation of the PORFLOW VZ ILV model. A more comprehensive set of transport model results is provided in Appendix E.

The ILV VZ is modeled as a 2-D treatment in the same way as the LAWV VZ (Section 5.2.1). For the ILV, Aleman and Hamm (2021) concluded that 20 generic radionuclides have a significant impact on dose as listed in Table 5-27 and explained in Section 2.3.7.

Table 5-27. Generic Parent Radionuclides for Intermediate-Level Vault Vadose Zone and Aquifer Zone Modeling

Radionuclides			
Ag-108m	Cl-36	K-40	Pu-241
Am-241	Cm-245	Ni-59	Ra-226
Ar-39	Cs-137	Ni-63	Sr-90
C-14	H-3	Np-237	Tc-99
Cf-249	I-129	Pu-239	U-235

The PORFLOW case studies considered for the ILV VZ are listed in Table 5-15. As outlined for the LAWV in Section 5.2.1, in addition to the nominal case model settings used for PA calculations, a best estimate case and eight sensitivity cases are run. The sensitivity cases are all one-sided calculations designed to investigate model response to changes in what are deemed to be model parameters having the most significant impact on radionuclide transport. The best estimate case primarily differs from the nominal PA case in that the ELLWF vault concrete is expected to maintain its integrity for longer than the 500-year limit recommended by the PAWG in NUREG-1573 (U.S. NRC, 2000) Each sensitivity case is executed separately to assess the individual effect of each variation.[3] For example, to simulate more extensive concrete cracking, Sensitivity Case 1 uses nominal PA case parameters except for an increase in the gravel content of the initial concrete composition. Except for Sensitivity Case 8 which addresses tritium diffusion in concrete, the sensitivity cases include all 20 generic parent radionuclides.

In addition to the ILV VZ model cases listed in Table 5-15, the disposal of five SWFs (C-14_KB, H-3_TPBAR, I-129_ETF, I-129_KB, and Tc-99_KB) is modeled. Except for H-3_TPBAR, SWF simulations use different K_d values in the waste zone as specified in the *GeoChem Data Package* (Kaplan, 2016b; SRNL, 2018). SWF simulation results are discussed in Section 5.3.1.3.

[3] Performing one-at-a-time sensitivity studies does not capture non-linear effects in the modeling; however, the parameters in this sensitivity study are largely independent.

As described in Section 4.6.3, three different conceptual models of an ILV cell are implemented in the PORFLOW ILV VZ model (Smith, 2021a):

1. "CenterCell" model of ILV Cell #4 in the middle of the ILNT seven-cell unit representing a closed cell containing generic waste only (i.e., no tritium-containing TPBAR disposal containers present)
2. Model with four TPBAR disposal containers representing a typical configuration for the nominal PA, best estimate, and sensitivity cases
3. Model with eight TPBAR containers assessing tritium release from TPBAR disposal containers, where it is assumed that more containers are placed in some ILV cells to accommodate a total of 28 TPBAR disposal containers

Figure 5-100 identifies materials in the ILV VZ model. Note that material zone colors are uniform within a set of plots but may change between sets to better display results.

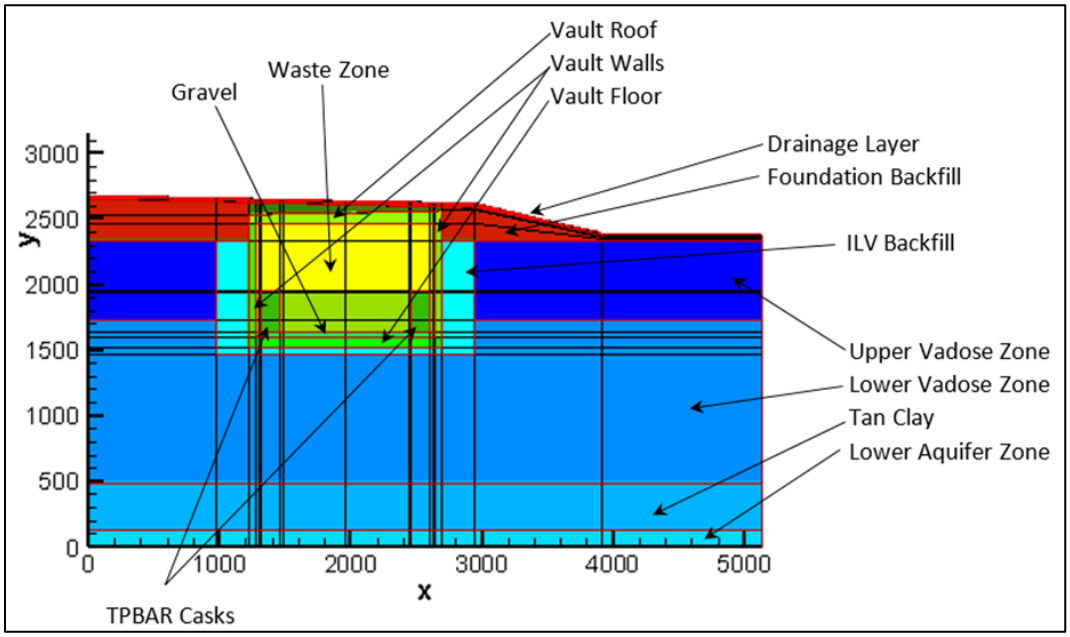

Figure 5-100. Material Zones Included in Intermediate-Level Vault Vadose Zone Model

5.3.1.1. Flow Model Results

Figure 5-101, Figure 5-102, and Figure 5-103 show infiltration flow over the computational mesh at selected time steps for the nominal PA case, best estimate case, and Sensitivity Case 6, respectively. As listed in Table 5-15, ILV concrete hydraulic performance degrades over 500 years in the nominal PA case and 1,000 years in the best estimate case. The infiltration flow rate increases in the ILV in Sensitivity Case 6. These three cases are expected to have the greatest impact on VZ flow. In all three figures, the first plot (Year 0 to Year 170) shows flow before the final closure cap is installed. The PORFLOW model simulations during this period include the backfill soil around the ILV even though the soil will not actually be placed until Year 170 when the final closure cap is installed. Nevertheless, water flow directly over the ILV during this period

is low and model-calculated flow lines display the expected behavior (i.e., relatively uniform flow on either side of the ILV, negligible flow through the vault, little flow directly under the ILV, and water encroachment under the ILV caused by the elevated suction created by the presence of dry soil beneath and moist, uncovered soil surrounding the ILV).

Degradation of the hydraulic properties of the ILV concrete occurs from Year 170 to Year 670 for the nominal PA case and Sensitivity Case 6 and from Year 170 to Year 1,170 for the best estimate case. From Year 170 to Year 5,770 when the vault roof is predicted to collapse (Peregoy, 2006b), the HDPE geomembrane and GCL composite barrier within the final closure cap progressively deteriorates and allows more water flow directly above and beside the ILV. All three simulations continue to show little flow through and below the ILV until Year 470. Because the vault concrete is not fully degraded hydraulically, the best estimate case displays lower flow through the ILV from Year 720 to Year 770 when compared to the nominal PA case. Otherwise, the flow patterns for Year 720 to Year 770 are quite similar. Close examination of flow rates for Sensitivity Case 6 indicates that they are higher than flow rates for the other two cases. Between Year 720 and Year 5,770, flow through the ILV and final closure cap steadily increases in all three cases as the performance of the geomembrane and GCL composite barrier declines. At Year 5,770 and beyond, water flow through the ILV is higher than background flow. The collapse of the ILV roof is assumed to create a hole in the final closure cap that allows surface runoff and lateral drainage from the upslope, intact area of the cap to drain into the vault region (Dyer, 2019b). After roof collapse (Year 5,770 and beyond), the flow rates are nearly identical for the nominal PA and best estimate cases and clearly higher for Sensitivity Case 6.

Figure 5-104 and Figure 5-105 present an expanded view of flow through the ILV region and the associated VZ from Year 570 to Year 620 for all seven flow cases modeled: nominal PA case, best estimate case, and Sensitivity Cases 1, 2, 4, 5, and 6. This time interval is selected because the ILV concrete remains somewhat intact in all the models, and the flux to the water table occurs early enough to impact the aquifer concentration during the 1,000-year compliance period. Flow profiles for the best estimate case and Sensitivity Case 2 are similar to each other yet are clearly different from the other five cases. The best estimate case and Sensitivity Case 2 assume slower degradation of the ILV concrete (1,000 years to degrade vs. 500 years for the nominal PA case). Although flow patterns for the five other cases appear similar to each other, closer examination shows that VZ flow rates for Sensitivity Case 6 are somewhat higher.

Figure 5-101 through Figure 5-105 display zero flow through the two TPBAR disposal areas, represented by the red rectangles located in the lower left-hand and right-hand corners of the ILV. Generic waste material is not placed in these TPBAR disposal areas; therefore, flow through the TPBAR disposal containers should not occur.

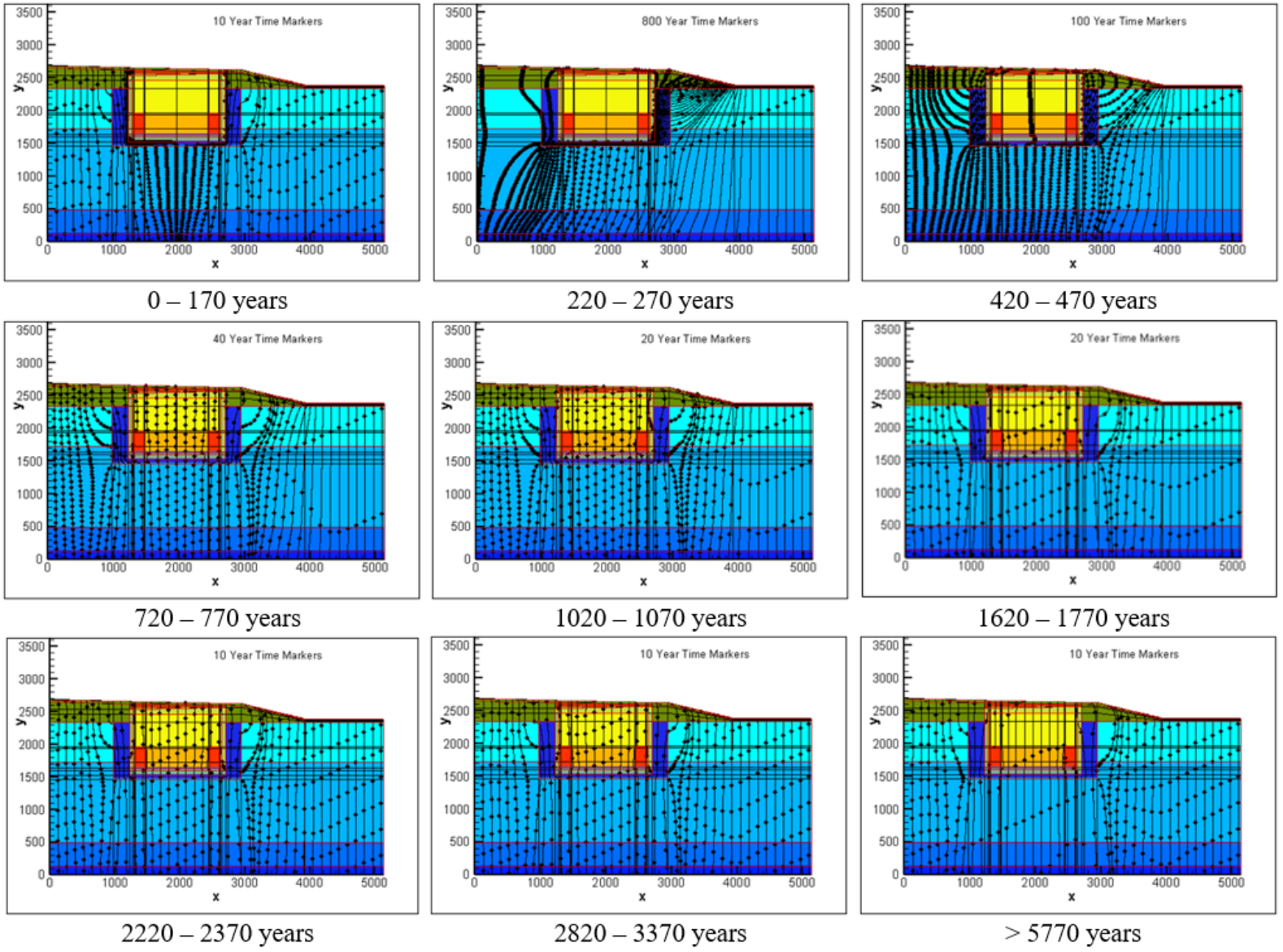

Figure 5-101. Flow through Intermediate-Level Vault Vadose Zone for Nominal PA Case

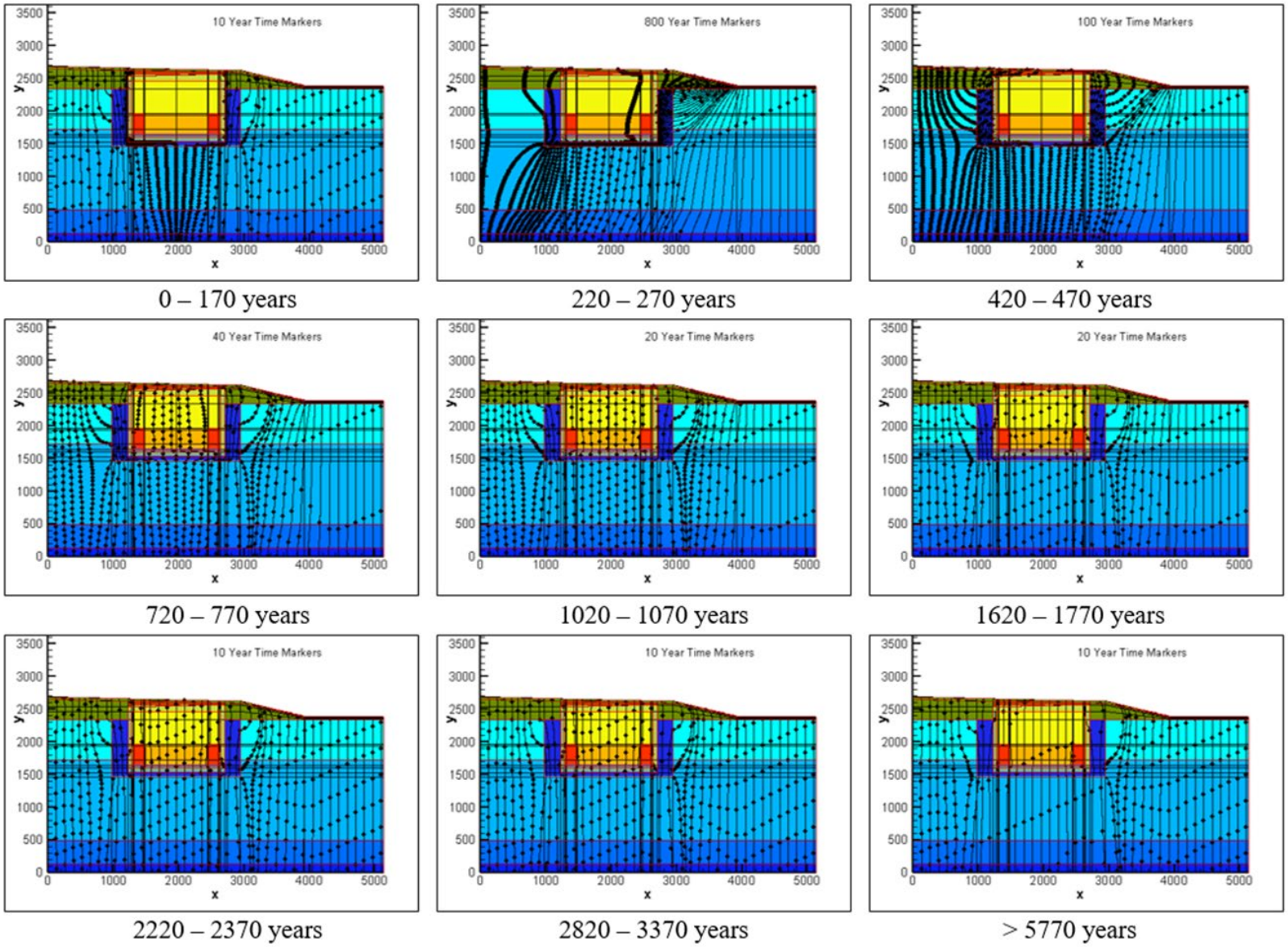

Figure 5-102. Flow through Intermediate-Level Vault Vadose Zone for Best Estimate Case

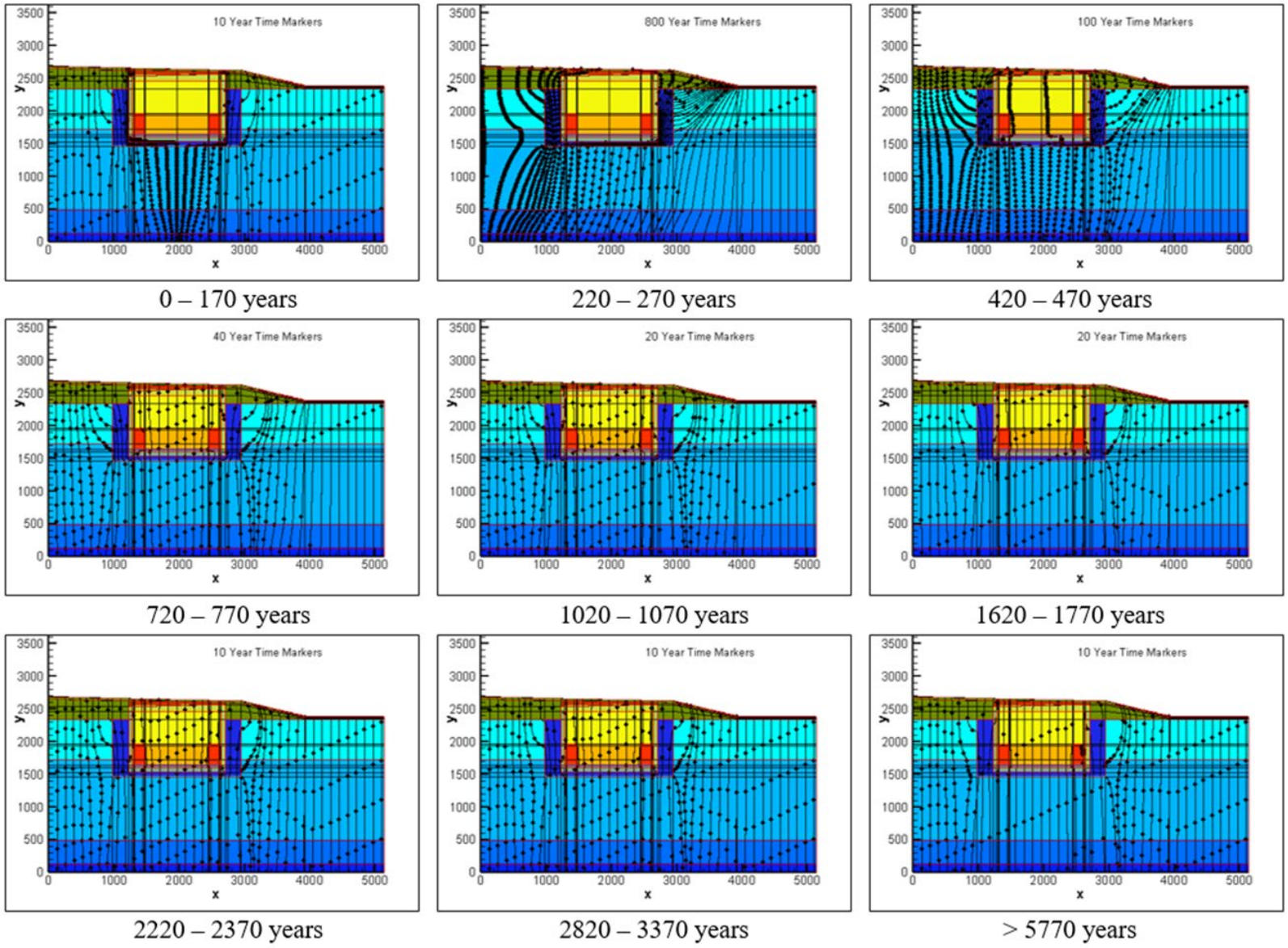

Figure 5-103. Flow through Intermediate-Level Vault Vadose Zone for Sensitivity Case 6

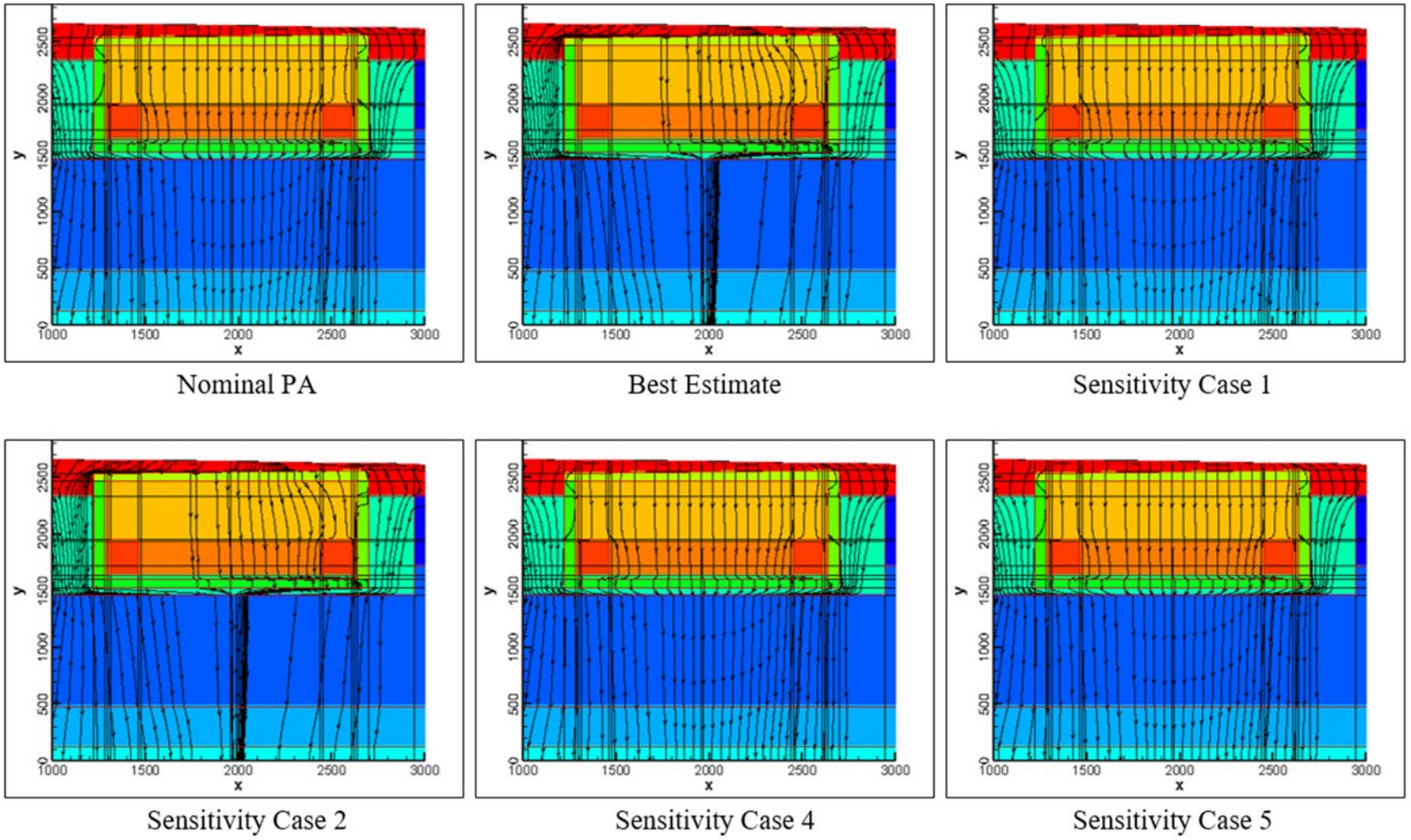

Figure 5-104. Year 570 to Year 620 Flow Lines of Intermediate-Level Vault Vadose Zone Model for Nominal PA Case; Best Estimate Case; and Sensitivity Cases 1, 2, 4 and 5

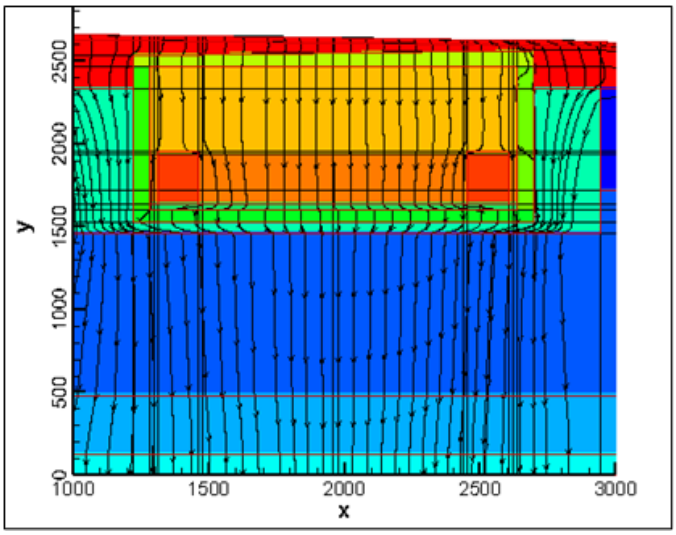

Figure 5-105. Year 570 to Year 620 Flow Lines of Intermediate-Level Vault Vadose Zone Model for Sensitivity Case 6

5.3.1.2. Transport Model Results for Generic Waste

This section summarizes PORFLOW modeling results for the transport of generic waste radionuclides through the ILV VZ. For comparison purposes and to analyze the vast quantity of data, this section includes transport model results used to establish PA limits, results for the best estimate case representing the expected behavior of the ILV, and results for the sensitivity cases listed in Table 5-15. The decay and transport of 46 total isotopes through the VZ are modeled over a 50,000-year period. The isotopes include the 20 generic ILV parent radionuclides listed in Table 5-27 as well as 26 progeny isotopes in the parent decay chains with half-lives equal to or greater than one year.

Table 5-28 and Table 5-29 compare peak flux to the water table and the time at which the peak flux occurs for each radionuclide and each case. To further reduce the size of the dataset, radionuclides are screened out if they do not peak within 50,000 years for the nominal PA case or if the peak flux is less than 1.0E-20 gmol yr^{-1} per gmole buried. Using this criterion, Cs-137 and Sr-90 with peak fluxes of 7.1E-30 gmol yr^{-1} and 4.5E-32 gmol yr^{-1}, respectively, are eliminated from consideration. Peak flux and time of occurrence for the remaining 33 parent and daughter radionuclides are listed in Table 5-28 and Table 5-29 for the nine cases that include these radionuclides. Except for Ar-39 and H-3, all radionuclides peak beyond the period of performance; however, the leading release curve may still impact limit calculations.

Table 5-30 further simplifies the results by normalizing peak flux values to the nominal PA case. Ratios greater than 1.0 in Table 5-30 indicate that the case exceeds the nominal PA case. Results are summarized in Table 5-31.

Table 5-28. Peak Flux to the Water Table of Intermediate-Level Vault Vadose Zone and Time of Occurrence for Nominal PA Case; Best Estimate Case; and Sensitivity Cases 1 to 3

Radionuclide		Nominal PA Case		Best Estimate Case		Sensitivity Case 1 Concrete Cracking		Sensitivity Case 2 Degraded Concrete		Sensitivity Case 3 Concrete Aging	
Parent	Progeny	Maximum (gmol yr^{-1})	Time (Year)	Maximum (gmol yr^{-1})	Time (Year)	Maximum (gmol yr^{-1})	Time (Year)	Maximum (gmol yr^{-1})	Time (Year)	Maximum (gmol yr^{-1})	Time (Year)
Ag-108m	-	1.14E-07	6,370	1.19E-07	6,380	1.14E-07	6,370	1.14E-07	6,370	1.25E-07	4,332
Am-241	Np-237	4.22E-03	6,010	4.16E-03	6,010	4.22E-03	6,010	4.22E-03	6,010	3.77E-03	6,010
Am-241	U-233	2.45E-07	17,600	2.43E-07	17,910	2.45E-07	17,590	2.45E-07	17,590	2.34E-07	17,710
Am-241	Th-229	1.17E-09	20,190	1.16E-09	20,480	1.17E-09	20,190	1.17E-09	20,190	1.12E-09	20,230
Ar-39	-	1.63E-03	771	6.66E-04	821	1.50E-03	746	6.73E-04	842	1.63E-03	771
C-14	-	1.11E-03	6,260	1.29E-03	6,260	1.10E-03	6,260	1.11E-03	6,260	7.04E-04	4,723
Cf-249	Np-237	1.35E-03	6,010	1.32E-03	6,010	1.35E-03	6,010	1.35E-03	6,010	1.09E-03	6,010
Cf-249	U-233	4.01E-08	17,660	3.99E-08	17,910	4.01E-08	17,660	4.01E-08	17,650	3.62E-08	17,670
Cf-249	Th-229	1.95E-10	20,260	1.95E-10	20,500	1.95E-10	20,260	1.95E-10	20,270	1.76E-10	20,200
Cl-36	-	4.25E-03	1,415	3.64E-03	1,471	4.13E-03	1,471	3.80E-03	1,471	4.09E-03	1,414
Cm-245	Np-237	1.47E-03	6,010	1.44E-03	6,010	1.47E-03	6,010	1.47E-03	6,010	1.20E-03	6,010
Cm-245	U-233	4.75E-08	17,640	4.72E-08	17,900	4.75E-08	17,640	4.75E-08	17,640	4.34E-08	17,680
Cm-245	Th-229	2.30E-10	20,240	2.29E-10	20,480	2.30E-10	20,240	2.30E-10	20,240	2.10E-10	20,200
H-3	-	4.06E-09	90	8.38E-09	89	4.06E-09	90	4.05E-09	90	4.06E-09	90
I-129	-	5.19E-03	1,241	3.27E-03	1,412	5.08E-03	1,238	5.04E-03	1,321	4.67E-03	1,237
K-40	-	2.22E-03	2,371	2.13E-03	2,433	2.16E-03	2,371	2.11E-03	2,414	2.20E-03	2,371
Ni-59	-	4.99E-04	4,214	1.00E-03	6,270	4.96E-04	4,211	5.04E-04	4,261	1.23E-03	4,135
Ni-63	-	5.74E-14	2,675	8.27E-15	2,954	6.39E-14	2,671	1.88E-14	2,995	2.80E-14	2,821
Np-237	-	6.69E-03	5,990	6.84E-03	5,990	6.69E-03	5,990	6.69E-03	5,990	6.02E-03	5,990
Np-237	U-233	2.74E-07	17,550	2.71E-07	17,900	2.74E-07	17,550	2.74E-07	17,550	2.62E-07	17,680
Np-237	Th-229	1.16E-09	20,150	1.15E-09	20,460	1.16E-09	20,150	1.16E-09	20,140	1.11E-09	20,190

Notes:

The reference point for time is the start of ILV operations in late 1994, and the compliance period is from Year 170 to Year 1,170.

Table 5-28 (cont'd). Peak Flux to the Water Table of Intermediate-Level Vault Vadose Zone and Time of Occurrence for Nominal PA Case, Best Estimate Case, and Sensitivity Cases 1 to 3

Radionuclide		Nominal PA Case		Best Estimate Case		Sensitivity Case 1 Concrete Cracking		Sensitivity Case 2 Degraded Concrete		Sensitivity Case 3 Concrete Aging	
Parent	Progeny	Maximum (gmol yr^{-1})	Time (Year)	Maximum (gmol yr^{-1})	Time (Year)	Maximum (gmol yr^{-1})	Time (Year)	Maximum (gmol yr^{-1})	Time (Year)	Maximum (gmol yr^{-1})	Time (Year)
Pu-239	U-235	3.95E-05	18,410	4.04E-05	18,650	3.95E-05	18,410	3.95E-05	18,410	3.91E-05	18,360
Pu-239	Pa-231	1.89E-09	6,000	1.84E-09	6,010	1.89E-09	6,000	1.89E-09	6,000	1.64E-09	6,010
Pu-239	Ac-227	3.38E-15	6,040	3.29E-15	6,050	3.38E-15	6,040	3.38E-15	6,040	2.93E-15	6,040
Pu-241	Np-237	4.22E-03	6,010	4.16E-03	6,010	4.22E-03	6,010	4.22E-03	6,010	3.77E-03	6,010
Pu-241	U-233	2.44E-07	17,600	2.42E-07	17,910	2.44E-07	17,600	2.44E-07	17,590	2.33E-07	17,710
Pu-241	Th-229	1.16E-09	20,200	1.15E-09	20,480	1.16E-09	20,200	1.16E-09	20,180	1.11E-09	20,230
Ra-226	-	2.41E-05	7,390	2.28E-05	7,530	2.41E-05	7,390	2.40E-05	7,390	3.56E-05	7,020
Ra-226	Pb-210	4.21E-09	7,420	3.98E-09	7,560	4.20E-09	7,420	4.19E-09	7,430	6.21E-09	7,060
Tc-99	-	3.92E-03	5,850	3.54E-03	5,850	3.94E-03	5,850	3.76E-03	5,850	1.54E-02	2,926
U-235	-	2.03E-04	16,530	2.14E-04	16,680	2.03E-04	16,530	2.03E-04	16,530	2.00E-04	16,570
U-235	Pa-231	2.37E-08	6,000	2.29E-08	6,010	2.37E-08	6,000	2.37E-08	6,000	1.98E-08	6,010
U-235	Ac-227	4.21E-14	6,030	4.08E-14	6,040	4.21E-14	6,030	4.21E-14	6,030	3.53E-14	6,040

Notes:

The reference point for time is the start of ILV operations in late 1994, and the compliance period is from Year 170 to Year 1,170.

Table 5-29. Peak Flux to the Water Table of Intermediate-Level Vault Vadose Zone and Time of Occurrence for Nominal PA Case, Best Estimate Case, and Sensitivity Cases 4 to 7

Radionuclide		Nominal PA Case		Sensitivity Case 4 LVZ Porosity		Sensitivity Case 5 Waste Porosity		Sensitivity Case 6 Infiltration		Sensitivity Case 7 K_d	
Parent	Progeny	Maximum (gmol yr^{-1})	Time (Year)	Maximum (gmol yr^{-1})	Time (Year)	Maximum (gmol yr^{-1})	Time (Year)	Maximum (gmol yr^{-1})	Time (Year)	Maximum (gmol yr^{-1})	Time (Year)
Ag-108m	-	1.14E-07	6,370	1.16E-07	6,360	1.13E-07	6,350	1.64E-07	6,240	2.39E-07	6,100
Am-241	Np-237	4.22E-03	6,010	4.20E-03	6,010	4.18E-03	6,010	5.04E-03	5,960	5.82E-03	5,910
Am-241	U-233	2.45E-07	17,600	2.50E-07	17,260	2.43E-07	17,900	3.12E-07	14,860	5.03E-07	11,470
Am-241	Th-229	1.17E-09	20,190	1.18E-09	19,800	1.16E-09	20,470	1.22E-09	17,100	1.39E-09	13,260
Ar-39	-	1.63E-03	771	1.68E-03	771	1.86E-03	737	2.93E-03	671	1.63E-03	771
C-14	-	1.11E-03	6,260	1.10E-03	6,260	4.79E-04	5,043	1.34E-03	6,150	1.47E-03	6,050
Cf-249	Np-237	1.35E-03	6,010	1.34E-03	6,010	1.35E-03	6,010	1.61E-03	5,960	1.87E-03	5,910
Cf-249	U-233	4.01E-08	17,660	4.09E-08	17,320	3.98E-08	17,830	5.02E-08	14,890	7.89E-08	11,540
Cf-249	Th-229	1.95E-10	20,260	1.97E-10	19,880	1.94E-10	20,430	2.01E-10	17,150	2.21E-10	13,320
Cl-36	-	4.25E-03	1,415	4.25E-03	1,411	4.17E-03	1,414	6.06E-03	1,171	6.60E-03	1,171
Cm-245	Np-237	1.47E-03	6,010	1.46E-03	6,010	1.47E-03	6,010	1.75E-03	5,960	2.03E-03	5,910
Cm-245	U-233	4.75E-08	17,640	4.84E-08	17,310	4.71E-08	17,840	5.97E-08	14,890	9.43E-08	11,530
Cm-245	Th-229	2.30E-10	20,240	2.33E-10	19,860	2.29E-10	20,430	2.37E-10	17,140	2.64E-10	13,310
H-3	-	4.06E-09	90	3.69E-09	91	8.41E-09	89	6.37E-09	84	4.06E-09	90
I-129	-	5.19E-03	1,241	5.21E-03	1,236	3.16E-03	1,321	7.07E-03	1,038	6.99E-03	1,071
K-40	-	2.22E-03	2,371	2.20E-03	2,316	2.23E-03	2,371	2.76E-03	1,937	3.68E-03	1,782
Ni-59	-	4.99E-04	4,214	5.00E-04	4,191	9.76E-04	6,270	5.78E-04	3,576	9.62E-04	2,821
Ni-63	-	5.74E-14	2,675	6.63E-14	2,671	2.73E-14	2,671	1.11E-12	2,441	5.96E-11	2,071
Np-237	-	6.69E-03	5,990	6.65E-03	5,990	6.79E-03	5,990	7.97E-03	5,940	1.00E-02	5,910
Np-237	U-233	2.74E-07	17,550	2.80E-07	17,210	2.72E-07	17,890	3.49E-07	14,820	5.66E-07	11,430
Np-237	Th-229	1.16E-09	20,150	1.18E-09	19,760	1.15E-09	20,460	1.22E-09	17,080	1.39E-09	13,220

Notes:

The reference point for time is the start of ILV operations in late 1994, and the compliance period is from Year 170 to Year 1,170.

Table 5-29 (cont'd). Peak Flux to the Water Table of Intermediate-Level Vault Vadose Zone and Time of Occurrence for Nominal PA Case and Sensitivity Cases 4 to 7

Radionuclide		Nominal PA Case		Sensitivity Case 4 LVZ Porosity		Sensitivity Case 5 Waste Porosity		Sensitivity Case 6 Infiltration		Sensitivity Case 7 K_d	
Parent	Progeny	Maximum (gmol yr^{-1})	Time (Year)	Maximum (gmol yr^{-1})	Time (Year)	Maximum (gmol yr^{-1})	Time (Year)	Maximum (gmol yr^{-1})	Time (Year)	Maximum (gmol yr^{-1})	Time (Year)
Pu-239	U-235	3.95E-05	18,410	4.01E-05	18,050	4.03E-05	18,610	4.53E-05	15,390	6.12E-05	11,710
Pu-239	Pa-231	1.89E-09	6,000	1.89E-09	6,000	1.85E-09	6,010	2.26E-09	5,950	2.66E-09	5,910
Pu-239	Ac-227	3.38E-15	6,040	3.36E-15	6,040	3.30E-15	6,040	3.90E-15	5,980	4.70E-15	5,940
Pu-241	Np-237	4.22E-03	6,010	4.20E-03	6,010	4.18E-03	6,010	5.04E-03	5,960	5.82E-03	5,910
Pu-241	U-233	2.44E-07	17,600	2.49E-07	17,260	2.42E-07	17,900	3.11E-07	14,860	5.01E-07	11,470
Pu-241	Th-229	1.16E-09	20,200	1.18E-09	19,800	1.15E-09	20,470	1.22E-09	17,110	1.39E-09	13,260
Ra-226		2.41E-05	7,390	2.45E-05	7,360	2.27E-05	7,530	4.10E-05	6,770	9.49E-05	5,970
Ra-226	Pb-210	4.21E-09	7,420	4.28E-09	7,390	3.96E-09	7,560	7.15E-09	6,800	1.66E-08	6,000
Tc-99		3.92E-03	5,850	3.85E-03	5,850	3.72E-03	5,850	3.09E-03	5,840	1.82E-03	5,880
U-235		2.03E-04	16,530	2.08E-04	16,200	2.14E-04	16,680	2.60E-04	14,070	3.81E-04	11,040
U-235	Pa-231	2.37E-08	6,000	2.36E-08	6,000	2.30E-08	6,010	2.84E-08	5,950	3.34E-08	5,910
U-235	Ac-227	4.21E-14	6,030	4.19E-14	6,030	4.10E-14	6,040	4.88E-14	5,980	5.88E-14	5,930

Notes:

The reference point for time is the start of ILV operations in late 1994, and the compliance period is from Year 170 to Year 1,170.

Table 5-30. Maximum Flux to Water Table of Intermediate-Level Vault Vadose Zone for Best Estimate and Sensitivity Cases Normalized to Nominal PA Case

Radionuclide		Best Estimate Case	Sensitivity Cases						
Parent	Progeny		1	2	3	4	5	6	7
Ag-108m	-	1.05	1.00	1.00	1.10	1.02	0.99	1.45	2.10
Am-241	Np-237	0.99	1.00	1.00	0.89	1.00	0.99	1.20	1.38
Am-241	U-233	0.99	1.00	1.00	0.96	1.02	0.99	1.27	2.05
Am-241	Th-229	0.99	1.00	1.00	0.96	1.01	0.99	1.05	1.19
Ar-39	-	0.41	0.92	0.41	1.00	1.03	1.14	1.80	1.00
C-14	-	1.17	1.00	1.00	0.64	0.99	0.43	1.21	1.33
Cf-249	Np-237	0.98	1.00	1.00	0.81	1.00	1.00	1.19	1.39
Cf-249	U-233	0.99	1.00	1.00	0.90	1.02	0.99	1.25	1.97
Cf-249	Th-229	1.00	1.00	1.00	0.90	1.01	0.99	1.03	1.13
Cl-36	-	0.86	0.97	0.90	0.96	1.00	0.98	1.43	1.55
Cm-245	Np-237	0.98	1.00	1.00	0.82	1.00	1.00	1.19	1.38
Cm-245	U-233	0.99	1.00	1.00	0.91	1.02	0.99	1.26	1.98
Cm-245	Th-229	1.00	1.00	1.00	0.91	1.01	0.99	1.03	1.15
H-3	-	2.06	1.00	1.00	1.00	0.91	2.07	1.57	1.00
I-129	-	0.63	0.98	0.97	0.90	1.00	0.61	1.36	1.35
K-40	-	0.96	0.97	0.95	0.99	0.99	1.00	1.24	1.66
Ni-59	-	2.01	0.99	1.01	2.47	1.00	1.96	1.16	1.93
Ni-63	-	0.14	1.11	0.33	0.49	1.15	0.47	19.34	1,037.21
Np-237	-	1.02	1.00	1.00	0.90	0.99	1.02	1.19	1.50
Np-237	U-233	0.99	1.00	1.00	0.96	1.02	0.99	1.27	2.06
Np-237	Th-229	0.99	1.00	1.00	0.96	1.01	0.99	1.05	1.19
Pu-239	U-235	1.02	1.00	1.00	0.99	1.01	1.02	1.15	1.55
Pu-239	Pa-231	0.97	1.00	1.00	0.87	1.00	0.98	1.19	1.40

Notes:

Concentrations greater than 10% above the nominal PA case (i.e., an exceedance) are shaded in light green.

Concentrations greater than 10% below the nominal PA case are shaded in light gold.

Radionuclides with concentration ratios greater than 50 are highlighted in yellow.

Table 5-30 (cont'd). Maximum Flux to Water Table of Intermediate-Level Vault Vadose Zone Best Estimate and Sensitivity Cases Normalized to Nominal PA Case

Radionuclide		Best Estimate Case	Sensitivity Cases						
Parent	Progeny		1	2	3	4	5	6	7
Pu-239	Ac-227	0.97	1.00	1.00	0.87	0.99	0.98	1.15	1.39
Pu-241	Np-237	0.99	1.00	1.00	0.89	1.00	0.99	1.20	1.38
Pu-241	U-233	0.99	1.00	1.00	0.96	1.02	0.99	1.27	2.05
Pu-241	Th-229	0.99	1.00	1.00	0.96	1.01	0.99	1.05	1.19
Ra-226	-	0.95	1.00	1.00	1.48	1.02	0.94	1.70	3.94
Ra-226	Pb-210	0.95	1.00	1.00	1.48	1.02	0.94	1.70	3.94
Tc-99	-	0.90	1.00	0.96	3.92	0.98	0.95	0.79	0.46
U-235	-	1.06	1.00	1.00	0.99	1.03	1.06	1.28	1.88
U-235	Pa-231	0.97	1.00	1.00	0.84	1.00	0.97	1.20	1.41
U-235	Ac-227	0.97	1.00	1.00	0.84	1.00	0.97	1.16	1.40

Notes:

Concentrations greater than 10% above the nominal PA case (i.e., an exceedance) are shaded in light green.

Concentrations greater than 10% below the nominal PA case are shaded in light gold.

Radionuclides with concentration ratios greater than 50 are highlighted in yellow.

Table 5-31. Summary of Maximum Concentration Ratios and Number of Concentration Ratios Greater or Less than 1.0 for Intermediate-Level Vault Vadose Zone

Parameter		Best Estimate	Sensitivity Cases						
			1	2	3	4	5	6	7
Maximum Conc. Ratios	Maximum Value	2.06	1.11	1.01	3.92	1.15	2.07	19.34	1,037.21
	Minimum Value	0.14	0.92	0.33	0.49	0.91	0.43	0.79	0.46
No. of Conc. Ratios < 1	Conc. Ratios < 0.5	2	0	2	1	0	2	0	1
	Conc. Ratios < 0.9	4	0	3	13	0	3	1	1
No. of Conc. Ratios > 1	Conc. Ratios > 1.1	3	1	0	4	1	3	27	30
	Conc. Ratios > 1.5	2	0	0	2	0	2	5	14

The impact of the sensitivity cases on peak flux to the water table can be generalized as follows:

Significant Impact

Sensitivity Case 6 – Raising the mean monthly infiltration rates by 0.5 standard deviation increases peak flux for all radionuclides except Tc-99.

Sensitivity Case 7 – Lowering K_d values by a factor of two (change greater than 2σ) increases peak flux for all radionuclides except Tc-99, H-3, and Ar-39.

Limited Impact

Sensitivity Case 3 – Decreasing the number of pore volume exchanges required for concrete aging lowers the maximum flux for most radionuclides. However, peak flux increases for Ni-59, Ra-226, Pb-210 (daughter of Ra-226), and Tc-99.

Sensitivity Case 5 – Lowering waste porosity relative to soil increases peak flux by a factor of approximately 2.0 for H-3 and Ni-59.

Minimal Impact

Sensitivity Case 1 – Doubling the gravel content to simulate an increase in concrete cracking of the vault roof and side walls when the final closure cap is installed increases concrete hydraulic conductivity and porosity without representing through-cracking of the concrete. This change has a minimal impact on peak flux for all radionuclides except Ni-63.

Sensitivity Case 2 – Extending concrete hydraulic degradation over 1,000 years instead of the 500-year limit suggested by the PAWG in NUREG-1573 (U.S. NRC, 2000) has a minimal impact on peak flux for all radionuclides except Ar-39, Cl-36, and Ni-63.

Sensitivity Case 4 – Increasing soil porosity in the LVZ by one standard deviation has a minimal impact on peak flux for all radionuclides except Ni-63.

The best estimate case combines Sensitivity Cases 2 and 5; therefore, the results for this case closely match those of the two sensitivity cases. The flux to the water table of Ni-63 is strongly impacted in Sensitivity Cases 5 and 6. Parameters that affect the timing of flux to the water table (e.g., higher water flow or lower K_d) substantially impact Ni-63 transport because of its relatively short 101-year half-life. Assuming 1.0 gmole of each isotope buried in the ILV for the nominal PA case, the maximum flux to the water table of Ni-59 (half-life 76,000 years) is 5.0E-04 gmol yr^{-1}. Using the same assumption, the maximum flux of Ni-63 is only 5.7E-14 gmol yr^{-1} because of its greater decay rate.

Figure 5-106 through Figure 5-108 compare flux to the water table for the nominal PA case, best estimate case, and Sensitivity Cases 6 and 7.

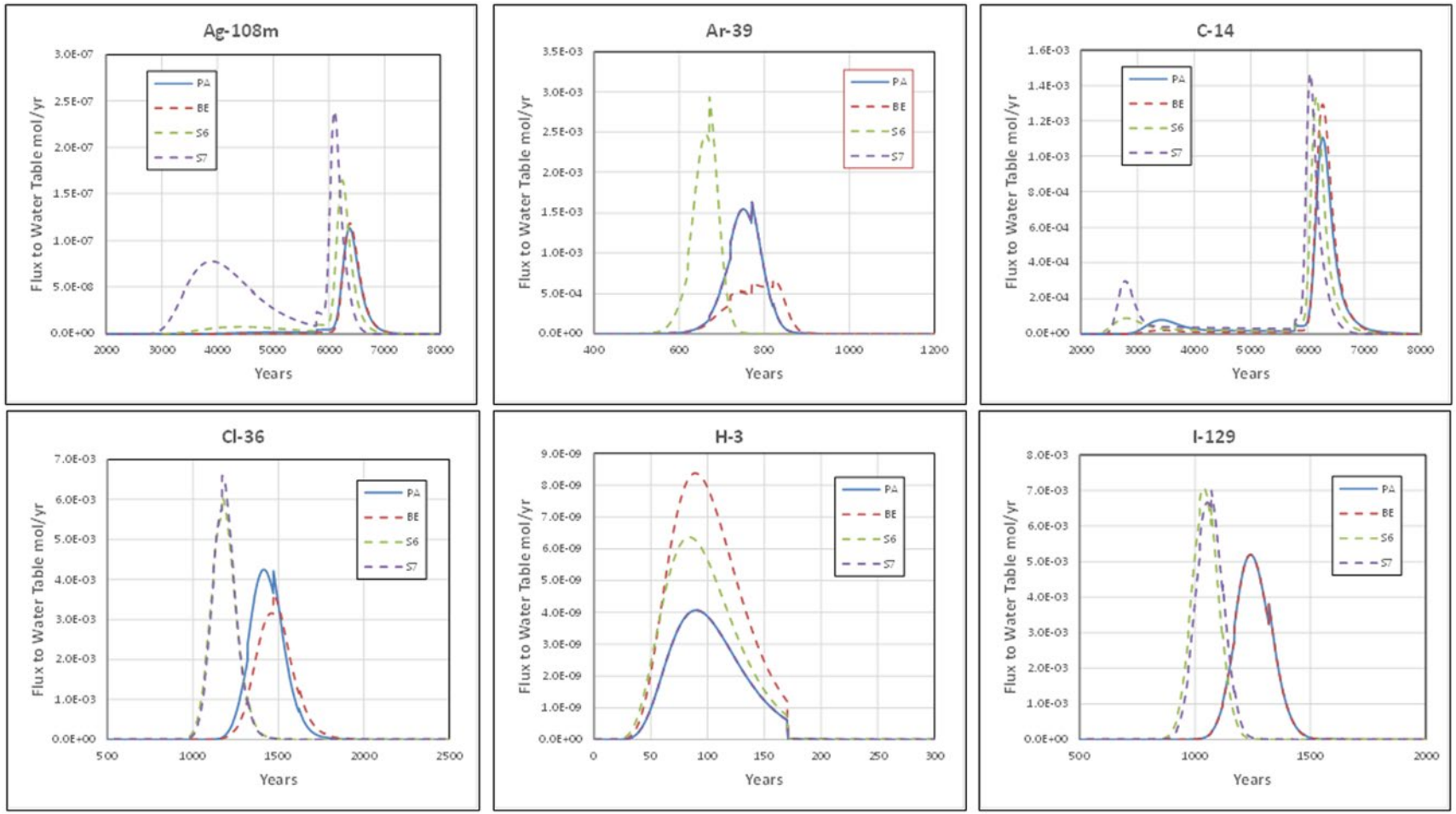

Figure 5-106. Flux-to-the-Water-Table Profiles of Ag-108m through I-129 for Nominal PA Case (PA), Best Estimate Case (BE), Sensitivity Case 6 (S6), and Sensitivity Case 7 (S7) in Intermediate-Level Vault Vadose Zone

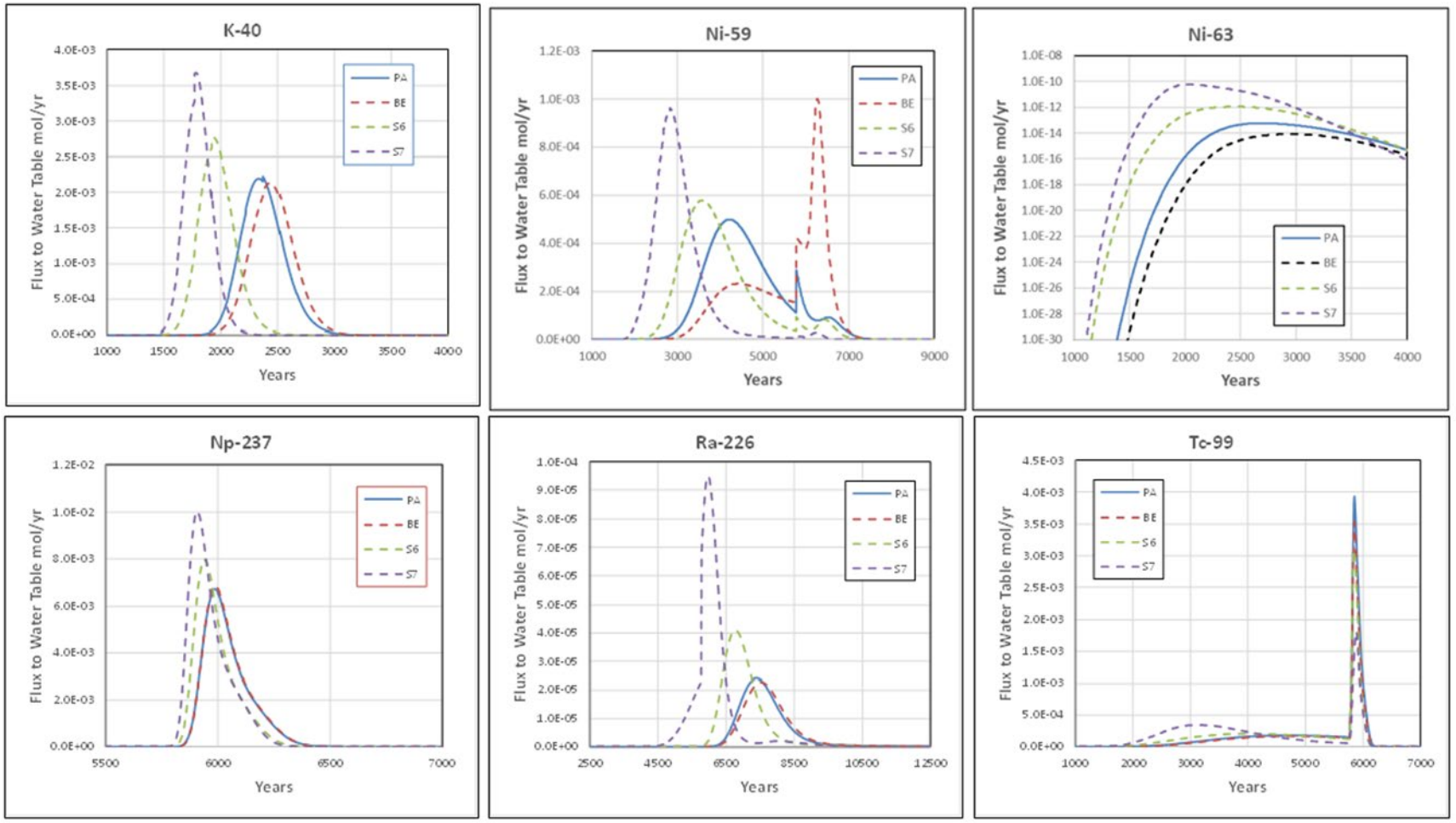

Figure 5-107. Flux-to-the-Water-Table Profiles of K-40 through Tc-99 for Nominal PA Case (PA), Best Estimate Case (BE), Sensitivity Case 6 (S6), and Sensitivity Case 7 (S7) in Intermediate-Level Vault Vadose Zone

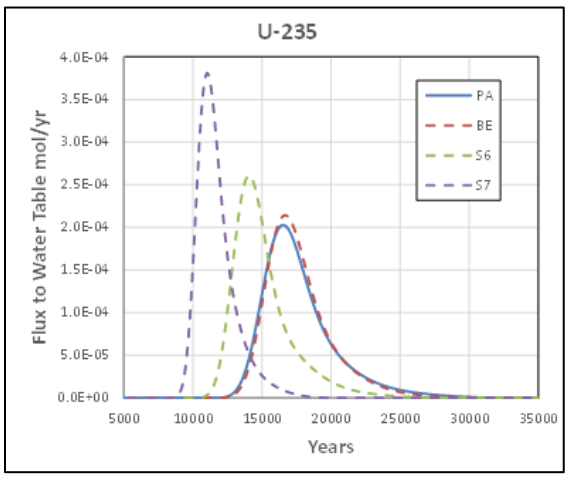

Figure 5-108. Flux-to-the-Water-Table Profiles of U-235 for Nominal PA Case (PA), Best Estimate Case (BE), Sensitivity Case 6 (S6), and Sensitivity Case 7 (S7) in Intermediate-Level Vault Vadose Zone

For most of the radionuclides evaluated, the nominal PA case and best estimate case are in close agreement and the sensitivity cases display fluxes that peak higher and earlier than the nominal PA case. The exceptions are H-3 where the maximum flux for the best estimate case is approximately twice the flux for the nominal PA case and Ni-59 where the maximum flux for the best estimate case peaks higher and later than the flux for the nominal PA case. In Figure 5-107, Ni-63 is plotted on a semi-log graph to clearly show all the cases.

Sensitivity Case 8 is designed to investigate the impact of increasing the diffusivity of tritium in concrete by one standard deviation as shown in Figure 5-109. A greater diffusion rate through the concrete increases the maximum H-3 flux to the water table by 30% from 4.06E-09 to 5.25E-09 gmol yr^{-1} per gmole buried.

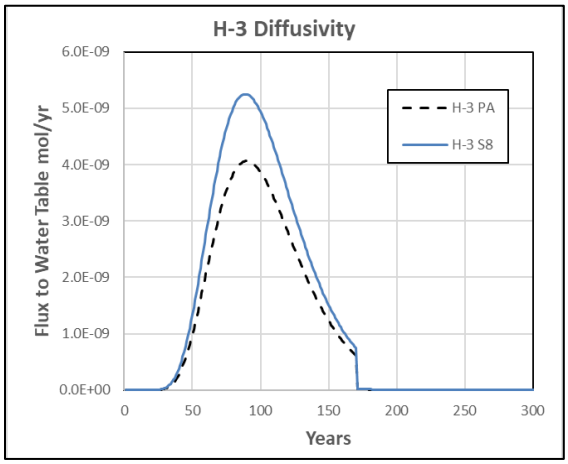

Figure 5-109. Flux-to-the-Water-Table Profiles of H-3 for Nominal PA Case (PA) and Sensitivity Case 8 (S8) in Intermediate-Level Vault Vadose Zone

Figure 5-110 and Figure 5-111 present flux-to-the-water-table profiles for all decay chains. Except for Pu-239, all decay chains shown in Figure 5-110 include Np-237, which is likely the leading contributor to dose from these parent radionuclides.

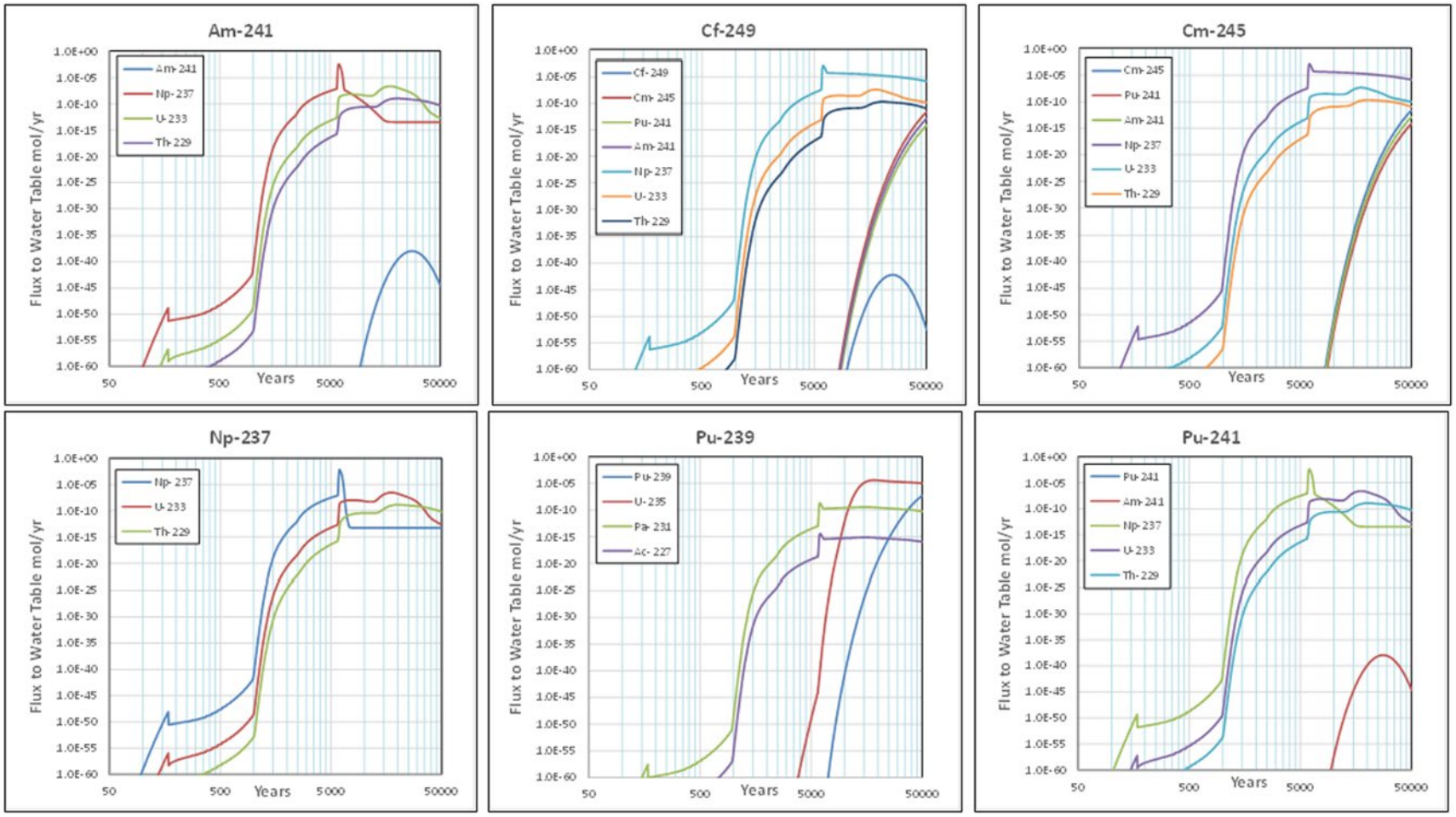

Figure 5-110. Flux-to-the-Water-Table Profiles of Am-241 through Pu-241 and Their Progeny for Nominal PA Case in Intermediate-Level Vault Vadose Zone

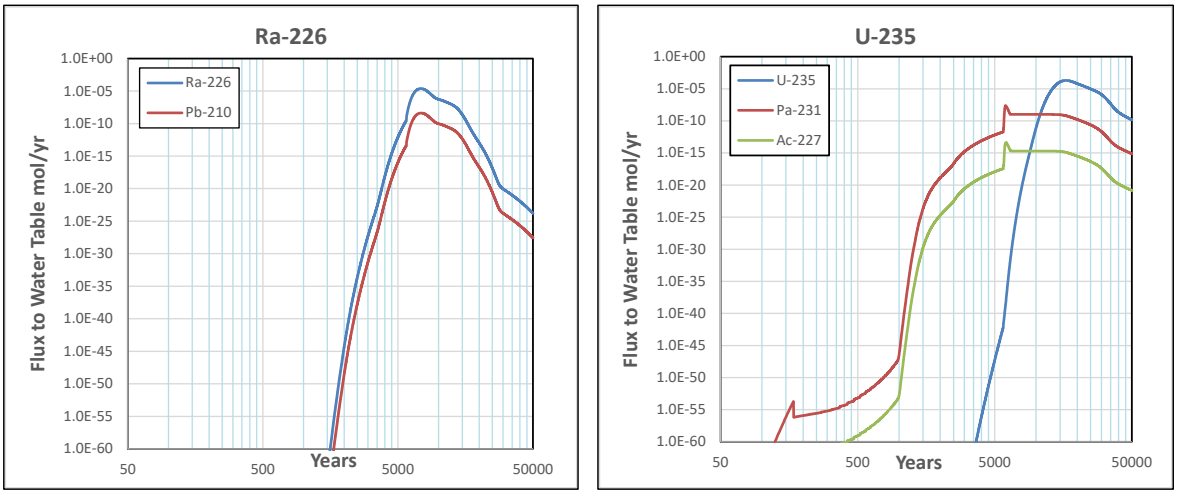

Figure 5-111. Flux-to-the-Water-Table Profiles of Ra-226 and U-235 and Their Progeny for the Nominal PA Case in Intermediate-Level Vault Vadose Zone

5.3.1.3. Transport Model Results for Special Waste Forms

In addition to generic waste, transport simulations are provided for the following six SWFs: C-14K, I-129K, and Tc-99K in resin from the K-Area Disassembly Basin (KB); I-129C in waste received from the ETF; Ar-39T and H-3T released from TPBAR disposal containers. The TPBAR H-3T and Ar-39T SWFs are discussed in Sections 5.3.1.4 and 5.3.1.5, respectively. The SWFs for H-3R and U-235D are set to their generic waste form values.

As described previously in Section 2.2.6.2, waste is added to the ILV in a layer and then grouted in place to form a base for the next waste layer. ILV waste, therefore, is largely contained in a cementitious environment and cementitious K_d values would normally be selected for ILV waste. In the ILV VZ model, however, the chemical SWFs are assigned K_d values in the waste zone that are different than the K_d values for reducing cement (Kaplan, 2016b) as shown in Table 5-32. The K_d for C-14K is much lower for KB Waste than for reducing cement while K_d values for I-129K and Tc-99K are much higher for the SWF than for reducing cement.

Table 5-32. K_d Values for Specific Radionuclides within Special Waste Forms

Isotope	Reducing Cement	KB Waste	ETF Waste
C-14	2,000	140	-
I-129	8	3,700	600
Tc-99	0.8	810	-

Figure 5-112 and Figure 5-113 present flux-to-the-water-table profiles of C-14, I-129, and Tc-99 in ILV SWFs as predicted by the model. As expected from the change in K_d, C-14_KB peaks approximately 2,800 years earlier while I-129_KB and I-129_ETF peak 1,000 and 5,000 years later, respectively, than in the nominal PA case (Figure 5-112). The peak fluxes for I-129_ETF and I-129_KB are approximately 20 and 40 times lower, respectively, than nominal PA case. (Note the two different y-axis scales used in the I-129 plot in Figure 5-112). As displayed in Figure 5-113, the peak flux of Tc-99 occurs at the same time for both generic waste and the

Tc-99_KB SWF. The peak in Tc-99 occurs shortly after the ILV roof collapse at Year 5,770. Before the roof collapse, Tc-99 undergoes a slow release. The sharp peak in Tc-99 (Figure 5-113) results from the large increase in flow through the ILV following roof collapse.

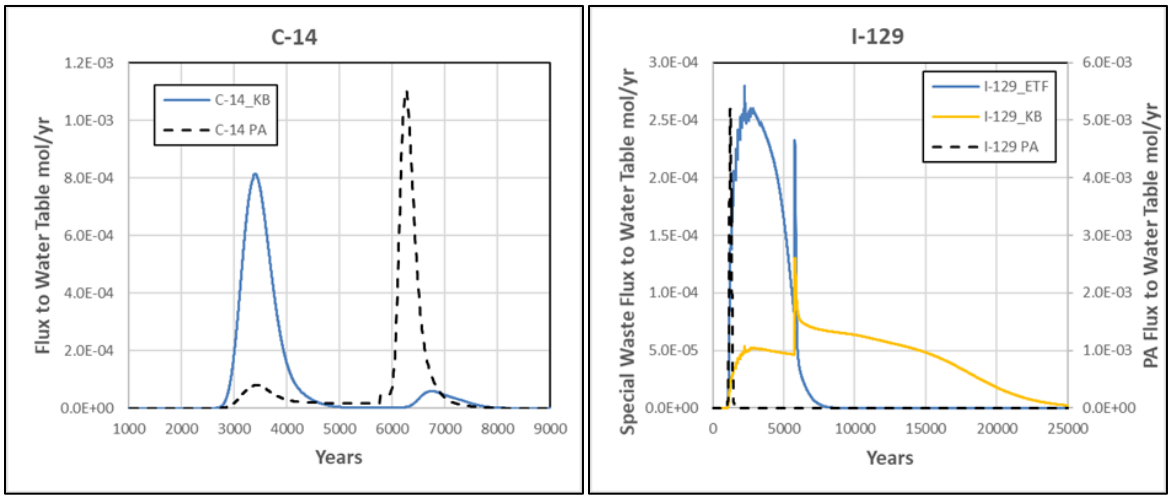

Figure 5-112. Flux-to-the-Water-Table Profiles of C-14 and I-129 in Intermediate-Level Vault Special Waste Forms

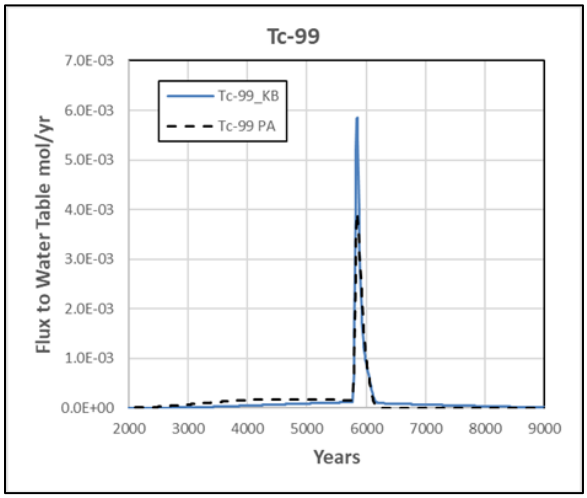

Figure 5-113. Flux-to-the-Water-Table Profile of Tc-99 in Intermediate-Level Vault Special Waste Forms

5.3.1.4. Transport of TPBAR Tritium

Following tritium extraction, reactor rods within TPBAR waste containers buried in the ILV have a large inventory of radioactive isotopes (Hiergesell, 2005; Table 1). However, with the exception of tritium which can diffuse through metals, the other radioactive elements cannot become mobile until the outer wall or welds in the disposal cask fail mechanically or through corrosion. The disposal cask has 13-inch-thick carbon steel walls, and the welds sealing the cask are 1-inch deep. Therefore, the most likely failure mechanism is corrosion of the welds. An analysis of TPBAR waste container corrosion (Vinson et al., 2004) calculated a weld penetration time of 12,600 years for the high-pH ILV disposal environment; therefore, only tritium is expected to be released from

the TPBAR disposal containers due to corrosion of the welds followed by hydrogen permeation through the carbon steel walls of the container.

In PA2008 (WSRC, 2008), the release of tritium from TPBAR disposal containers was modeled using a "bounding conservative" source term calculated by Pacific Northwest National Laboratory (Lanning and Gilbert, 2005) assuming all TPBAR disposal occurs at the end of operations. SRNL (Gorensek, 2021) recently recalculated the source term for TPBAR tritium release for use in this PA. As explained in Section 4.6.3.6, the computed tritium release rates are pessimistically bounding, considering both permeation loss due to corrosion plus leak loss at the maximum allowable leak rate of 1.0E-04 std. cm^3 s^{-1} (Snider, 2007). The ILV VZ model in this PA involves placing a total of 28 TPBAR disposal containers in the ILV based on the schedule outlined in Table 4-63. The current model further assumes that the first 12 TPBAR disposal containers are placed in three ILV cells with four containers per cell, and the last 16 TPBAR disposal containers are placed in two ILV cells with eight containers per cell. This disposal configuration uses five of the six ILV cells available for TPBAR disposal.

Section 4.6.3.6 summarizes the four tritium release cases for this PA. SRNL Case 1 (one-year-old TPBAR disposal containers, eight per ILV cell) and SRNL Case 3 (one-year-old TPBAR disposal containers, four per ILV cell) are selected because they release the most total tritium (6,507 Ci and 3,279 Ci, respectively). The first 12 TPBAR disposal containers are modeled using the SRNL Case 3 tritium release rate; the last 16 disposal containers are modeled using the SRNL Case 1 tritium release rate. Figure 5-114 (left) displays the tritium release rate from all TPBAR disposal containers for SRNL Cases 1 and 3 as well as the total release rate. Figure 5-114 (right) shows the flux of tritium to the water table for each case as well as the total flux to the water table based on the sum of the two cases. In this calculation, the flux to the water table represents the total flux of tritium from the TPBAR disposal containers and is not based on disposal of 1.0 gmole of H-3. As a result, the SWF release rate cannot be compared to the release rate of generic tritium waste described in Section 5.3.1.2.

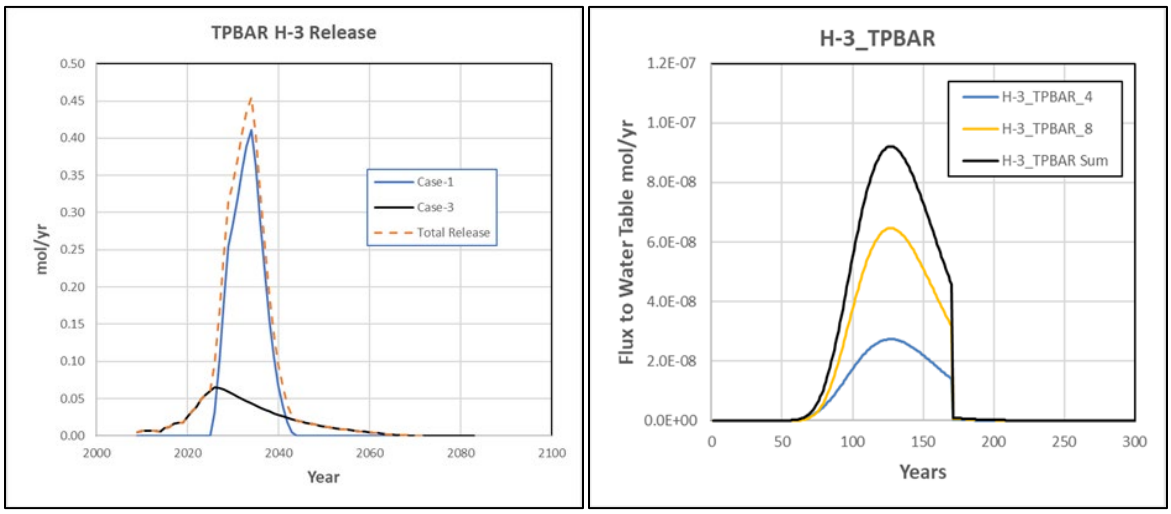

Figure 5-114. Tritium Release Rate and Flux to the Water Table for TPBAR Tritium Special Waste Form

5.3.1.5. Transport of TPBAR Argon-39

Argon as Ar-39 may also be released from TPBAR disposal containers due to a leak. As a pessimistically bounding approach, a release rate is calculated by (Gorensek, 2021) assuming that 1 Ci Ar-39 instantaneously enters the void volume of a TPBAR cask at the time of disposal. The Ar-39 is subsequently released from the cask into the ILV waste zone at the maximum allowed leak rate (Gorensek, 2021; Snider, 2007). The ILV VZ PORFLOW model is used to calculate the resulting Ar-39 flux to the water table.

Figure 5-115 compares the flux to the water table from 1.0 Ci generic Ar-39 and 1.0 Ci Ar-39 released from TPBAR disposal containers. At its peak, the SWF TPBAR flux is about one-eighth the generic Ar-39 flux. The TPBAR SA (Hiergesell, 2005) reports an inventory of 193 Ci Ar-39 for 17 TPBAR disposal containers, which scales to 318 Ci for 28 TPBAR casks. Table H-66 (Appendix H) in this PA provides a disposal limit of 1.12E+06 Ci for ILV generic Ar-39. Assuming the generic waste form disposal limit to include Ar-39 present in TPBAR casks is therefore pessimistically bounding and, by a large margin, exceeds any expected Ar-39 disposal in the ILV.

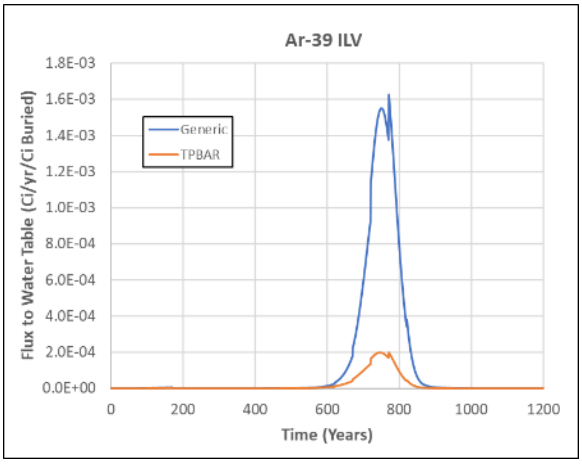

Figure 5-115 Flux to the Water Table Resulting from the Release of 1.0 Ci Generic Ar-39 and 1.0 Ci TPBAR Ar-39

5.3.2. Aquifer Zone Model

ILV aquifer modeling includes all case studies listed in Table 5-15 for the ILV VZ transport calculations. The same approach is taken as described for the LAWV in Section 5.2.2. Sensitivity cases are modeled for all 20 generic parent radionuclides listed in Table 5-27 as outlined in Section 5.3.2.1 for the LAWV. SWF simulation results for the aquifer zone are discussed in Section 5.3.2.2. As noted for other types of DUs, only a "cutout" of the full GSA flow model is used. For the ILV, the West_B cutout is used. Implementation of the aquifer flow model for the ILV is described in Section 3.5.3.

There is a slight discrepancy between the ILV flux to the water table and the aquifer flow timing. As described in Section 5.3.1, the ILV began operation one year later than the ELLWF. The VZ model established the starting point of ILV operations as time zero. To align ILV flux to the water

table with the aquifer flow, one year is added to the flux timing. Maintaining two sets of ILV flux tables proved awkward and was not implemented. This introduces a slight pessimistic bias into the ILV 100-meter POA concentration calculations because model Year 1,171 (end of the compliance period when most radionuclides reach a maximum concentration) is using the slightly greater ILV flux for Year 1,172. A decision was made to simply accept this pessimistic bias in the calculation instead of modifying the flux tables used in the aquifer analysis by one year.

5.3.2.1. Transport Model Results for Generic Waste

For comparison purposes and to analyze the large quantity of data, this section summarizes the aquifer transport model results used to establish PA limits, the best estimate case representing the expected behavior of the ILV, and the sensitivity results for the aquifer model based on the VZ sensitivity cases outlined in Table 5-15. The 20 generic ILV parent radionuclides and 26 progeny isotopes in parent decay chains with half-lives equal to or greater than one year yield a total of 46 isotopes (counting duplicate daughters and 31 unique isotopes) whose transport and decay through the aquifer are modeled over a 50,000-year simulation time.

The simplest way to analyze the large simulation dataset is to compare peak concentrations at the 100-meter POA and the time when the peak occurs for each radionuclide and each case. To further reduce the dataset, radionuclides that do not peak within 50,000 years for the nominal PA case and those with peak concentrations less than 1.0E-10 pCi L^{-1} per Ci buried are not included in the comparison. Cs-137 and Sr-90 (with peak concentrations of 3.17E-27 pCi L^{-1} Ci^{-1} and 1.62E-28 pCi L^{-1} Ci^{-1}, respectively) fall below this threshold even though they typically are radionuclides of concern in dose calculations. Peak concentrations and the time of occurrence for the 33 parent and daughter radionuclides retained after this preliminary screening are listed in Table 5-33 and Table 5-34 for the nine cases that included all generic parent radionuclides. Except for Ar-39 and H-3 which have zero K_d values, all radionuclide concentrations peak beyond the compliance period. However, the leading edge of the release curve impacts limit calculations.

Table 5-35 further simplifies the results by ratioing peak concentrations to the values obtained for the nominal PA case. Ratios greater than 1.0 in Table 5-35 indicate that a case exceeds the nominal PA value. In the table, Ni-63 concentrations at the 100-meter POA are strongly impacted by Sensitivity Cases 6 and 7. Because Ni-63 has a relatively short half-life of 101 years, effects that alter the timing of when the 100-meter POA concentration is reached significantly impact its concentration because of radioactive decay.

Table 5-33. Peak Concentrations for Intermediate-Level Vault at 100-meter POA and Time of Occurrence for Nominal PA Case, Best Estimate Case, and Sensitivity Cases 1 to 3

Radionuclide		Nominal PA Case		Best Estimate Case		Sensitivity Case 1 Concrete Cracking		Sensitivity Case 2 Degraded Concrete		Sensitivity Case 3 Concrete Aging	
Parent	Progeny	Maximum (pCi L^{-1} Ci^{-1})	Time (Year)	Maximum (pCi L^{-1} Ci^{-1})	Time (Year)	Maximum (pCi L^{-1} Ci^{-1})	Time (Year)	Maximum (pCi L^{-1} Ci^{-1})	Time (Year)	Maximum (pCi L^{-1} Ci^{-1})	Time (Year)
Ag-108m	-	3.43E-03	6,600	3.58E-03	6,610	3.43E-03	6,600	3.43E-03	6,600	3.99E-03	4,556
Am-241	Np-237	3.78E-02	6,110	3.73E-02	6,110	3.78E-02	6,110	3.78E-02	6,110	3.38E-02	6,100
Am-241	U-233	2.50E-05	23,900	2.48E-05	24,200	2.50E-05	23,900	2.50E-05	23,900	2.38E-05	23,900
Am-241	Th-229	4.31E-06	27,500	4.28E-06	27,800	4.31E-06	27,500	4.31E-06	27,500	4.13E-06	27,500
Ar-39	-	8.33E+01	759	3.49E+01	833	8.03E+01	754	3.61E+01	850	8.33E+01	759
C-14	-	5.12E+01	6,330	5.99E+01	6,330	5.12E+01	6,330	5.13E+01	6,330	3.31E+01	4,776
Cf-249	Np-237	9.82E-03	6,110	9.65E-03	6,110	9.82E-03	6,110	9.82E-03	6,110	7.94E-03	6,100
Cf-249	U-233	3.38E-06	24,000	3.36E-06	24,200	3.38E-06	24,000	3.38E-06	24,000	3.03E-06	23,900
Cf-249	Th-229	6.04E-07	27,600	6.02E-07	27,800	6.04E-07	27,600	6.04E-07	27,600	5.44E-07	27,400
Cl-36		2.01E+02	1,444	1.68E+02	1,508	1.93E+02	1,446	1.75E+02	1,509	1.93E+02	1,442
Cm-245	Np-237	2.59E-01	6,110	2.55E-01	6,110	2.59E-01	6,110	2.59E-01	6,110	2.12E-01	6,100
Cm-245	U-233	9.66E-05	24,000	9.59E-05	24,200	9.66E-05	24,000	9.66E-05	24,000	8.76E-05	23,900
Cm-245	Th-229	1.71E-05	27,500	1.70E-05	27,800	1.71E-05	27,500	1.71E-05	27,500	1.56E-05	27,400
H-3	-	1.85E-04	98	3.81E-04	97	1.85E-04	98	1.84E-04	98	1.85E-04	98
I-129	-	2.46E+02	1,268	1.57E+02	1,439	2.41E+02	1,265	2.28E+02	1,351	2.21E+02	1,265
K-40	-	1.03E+02	2,465	9.96E+01	2,549	9.95E+01	2,476	9.79E+01	2,536	1.01E+02	2,494
Ni-59	-	2.36E+01	4,386	4.49E+01	6,440	2.35E+01	4,386	2.39E+01	4,436	5.71E+01	4,296
Ni-63	-	9.36E-10	2,857	1.45E-10	3,136	1.04E-09	2,829	3.09E-10	3,156	4.59E-10	2,976
Np-237	-	2.90E+02	6,090	2.96E+02	6,090	2.90E+02	6,090	2.90E+02	6,090	2.61E+02	6,080
Np-237	U-233	1.39E-01	23,900	1.37E-01	24,200	1.39E-01	23,900	1.39E-01	23,900	1.32E-01	23,900
Np-237	Th-229	2.40E-02	27,500	2.38E-02	27,800	2.40E-02	27,500	2.40E-02	27,500	2.31E-02	27,400

Table 5-33 (cont'd). Peak Concentrations for Intermediate-Level Vault at 100-meter POA and Time of Occurrence for Nominal PA Case, Best Estimate Case, and Sensitivity Cases 1 to 3

Radionuclide		Nominal PA Case		Best Estimate		Sensitivity Case 1 Concrete Cracking		Sensitivity Case 2 Degraded Concrete		Sensitivity Case 3 Concrete Aging	
Parent	Progeny	Maximum ($pCi\ L^{-1}\ Ci^{-1}$)	Time (Year)	Maximum ($pCi\ L^{-1}\ Ci^{-1}$)	Time (Year)	Maximum ($pCi\ L^{-1}\ Ci^{-1}$)	Time (Year)	Maximum ($pCi\ L^{-1}\ Ci^{-1}$)	Time (Year)	Maximum ($pCi\ L^{-1}\ Ci^{-1}$)	Time (Year)
Pu-239	U-235	5.49E-05	25,000	5.61E-05	25,300	5.49E-05	25,000	5.49E-05	25,000	5.43E-05	24,900
Pu-239	Pa-231	6.20E-05	6,100	6.04E-05	6,110	6.20E-05	6,100	6.20E-05	6,100	5.38E-05	6,100
Pu-239	Ac-227	1.69E-07	6,140	1.65E-07	6,150	1.69E-07	6,140	1.69E-07	6,140	1.47E-07	6,130
Pu-241	Np-237	1.26E-03	6,110	1.24E-03	6,110	1.26E-03	6,110	1.26E-03	6,110	1.12E-03	6,100
Pu-241	U-233	8.27E-07	23,900	8.20E-07	24,200	8.27E-07	23,900	8.27E-07	23,900	7.88E-07	23,900
Pu-241	Th-229	1.43E-07	27,500	1.42E-07	27,800	1.43E-07	27,500	1.43E-07	27,500	1.37E-07	27,500
Ra-226	-	8.70E-01	7,940	8.24E-01	8,070	8.69E-01	7,940	8.66E-01	7,940	1.27E+00	7,560
Ra-226	Pb-210	1.10E-02	7,970	1.04E-02	8,600	1.09E-02	7,970	1.09E-02	7,970	1.59E-02	7,590
Tc-99	-	1.74E+02	5,910	1.55E+02	5,910	1.74E+02	5,910	1.68E+02	5,910	5.54E+02	2,976
U-235	-	7.11E+00	22,900	7.42E+00	23,000	7.11E+00	22,900	7.13E+00	22,900	7.07E+00	22,800
U-235	Pa-231	2.26E+01	6,100	2.19E+01	6,110	2.26E+01	6,100	2.26E+01	6,100	1.89E+01	6,100
U-235	Ac-227	6.15E-02	6,130	5.98E-02	6,140	6.15E-02	6,130	6.14E-02	6,130	5.16E-02	6,130

Table 5-34. Peak Concentrations for Intermediate-Level Vault at 100-meter POA and Time of Occurrence for Nominal PA Case and Sensitivity Cases 4 to 7

Radionuclide		Nominal PA Case		Sensitivity Case 4 LVZ Porosity		Sensitivity Case 5 Waste Porosity		Sensitivity Case 6 Infiltration		Sensitivity Case 7 Kd	
Parent	Progeny	Maximum (pCi L^{-1} Ci^{-1})	Time (Year)	Maximum (pCi L^{-1} Ci^{-1})	Time (Year)	Maximum (pCi L^{-1} Ci^{-1})	Time (Year)	Maximum (pCi L^{-1} Ci^{-1})	Time (Year)	Maximum (pCi L^{-1} Ci^{-1})	Time (Year)
Ag-108m	-	3.43E-03	6,600	3.50E-03	6,580	3.42E-03	6,570	4.79E-03	6,460	8.65E-03	6,320
Am-241	Np-237	3.78E-02	6,110	3.76E-02	6,100	3.75E-02	6,100	4.39E-02	6,050	5.18E-02	5,990
Am-241	U-233	2.50E-05	23,900	2.54E-05	23,500	2.48E-05	24,100	2.98E-05	21,100	5.23E-05	14,648
Am-241	Th-229	4.31E-06	27,500	4.35E-06	27,100	4.28E-06	27,700	4.65E-06	24,400	5.77E-06	17,162
Ar-39	-	8.33E+01	759	8.62E+01	782	9.96E+01	745	1.60E+02	681	8.33E+01	759
C-14	-	5.12E+01	6,330	5.09E+01	6,320	2.26E+01	5,100	6.14E+01	6,210	6.79E+01	6,100
Cf-249	Np-237	9.82E-03	6,110	9.77E-03	6,100	9.83E-03	6,100	1.14E-02	6,050	1.35E-02	5,990
Cf-249	U-233	3.38E-06	24,000	3.44E-06	23,500	3.35E-06	24,000	3.96E-06	21,100	6.72E-06	14,705
Cf-249	Th-229	6.04E-07	27,600	6.09E-07	27,100	6.00E-07	27,600	6.39E-07	24,500	7.57E-07	17,162
Cl-36		2.01E+02	1,444	2.01E+02	1,439	1.97E+02	1,442	2.82E+02	1,177	3.09E+02	1,196
Cm-245	Np-237	2.59E-01	6,110	2.58E-01	6,100	2.59E-01	6,100	3.00E-01	6,050	3.54E-01	5,990
Cm-245	U-233	9.66E-05	24,000	9.82E-05	23,500	9.58E-05	24,100	1.14E-04	21,100	1.94E-04	14,705
Cm-245	Th-229	1.71E-05	27,500	1.73E-05	27,100	1.70E-05	27,600	1.82E-05	24,400	2.18E-05	17,162
H-3	-	1.85E-04	98	1.68E-04	99	3.83E-04	97	2.90E-04	92	1.85E-04	98
I-129	-	2.46E+02	1,268	2.47E+02	1,263	1.44E+02	1,358	3.81E+02	1,067	3.67E+02	1,091
K-40	-	1.03E+02	2,465	1.03E+02	2,432	1.02E+02	2,476	1.28E+02	2,058	1.72E+02	1,851
Ni-59	-	2.36E+01	4,386	2.36E+01	4,356	4.38E+01	6,430	2.73E+01	3,736	4.53E+01	2,946
Ni-63	-	9.36E-10	2,857	1.08E-09	2,829	4.43E-10	2,838	1.83E-08	2,589	1.60E-06	2,107
Np-237	-	2.90E+02	6,090	2.88E+02	6,070	2.94E+02	6,080	3.35E+02	6,030	4.39E+02	5,980
Np-237	U-233	1.39E-01	23,900	1.41E-01	23,400	1.37E-01	24,100	1.65E-01	21,000	2.92E-01	14,592
Np-237	Th-229	2.40E-02	27,500	2.42E-02	27,000	2.38E-02	27,700	2.59E-02	24,400	3.23E-02	17,081

Table 5-34 (cont'd). Peak Concentrations for Intermediate-Level Vault at 100-meter POA and Time of Occurrence for Nominal PA Case and Sensitivity Cases 4 to 7

Radionuclide		Nominal PA Case		Sensitivity Case 4 LVZ Porosity		Sensitivity Case 5 Waste Porosity		Sensitivity Case 6 Infiltration		Sensitivity Case 7 Kd	
Parent	Progeny	Maximum (pCi L^{-1} Ci^{-1})	Time (Year)	Maximum (pCi L^{-1} Ci^{-1})	Time (Year)	Maximum (pCi L^{-1} Ci^{-1})	Time (Year)	Maximum (pCi L^{-1} Ci^{-1})	Time (Year)	Maximum (pCi L^{-1} Ci^{-1})	Time (Year)
Pu-239	U-235	5.49E-05	25,000	5.55E-05	24,600	5.59E-05	25,100	5.99E-05	21,900	8.42E-05	14,936
Pu-239	Pa-231	6.20E-05	6,100	6.17E-05	6,090	6.07E-05	6,100	7.18E-05	6,040	8.58E-05	5,980
Pu-239	Ac-227	1.69E-07	6,140	1.68E-07	6,130	1.66E-07	6,130	1.92E-07	6,070	2.36E-07	6,010
Pu-241	Np-237	1.26E-03	6,110	1.25E-03	6,100	1.24E-03	6,100	1.46E-03	6,050	1.72E-03	5,990
Pu-241	U-233	8.27E-07	23,900	8.41E-07	23,500	8.20E-07	24,100	9.85E-07	21,100	1.73E-06	14,648
Pu-241	Th-229	1.43E-07	27,500	1.44E-07	27,100	1.42E-07	27,700	1.54E-07	24,400	1.91E-07	17,162
Ra-226	-	8.70E-01	7,940	8.85E-01	7,900	8.22E-01	8,060	1.45E+00	7,310	3.78E+00	6,260
Ra-226	Pb-210	1.10E-02	7,970	1.11E-02	7,930	1.04E-02	8,590	1.83E-02	7,340	5.04E-02	6,570
Tc-99	-	1.74E+02	5,910	1.70E+02	5,900	1.63E+02	5,900	1.39E+02	5,890	8.27E+01	5,930
U-235	-	7.11E+00	22,900	7.25E+00	22,400	7.42E+00	22,900	8.29E+00	20,300	1.38E+01	14,216
U-235	Pa-231	2.26E+01	6,100	2.25E+01	6,090	2.20E+01	6,100	2.62E+01	6,040	3.15E+01	5,980
U-235	Ac-227	6.15E-02	6,130	6.12E-02	6,120	6.00E-02	6,130	6.99E-02	6,070	8.62E-02	6,010

Table 5-35. Ratios of Peak Concentrations for Intermediate-Level Vault at 100-meter POA for Best Estimate and Sensitivity Cases to Nominal PA Case

Radionuclide		Best Estimate	Sensitivity Cases						
Parent	Progeny		1	2	3	4	5	6	7
Ag-108m	-	1.04	1.00	1.00	1.16	1.02	1.00	1.40	2.52
Am-241	Np-237	0.99	1.00	1.00	0.89	1.00	0.99	1.16	1.37
Am-241	U-233	0.99	1.00	1.00	0.95	1.02	0.99	1.19	2.09
Am-241	Th-229	0.99	1.00	1.00	0.96	1.01	0.99	1.08	1.34
Ar-39	-	0.42	0.96	0.43	1.00	1.04	1.20	1.92	1.00
C-14	-	1.17	1.00	1.00	0.65	0.99	0.44	1.20	1.33
Cf-249	Np-237	0.98	1.00	1.00	0.81	1.00	1.00	1.16	1.34
Cf-249	U-233	0.99	1.00	1.00	0.90	1.02	0.99	1.17	1.99
Cf-249	Th-229	1.00	1.00	1.00	0.90	1.01	0.99	1.06	1.25
Cl-36		0.84	0.96	0.87	0.96	1.00	0.98	1.41	1.54
Cm-245	Np-237	0.98	1.00	1.00	0.82	1.00	1.00	1.16	1.37
Cm-245	U-233	0.99	1.00	1.00	0.91	1.02	0.99	1.18	2.01
Cm-245	Th-229	1.00	1.00	1.00	0.91	1.01	0.99	1.06	1.27
H-3	-	2.06	1.00	1.00	1.00	0.91	2.07	1.57	1.00
I-129	-	0.64	0.98	0.93	0.90	1.00	0.58	1.55	1.49
K-40	-	0.97	0.97	0.95	0.98	1.00	1.00	1.24	1.67
Ni-59	-	1.90	0.99	1.01	2.42	1.00	1.85	1.16	1.92
Ni-63	-	0.16	1.11	0.33	0.49	1.15	0.47	19.55	1712.33
Np-237	-	1.02	1.00	1.00	0.90	0.99	1.02	1.16	1.51
Np-237	U-233	0.99	1.00	1.00	0.95	1.02	0.99	1.19	2.10
Np-237	Th-229	0.99	1.00	1.00	0.96	1.01	0.99	1.08	1.35
Pu-239	U-235	1.02	1.00	1.00	0.99	1.01	1.02	1.09	1.53

Notes:

Concentrations greater than 10% above the nominal PA case (i.e., an exceedance) are shaded in light green.

Concentrations greater than 10% below the nominal PA case are shaded in light gold.

Radionuclides with concentration ratios greater than 10 are highlighted in yellow.

Table 5-35 (cont'd). Ratios of Peak Concentrations for Intermediate-Level Vault at 100-meter POA for Best Estimate and Sensitivity Cases to Nominal PA Case

Radionuclide		Best Estimate	Sensitivity Cases						
Parent	Progeny		1	2	3	4	5	6	7
Pu-239	Pa-231	0.97	1.00	1.00	0.87	1.00	0.98	1.16	1.38
Pu-239	Ac-227	0.98	1.00	1.00	0.87	0.99	0.98	1.13	1.39
Pu-241	Np-237	0.99	1.00	1.00	0.89	1.00	0.99	1.16	1.37
Pu-241	U-233	0.99	1.00	1.00	0.95	1.02	0.99	1.19	2.09
Pu-241	Th-229	0.99	1.00	1.00	0.96	1.01	0.99	1.08	1.34
Ra-226	-	0.95	1.00	1.00	1.45	1.02	0.94	1.67	4.34
Ra-226	Pb-210	0.95	1.00	1.00	1.45	1.02	0.95	1.67	4.60
Tc-99	-	0.89	1.00	0.96	3.19	0.98	0.94	0.80	0.48
U-235	-	1.04	1.00	1.00	0.99	1.02	1.04	1.17	1.94
U-235	Pa-231	0.97	1.00	1.00	0.84	1.00	0.97	1.16	1.39
U-235	Ac-227	0.97	1.00	1.00	0.84	1.00	0.98	1.14	1.40

Notes:

Concentrations greater than 10% above the nominal PA case (i.e., an exceedance) are shaded in light green.

Concentrations greater than 10% below the nominal PA case are shaded in light gold.

Radionuclides with concentration ratios greater than 10 are highlighted in yellow.

A summary of the ratios of the peak concentrations at the 100-meter POA for the cases in Table 5-35 to the nominal PA case is presented in Table 5-36.

Table 5-36. Summary of Maximum Concentration Ratios and Number of Concentration Ratios Greater or Less than 1 for Intermediate-Level Vault Aquifer Zone

Parameter		Best Estimate	Sensitivity Cases						
			1	2	3	4	5	6	7
Maximum Conc. Ratios*	Maximum Value	2.06	1.11	1.01	3.19	1.15	2.07	1.92	4.60
	Minimum Value	0.16	0.96	0.33	0.49	0.91	0.44	0.80	0.48
No. of Conc. Ratios < 1	Conc. Ratios < 0.5	2	0	2	1	0	2	0	1
	Conc. Ratios < 0.9	5	0	3	10	0	3	1	1
No. of Conc. Ratios > 1	Conc. Ratios > 1.1	3	1	0	5	1	3	26	30
	Conc. Ratios > 1.5	2	0	0	2	0	2	6	15

Notes:

* Excluding Ni-63 which is sensitive to peak timing because of its short half-life.

The impact of the sensitivity cases on peak concentrations at the 100-meter POA is as follows:

Significant Impact

Sensitivity Case 6 – Increasing the background infiltration in the VZ by 0.5 standard deviation increases peak concentrations at the 100-meter POA for most radionuclides. Notably, only the concentration of Tc-99 decreases.

Sensitivity Case 7 – Decreasing K_d values in the VZ and aquifer by a factor of two, which represents a change of more than 2.5 standard deviations (95% confidence limit), significantly increases peak flux for all radionuclides with nonzero K_d except for Tc-99 which shows about a 50% decrease in peak concentration. Overall, lowering K_d values has the most significant impact on peak concentrations at the 100-meter POA.

Limited Impact

Sensitivity Case 3 – Decreasing the number of pore volume exchanges required for concrete aging tends to lower the peak concentrations. However, peak concentrations of Ag-108m, Ni-59, Ra-226, Pb-210 (Ra-226), and Tc-99 increase at the 100-meter POA. Tc-99 increases by a factor of three.

Sensitivity Case 5 – Lowering waste porosity relative to soil increases peak concentrations at the 100-meter POA by a factor of about two for H-3 and Ni-59. The peak concentration of Ar-39 increases by 20% while C-14, I-129 and Ni-63 decreases by about 50%.

Minimal Impact

Sensitivity Case 1 – Doubling the gravel content to simulate an increase in concrete cracking of the vault roof and side walls when the final closure cap is installed increases concrete hydraulic conductivity and porosity without representing through-cracking of the concrete. This change has a minimal impact on peak flux for all radionuclides except Ni-63.

Sensitivity Case 2 – Extending concrete hydraulic degradation over 1,000 years instead of the 500-year limit suggested by the PAWG in NUREG-1573 (U.S. NRC, 2000) has a minimal impact on peak flux for all radionuclides except Ar-39, Cl-36, and Ni-63 – all of which have lower concentrations.

Sensitivity Case 4 – Increasing soil porosity in the LVZ by one standard deviation has a minimal impact on peak flux for all radionuclides except Ni-63 which has a 15% increase in concentration.

The best estimate case combines Sensitivity Cases 2 and 5; therefore, results for this case closely match those of the two sensitivity cases. These general conclusions are similar as those obtained for flux to the water table, which emphasizes the importance of accurately modeling VZ transport.

Figure 5-116 through Figure 5-120 compare 100-meter POA concentrations for the nominal PA case, best estimate case, Sensitivity Case 6, and Sensitivity Case 7 for 13 parent radionuclides. For most isotopes, the nominal PA and best estimate cases closely match while the sensitivity cases show concentrations peaking higher and earlier than for the nominal PA case. H-3 transport is primarily from diffusion, and all transport curves peak at nearly the same time. Ni-59 and Ni-63 show significantly different behavior. For Ni-59, the peak concentration for the best estimate case occurs higher and later than the nominal PA case. The nominal PA case for Ni-59 has a shoulder on the trailing edge of the peak, which appears to become the dominant peak for the best estimate case. This behavior is not investigated further. Ni-63, where results are strongly influenced by timing, is plotted on a semi-log graph to clearly show all cases.

Sensitivity Case 8 investigates the impact of increasing the diffusivity of tritium in concrete by one standard deviation. Results are shown in Figure 5-121. Higher diffusion through the concrete increases the maximum 100-meter POA concentration for H-3 by about 30%. This is equal to the increase found in flux to the water table (Figure 5-109).

Figure 5-122 through Figure 5-126 show a comparison of 100-meter POA concentrations for the same radionuclides in Figure 5-116 through Figure 5-120 during the 1,000-year compliance period from Year 171 to Year 1,171. In general, the nominal PA and best estimate cases are in close agreement. However, C-14 and Tc-99 concentrations for the best estimate case fall significantly below the nominal PA case values during the last 300 to 400 years of the compliance period when the highest concentrations are reached. Also, except for fast eluting H-3 and Ar-39, Sensitivity Cases 6 and 7 have the most impact on peak concentrations and result in significantly higher 100-meter POA concentrations during the compliance period. Sensitivity Case 7, which decreases K_d in the VZ and aquifer by 2.5 standard deviations, gives the highest 100-meter POA concentrations, which may be considered an approximation to the 95% confidence bound on radionuclide concentrations.

Peak concentrations at the 100-meter POA for all decay chains in the nominal PA case are presented in Figure 5-127 through Figure 5-129. Except for Pu-239, all decay chains in Figure 5-127 and Figure 5-128 include Np-237, which is likely the leading contributor to dose from these parent radionuclides.

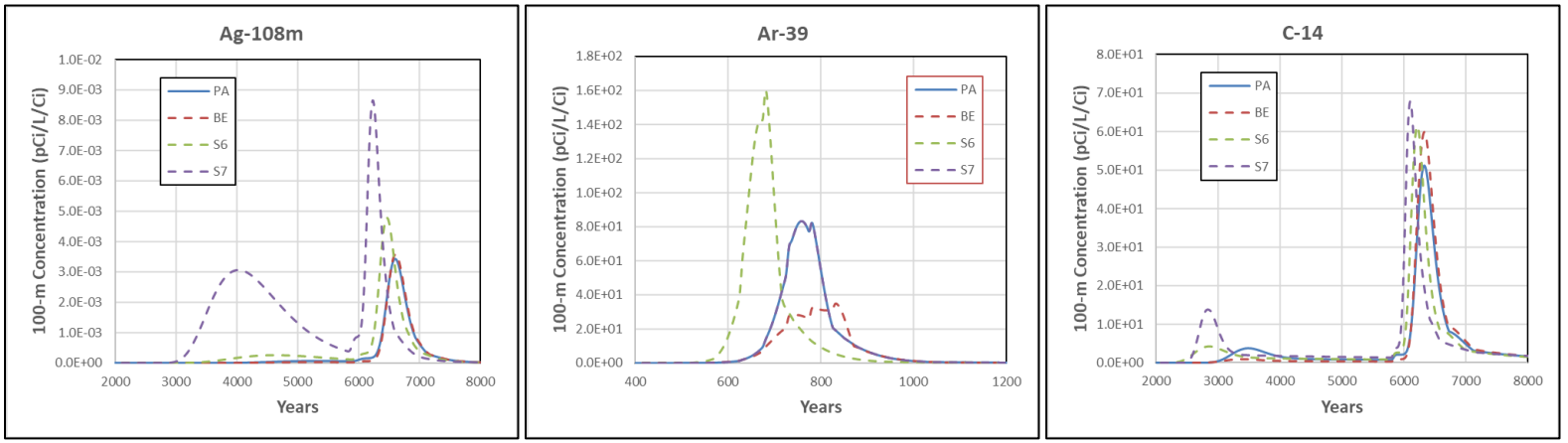

Figure 5-116. Nominal PA Case, Best Estimate (BE) Case, Sensitivity Case 6 (S6), and Sensitivity Case 7 (S7) Concentrations for Intermediate-Level Vault at 100-meter POA for Ag-108m, Ar-39, and C-14

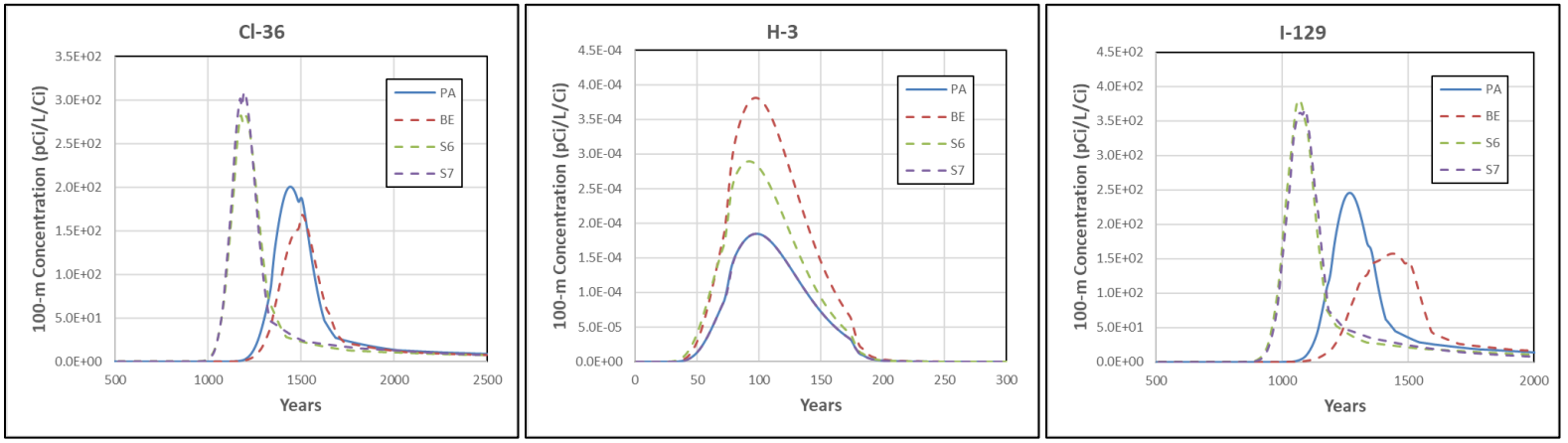

Figure 5-117. Nominal PA Case, Best Estimate (BE) Case, Sensitivity Case 6 (S6), and Sensitivity Case 7 (S7) Concentrations for Intermediate-Level Vault at 100-meter POA for Cl-36, H-3, and I-129

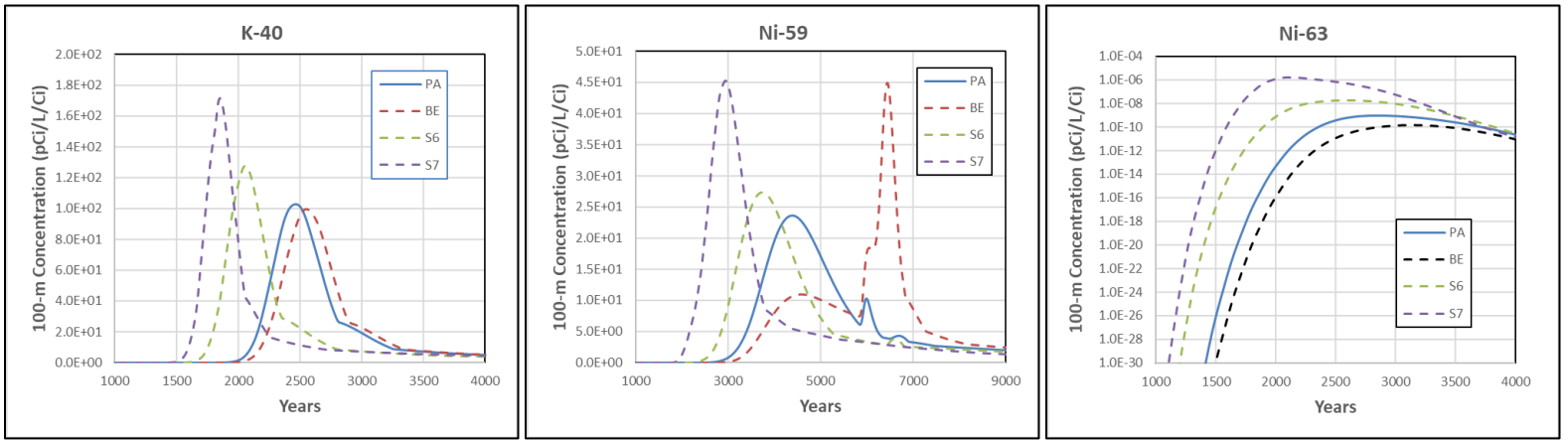

Figure 5-118. Nominal PA Case, Best Estimate (BE) Case, Sensitivity Case 6 (S6), and Sensitivity Case 7 (S7) Concentrations for Intermediate-Level Vault at 100-meter POA for K-40, Ni-59, and Ni-63

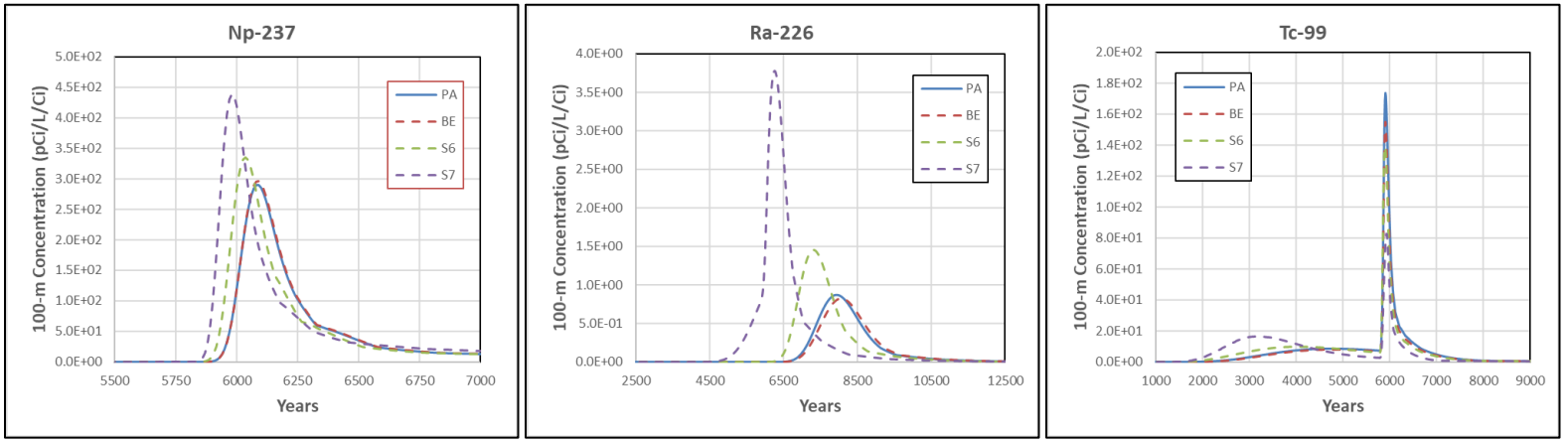

Figure 5-119. Nominal PA Case, Best Estimate (BE) Case, Sensitivity Case 6 (S6), and Sensitivity Case 7 (S7) Concentrations for Intermediate-Level Vault at 100-meter POA for Np-237, Ra-226, and Tc-99

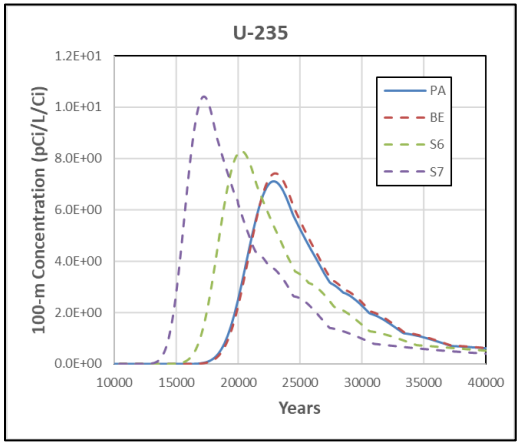

Figure 5-120. Nominal PA Case, Best Estimate (BE) Case, Sensitivity Case 6 (S6), and Sensitivity Case 7 (S7) Concentrations for Intermediate-Level Vault at 100-meter POA for U-235

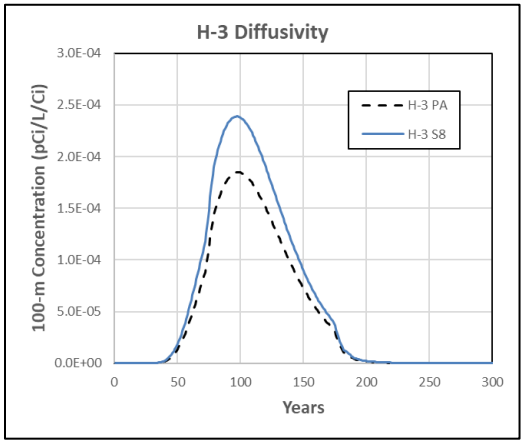

Figure 5-121. Nominal PA Case and Sensitivity Case 8 (S8) Concentrations for Intermediate-Level Vault at 100-meter POA for H-3

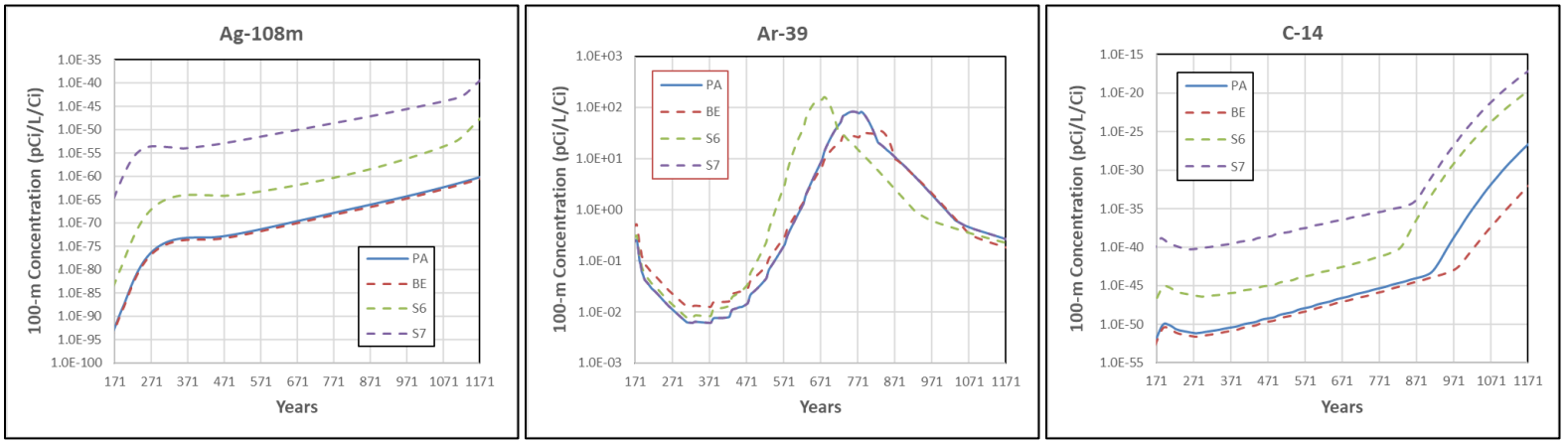

Figure 5-122. Nominal PA Case, Best Estimate (BE) Case, Sensitivity Case 6 (S6), and Sensitivity Case 7 (S7) Concentrations for Intermediate-Level Vault at 100-meter POA for Ag-108m, Ar-39, and C-14 During Compliance Period

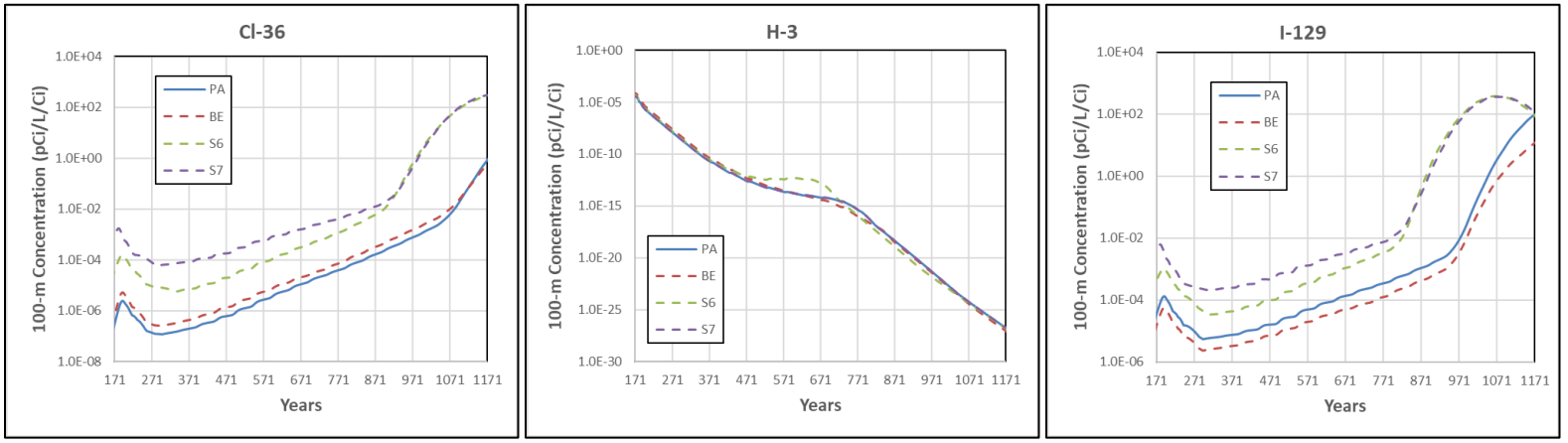

Figure 5-123. Nominal PA Case, Best Estimate (BE) Case, Sensitivity Case 6 (S6), and Sensitivity Case 7 (S7) Concentrations for Intermediate-Level Vault at 100-meter POA for Cl-36, H-3, and I-129 During Compliance Period

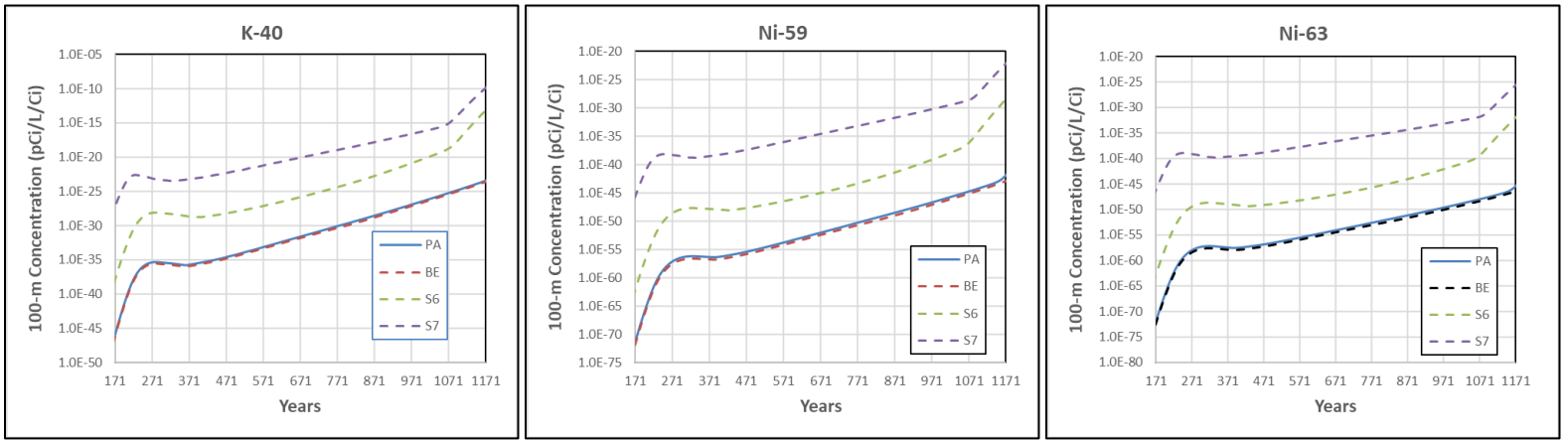

Figure 5-124. Nominal PA Case, Best Estimate (BE) Case, Sensitivity Case 6 (S6), and Sensitivity Case 7 (S7) Concentrations for Intermediate-Level Vault at 100-meter POA for K-40, Ni-59, and Ni-63 During Compliance Period

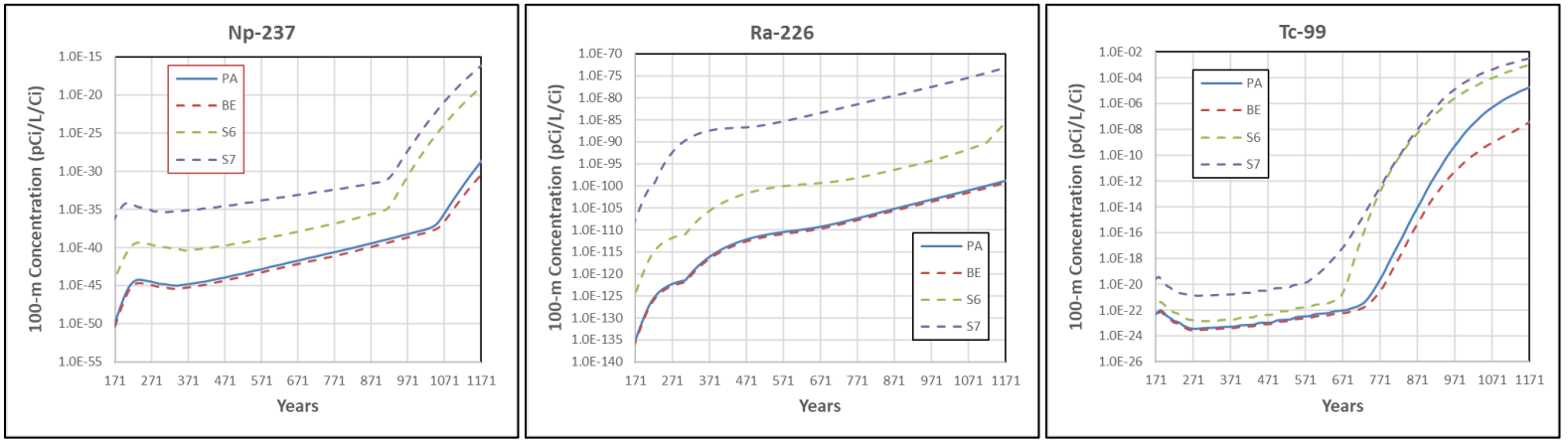

Figure 5-125. Nominal PA Case, Best Estimate (BE) Case, Sensitivity Case 6 (S6), and Sensitivity Case 7 (S7) Concentrations for Intermediate-Level Vault at 100-meter POA for Np-237, Ra-226, and Tc-99 During Compliance Period

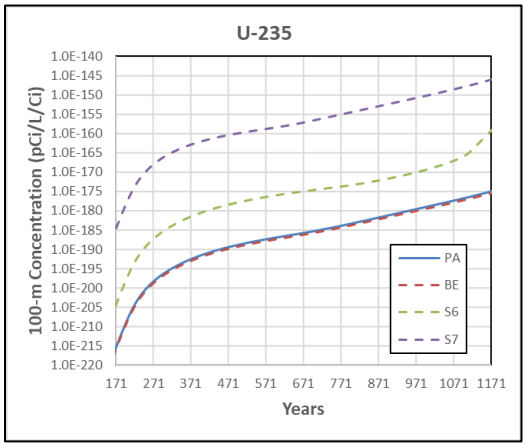

Figure 5-126. Nominal PA Case, Best Estimate (BE) Case, Sensitivity Case 6 (S6), and Sensitivity Case 7 (S7) Concentrations for Intermediate-Level Vault at 100-meter POA for U-235 During the Compliance Period

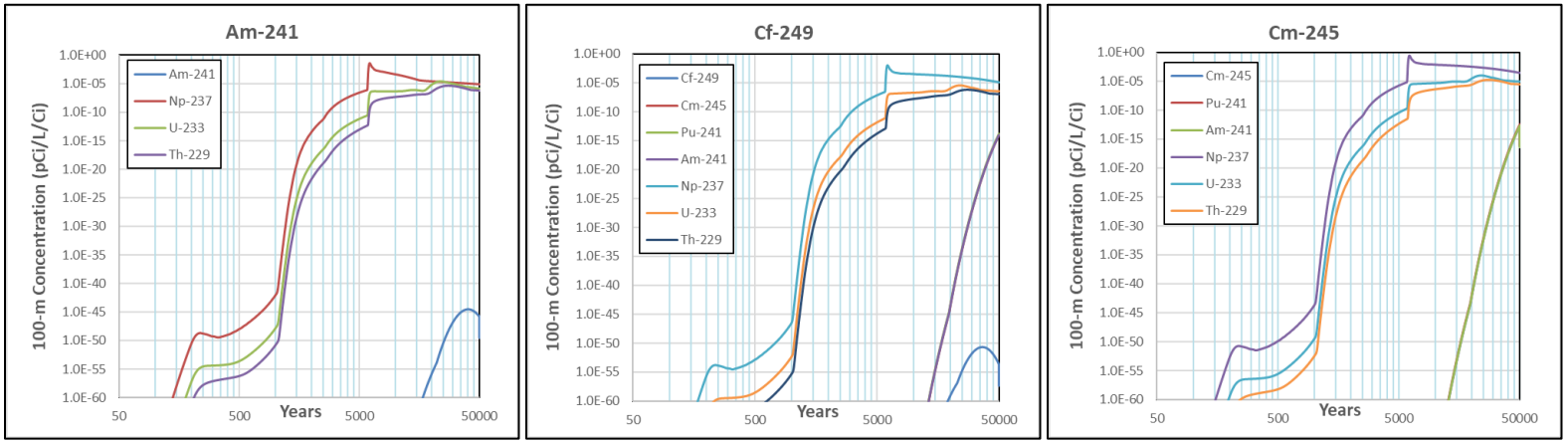

Figure 5-127. Nominal PA Case Concentrations for Intermediate-Level Vault at 100-meter POA for Am-241, Cf-249, and Cm-245 Decay Chains

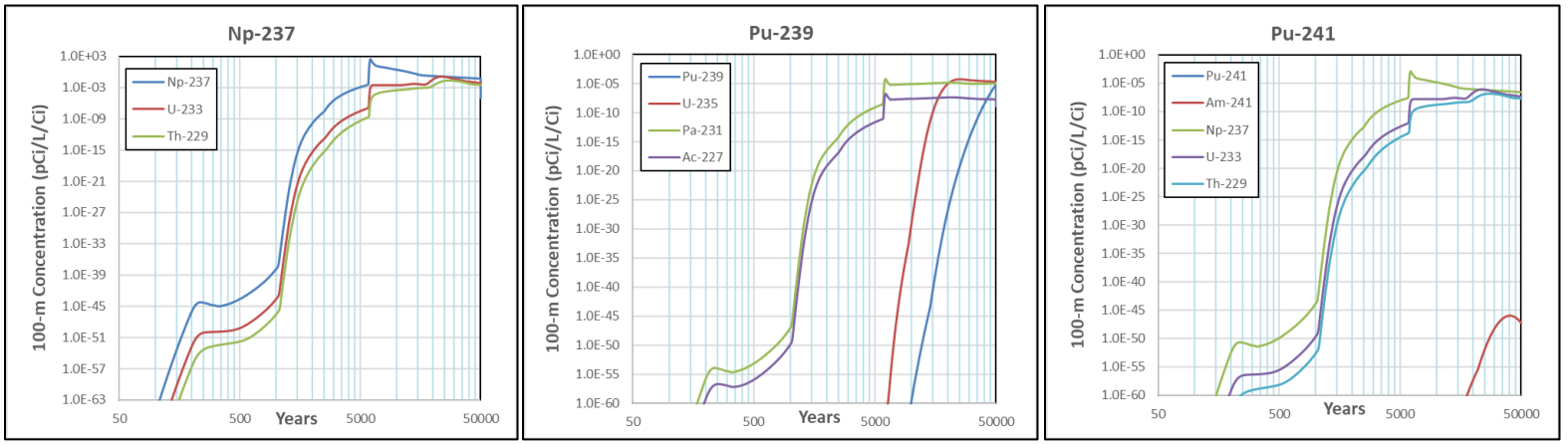

Figure 5-128. Nominal PA Case Concentrations for Intermediate-Level Vault at 100-meter POA for Np-237, Pu-239, and Pu-241 Decay Chains

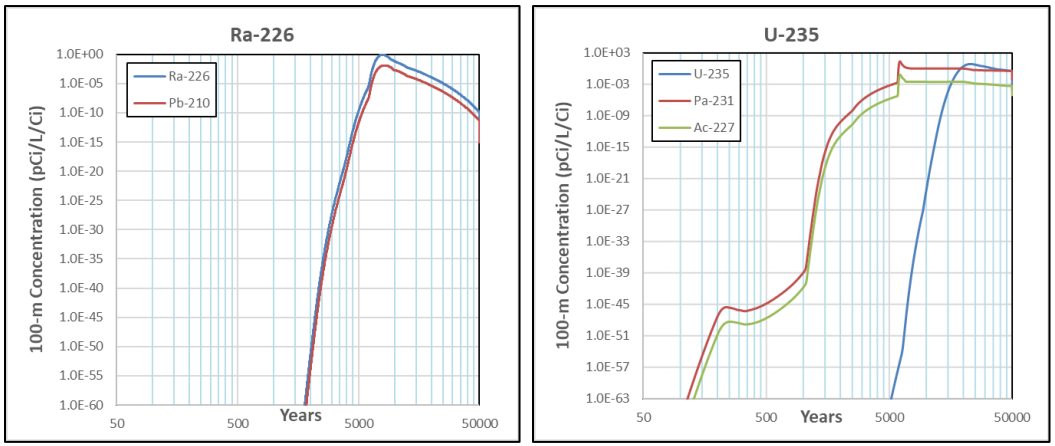

Figure 5-129. Nominal PA Case Concentrations for Intermediate-Level Vault at 100-meter POA for Ra-226 and U-235 Decay Chains

5.3.2.2. Transport Model Results for Special Waste Forms

In addition to generic waste, the transport of five SWFs is modeled for the ILV: C-14; I-129; Tc-99 in resin from the K-Area Disassembly Basin (KB); I-129 in waste received from the ETF; and H-3 released from TPBAR disposal containers. These chemical SWFs are assigned different K_d values in the waste zone (Kaplan, 2016b; SRNL, 2018). Cementitious K_d values are normally used for ILV waste because, as layers of waste within the ILV are completed, they are grouted in place to form a base for the next layer. Therefore, ILV waste is largely within a cementitious environment. Release of H-3 from TPBAR disposal containers is derived from the model by Gorensek (2021).

Results of modeling the concentration at the 100-meter POA for C-14, I-129, and Tc-99 SWFs are shown in Figure 5-130 and Figure 5-131. Like the flux-to-the-water-table results, C-14_KB concentration peaks earlier while I-129_KB and I-129_ETF peak later than the nominal PA case. Peak concentrations for I-129_ETF and I-129_KB are approximately 20 and 40 times smaller, respectively, than the nominal PA case peak concentration.

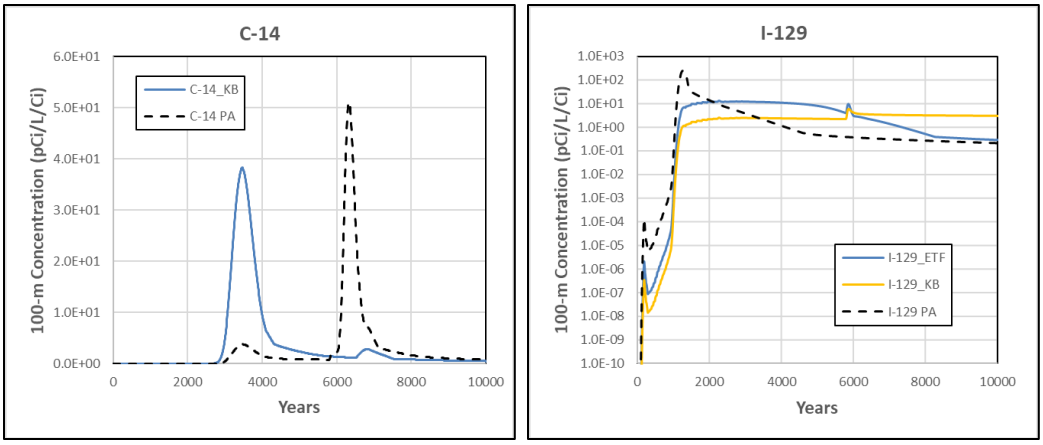

Figure 5-130. C-14 and I-129 Special Waste Form Concentrations for Intermediate-Level Vault at 100-meter POA

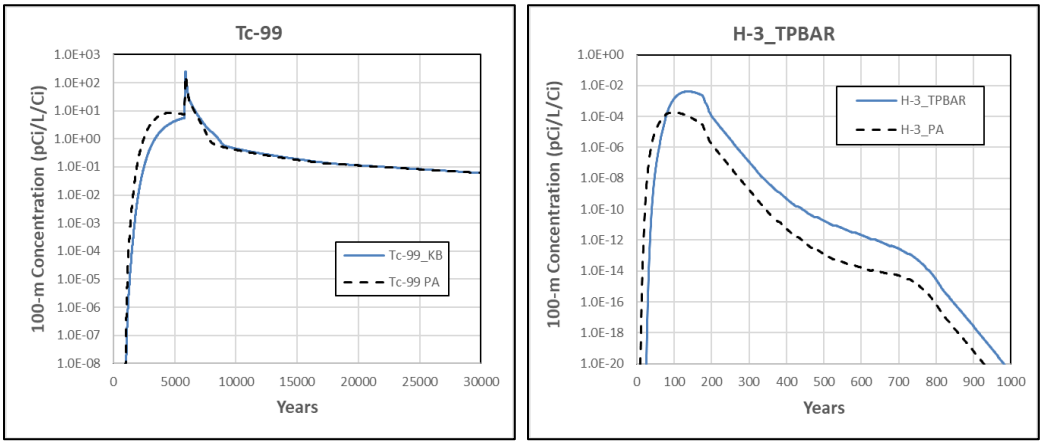

Figure 5-131. Tc-99 and TPBAR H-3 Special Waste Form Concentrations for Intermediate-Level Vault at 100-meter POA

As shown in Figure 5-131, the peak Tc-99 concentration occurs at the same time for both the generic waste form (Tc-99 PA) and the SWFs (Tc-99_KB). The Tc-99 peak occurs shortly after ILV roof collapse in Year 5,770. Conversely, the release rate of Tc-99 is slow before Year 5,770. The sharp peak occurs because of the large increase in flow through the ILV following roof collapse.

For the TPBAR calculation shown in Figure 5-131, the concentration at the 100-meter POA represents the total of all tritium released from the TPBAR disposal containers; it is not based on the usual assumed disposal of one curie in the ILV. Therefore, while TPBAR H-3 (H-3_TPBAR) is plotted together with the concentration resulting from disposal of one curie of generic waste form H-3 (H-3_PA), the two peaks are not directly comparable. Still, they seem to follow the same general elution pattern.

5.3.2.3. Concentration Contour Plots

The movement of radionuclides through the aquifer is best described through contour plots using the ELLWF map scheme in Figure 5-132 to create x-y contours of the maximum concentration (pCi L^{-1} Ci^{-1} parent buried) in the vertical z direction. Refer to Section 5.2.2.2 for more background. The PORFLOW aquifer model simulates 50,000 years, starting in 1994 when ELLWF operations began. ILV plume concentrations are saved at only eight discrete times to limit model output to a manageable size: Years 71 (end of ELLWF operations); 451; 731; 1,171 (end of compliance period); 2,000; 10,000; 20,000; and 50,000. Snapshots of the maximum concentration in the z-direction are subsequently plotted. Figure 5-133 through Figure 5-142 illustrate the evolution of plumes for select radionuclides. A sampling of results from the nominal PA case and Sensitivity Cases 6 and 7 are shown. Sensitivity Case 7 displays the largest deviations from nominal PA behavior.

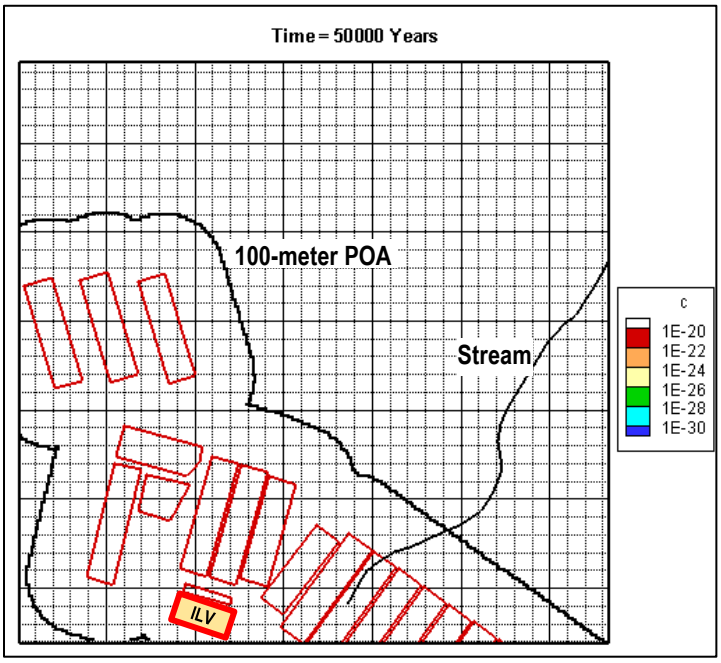

Figure 5-132. Grid Used for Intermediate-Level Vault Contour Plots

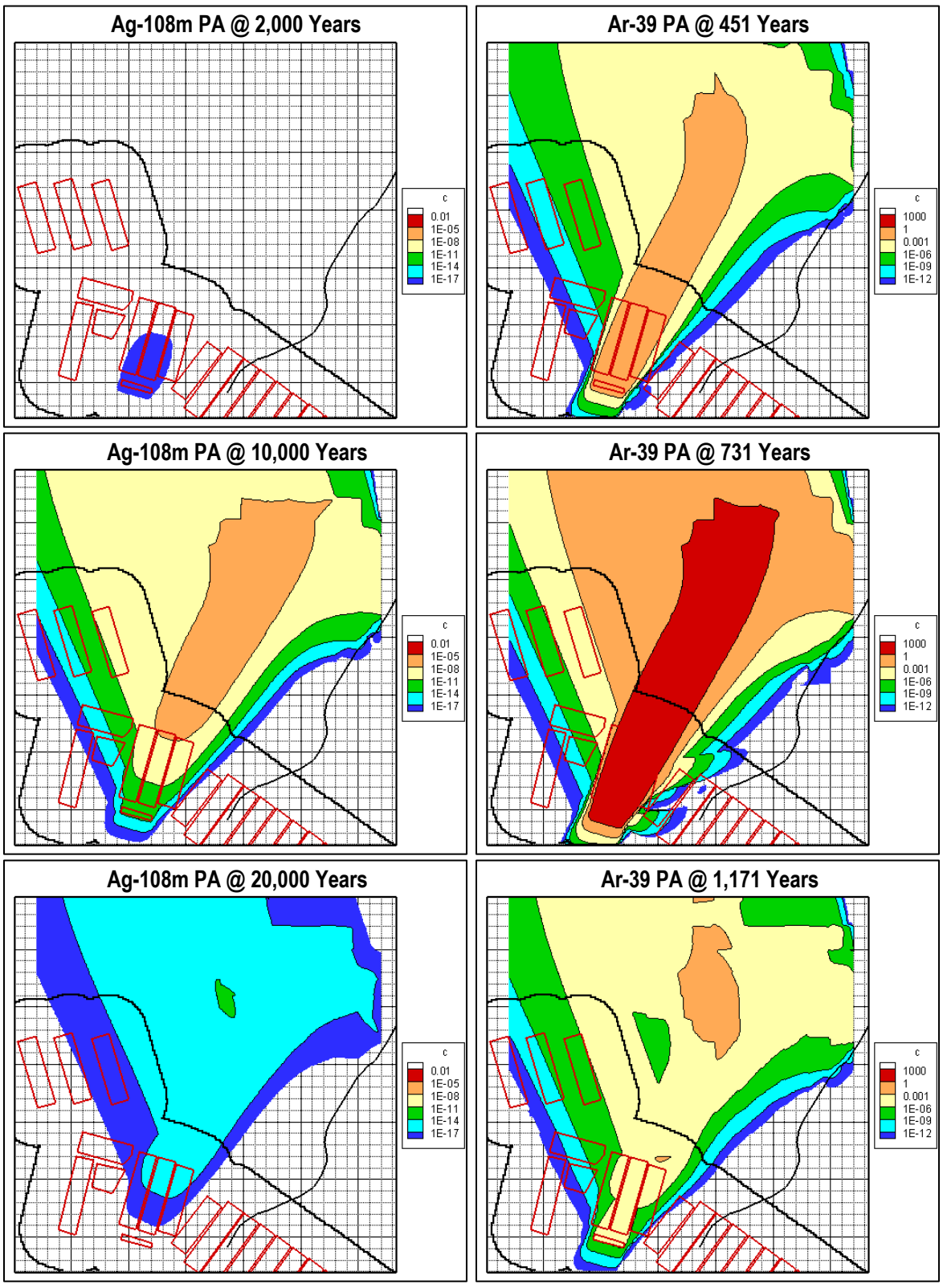

Figure 5-133. Contours of Maximum Concentration (pCi L^{-1} Ci^{-1} parent buried) for Ag-108m PA (left) and Ar-39 PA (right) Cases

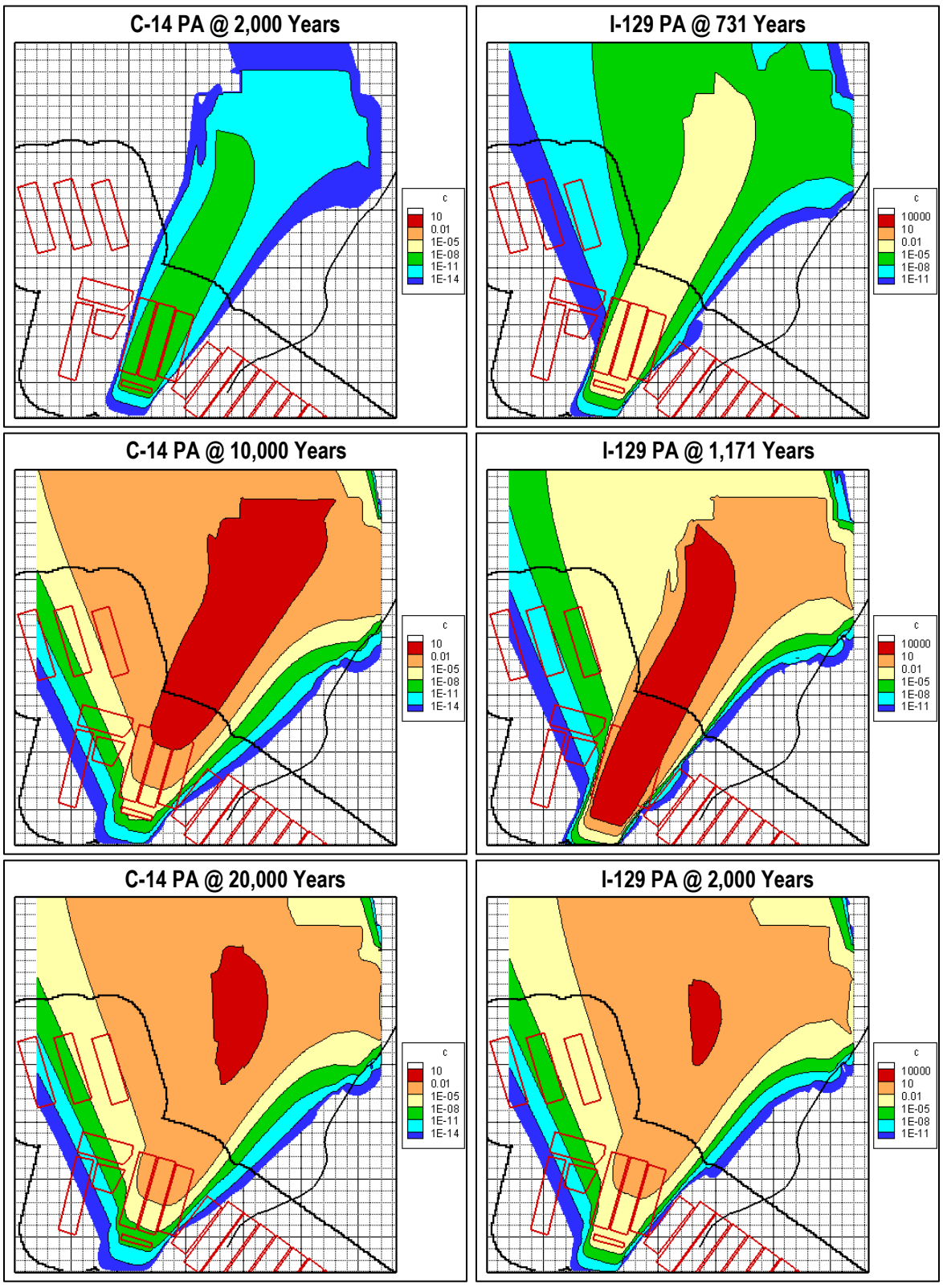

Figure 5-134. Contours of Maximum Concentration (pCi L^{-1} Ci^{-1} parent buried) for C-14 PA (left) and I-129 PA (right) Cases

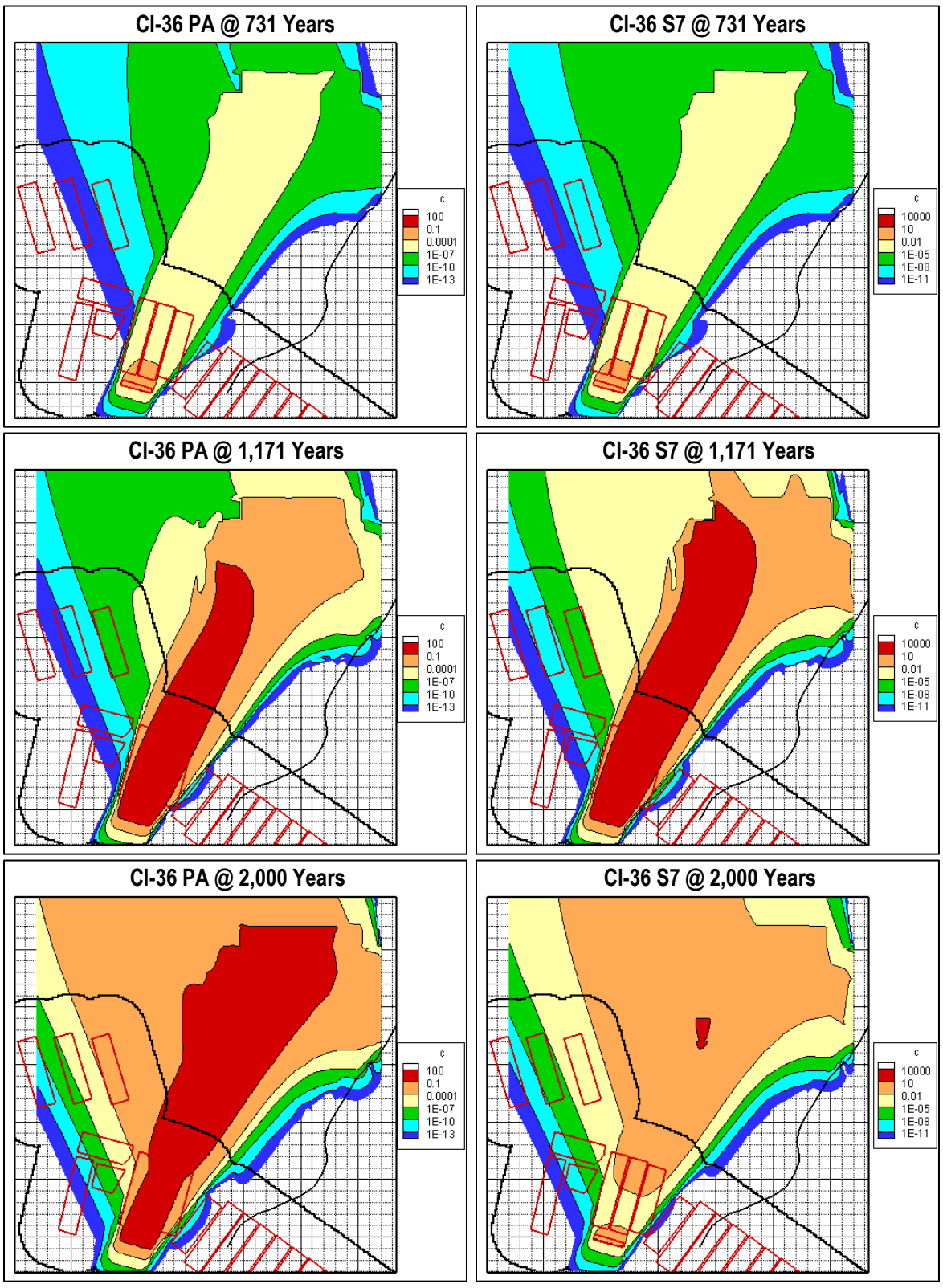

Figure 5-135. Contours of Maximum Concentration (pCi L^{-1} Ci^{-1} parent buried) for Cl-36 PA (left) and Cl-36 S7 (right) Cases

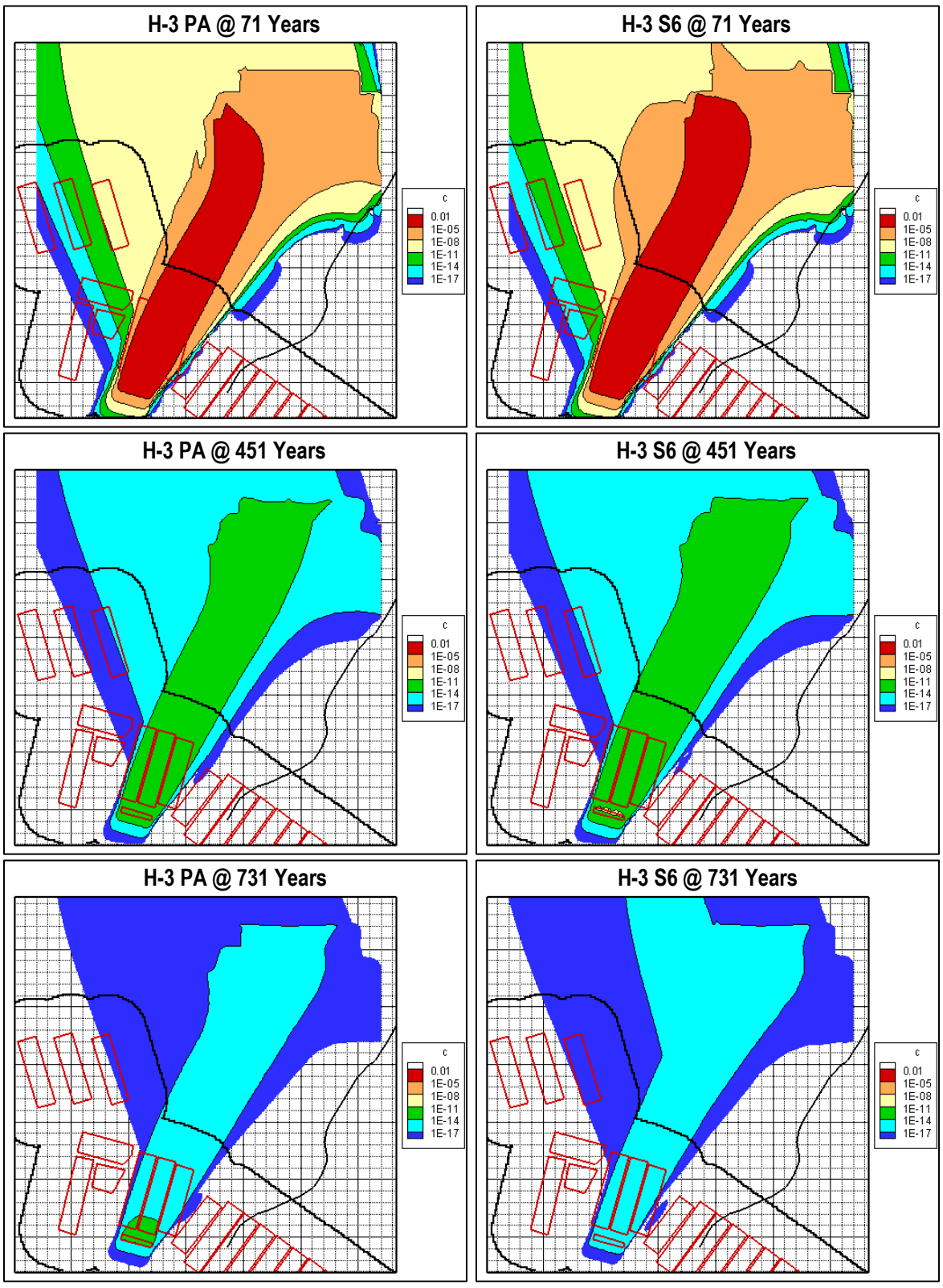

Figure 5-136. Contours of Maximum Concentration (pCi L^{-1} Ci^{-1} parent buried) for H-3 PA (left) and H-3 S6 (right) Cases

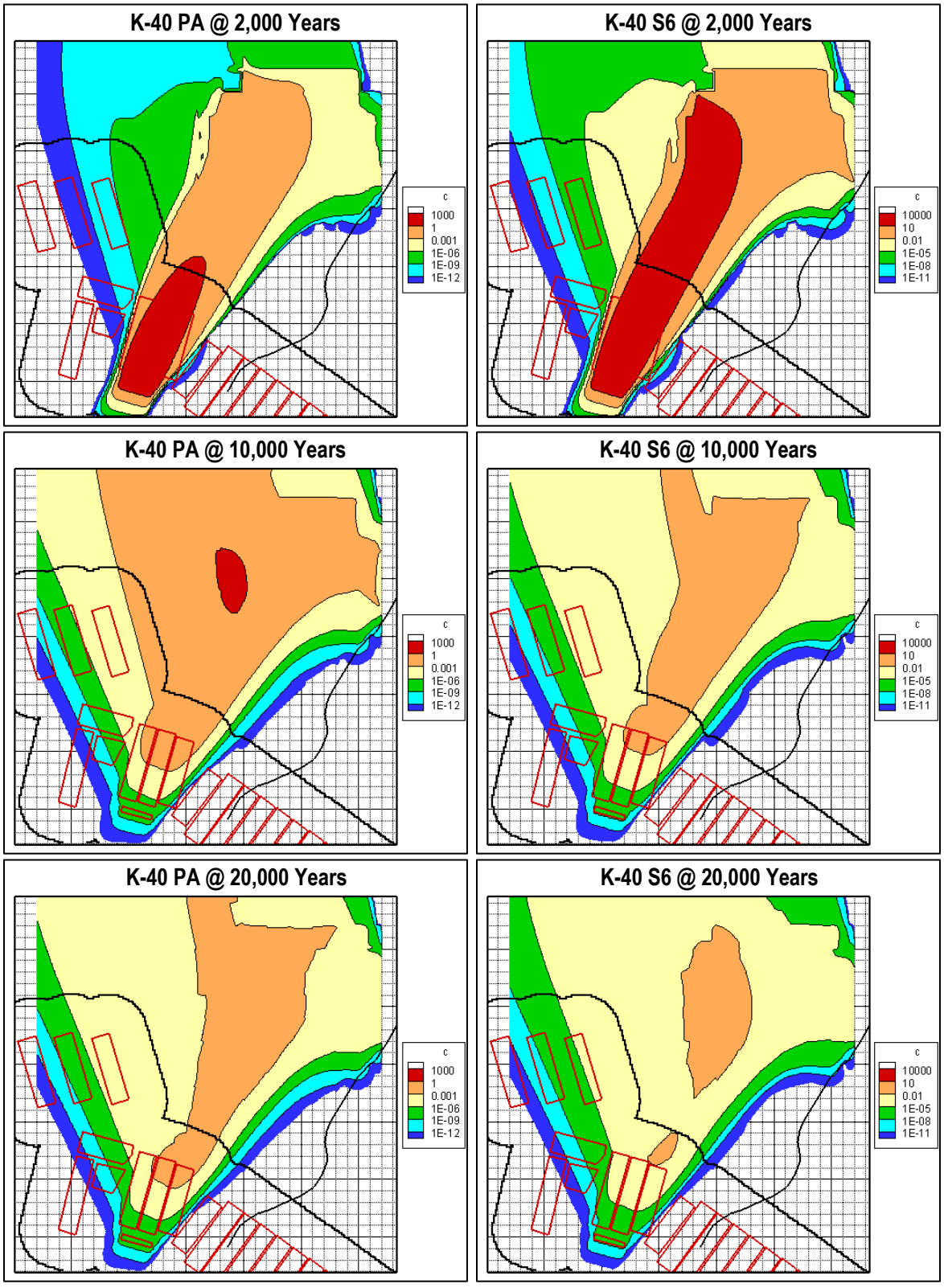

Figure 5-137. Contours of Maximum Concentration (pCi L^{-1} Ci^{-1} parent buried) for K-40 PA (left) and K-40 S6 (right) Cases

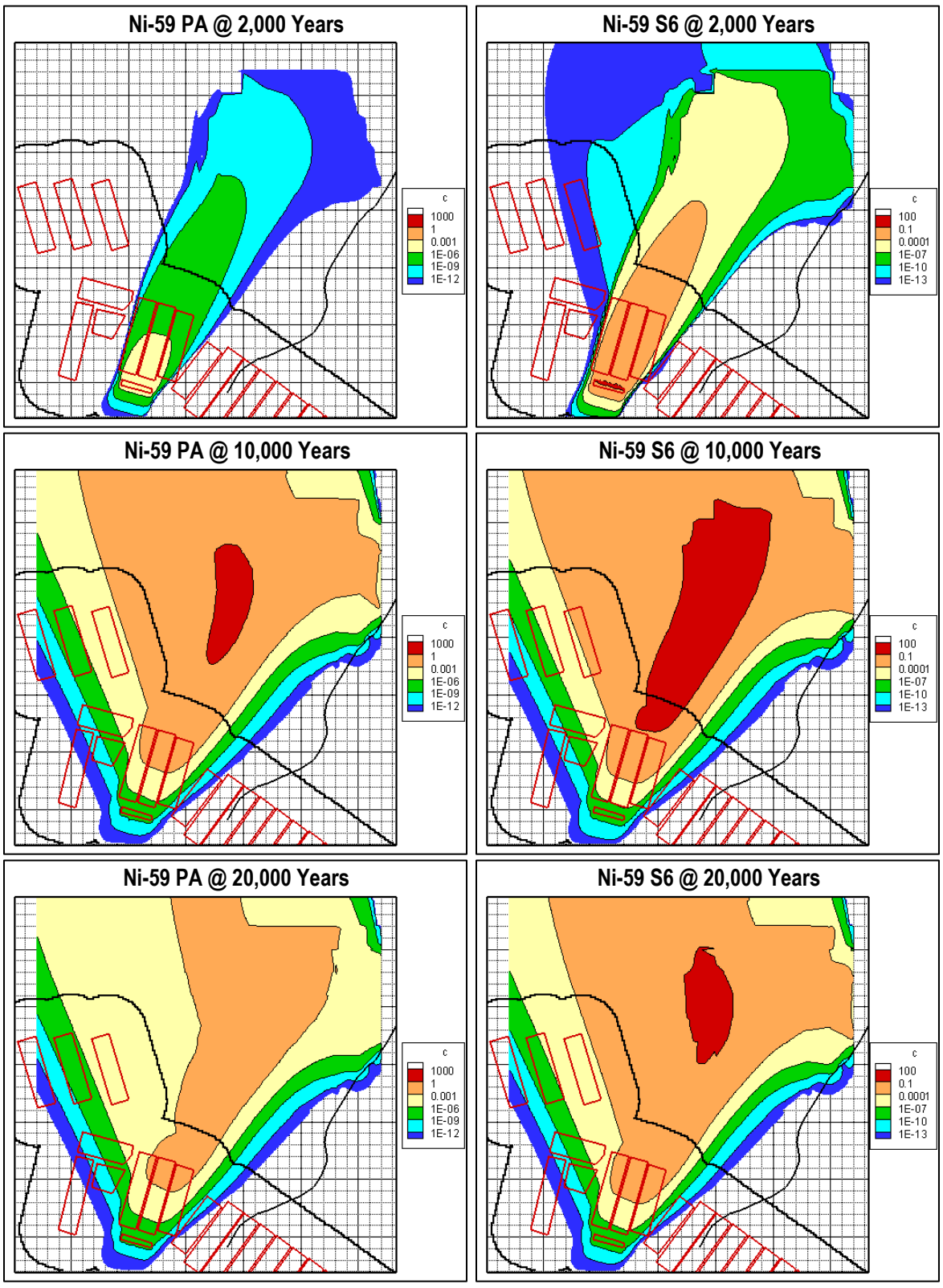

Figure 5-138. Contours of Maximum Concentration (pCi L^{-1} Ci^{-1} parent buried) for Ni-59 PA (left) and Ni-59 S6 (right) Cases

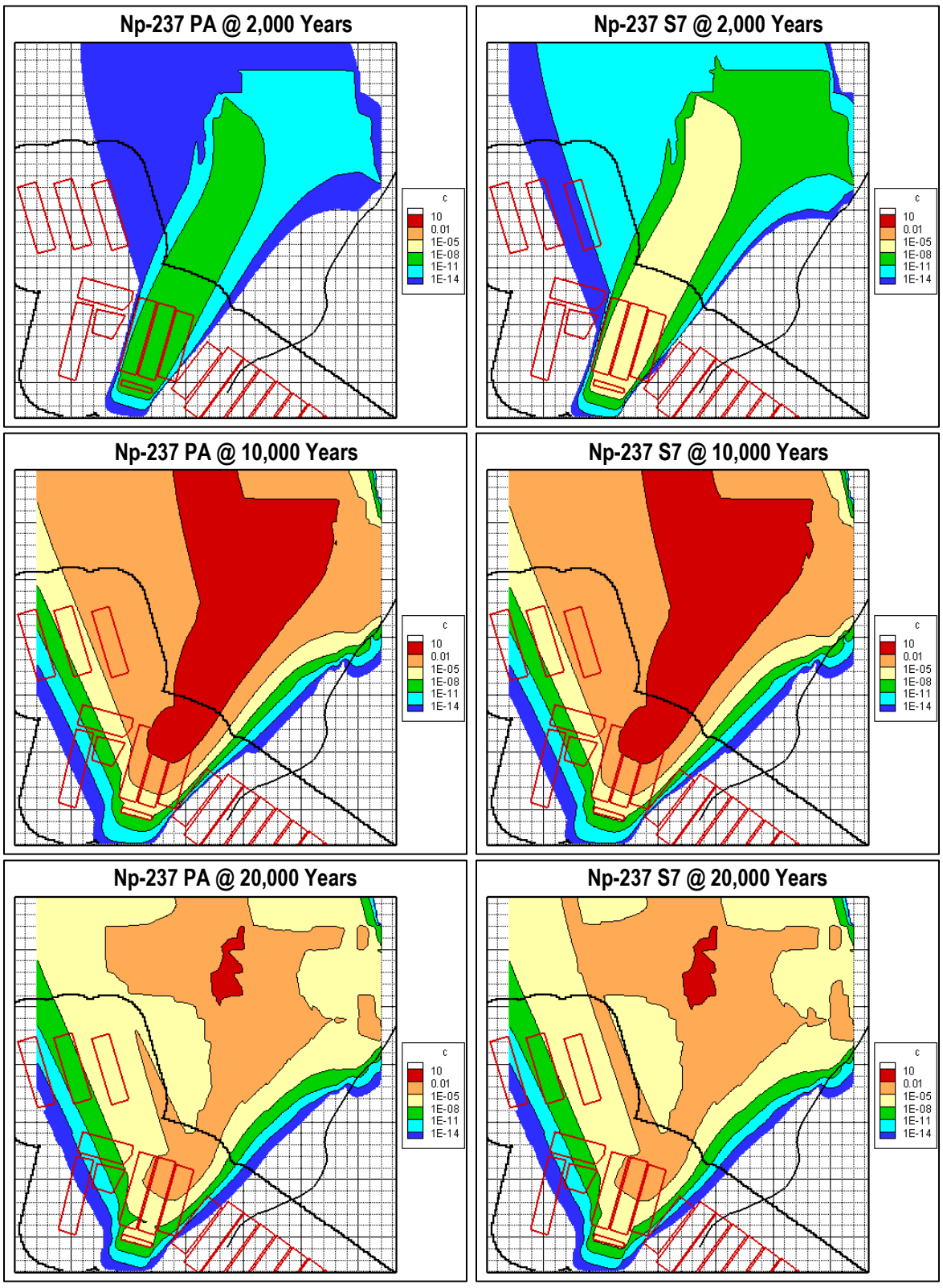

Figure 5-139. Contours of Maximum Concentration (pCi L^{-1} Ci^{-1} parent buried) for Np-237 PA (left) and Np-237 S7 (right) Cases

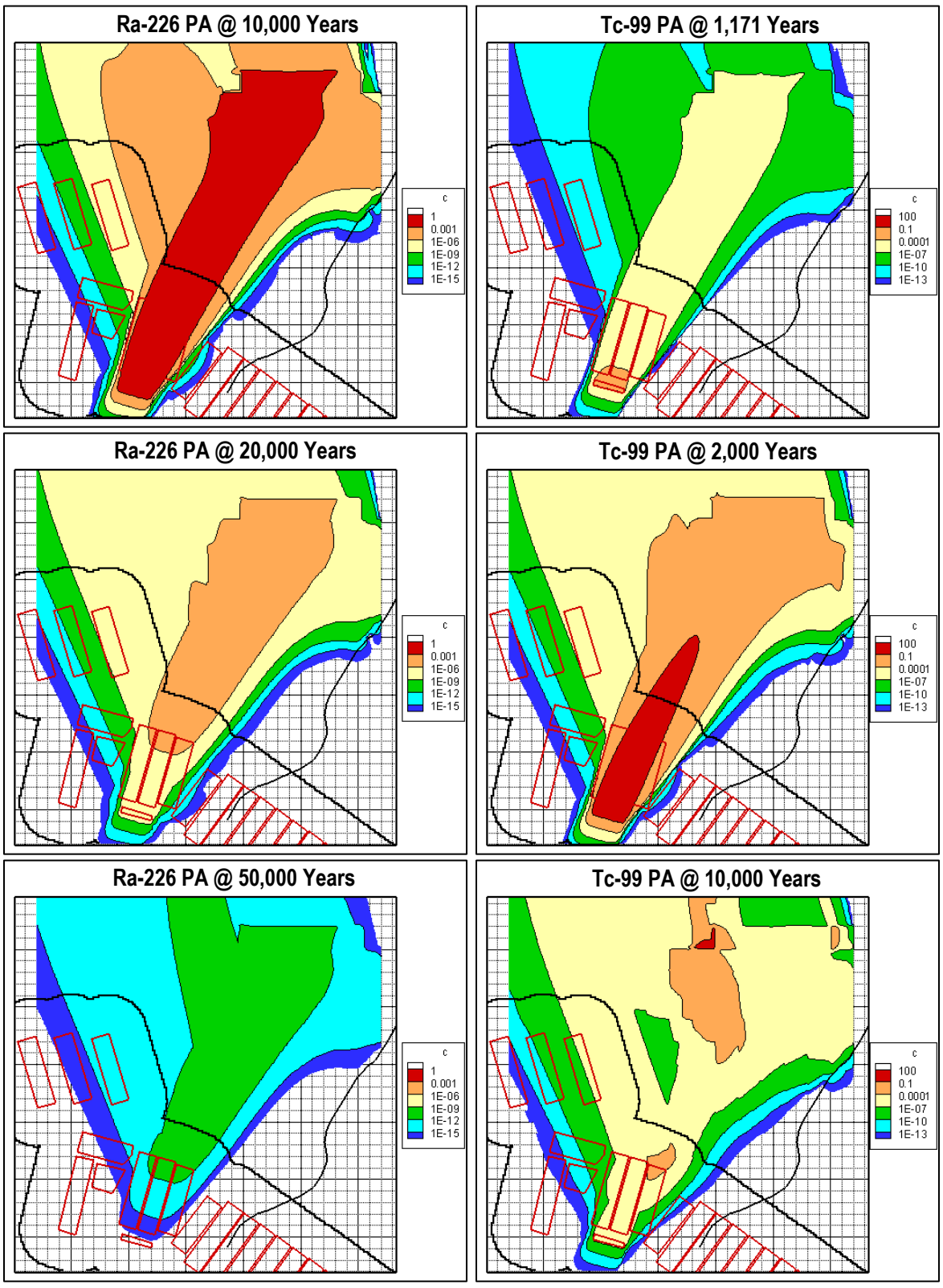

Figure 5-140. Contours of Maximum Concentration (pCi L^{-1} Ci^{-1} parent buried) for Ra-226 PA (left) and Tc-99 PA (right) Cases

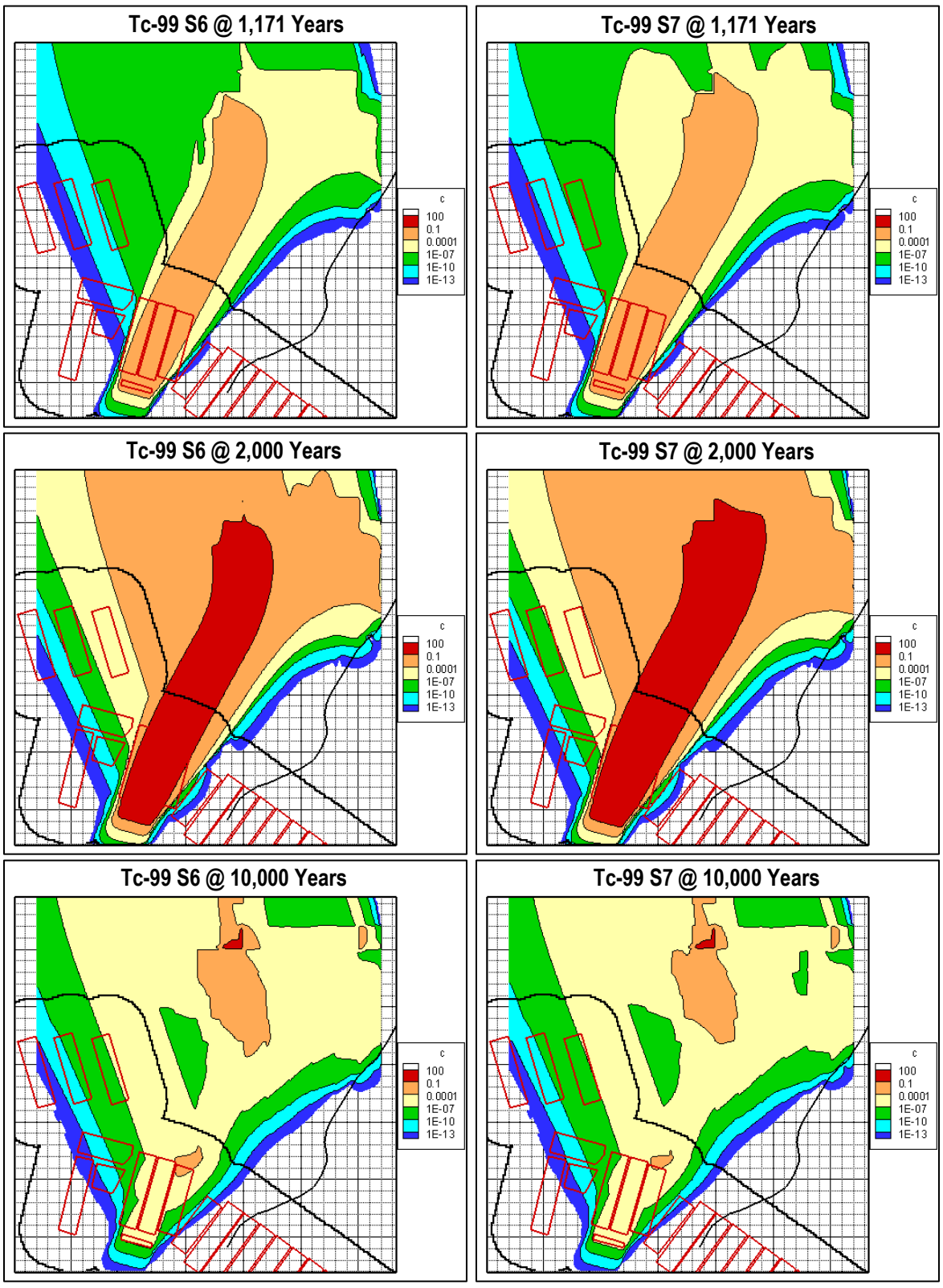

Figure 5-141. Contours of Maximum Concentration (pCi L^{-1} Ci^{-1} parent buried) for Tc-99 S6 (left) and Tc-99 S7 (right) Cases

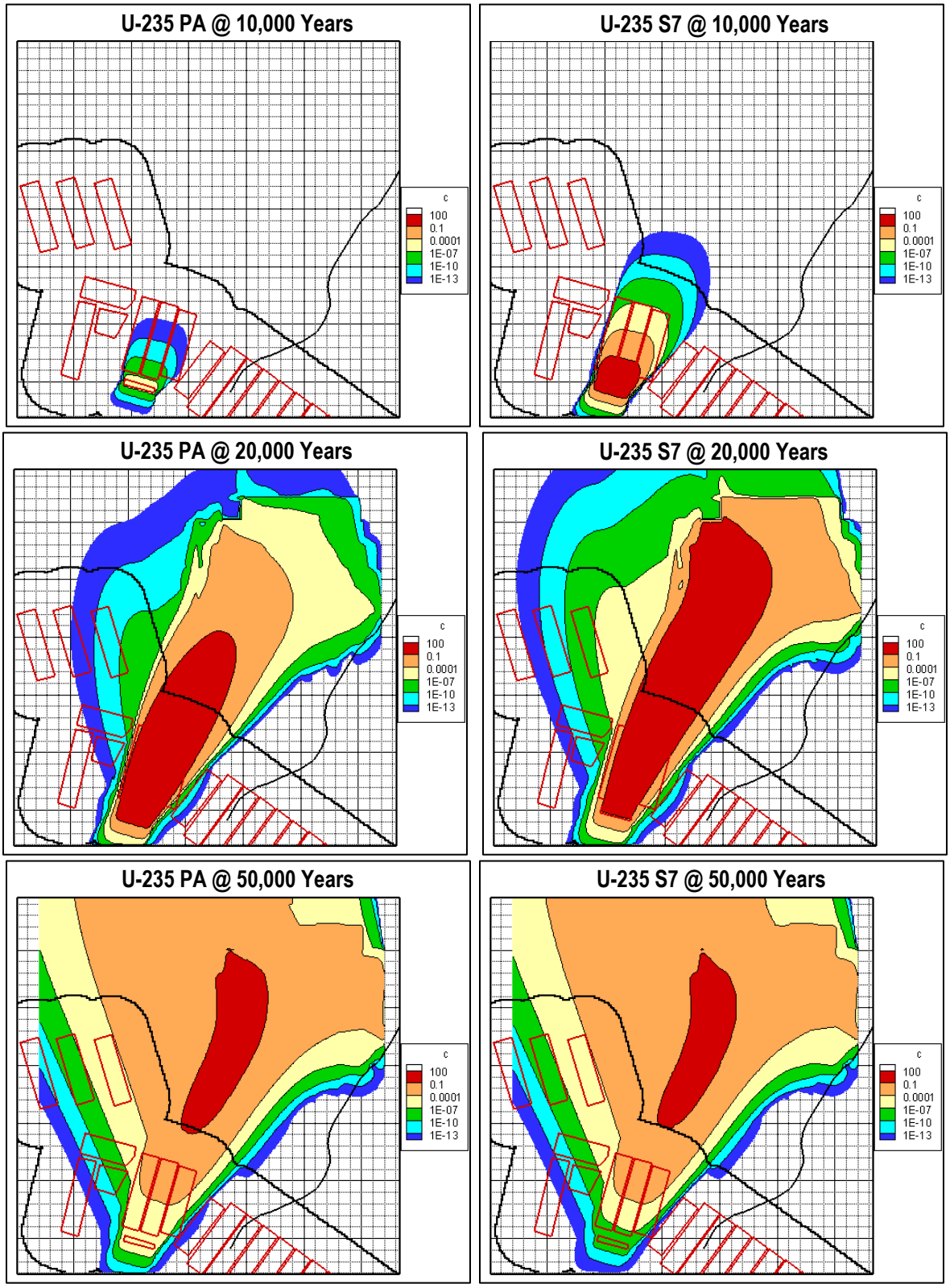

Figure 5-142. Contours of Maximum Concentration (pCi L^{-1} Ci^{-1} parent buried) for U-235 PA (left) and U-235 S7 (right) Cases

5.3.3. Air Pathway and Radon Flux Analyses

This section presents the air pathway and radon flux modeling results for the ILV. The configuration of the ARM for the ILV consists of a 1-D vertical stack of cells from the base of the waste zone to a clean layer of CLSM and a concrete roof. The top of the concrete roof is considered the ground surface before closure. Following closure at Year 171, the roof is linked to the bottom of the closure cap (Section 3.6.1.9) with the top of the erosion barrier considered the ground surface. The pertinent information regarding specific material zones, thicknesses, and properties for the ILV ARM is provided in Table 5-37. The waste is assumed to be equally distributed throughout the waste zone.

Table 5-37. Layer and Material Properties for Intermediate-Level Vault Atmospheric Release Model

Layer	Thickness (ft)	Number of Cells	Bulk Dry Density (g cm^{-3})	Porosity	Residual Water Saturation
Before Closure (Year 71 to Year 171)					
ILV Roof	2.25	8	2.54[a]	0.158[a]	0.823[a]
Clean CLSM	0.25	2	1.78[a]	0.328[a]	0.66[a]
Waste Zone	27.25	18	0.612[a]	0.736[a]	0.00001[b]
After Closure (Year 171 to Year 1,171)					
Closure Cap	Per Section 3.6.1.9				
ILV Roof	2.25	8	2.54[a]	0.158[a]	0.823[a]
Clean CLSM	0.25	2	1.78[a]	0.328[a]	0.66[a]
Waste Zone	27.25	18	0.612[a]	0.736[a]	0.00001[b]

Notes:

[a] From Nichols (2020).

[b] Waste is assumed to be dry resulting in the air-filled porosity equaling the total porosity (WSRC, 2008)

5.3.3.1. Air Pathway

The surface flux time histories of screened-in air pathway radionuclides (C-14, H-3, and Kr-85; Section 2.3.8) generated by the ARM for the ILV are converted to dose by multiplying by the DRFs of the corresponding time period (Section 3.6.2.2.5). The time histories of these doses are used to determine the grouping (immediate, delayed, or non-factor) of the radionuclide-DU pairs to account for temporal differences in dose impact (Section 8.5). The peak dose and grouping-specific effective PO are used to develop a disposal limit for each radionuclide (Section 8.5). Dose results for the ILV are presented below.

The surface flux and resulting atmospheric dose of the radionuclides buried in the ILV (Table 5-38 and Figure 5-143) are similar to those for the LAWV. Doses from C-14 peak after Year 171. C-14, which is solubility limited as it diffuses through the concrete roof, has a delayed peak at Year 1,171. Kr-85 has a short half-life compared to the other radionuclides and peaks before Year 171, decaying away after the end of IC. H-3 is not released from the ILV before decaying away. Note that truncation of the H-3 curve in Year 171 is an artifact of the GoldSim® model, wherein the H-3 dose drops below the model quantification limit of 1.0E-26 mrem yr^{-1} when the final closure cap is installed.

Table 5-38. Peak Doses from 1 Curie of C-14, H-3, and Kr-85 Buried for the Intermediate-Level Vault Air Pathway

Radionuclide	Peak Dose (mrem yr^{-1} Ci^{-1})	Peak Time (Year)
C-14	1.46E-17	1,171
H-3	---	170.99
Kr-85	1.64E-10	71.47

Notes:

--- Peak dose < 10^{-20} mrem yr^{-1}

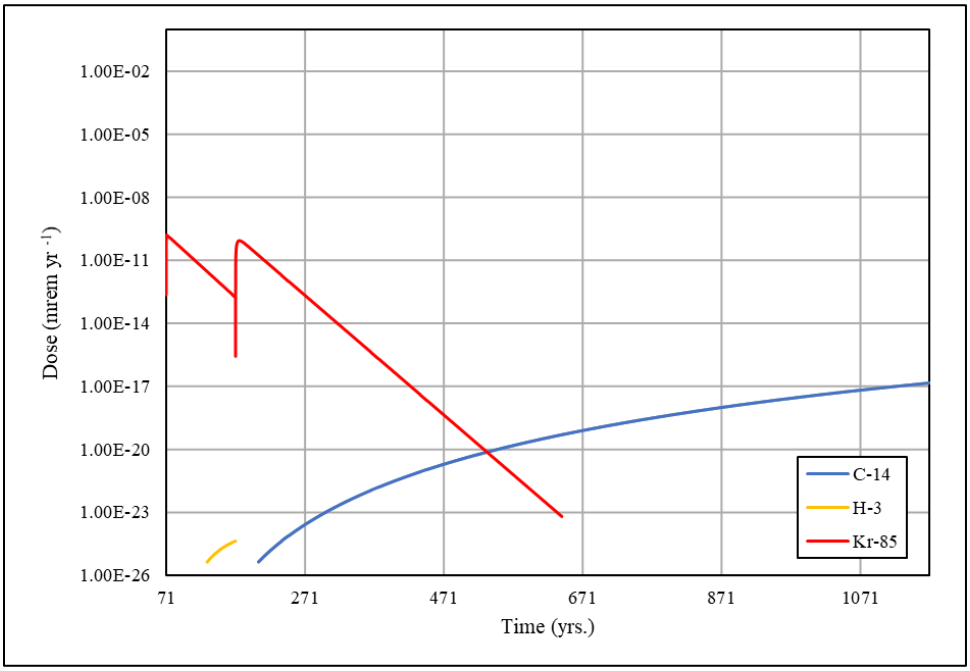

Figure 5-143. Air Pathway Dose Time Histories for 1 Curie of C-14, H-3, and Kr-85 Buried in the Intermediate-Level Vault

5.3.3.2. Radon Pathway

Surface-flux time histories are generated for Rn-222 from each of its 20 parent radionuclides for the ILV as explained in Section 5.1.5.3. Rn-222 flux time history characteristics for the ILV are as detailed for STs and ETs in Section 5.1.5.3 and are largely the same as for the LAWV but with slightly lower fluxes overall (Figure 5-144). Rn-222 peak fluxes from each parent are provided in Table 5-39. These fluxes are used for radionuclide screening in Section 2.3.8 and to determine disposal limits in Section 8.6. Radionuclides that are screened in and require further analysis and limits determination are denoted in Table 5-39 by "Limit" in the last column.

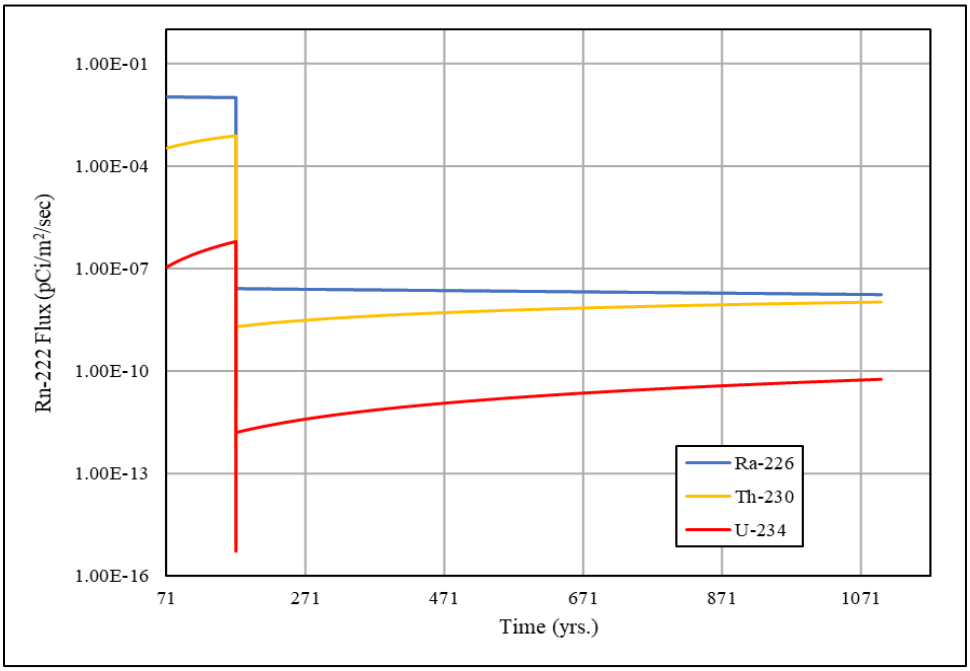

Figure 5-144. Rn-222 Flux Time Histories for 1 Curie of Ra-226, Th-230, and U-234 Buried in the Intermediate-Level Vault

Table 5-39. Peak Rn-222 Flux from 1 Curie of Rn-222 Parent Radionuclides and Rn-222 Buried for the Intermediate-Level Vault Radon Pathway

Radionuclide	Peak Rn-222 Flux (pCi m^{-2} s^{-1})	Peak Time (Year)	Limit or Trigger Required? [a]
Am-242	1.26E-15	170.99	--
Am-242m	1.84E-11	170.99	--
Am-246m	0.00E+00	--	--
Bk-250	3.06E-16	170.99	--
Cf-250	0.00E+00	--	--
Cm-242	3.72E-13	170.99	--
Cm-246	4.25E-23	170.99	--
Cm-250	0.00E+00	--	--
Np-238	4.88E-15	170.99	--
Pa-234	1.93E-15	170.99	--
Pa-234m	5.61E-18	170.99	--
Pu-238	7.39E-11	170.99	--
Pu-242	6.70E-19	170.99	--
Pu-246	0.00E+00	--	--
Ra-226	1.06E-02	72	Limit
Rn-222	0.00E+00	--	--
Th-230	7.78E-04	170.99	--
Th-234	1.66E-13	170.99	--
U-234	6.20E-07	170.99	--
U-238	1.00E-10	170.99	--

Notes:

[a] Based on radionuclide screening in Section 2.3.8.

5.4. NAVAL REACTOR COMPONENT DISPOSAL AREAS

5.4.1. Vadose Zone Model

PORFLOW VZ radionuclide transport for NR07E and NR26E are simulated to evaluate dose impacts and produce disposal limits for the ELLWF. This section presents selected flow and radionuclide contaminant transport results for the PORFLOW VZ NRCDA model. The GW pathway conceptual models for the two NRCDAs are described in Section 4.7.8 (Hang and Hamm, 2022). Radionuclide, chemical, and material properties, as well as subsurface features represented in the models, are obtained from data packages (SRNL, 2017; 2018; 2019a; 2019b; 2020).

Four modeling cases are evaluated to account for the uncertainty associated with the waste release characteristics of generic waste and SWFs: time to hydraulic failure of both the outer container and the type of metal alloy component for bolted containers versus welded casks, respectively. Table 4-83 and Table 4-84 summarize the four PORFLOW simulation cases for each NRCDA pad for the flow and radionuclide transport models, respectively. The four cases are:

- **Cases 1 and 2:** Instantaneous release of radionuclide inventory from generic waste in bolted containers. Separate VZ analyses are performed for two release times to evaluate the impact of early and delayed hydraulic failure of containers. The two release times are the initial soil cover (NR07E) or start of IC (NR26E) for Case 1, and 750 years following burial for Case 2. Subsequent aquifer analyses combine results to establish a compliance case.
- **Cases 3 and 4:** Corrosion-controlled release of radionuclides from SWFs (Inconel and Zircaloy reactor components) in welded casks. Separate VZ analyses are performed for Inconel and Zircaloy components to evaluate the impact of the different corrosion rates for the two material alloys. Subsequent aquifer analyses combine results to establish a compliance case.

The list of parent nuclides consistent with GW screening criteria (Aleman and Hamm, 2021) considered in these transport cases is provided in Table 4-86 along with radionuclide decay and elemental chemical properties (Kaplan, 2016b; SRNL, 2018).

5.4.1.1. Flow Model Results

In each flow simulation case setup, a sequence of 100 (NR07E) or 99 (NR26E) flow fields are computed spanning 10,171 years and representing various stages of the operational, IC, and final closure periods. Waste form properties and boundary conditions based on installation and degradation of infiltration barriers are considered across the three periods. This section presents a limited subset of the PORFLOW computed flow fields to display the impact of different geometries and varying boundary conditions.

The water saturation profiles for time periods corresponding to the operational and IC periods (Years -8 to 171), the first time period of final closure (Years 171 to 181), and the first time period when hydraulic failure occurs (Years 742 to 762) are shown in Figure 5-145 through Figure 5-147 for NR07E bolted containers and Figure 5-148 through Figure 5-150 for NR07E welded casks. Note that water saturation is dimensionless (vol/vol).

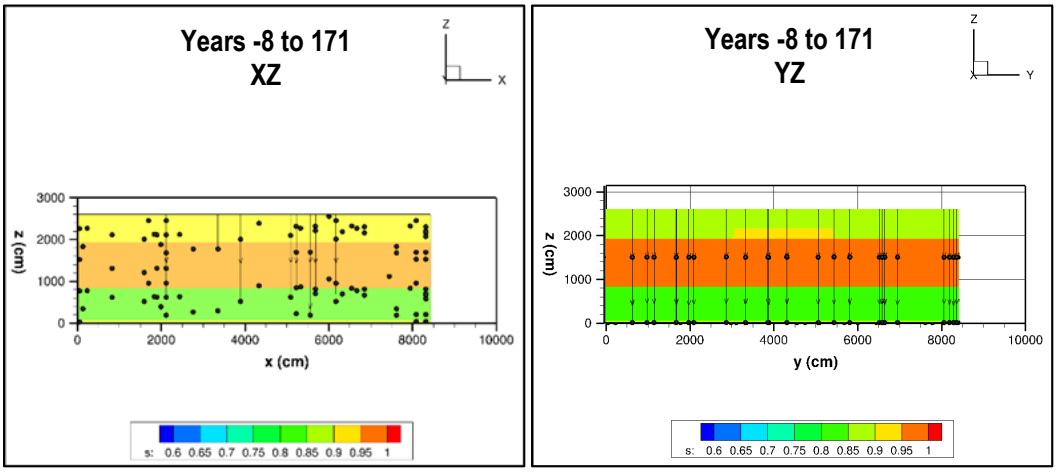

Figure 5-145. NR07E/Cases 1 and 2 – Saturation Profiles and Flow Stream Traces with 100-Year Time Markers in XZ and YZ Planes During Operational and IC Periods (Years -8 to 171)

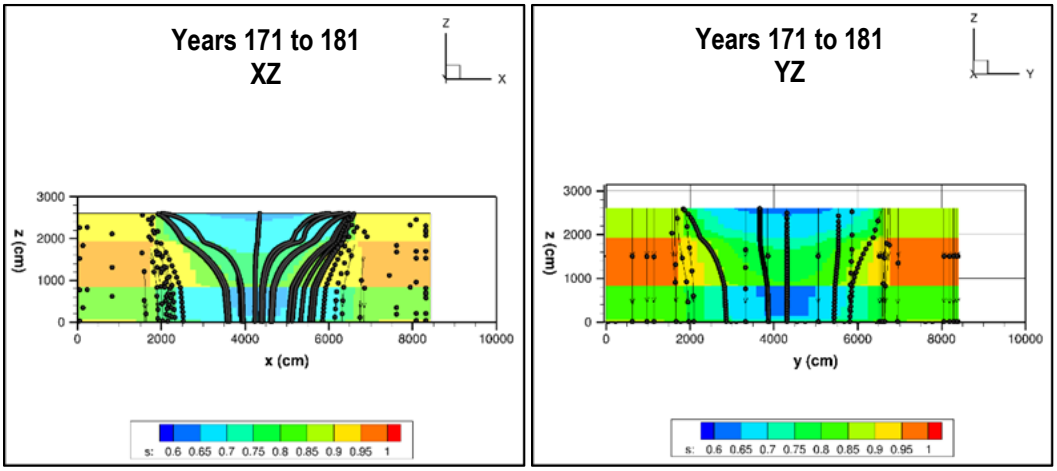

Figure 5-146. NR07E/Cases 1 and 2 – Saturation Profiles and Flow Stream Traces with 100-Year Time Markers in XZ and YZ Planes During First Time Period of Final Closure (Years 171 to 181)

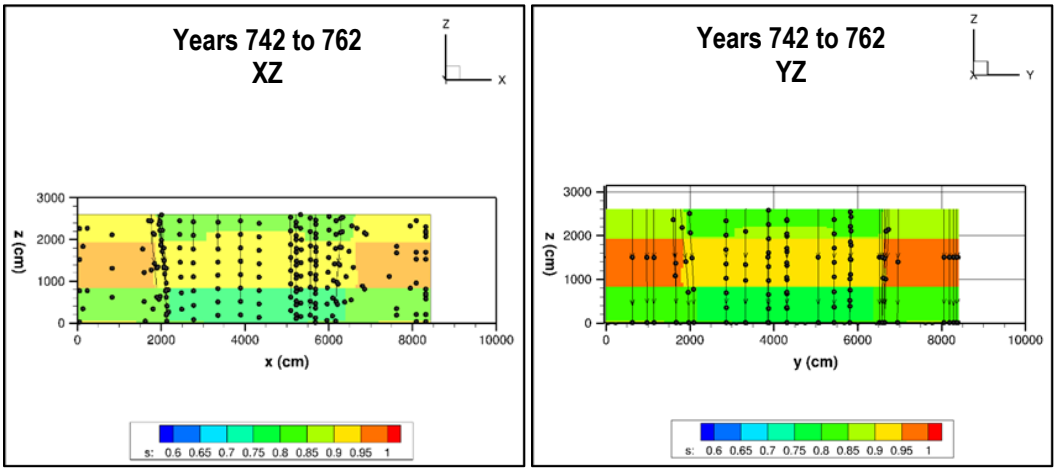

Figure 5-147. NR07E/Cases 1 and 2 – Saturation Profiles and Flow Stream Traces with 100-Year Time Markers in XZ and YZ Planes During First Period When Hydraulic Failure Occurs (Years 742 to 762)

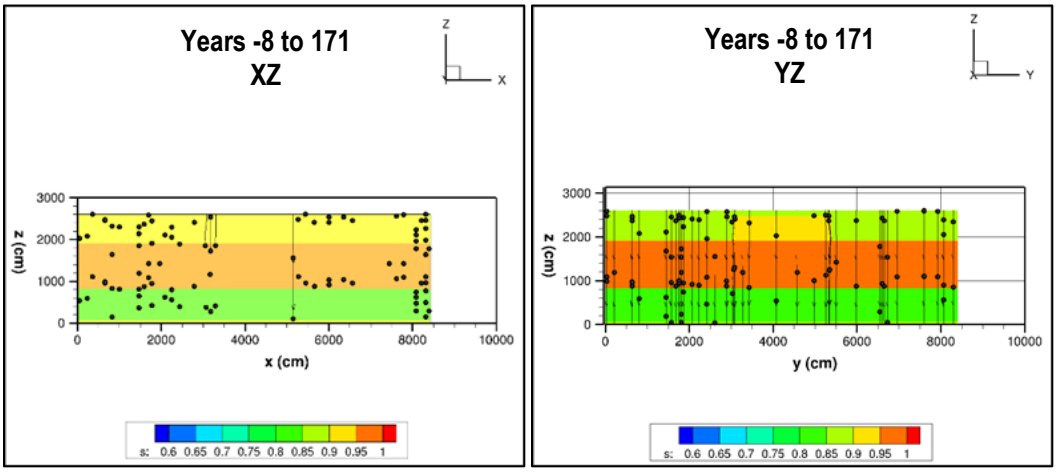

Figure 5-148. NR07E/Cases 3 and 4 – Saturation Profiles and Flow Stream Traces with 100-Year Time Markers in XZ and YZ Planes During Operational and IC Periods (Years -8 to 171)

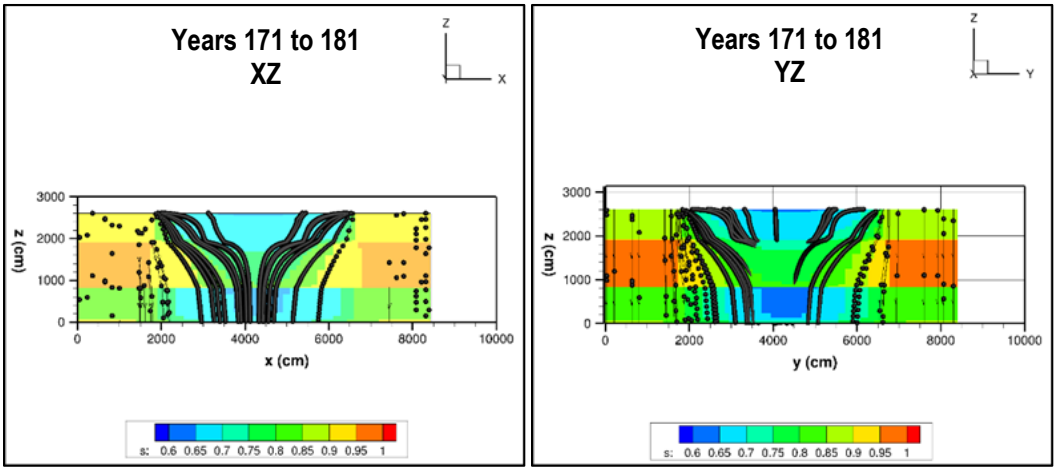

Figure 5-149. NR07E/Cases 3 and 4 – Saturation Profiles and Flow Stream Traces with 100-Year Time Markers in XZ and YZ Planes During First Time Period of Final Closure (Years 171 to 181)

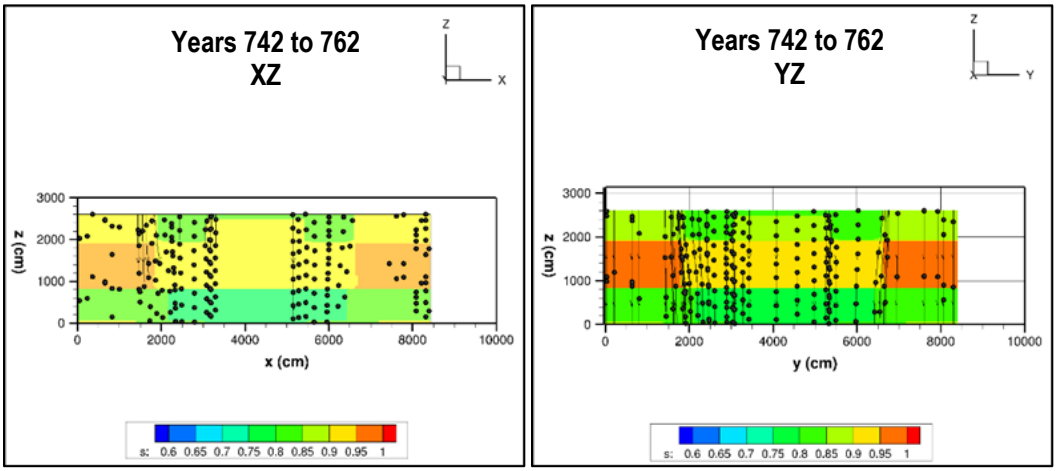

Figure 5-150. NR07E/Cases 3 and 4 – Saturation Profiles and Flow Stream Traces with 100-Year Time Markers in XZ and YZ Planes During First Period When Hydraulic Failure Occurs (Years 742 to 762)

The flow model predicts a low saturation level immediately after installation of the final closure cap due to low rainfall infiltration rates at the top boundaries. The 100-year streamtrace time markers correctly reflect the different infiltration conditions for the selected periods.

The saturation profiles for time periods corresponding to the operational and IC periods (Years 0 to 171), the first time period of final closure (Years 171 to 181), and the first time period when hydraulic failure occurs (Years 753 to 762) are shown in Figure 5-151 through Figure 5-153 for NR26E bolted containers and Figure 5-154 through Figure 5-156 for NR26E welded casks. Note that water saturation is dimensionless (vol/vol).

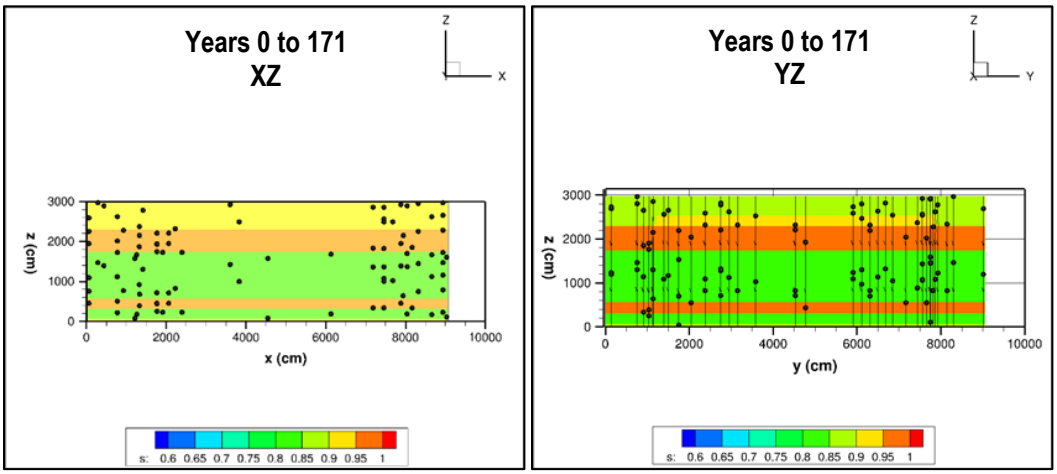

Figure 5-151. NR26E/Cases 1 and 2 – Saturation Profiles and Flow Stream Traces with 100-Year Time Markers in XZ and YZ Planes During Operational and IC Periods (Years 0 to 171)

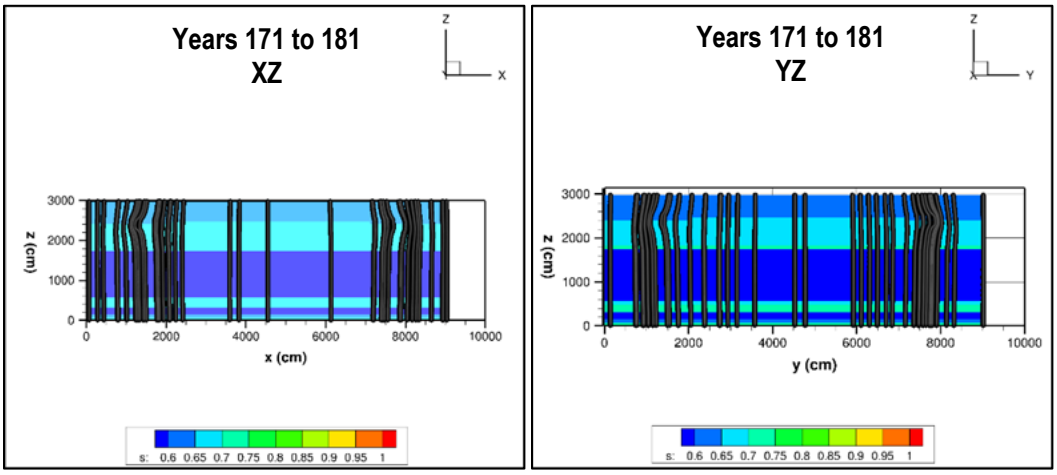

Figure 5-152. NR26E/Cases 1 and 2 – Saturation Profiles and Flow Stream Traces with 100-Year Time Markers in XZ and YZ Planes During First Time Period of Final Closure (Years 171 to 181)

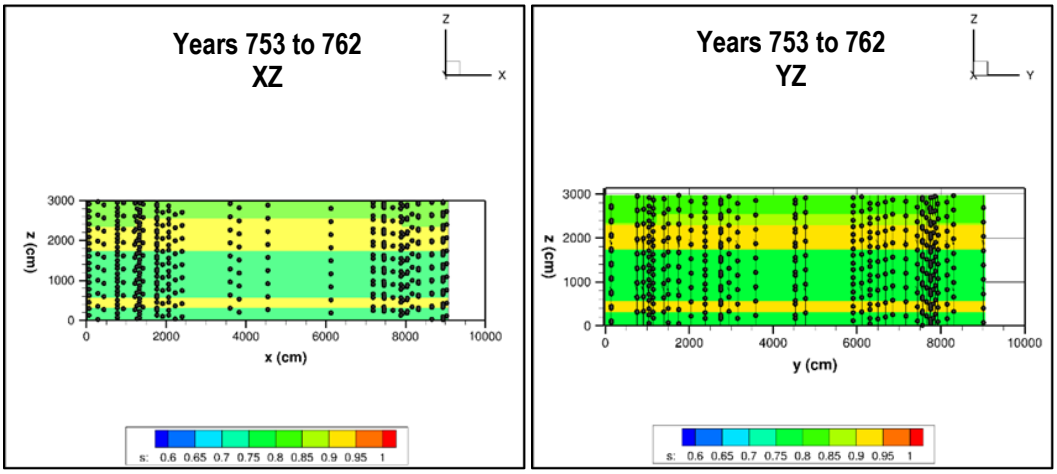

Figure 5-153. NR26E/Cases 1 and 2 – Saturation Profiles and Flow Stream Traces with 100-Year Time Markers in XZ and YZ Planes During First Period When Hydraulic Failure Occurs (Years 753 to 762)

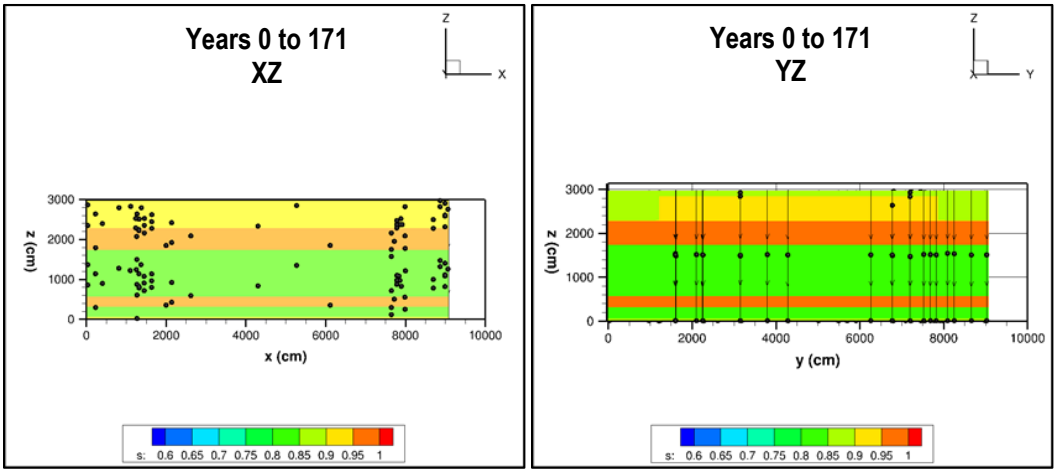

Figure 5-154. NR26E/Cases 3 and 4 – Saturation Profiles and Flow Stream Traces with 100-Year Time Markers in XZ and YZ Planes During Operational and IC Periods (Years 0 to 171)

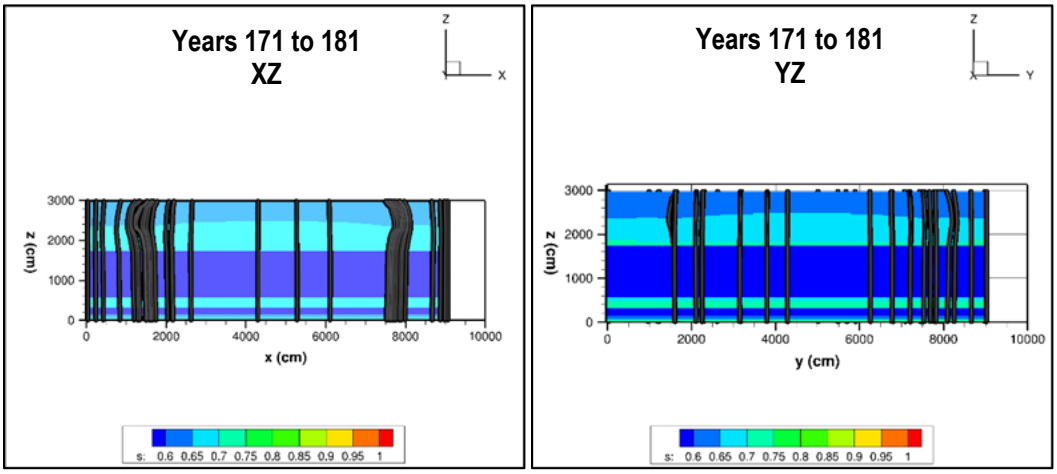

Figure 5-155. NR26E/Cases 3 and 4 – Saturation Profiles and Flow Stream Traces with 100-Year Time Markers in XZ and YZ Planes During First Time Period of Final Closure (Years 171 to 181)

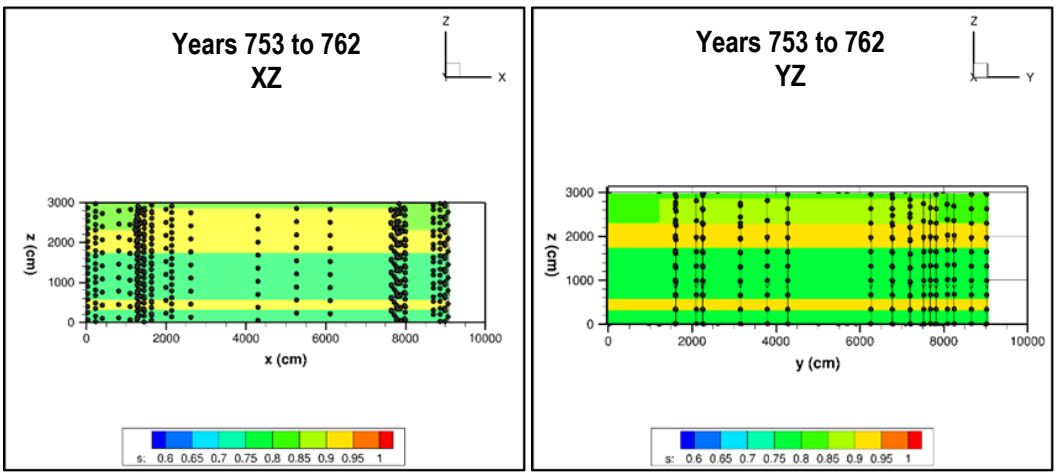

Figure 5-156. NR26E/Cases 3 and 4 – Saturation Profiles and Flow Stream Traces with 100-Year Time Markers in XZ and YZ Planes During First Period When Hydraulic Failure Occurs (Years 753 to 762)

The flow model predicts saturation trends for NR26E that are like those for NR07E. Note that the saturation levels following installation of the final closure cap are lower than those for NR07E. The reason for this is apparent by comparing Figure 4-210 (NR07E) to Figure 4-211 (NR26E). Because of their locations in the ELLWF relative to other DUs, different final closure cap configurations are required. NR07E is somewhat isolated from the other ELLWF DUs (see Figure 2-78). At the end of the IC period, a final closure cap that extends 40 feet beyond the edge of the disposal pad on all sides will be placed over NR07E. Beyond the reach of the closure cap is undisturbed soil that extends to the edge of the model domain. Conversely, NR26E is surrounded by other DUs (i.e., ET03, ET04, and ST08) and can be represented in the PORFLOW model by an essentially infinite cap that extends to the edge of the model domain.

5.4.1.2. Transport Model Results

Radionuclide transport is simulated for each NRCDA DU according to the operational timeline presented in Section 4.7.8.1. Steady-state flow fields are input to PORFLOW to solve transport equations for radionuclide species identified in the GW screening, which includes 13 radionuclides for the generic waste form (bolted, gasketed containers) and 11 radionuclides for the SWF (welded steel casks) as listed in Table 4-86. The flux to water table is computed for at least up to a 10,171-year simulation period and is used as the source term at the water table for contaminant transport in aquifer GW. This section presents a subset of the PORFLOW transport model results to demonstrate the differences in the flux to water table for mobile versus immobile and short- versus longer-lived radionuclides. Both generic waste form and SWF radionuclides are uniformly distributed throughout the waste zones.

The following radionuclides are selected for display: Be-10 (SWF only), C-14, H-3 (generic waste only), I-129, Ni-59, Pu-241, and Tc-99. Table 5-40 presents decay properties for these radionuclides along with their corresponding elemental chemical sorption properties assigned to each layer in the model.

Table 5-40. Radionuclide and Chemical Properties

Radionuclide		Half-Life (yr)	K_d (mL g^{-1})		
Parent	Progeny		LAZ and LVZ	TCCZ and UVZ	Backfill and Waste
Be-10	-	1.510E+06	5	17	17
C-14	-	5.700E+03	1	30	30
H-3	-	1.232E+01	0	0	0
I-129	-	1.570E+07	1	3	3
Ni-59	-	1.010E+05	7	30	30
Pu-241	-	1.435E+01	650	6,000	6,000
-	Am-241	4.322E+02	8,500	8,500	8,500
-	Np-237	2.144E+06	3	9	9
-	U-233	1.592E+05	300	400	400
-	Th-229	7.340E+03	900	2,000	2,000
Tc-99	-	2.111E+05	0.6	1.8	1.8

Graphical results of flux to the water table are displayed in the following sequence of figures:

- Figure 5-157 NR07E/Case 1 (generic waste, bolted container)
- Figure 5-158 NR07E/Case 2 (generic waste, bolted container)
- Figure 5-159 NR07E/Case 3 (special waste, activated Inconel, welded cask)
- Figure 5-160 NR07E/Case 4 (special waste, activated Zircaloy, welded cask)
- Figure 5-161 NR26E/Case 1 (generic waste, bolted container)
- Figure 5-162 NR26E/Case 2 (generic waste, bolted container)
- Figure 5-163 NR26E/Case 3 (special waste, activated Inconel, welded cask)
- Figure 5-164 NR26E/Case 4 (special waste, activated Zircaloy, welded cask)

The peak flux at the water table and the time of its occurrence (i.e., peak flux time) are captured from the PORFLOW transport runs and are listed for the selected radionuclides in the following tables:

- Table 5-41 NR07E/Case 1 (generic waste, bolted container)
- Table 5-42 NR07E/Case 2 (generic waste, bolted container)
- Table 5-43 NR07E/Case 3 (special waste, activated Inconel, welded cask)
- Table 5-44 NR07E/Case 4 (special waste, activated Zircaloy, welded cask)
- Table 5-45 NR26E/Case 1 (generic waste, bolted container)
- Table 5-46 NR26E/Case 2 (generic waste, bolted container)
- Table 5-47 NR26E/Case 3 (special waste, activated Inconel, welded cask)
- Table 5-48 NR26E/Case 4 (special waste, activated Zircaloy, welded cask)

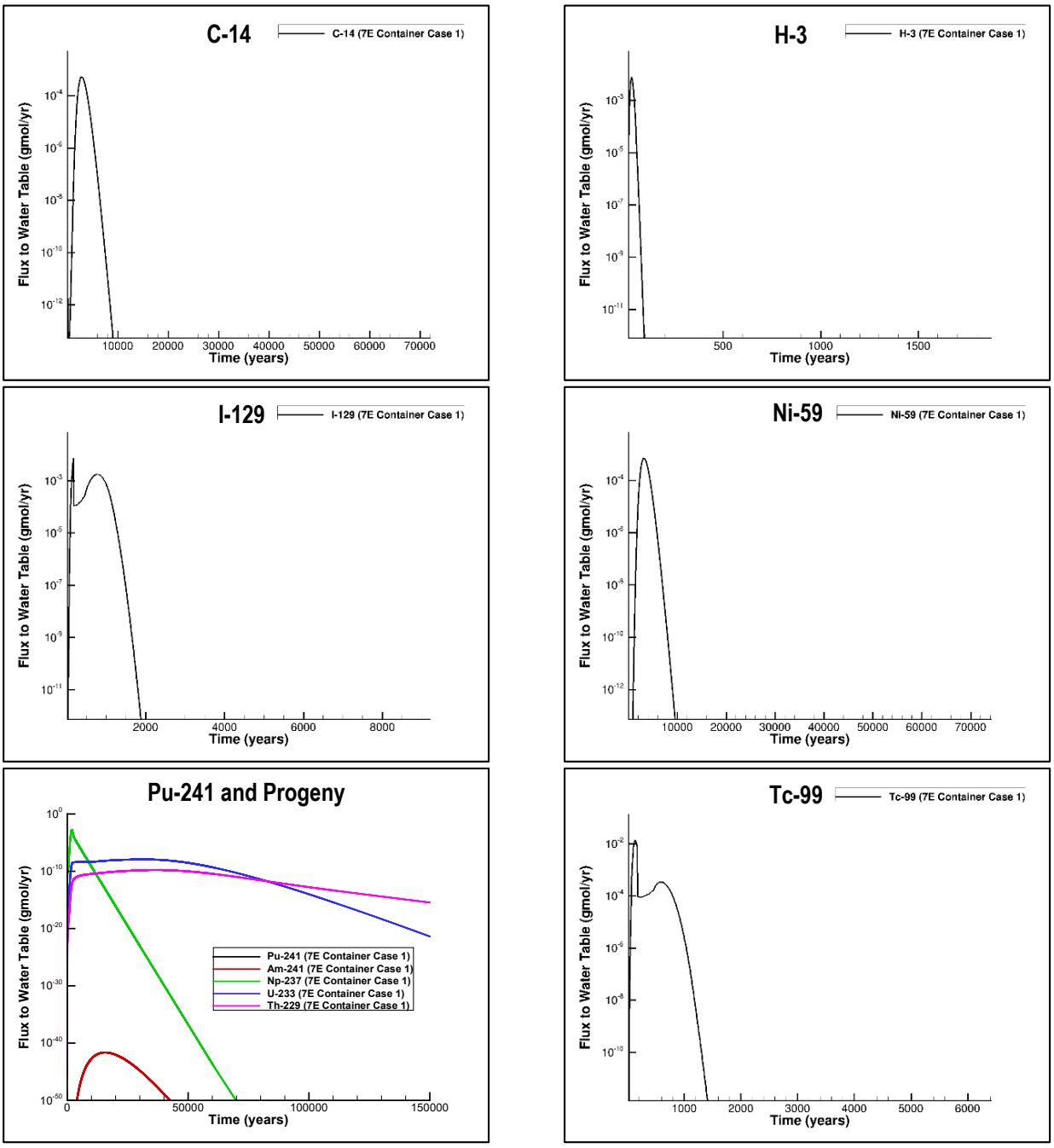

Figure 5-157. Flux at Water Table for NR07E/Case 1 (Generic Waste, Bolted Container)

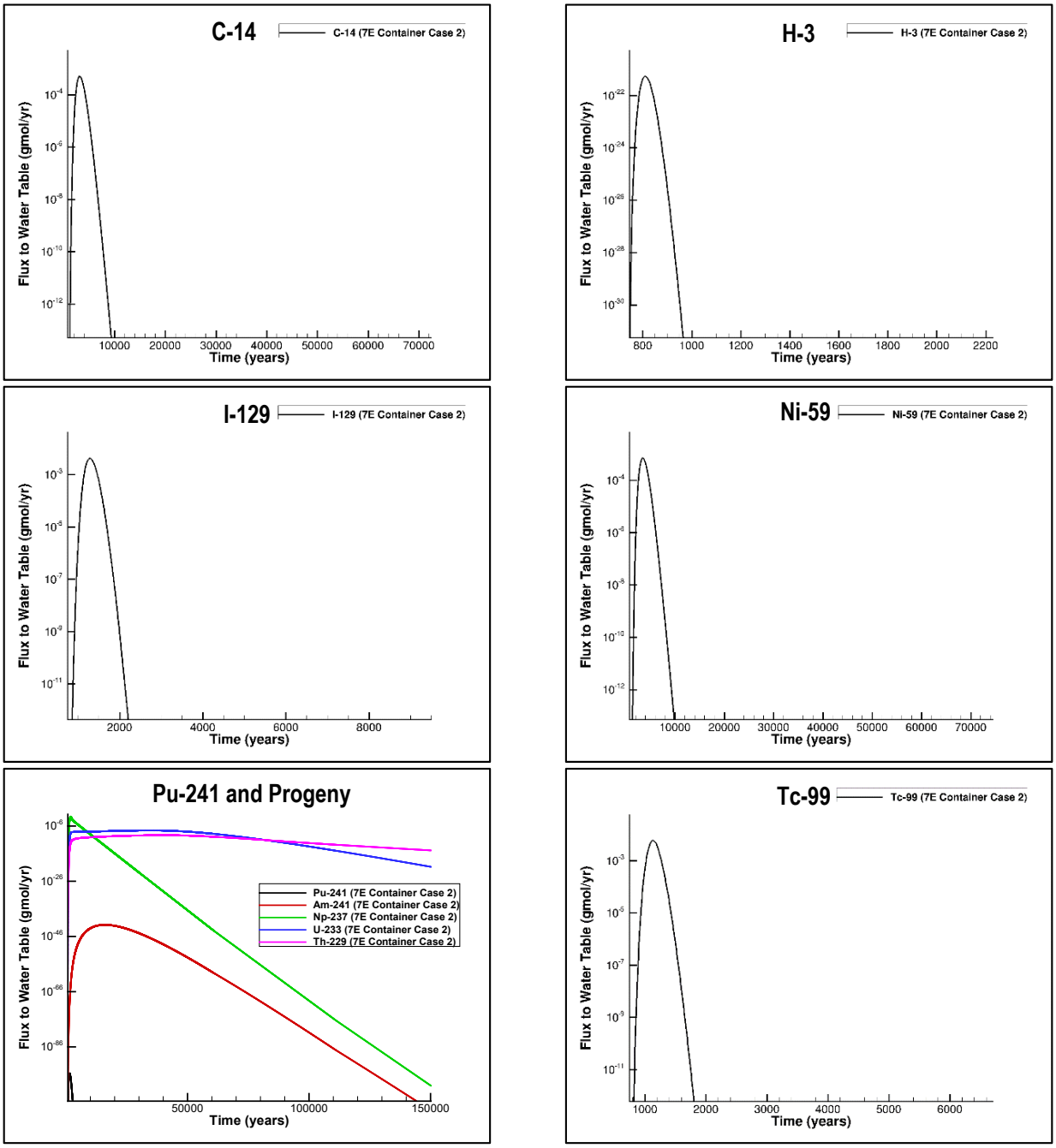

Figure 5-158. Flux at Water Table for NR07E/Case 2 (Generic Waste, Bolted Container)

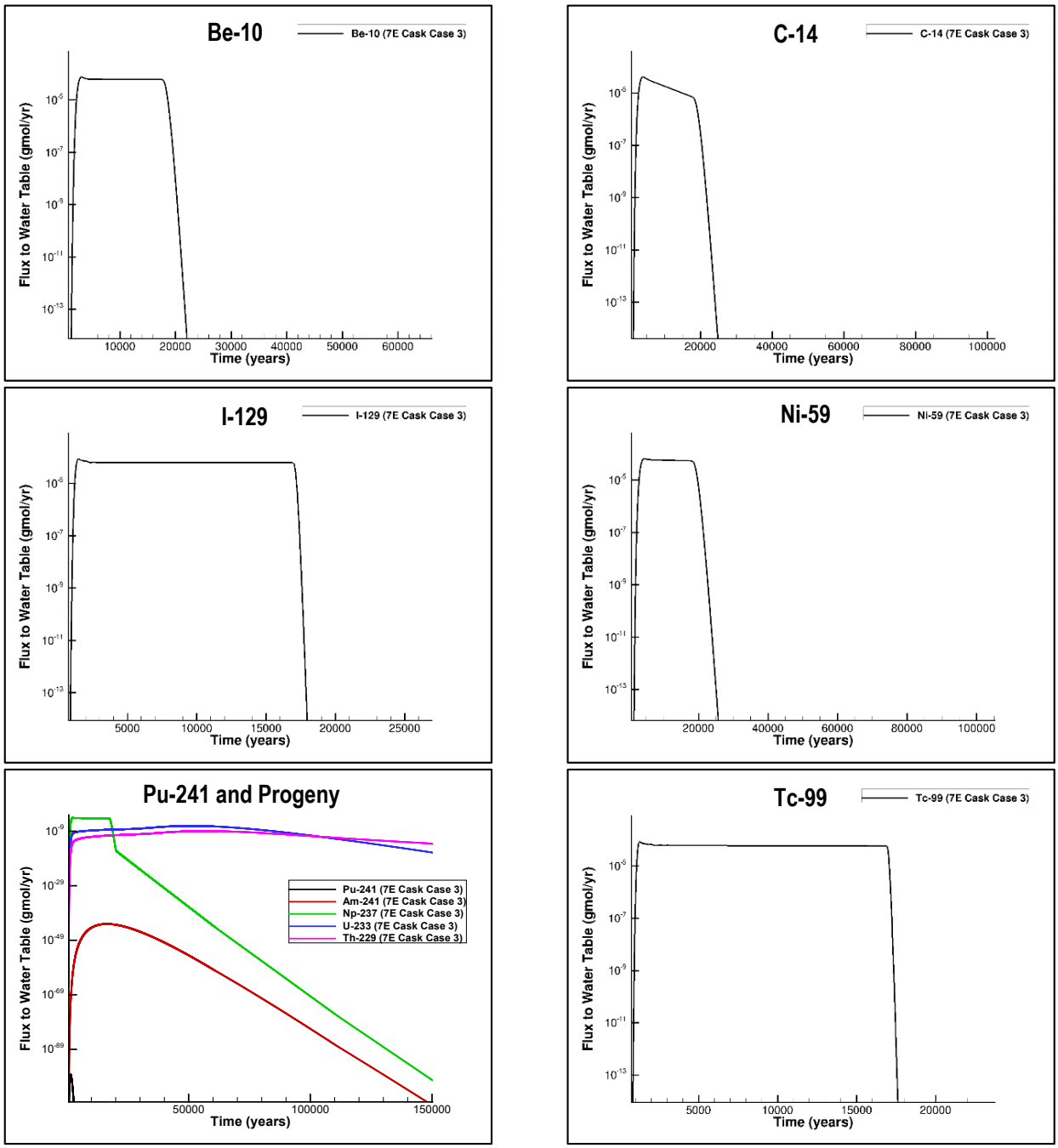

Figure 5-159. Flux at the Water Table for NR07E/Case 3 (Special Waste, Activated Inconel, Welded Cask)

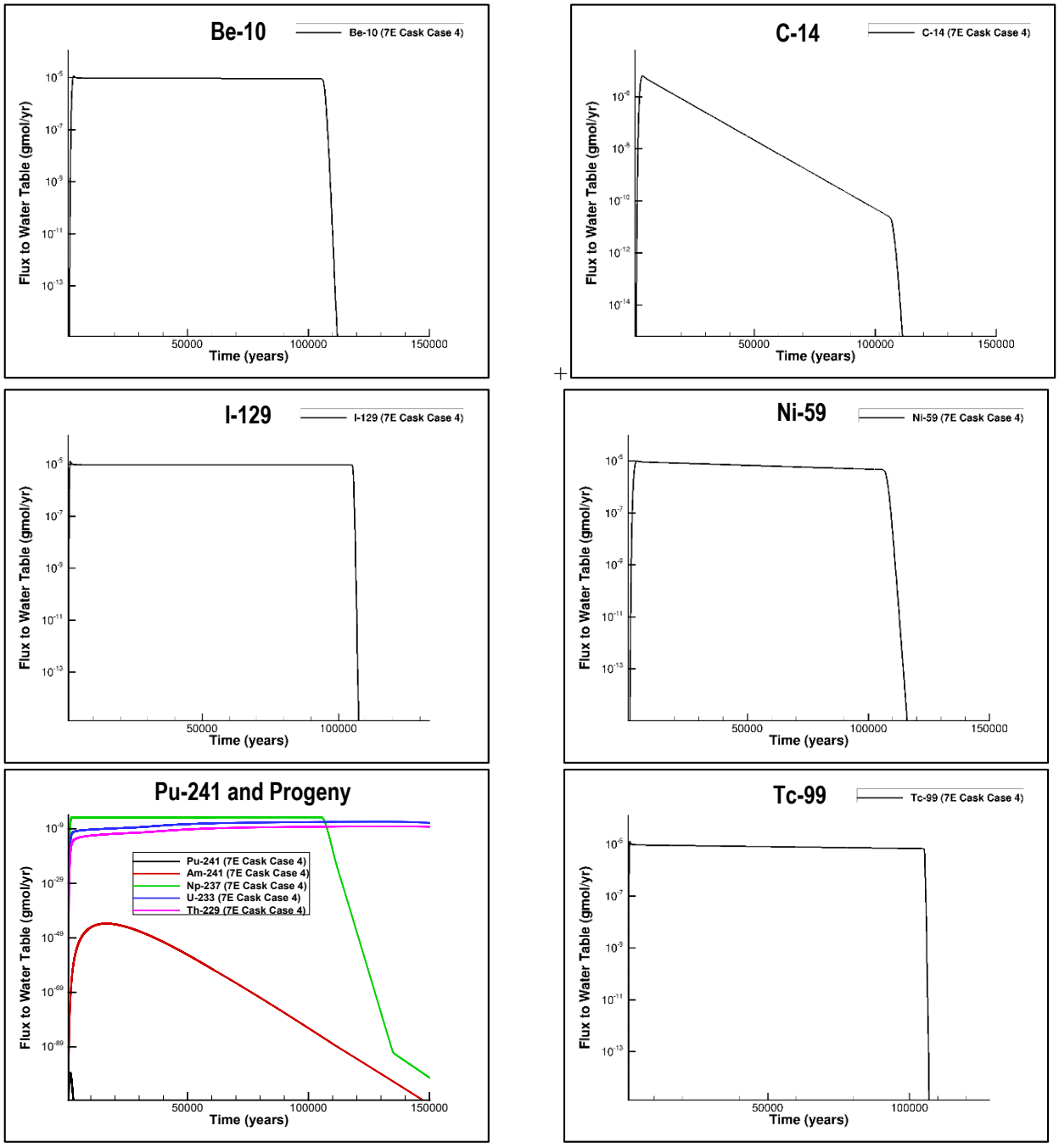

Figure 5-160. Flux at Water Table for NR07E/Case 4 (Special Waste, Activated Zircaloy, Welded Cask)

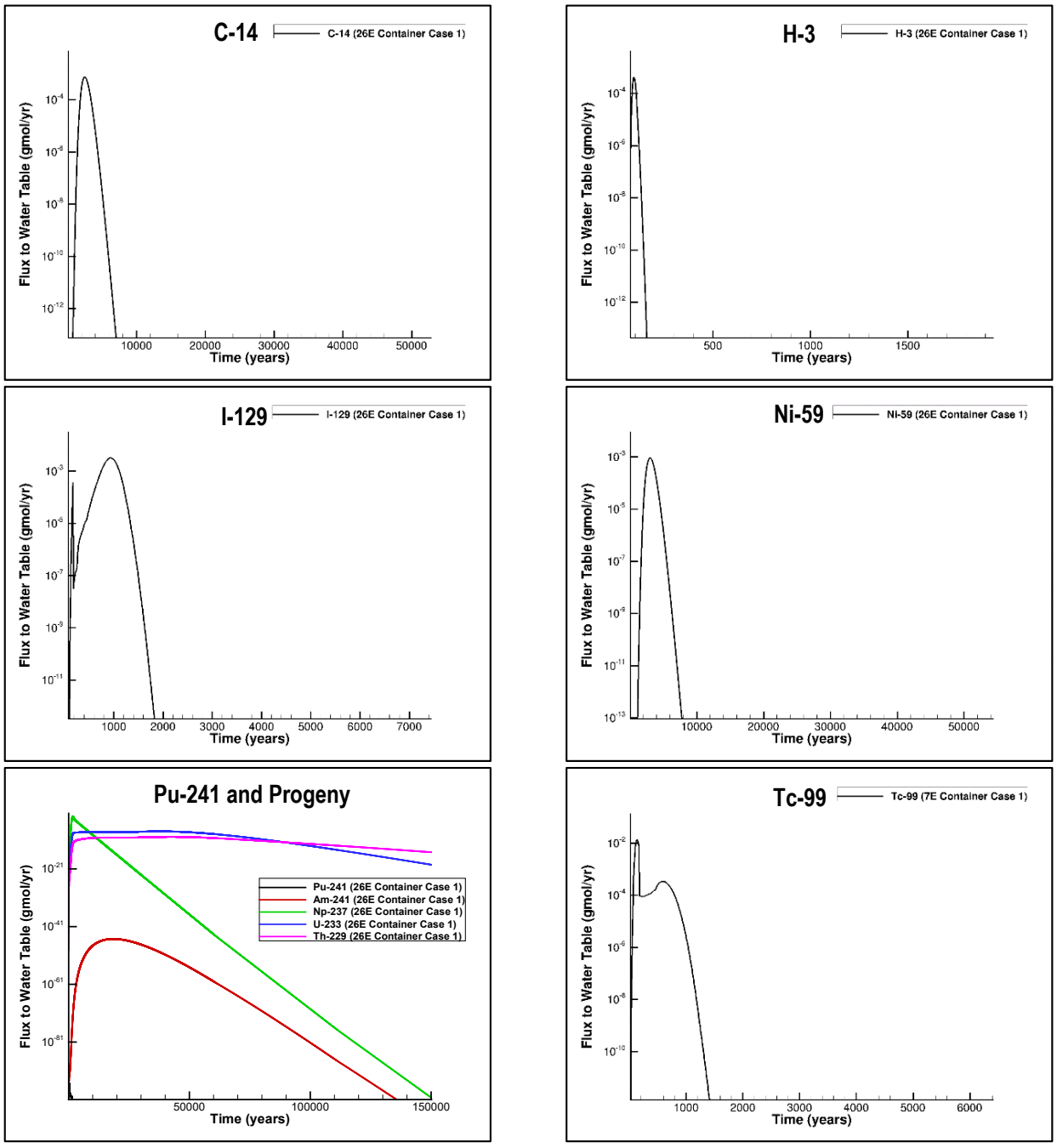

Figure 5-161. Flux at Water Table for NR26E/Case 1 (Generic Waste, Bolted Container)

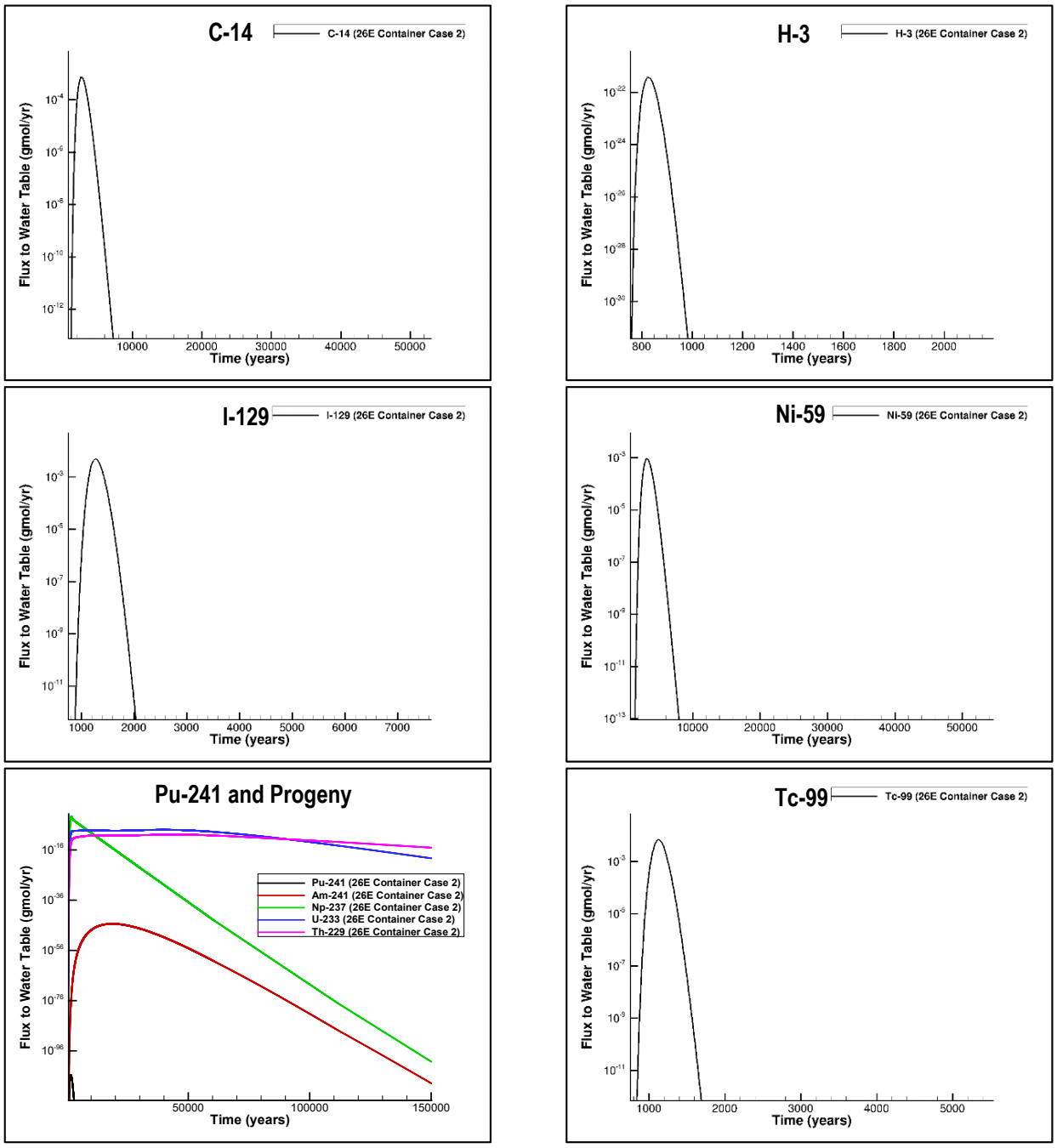

Figure 5-162. Flux at the Water Table for NR26E/Case 2 (Generic Waste, Bolted Container)

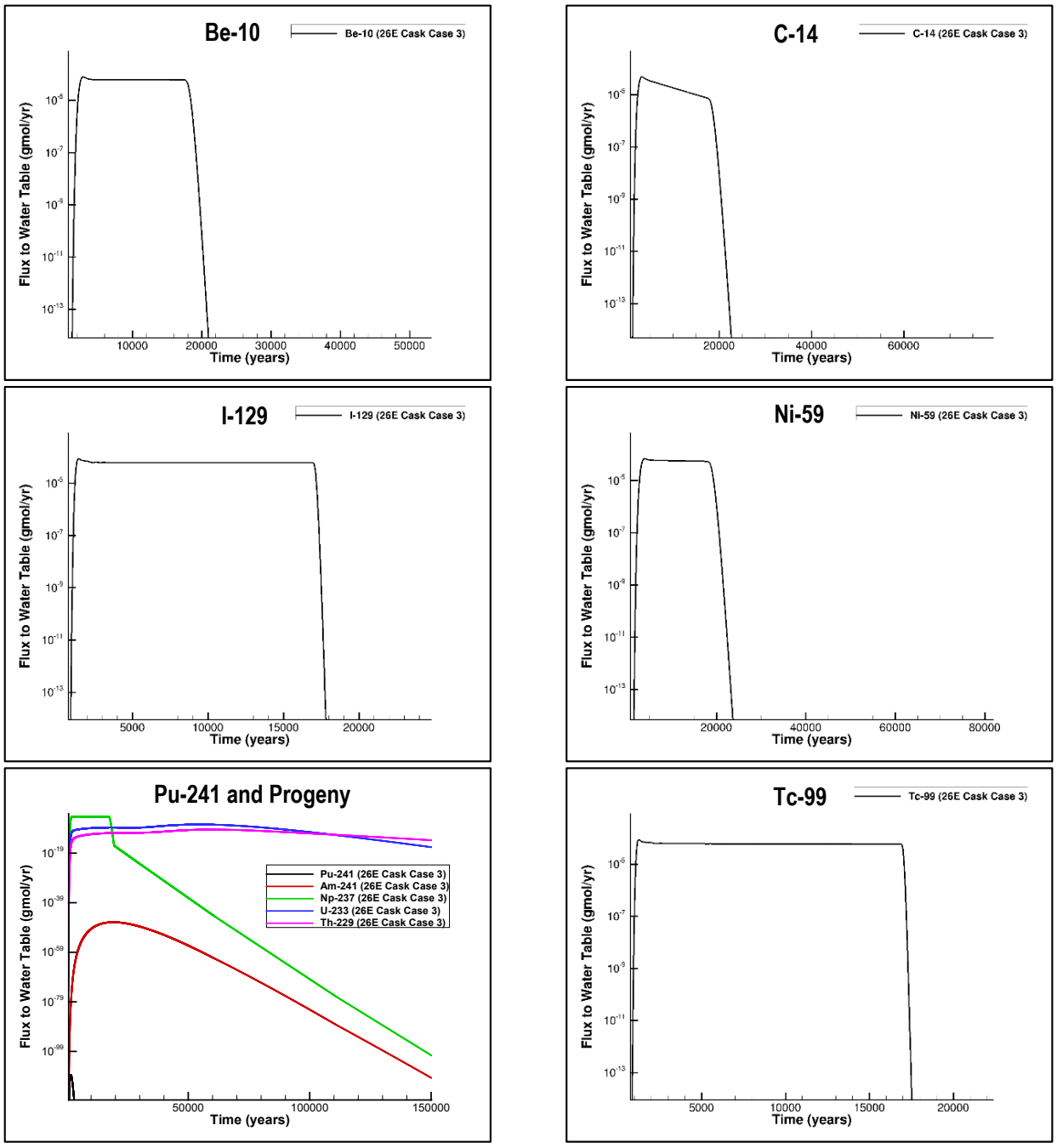

Figure 5-163. Flux at the Water Table for NR26E/Case 3 (Special Waste, Activated Inconel, Welded Cask)

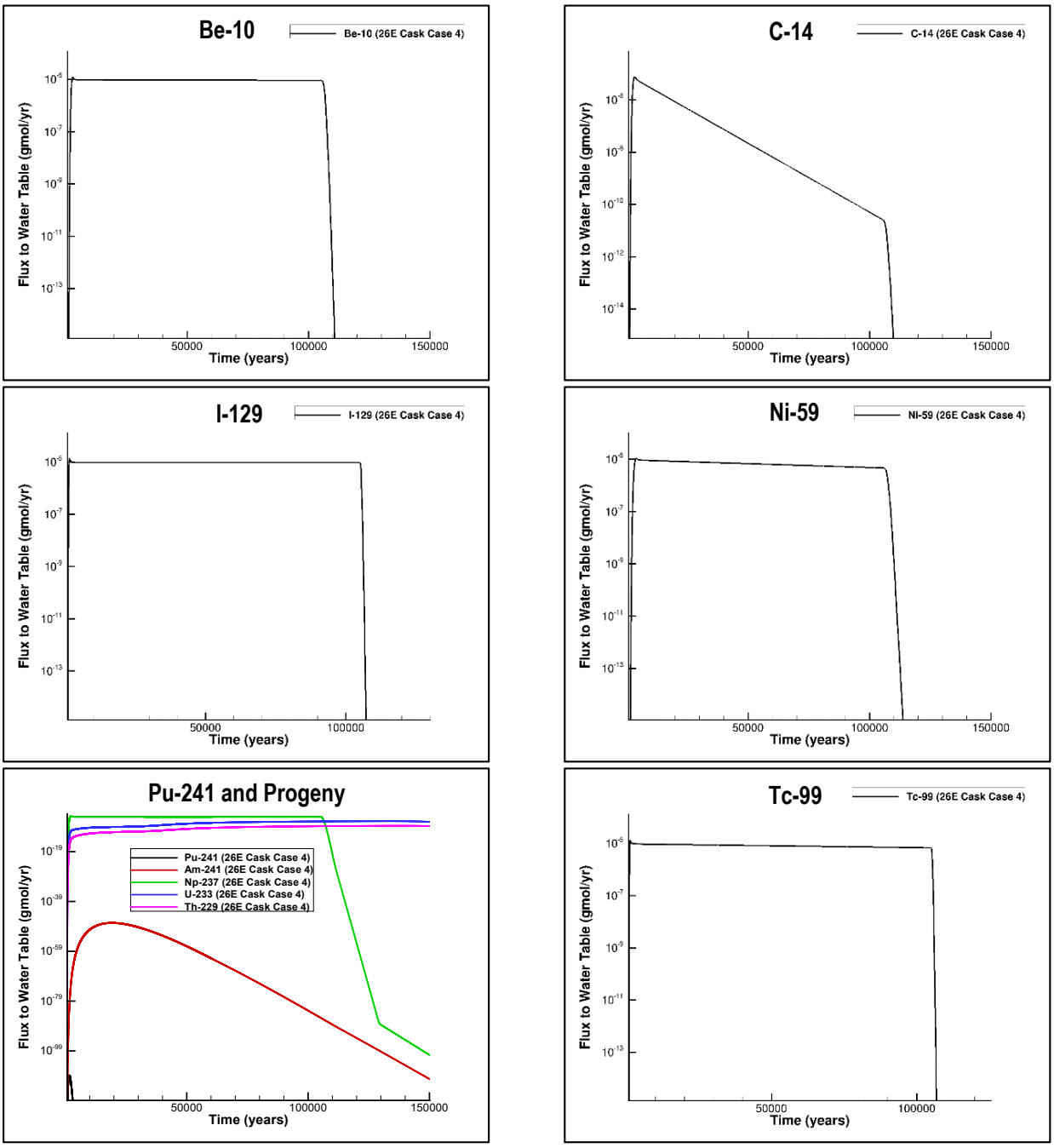

Figure 5-164. Flux at Water Table for NR26E/Case 4 (Special Waste, Activated Zircaloy, Welded Cask)

Table 5-41. Peak Flux and Peak Flux Time for NR07E/Case 1 (Bolted Container, Generic Waste)

Radionuclide		Peak Flux Time (Year)	Peak Flux (gmol yr^{-1})
Parent	Progeny		
C-14	-	2,816	5.27E-04
H-3	-	30	7.96E-03
I-129	-	170	7.41E-03
Ni-59	-	3,146	7.22E-04
Pu-241	-	170	6.56E-75
-	Am-241	15,661	2.28E-42
-	Np-237	1,876	1.54E-03
-	U-233	31,387	1.18E-08
-	Th-229	36,591	1.64E-10
Tc-99	-	130	1.39E-02

Table 5-42. Peak Flux and Peak Flux Time for NR07E/Case 2 (Bolted Container, Generic Waste)

Radionuclide		Peak Flux Time (Year)	Peak Flux (gmol yr^{-1})
Parent	Progeny		
C-14	-	3,101	5.18E-04
H-3	-	810	5.56E-22
I-129	-	1,276	4.38E-03
Ni-59	-	3,426	7.21E-04
Pu-241	-	1,436	2.32E-96
-	Am-241	15,951	1.41E-42
-	Np-237	1,911	1.73E-03
-	U-233	34,347	1.21E-08
-	Th-229	39,131	1.68E-10
Tc-99	-	1,125	6.03E-03

Table 5-43. Peak Flux and Peak Flux Time for NR07E/Case 3 (Activated Inconel, Welded Cask, Special Waste)

Radionuclide		Peak Flux Time (Year)	Peak Flux (gmol yr^{-1})
Parent	Progeny		
Be-10	-	3,081	7.62E-05
C-14	-	3,976	4.13E-05
I-129	-	1,476	8.81E-05
Ni-59	-	4,476	6.56E-05
Pu-241	-	1,486	5.20E-99
-	Am-241	16,361	9.69E-44
-	Np-237	2,476	8.13E-05
-	U-233	50,931	9.39E-08
-	Th-229	56,511	1.23E-09
Tc-99	-	1,276	8.88E-05

Table 5-44. Peak Flux and Peak Flux Time for NR07E/Case 4 (Activated Zircaloy, Welded Cask, Special Waste)

Radionuclide		Peak Flux Time (Year)	Peak Flux (gmol yr^{-1})
Parent	Progeny		
Be-10	-	3,081	1.17E-05
C-14	-	3,976	6.37E-06
I-129	-	1,476	1.36E-05
Ni-59	-	4,476	1.01E-05
Pu-241	-	1,491	2.89E-99
-	Am-241	16,361	1.50E-44
-	Np-237	2,476	1.25E-05
-	U-233	129,929	1.82E-07
-	Th-229	134,171	2.72E-09
Tc-99	-	1,276	1.37E-05

Table 5-45. Peak Flux and Peak Flux Time for NR26E/Case 1 (Bolted Container, Generic Waste)

Radionuclide		Peak Flux Time (Year)	Peak Flux (gmol yr^{-1})
Parent	Progeny		
C-14	-	2,476	7.61E-04
H-3	-	90	4.30E-04
I-129	-	925	3.28E-03
Ni-59	-	3,001	9.23E-04
Pu-241	-	170	1.19E-91
-	Am-241	18,541	5.28E-46
-	Np-237	1,801	1.75E-03
-	U-233	37,771	1.01E-08
-	Th-229	42,471	1.25E-10
Tc-99	-	170	1.21E-02

Table 5-46. Peak Flux and Peak Flux Time for NR26E/Case 2 (Bolted Container, Generic Waste)

Radionuclide		Peak Flux Time (Year)	Peak Flux (gmol yr^{-1})
Parent	Progeny		
C-14	-	2,641	7.46E-04
H-3	-	825	3.86E-22
I-129	-	1,276	5.10E-03
Ni-59	-	3,196	9.22E-04
Pu-241	-	1,606	1.89E-106
-	Am-241	18,751	3.75E-46
-	Np-237	1,876	2.03E-03
-	U-233	39,691	1.06E-08
-	Th-229	44,431	1.32E-10
Tc-99	-	1,125	6.98E-03

Table 5-47. Peak Flux and Peak Flux Time for NR26E/Case 3 (Activated Inconel, Welded Cask, Special Waste)

Radionuclide		Peak Flux Time (Year)	Peak Flux (gmol yr^{-1})
Parent	Progeny		
Be-10	-	2,976	8.02E-05
C-14	-	3,251	4.86E-05
I-129	-	1,476	8.85E-05
Ni-59	-	3,976	6.96E-05
Pu-241	-	1,626	2.48E-109
-	Am-241	19,181	1.59E-47
-	Np-237	2,191	8.41E-05
-	U-233	54,911	9.08E-08
-	Th-229	60,111	1.09E-09
Tc-99	-	1,276	8.93E-05

Table 5-48. Peak Flux and Peak Flux Time for NR26E/Case 4 (Activated Zircaloy, Welded Cask, Special Waste)

Radionuclide		Peak Flux Time (Year)	Peak Flux (gmol yr^{-1})
Parent	Progeny		
Be-10	-	2,976	1.24E-05
C-14	-	3,251	7.48E-06
I-129	-	1,476	1.36E-05
Ni-59	-	3,976	1.07E-05
Pu-241	-	1,631	1.39E-109
-	Am-241	19,181	2.46E-48
-	Np-237	2,191	1.30E-05
-	U-233	133,571	1.79E-07
-	Th-229	137,771	2.43E-09
Tc-99	-	1,276	1.38E-05

H-3, I-129, and Tc-99 have low K_d values (i.e., 0, 3, and 1.8 mL g^{-1}, respectively) in the waste zone, resulting in an early appearance of peak fluxes at the water table. With moderate K_d values (i.e., 30 mL g^{-1}), C-14 and Ni-59 display peak flux times ranging from about Years 2,500 to 4,000 and Years 3,000 to 4,500, respectively. Pu-241, which has a short half-life (14.35 years) but a high K_d value (6,000 mL g^{-1}), displays a low peak flux at a relatively early time. Pu-241 generates Am-241, Np-237, U-233, and Th-229 as daughter products. The daughter products, except for Np-237, have high K_d values (greater than 400 mL g^{-1}) and display late peak flux times (>> Year 10,000) that fall outside of the compliance period of 1,171 years.

For the bolted, gasketed containers, the models correctly display the difference between early release (Case 1) and late release (Case 2) due to hydraulic failure. For example, for NR07E, H-3 flux at the water table peaks at Year 30 for Case 1 and Year 810 for Case 2.

The results for the welded casks (Figure 5-159, Figure 5-160, Figure 5-163, and Figure 5-164) show a steep decline in flux values for nuclides with low and moderate K_d values because of the completion of radionuclide inventory release from the metal alloy due to corrosion. The difference

in the corrosion rates of activated Inconel and Zircaloy in welded casks is also correctly captured by the PORFLOW transport models (Figure 5-159 versus Figure 5-160; Figure 5-163 versus Figure 5-164).

The flux to the water table results provided in this section are calibrated to 1-D GoldSim® models of the NRCDAs using the final set of PORFLOW transport model runs. This calibration is described separately by Smith (2020).

5.4.1.3. Sensitivity Case Results

Among the nominal PA cases, Case 1 and Case 2 represent bounding scenarios for evaluating the effect of ACP contaminant release timing. Because of uncertainties in many of the variables and properties employed in the models, a series of sensitivity cases are defined below to evaluate the impact of these major uncertainties on final dose limits to comply with performance measures at the 100-meter POA in the aquifer.

Table 5-49 shows the list of all sensitivity cases under consideration, which include variations in K_{sat} for the waste zone, porosity of the LVZ and waste zone, infiltration rate, K_d, and waste placement timing. Table 5-50 provides the sensitivity cases of waste placement timing for both NR07E and NR26E. Note that Table 5-50 is like Table 4-84, except for waste placement timing.

Table 5-49. List of Naval Reactor Component Disposal Area Vadose Zone Sensitivity Cases

Sensitivity Case	Topic	Nominal PA Values	Best Estimate Values	Sensitivity Case Values	Number of Sensitivity Cases [2]	Flow Runs Performed?
a	Waste Zone Hydraulic Conductivity (cm s^{-1})	2.2E-05	2.2E-05	4.08E-05 (+1σ)	3	Yes
b	LVZ Porosity	0.380	0.380	0.420 (+1σ)	3	Yes
c	Waste Zone Porosity	0.889	0.889	0.939 (+1σ)	3	Yes
d	Infiltration [1]	HELP Model Intact Case (Table 4-81)	HELP Model Intact Case (Table 4-81)	HELP Model Pessimistic Case (Table 4-81)	3	Yes
e	Distribution Coefficient	2016 Chemistry Database K_d Values	2016 Chemistry Database K_d Values	0.5 K_d	3	No
f	Waste Placement at Time of Initial Soil Cover (see detail below)	--	--	--	--	Yes[3]

Dn't aanythioNotes:

1 For the HELP model intact case (Table 4-81), infiltration rates are calculated using the HELP model (Dyer, 2019b) and SRS historical mean monthly rainfall data (49.14 in yr^{-1} annual average). For Sensitivity Case d (pessimistic rainfall assumption), infiltration rates are based on an annual average rainfall of 61.68 in yr^{-1} (+½σ based on SRS historical mean monthly rainfall or +1.6σ on annual average basis).

2 Only for Vadose26E_Container_Case1, Vadose7E_Cask_Case3, and Vadose26E_Cask_Case4.

3 Partial rerun of time intervals.

Table 5-50. List of Waste Placement Timing for Naval Reactor Component Disposal Area Sensitivity Cases

DU	Waste Form	Waste Material	Release Time	Case ID
NR07E	Generic	Soil	Waste placement at time of initial soil cover in 2005 (model time: Year 11). Instantaneous release at Year 11	Case 1f
			Waste placement at time of initial soil cover in 2005 (model time: Year 11). Instantaneous release at Year 750 post-disposal (model time: Year 761)	Case 2f
	Special	Inconel	Waste placement at time of initial soil cover in 2005 (model time: Year 11). Corrosion-limited starting at Year 750 post-disposal (model time: Year 761)	Case 3f
		Zircaloy		Case 4f
NR26E	Generic	Soil	Waste placement at time of initial soil cover in 2065 (model time: Year 71). Instantaneous release at start of IC (model time: Year 71)	Case 1f
			Waste placement at time of initial soil cover in 2065 (motel time: Year 71). Instantaneous release at Year 750 post-disposal (model time: Year 821)	Case 2f
	Special	Inconel	Waste placement at time of initial soil cover in 2065 (model time: Year 71). Corrosion-limited starting at Year 750 post-disposal (model time: Year 821)	Case 3f
		Zircaloy		Case 4f

To demonstrate the impact of the sensitivity cases on radionuclide fluxes at the water table, three radionuclides are selected for discussion: C-14 (moderate half-life, moderate K_d), I-129 (long half-life, low K_d), and Pu-241 (a chain nuclide with Am-241, Np-237, U-233, and Th-229 as progenies). The sensitivity cases address both NR07E and NR26E as well as the two waste forms (generic waste for bolted containers and special waste for welded casks). Comparisons between the nominal PA and sensitivity cases are shown as follows:

- Figure 5-165 NR07E/Case 3 for C-14 (left) and I-129 (right)
- Figure 5-166 NR26E/Case 1 for C-14 (left) and I-129 (right)
- Figure 5-167 NR26E/Case 4 for C-14 (left) and I-129 (right)
- Figure 5-168 NR07E/Case 3 for Pu-241 and its progenies
- Figure 5-169 NR26E/Case 1 for Pu-241 and its progenies
- Figure 5-170 NR26E/Case 4 for Pu-241 and its progenies

In general, the sensitivity cases in which K_d is reduced by half appear to have the greatest impact on the peak flux at the water table. The reduction in K_d increases the peak flux; however, the flux dissipates more quickly. On the other hand, this effect is much less pronounced for radionuclides with a low K_d, such as I-129. For the SWF with activated Zircaloy metal that has a long corrosion time (104,349 years), the impact of sensitivity cases on the peak flux is negligible because of the long nuclide release process.

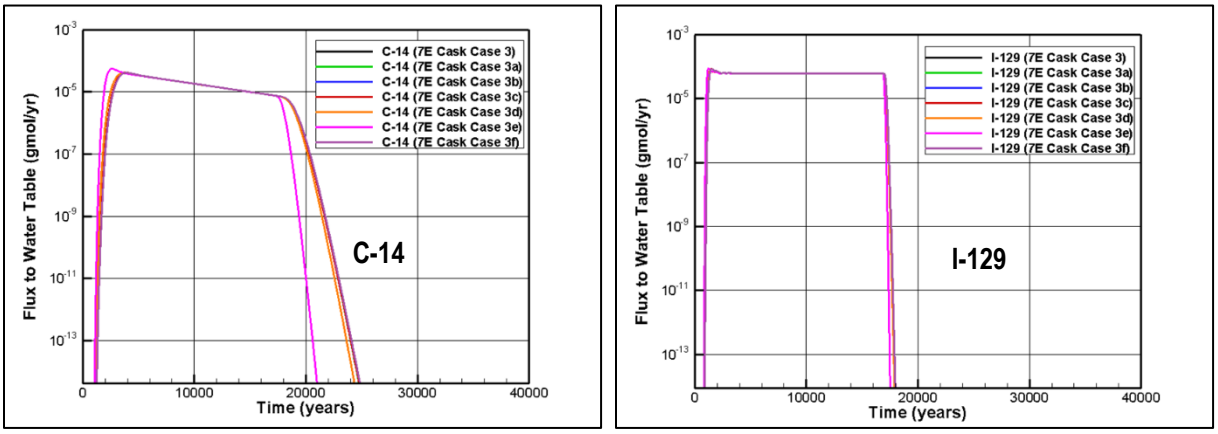

Figure 5-165. Comparison of Nominal PA Case 3 (Special Waste, Activated Inconel, Welded Cask) and Sensitivity Cases Flux to Water Table for C-14 (left) and I-129 (right) in Vadose Zone at NR07E

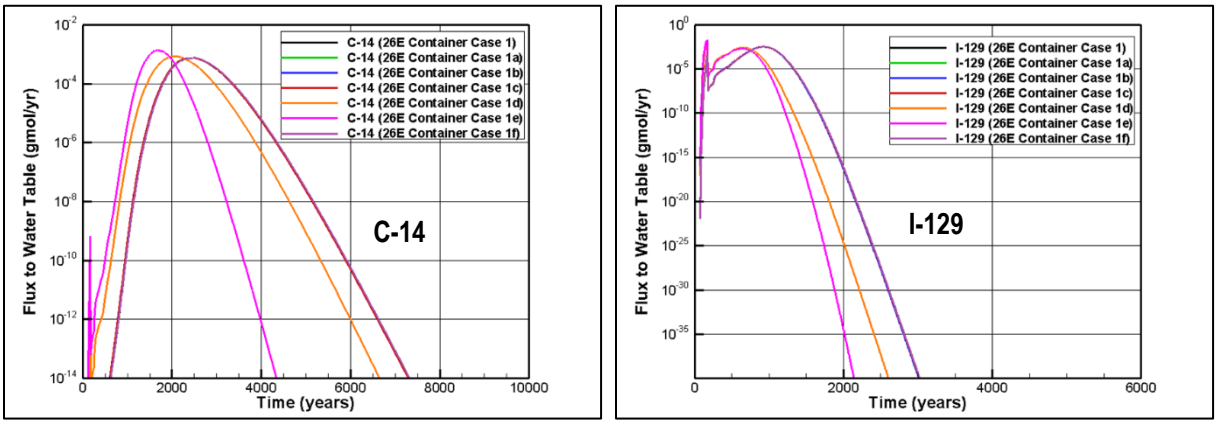

Figure 5-166. Comparison of Nominal PA Case 1 (Generic Waste, Bolted Container) and Sensitivity Cases Flux to Water Table for C-14 (left) and I-129 (right) in Vadose Zone at NR26E

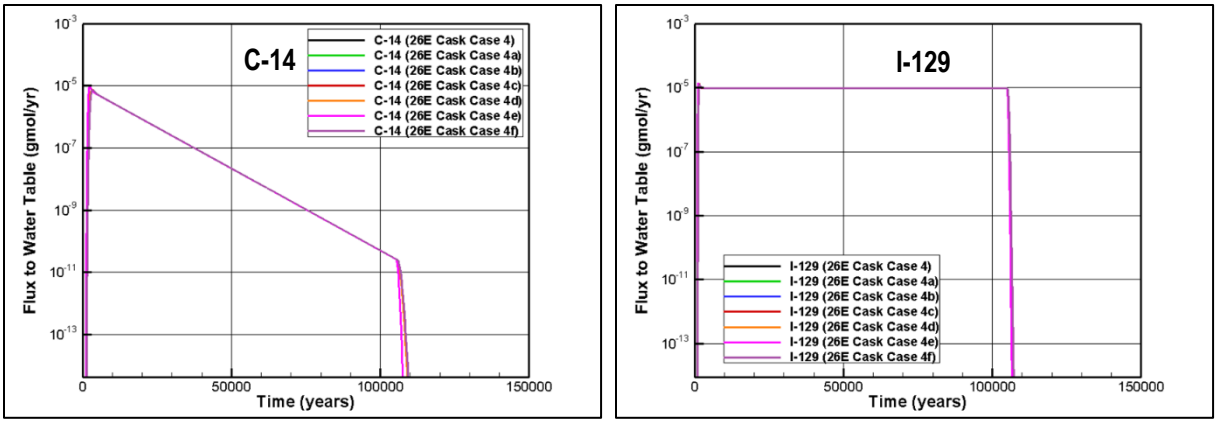

Figure 5-167. Comparison of Nominal PA Case 4 (Special Waste, Activated Zircaloy, Welded Cask) and Sensitivity Cases Flux to Water Table for C-14 (left) and I-129 (right) in Vadose Zone at NR26E

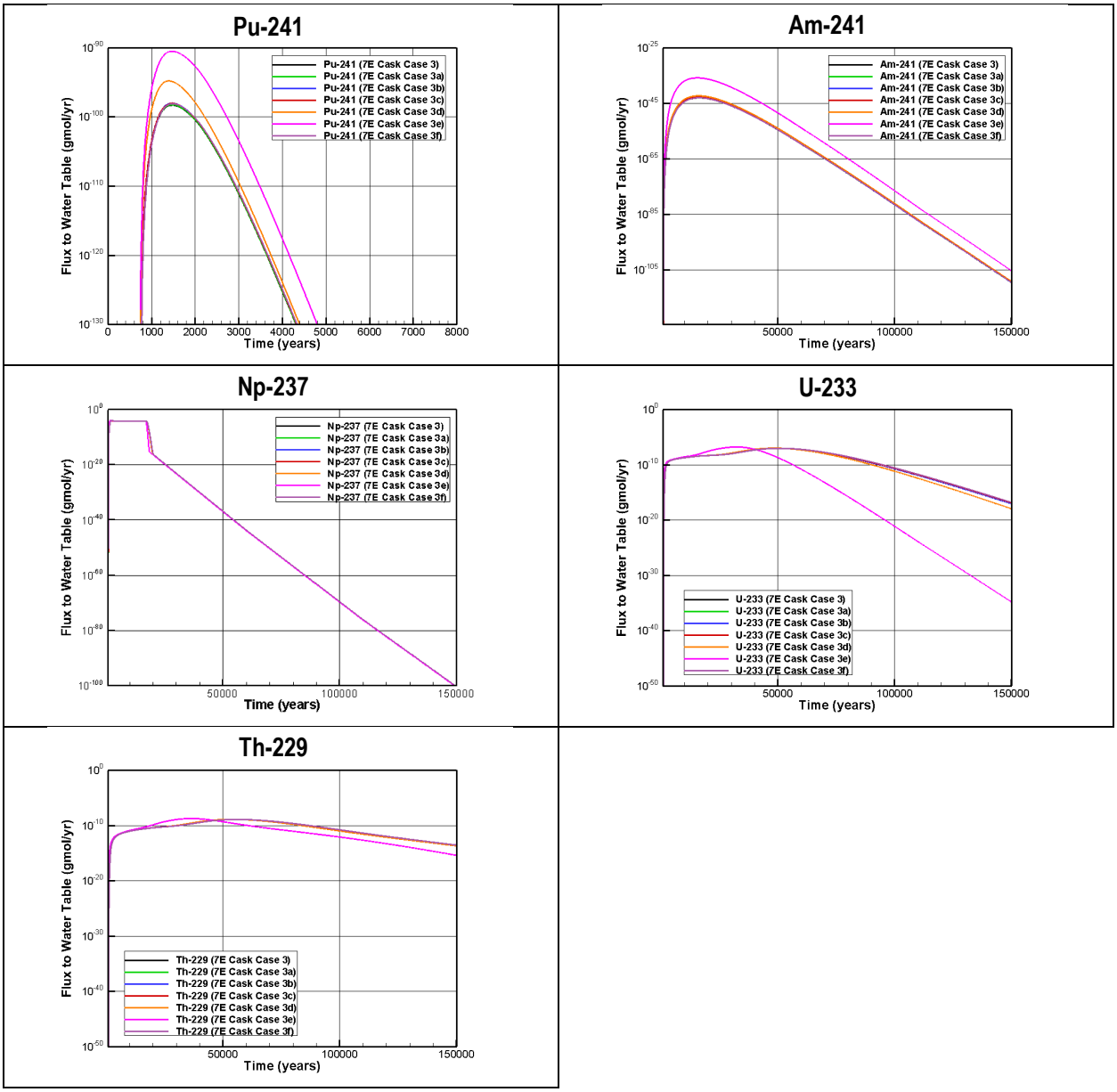

Figure 5-168. Comparison of Nominal PA Case 3 (Special Waste, Activated Inconel, Welded Cask) and Sensitivity Cases Flux to Water Table for Pu-241 and Progeny in Vadose Zone at NR07E

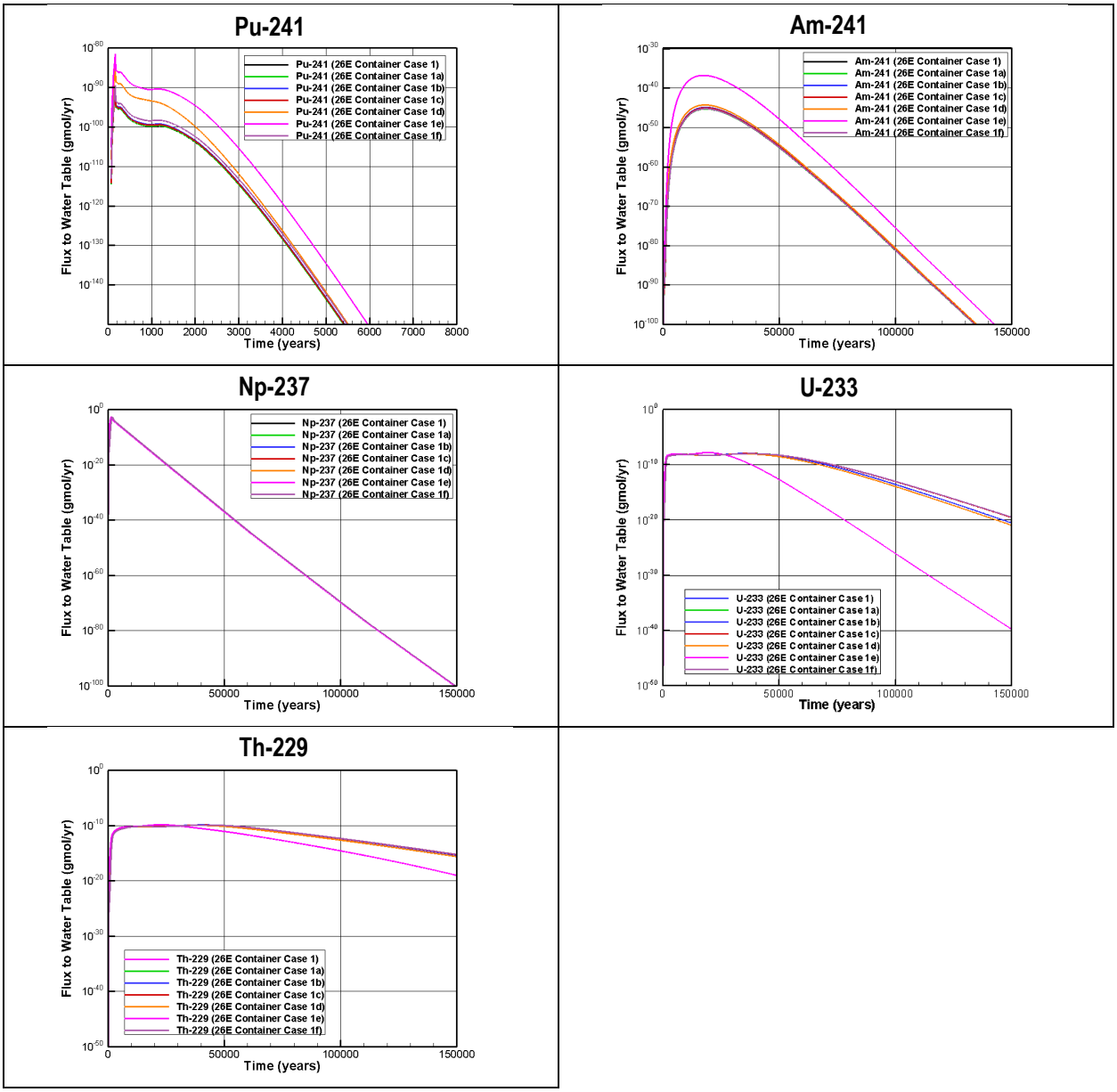

Figure 5-169. Comparison of Nominal PA Case 1 (Generic Waste, Bolted Container) and Sensitivity Cases Flux to Water Table for Pu-241 and Progeny in Vadose Zone at NR26E

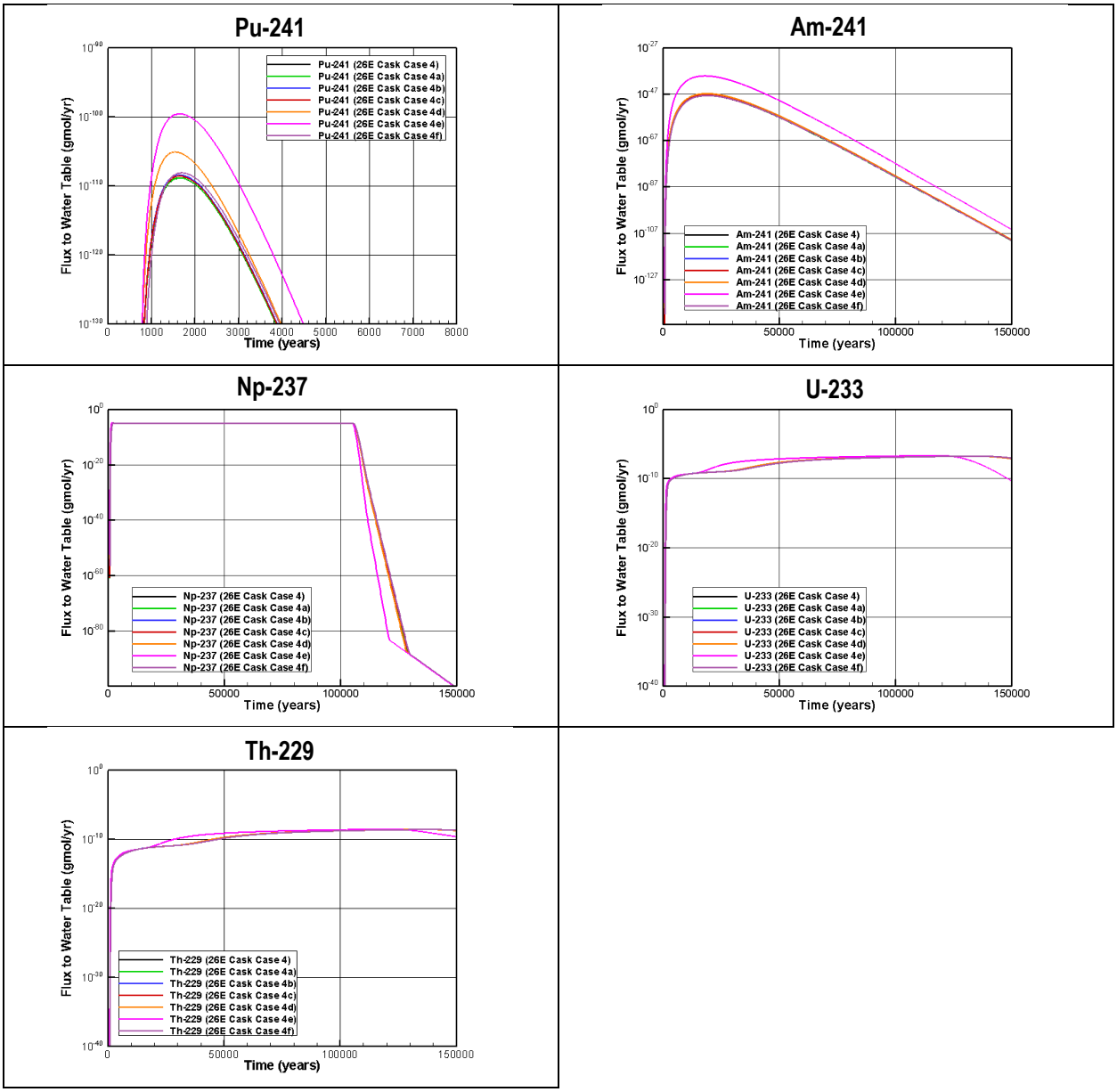

Figure 5-170. Comparison of Nominal PA Case 4 (Special Waste, Activated Zircaloy, Welded Cask) and Sensitivity Cases Flux to Water Table for Pu-241 and Progeny in Vadose Zone at NR26E

5.4.2. Aquifer Zone Model

Radionuclide contaminant transport through the aquifer is simulated for all nominal PA cases for each NRCDA pad. The source terms, obtained from the VZ flux-to-the-water-table profiles, are applied at the water table surface directly under the footprint of each DU in the GSA flow model(s).

5.4.2.1. Flow Model Results

Due to the large size of the full 3-D PORFLOW aquifer flow model for the GSA, the performance of individual waste DUs is modeled using only a "cutout" portion of the full model as described in Section 3.5.3. NR07E is in the East2_A cutout, and NR26E is in the West_B cutout. Additional

details on the implementation of the aquifer flow model for the NRCDAs are provided in Section 3.5.3.

5.4.2.2. Transport Model Results

As discussed in Section 5.1.3.2 for STs and ETs, the concentration profile at the 100-meter POA depends on DU-specific features (e.g., source location, cover geometries, disposal timing, hydraulic failure of seals) as well as the physical and geochemical parameters for the radionuclides of interest. For regulatory compliance, concentration data at the 100-meter POA are used to establish the inventory limit for each radionuclide in each NRCDA DU.

Figure 5-171 through Figure 5-174 display a 2-D projection of the maximum concentration for select radionuclides. The figures highlight how the concentration plumes evolve over time.

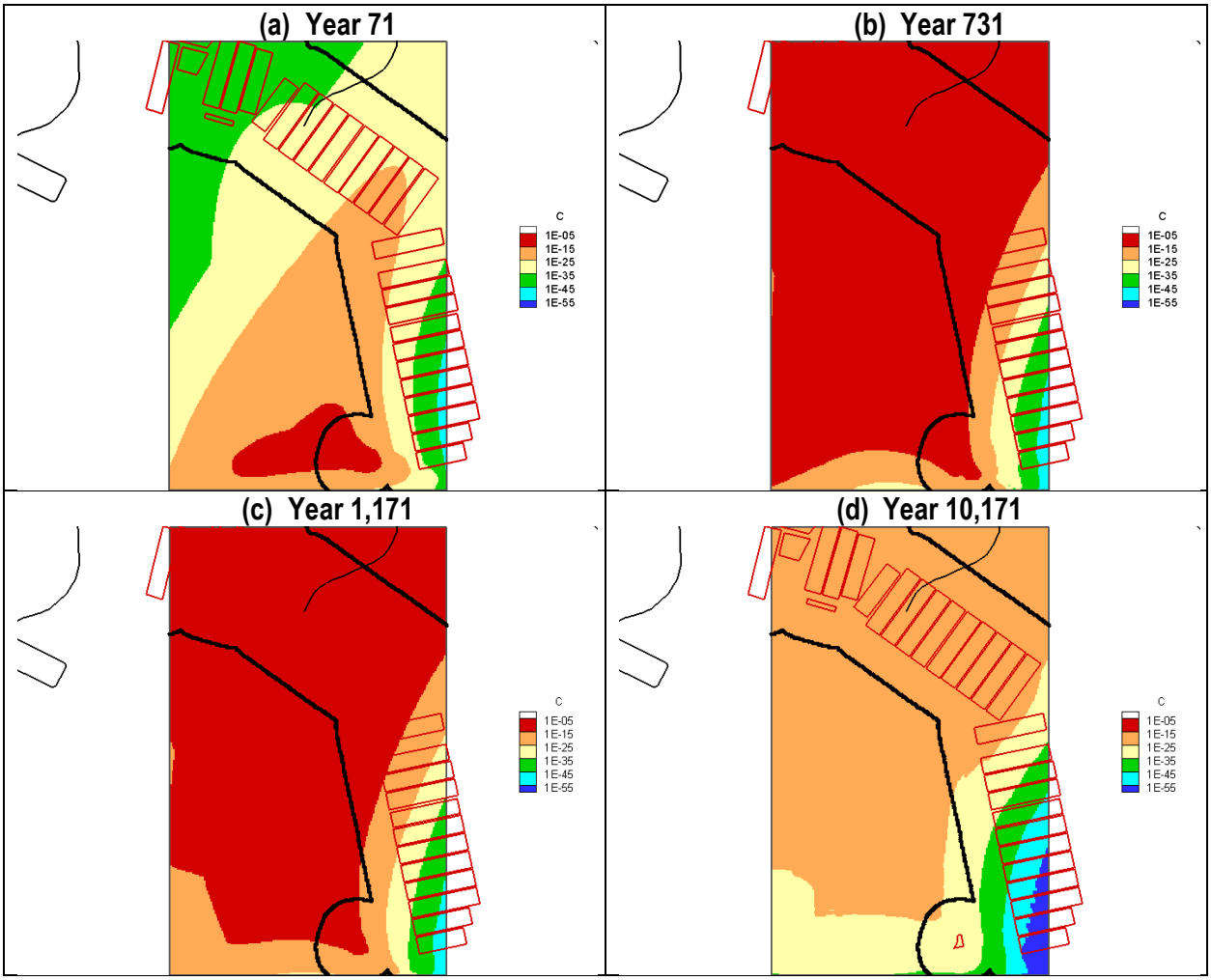

Figure 5-171. 2-D Projection of Maximum Concentration Profile (gmol ft^{-3} per gmole parent buried) of Tc-99 Emanating from NR07E (Nominal PA Case 1 - Generic Waste, Bolted Container) at (a) Year 71; (b) Year 731; (c) Year 1,171; and (d) Year 10,171

Figure 5-171 shows the 2-D projection of the maximum concentration profile for Tc-99 released from NR07E/Case 1 at four different times: Years 71; 731; 1,171; and 10,171. As indicated in

Table 4-82 for NR07E/Case 1, the release of radionuclides is assumed to occur immediately when bolted containers experience early hydraulic failure with placement of the soil cover in calendar year 2005 (Year 11 in model time). Therefore, Figure 5-171 suggests that the plume is already developed at Year 71 (i.e., start of IC) and progresses over time. By Year 1,171 (end of PA compliance period), an intense concentration profile is well established, and at the end of the aquifer transport model simulation (i.e., Year 10,171), most Tc-99 has been released from NR07E. Note that NR07E is only partially covered by the final closure cap as schematically exhibited in Figure 4-208. Consequently, the partial coverage accelerates the spread of the concentration plume.

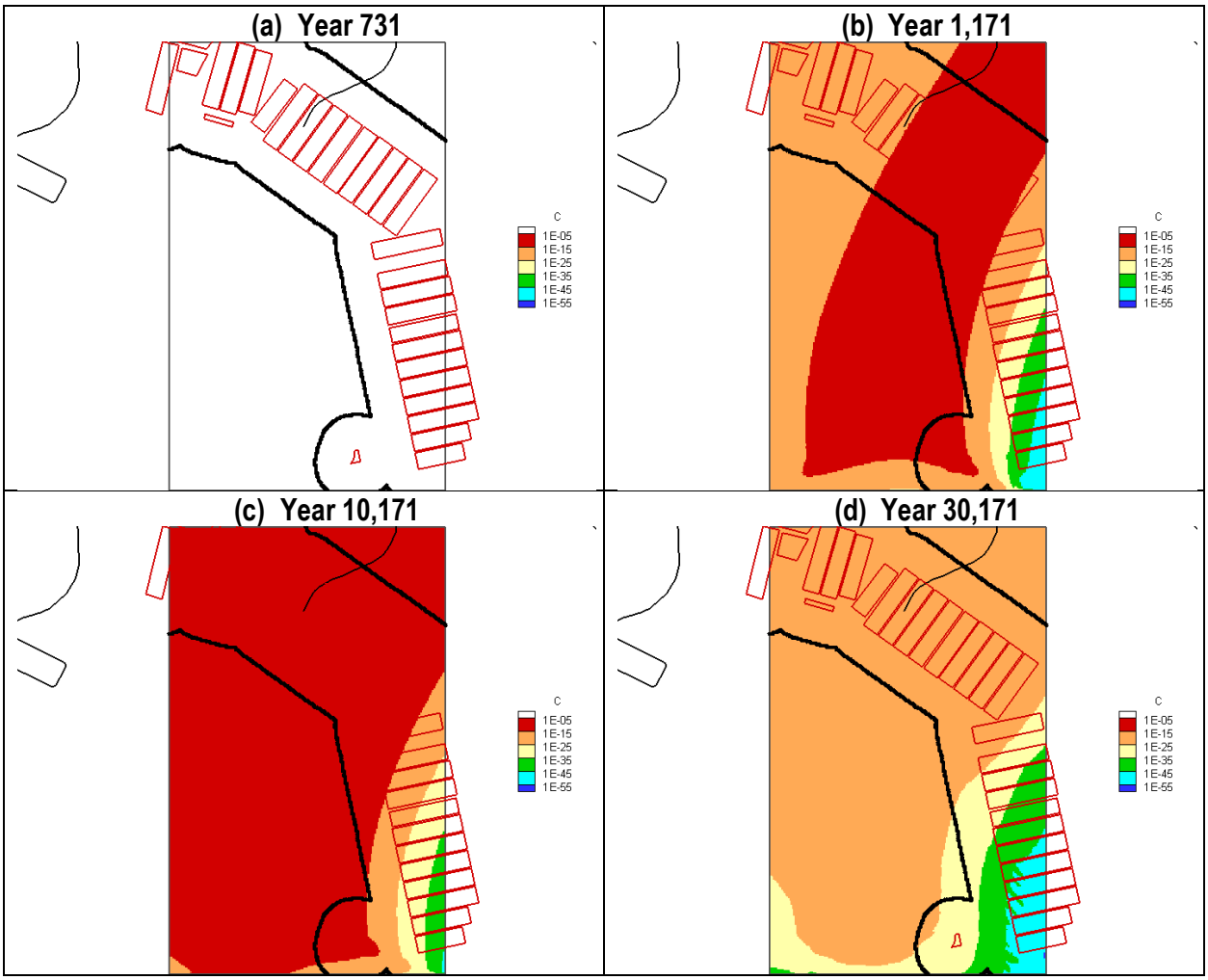

Figure 5-172. 2-D Projection of Maximum Concentration Profile (gmol ft^{-3} per gmole parent buried) of Tc-99 Emanating from NR07E (Nominal PA Case 3 - Special Waste, Activated Inconel, Welded Cask) at (a) Year 731; (b) Year 1,171; (c) Year 10,171; and (d) Year 30,171

The development of the concentration profile for Tc-99 in NR07E/Case 3 (with activated Inconel) is captured in Figure 5-172. In this case, the corrosion-controlled release of radionuclides from welded casks begins in Year 742 when the hydraulic failure of cask welds occurs. As expected, in Year 731, no concentration plume is observed (Figure 5-172(a). By Year 1,171, the plume is established, although the intensity is much less when compared with NR07E/Case 1 because of

the late release timing and slow corrosion rate. By Year 10,171, an intense plume is observed; however, the corrosion-controlled release is not complete until Year 16,821 when the Tc-99 inventory is completely depleted. By Year 30,171, Figure 5-172(d) shows that much of the Tc-99 has been released from the NR07E casks.

Figure 5-173 provides the Ni-59 plume results for NR26E/Case 2. In NR26E/Case 2, waste containers are placed on the NR26E pad in Year 3 and hydraulic failure of seals on all bolted containers is assumed to occur in Year 753; therefore, no plume is seen in Figure 5-173(a) (i.e., at Year 731). By Year 1,171, however, a concentration plume is observed at a low-intensity level when compared with NR07E/Case 1. The complete coverage of NR26E by the final closure cap at Year 171, together with the higher K_d values for Ni-59, evidently retard plume spread. By Year 10,171, a large concentration plume is established.

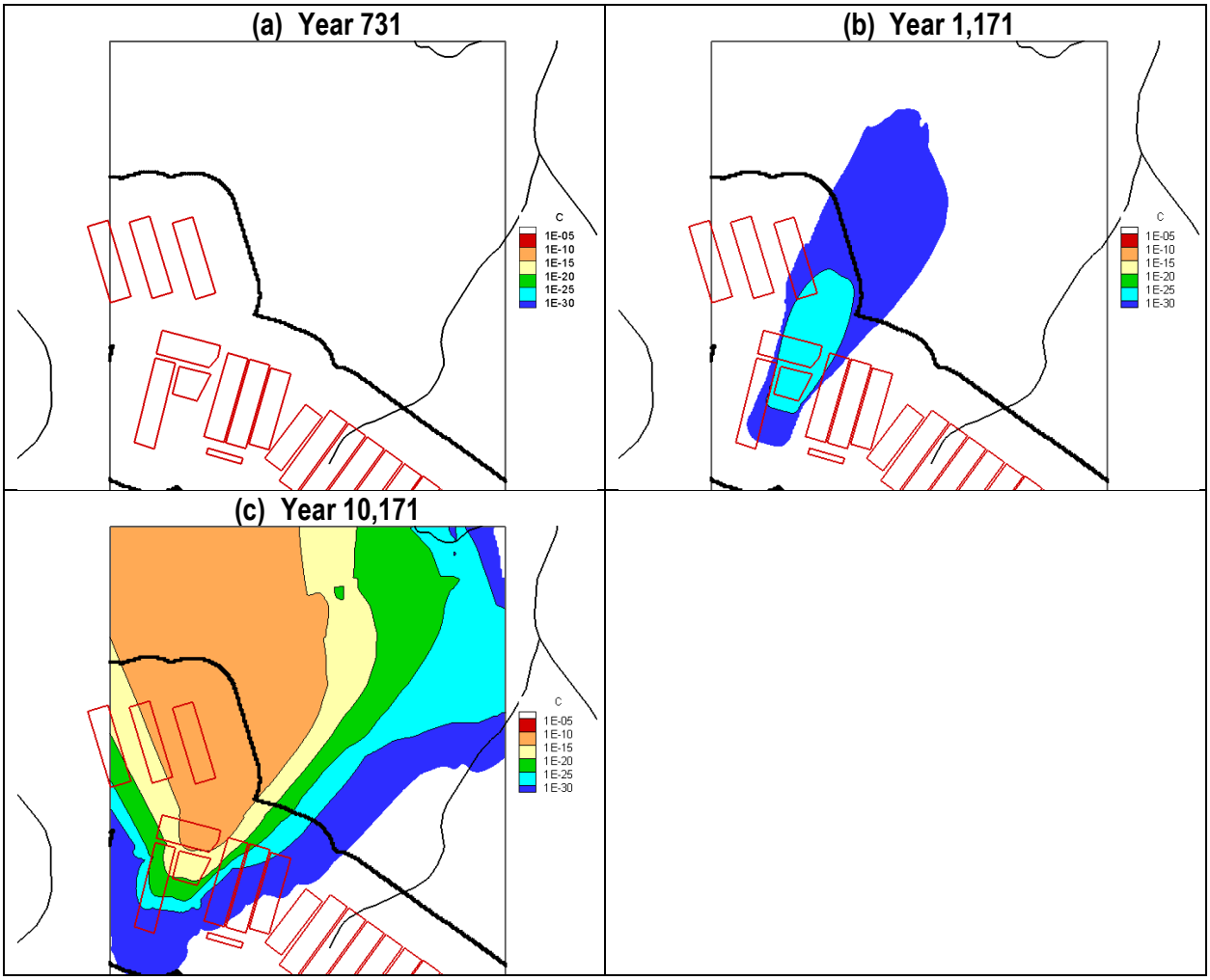

Figure 5-173. 2-D Projection of Maximum Concentration Profile (gmol ft^{-3} per gmole parent buried) of Ni-59 Emanating from NR26E (Nominal PA Case 2 - Generic Waste, Bolted Container) at (a) Year 731; (b) Year 1,171; and (c) Year 10,171

Plume results for Ni-59 for NR26E/Case 4 (activated Zircaloy) are shown in Figure 5-174. Again, as for NR26E/Case 2, no radionuclide release is assumed to occur before hydraulic failure of the

KAPL CB/TS cask welds in Year 753. For this reason, Figure 5-174(a) displays no plume at Year 731. A concentration plume of low intensity is exhibited in Figure 5-174(b), while the intensity of the plume spread accelerates at Year 10,171 in Figure 5-174(c). Because of the slow corrosion rate for activated Zircaloy, corrosion is not complete until Year 105,102. By Year 150,170, Figure 5-174(d) indicates that much of the Ni-59 has been released from the NR26E casks.

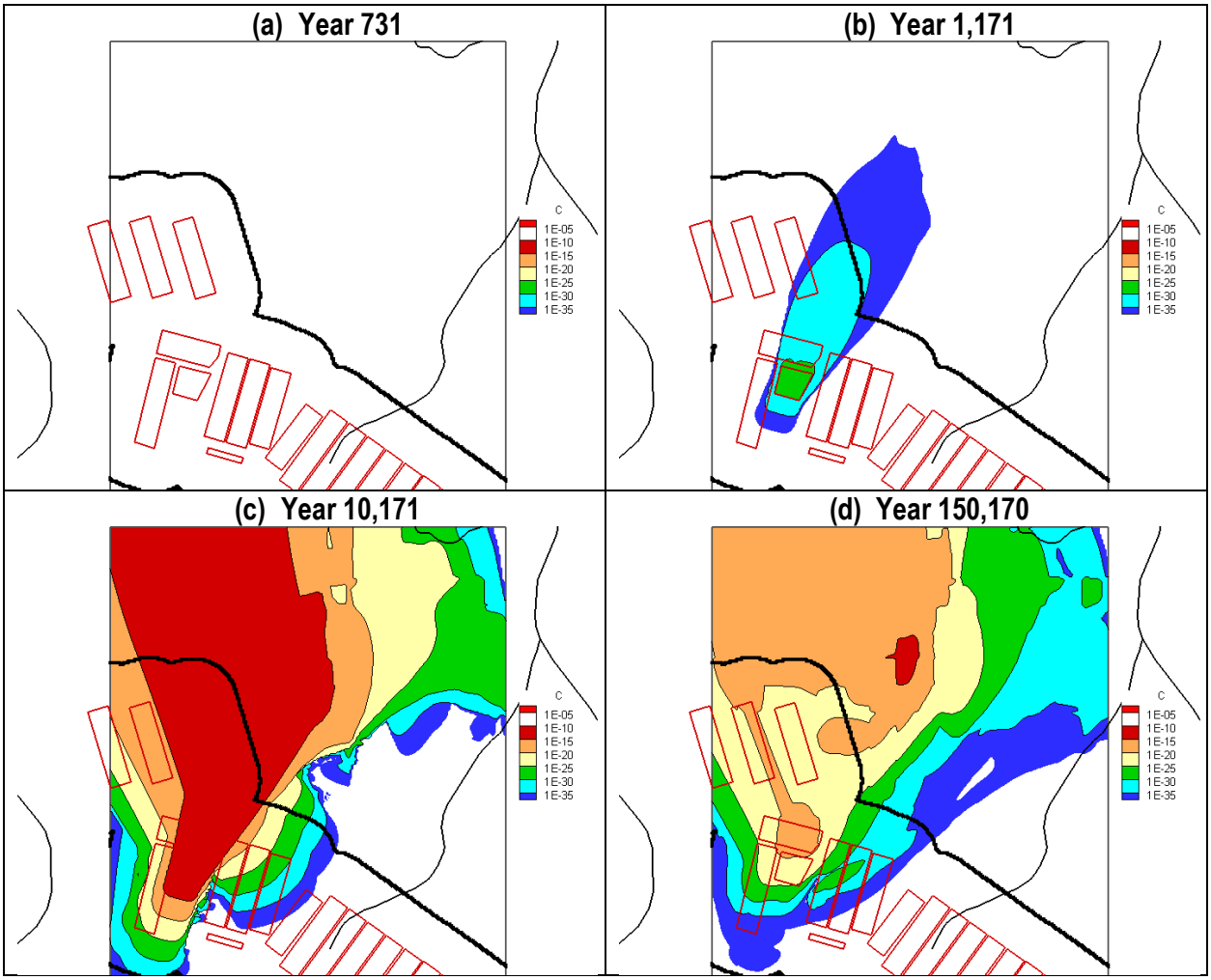

Figure 5-174. 2-D Projection of Maximum Concentration Profile (gmol ft^{-3} per gmole parent buried) of Ni-59 Emanating from NR26E (Nominal PA Case 4 - Special Waste, Activated Zircaloy, Welded Cask) at (a) Year 731; (b) Year 1,171; (c) Year 10,171; and (d) Year 150,170

Simulations of radionuclide contaminant transport in the aquifer GW are performed for radionuclide species identified in the GW screening (see Table 4-86) for each NRCDA DU utilizing, as the source term for contaminants, flux-to-the-water-table data computed for the VZ (Section 5.4.1.2). For consistency with the VZ computational results, the same limited set of radionuclides is selected for demonstration: Be-10 (special waste only), C-14, H-3 (generic waste only), I-129, Ni-59, Pu-241, and Tc-99. Properties of these radionuclide are summarized in Table 5-40. The objective of the aquifer transport calculations is to capture the peak concentration

for each radionuclide at the 100-meter POA, hence allowing the computation of nuclide inventory limits that comply with DOE M 435.1-1, Chg. 3, POs (U.S. DOE, 2021b).

Radionuclide concentrations at the 100-meter POA are presented in the following graphs:

- Figure 5-175 NR07E/Case 1 (generic waste, bolted container)
- Figure 5-176 NR07E/Case 2 (generic waste, bolted container)
- Figure 5-177 NR07E/Case 3 (special waste, activated Inconel, welded cask)
- Figure 5-178 NR07E/Case 4 (special waste, activated Zircaloy, welded cask)
- Figure 5-179 NR26E/Case 1 (generic waste, bolted container)
- Figure 5-180 NR26E/Case 2 (generic waste, bolted container)
- Figure 5-181 NR26E/Case 3 (special waste, activated Inconel, welded cask)
- Figure 5-182 NR26E/Case 4 (special waste, activated Zircaloy, welded cask)

Peak concentration and time of occurrence at the 100-meter POA for the PORFLOW aquifer transport runs are listed in the following tables for the selected radionuclides:

- Table 5-51 NR07E/Case 1 (generic waste, bolted container)
- Table 5-52 NR07E/Case 2 (generic waste, bolted container)
- Table 5-53 NR07E/Case 3 (special waste, activated Inconel, welded cask)
- Table 5-54 NR07E/Case 4 (special waste, activated Zircaloy, welded cask)
- Table 5-55 NR26E/Case 1 (generic waste, bolted container)
- Table 5-56 NR26E/Case 2 (generic waste, bolted container)
- Table 5-57 NR26E/Case 3 (special waste, activated Inconel, welded cask)
- Table 5-58 NR26E/Case 4 (special waste, activated Zircaloy, welded cask)

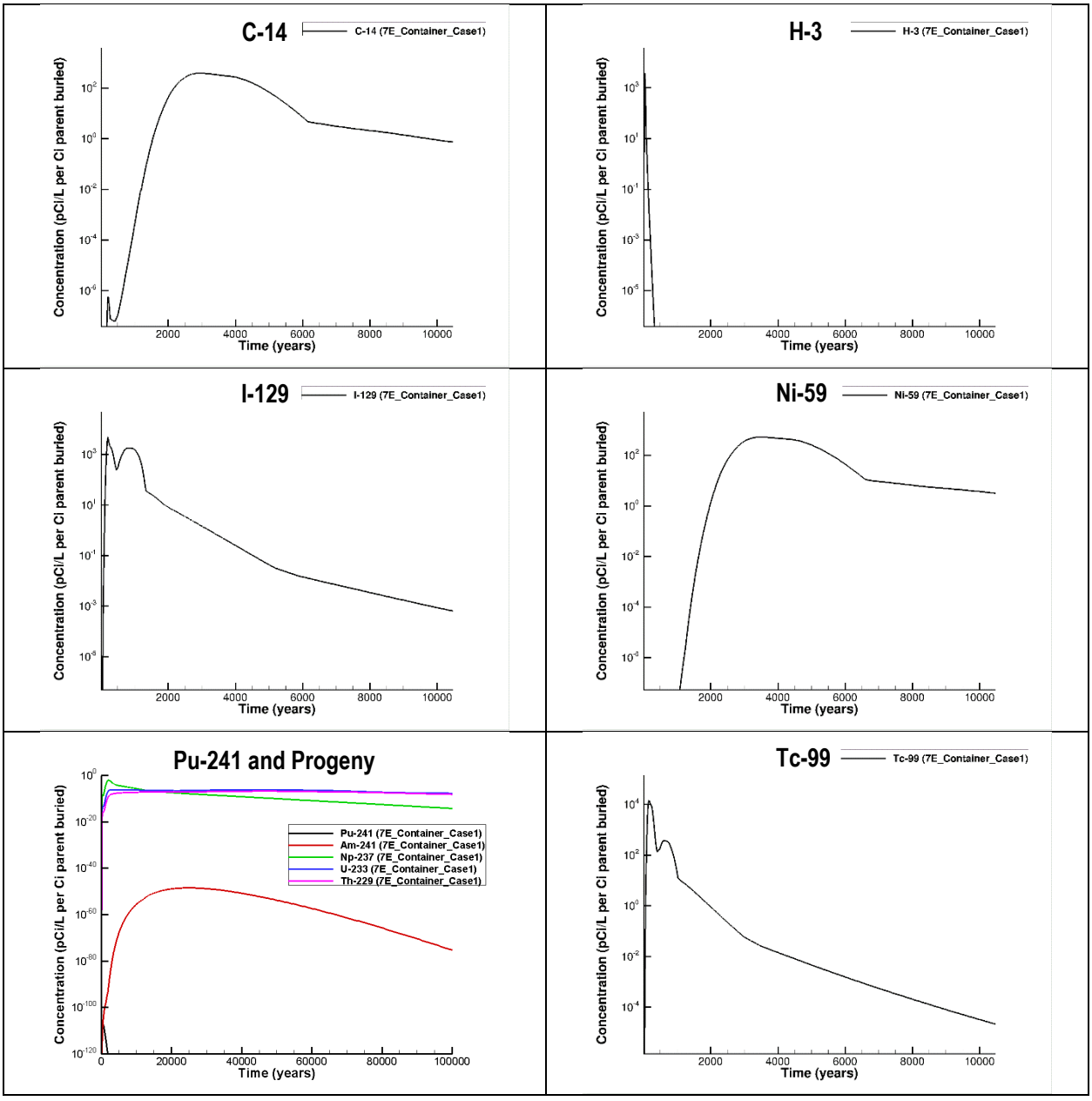

Figure 5-175. NR07E/Case 1 (Generic Waste, Bolted Container) Maximum Concentration at 100-meter POA

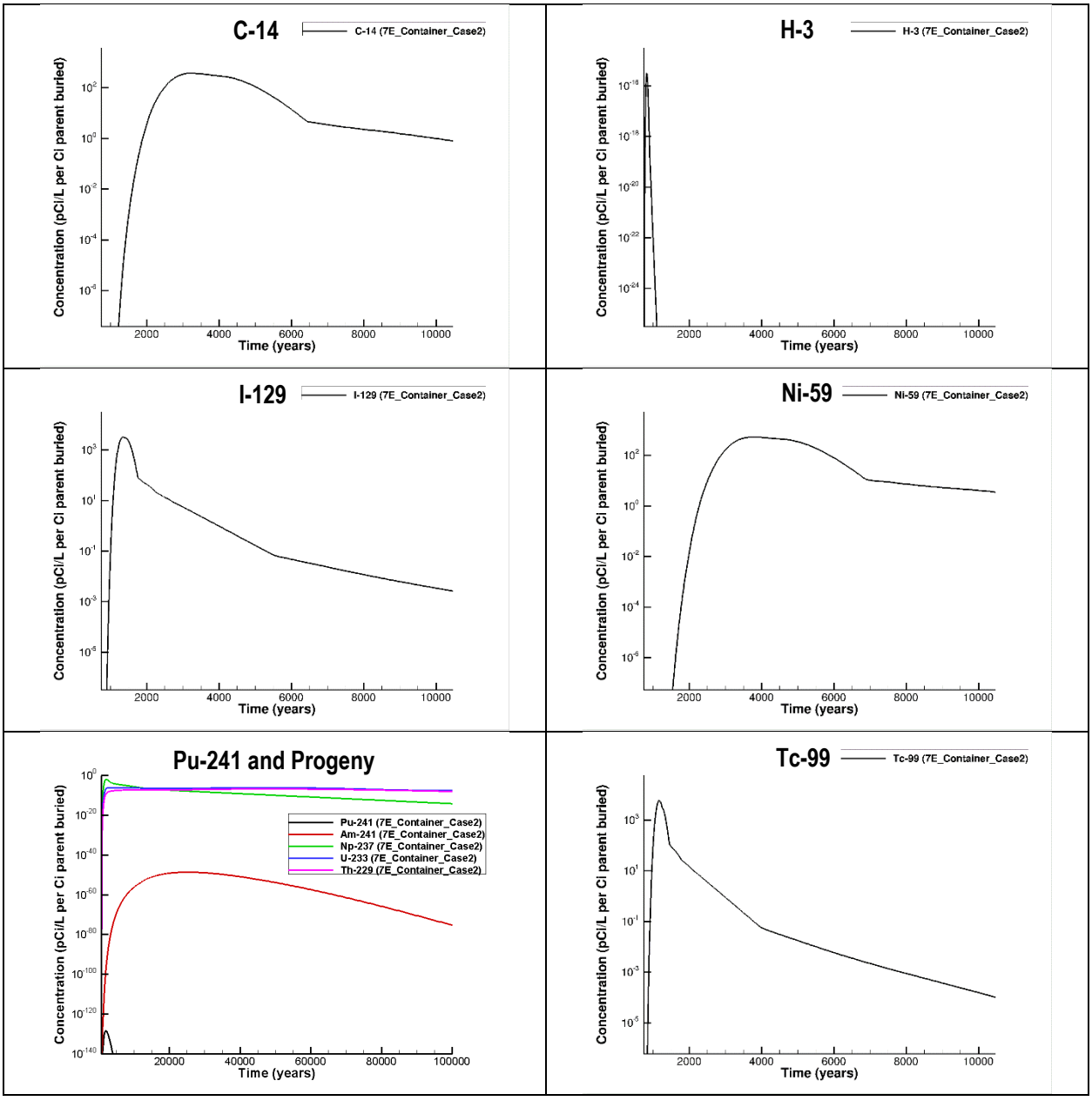

Figure 5-176. NR07E/Case 2 (Generic Waste, Bolted Container) Maximum Concentration at 100-meter POA

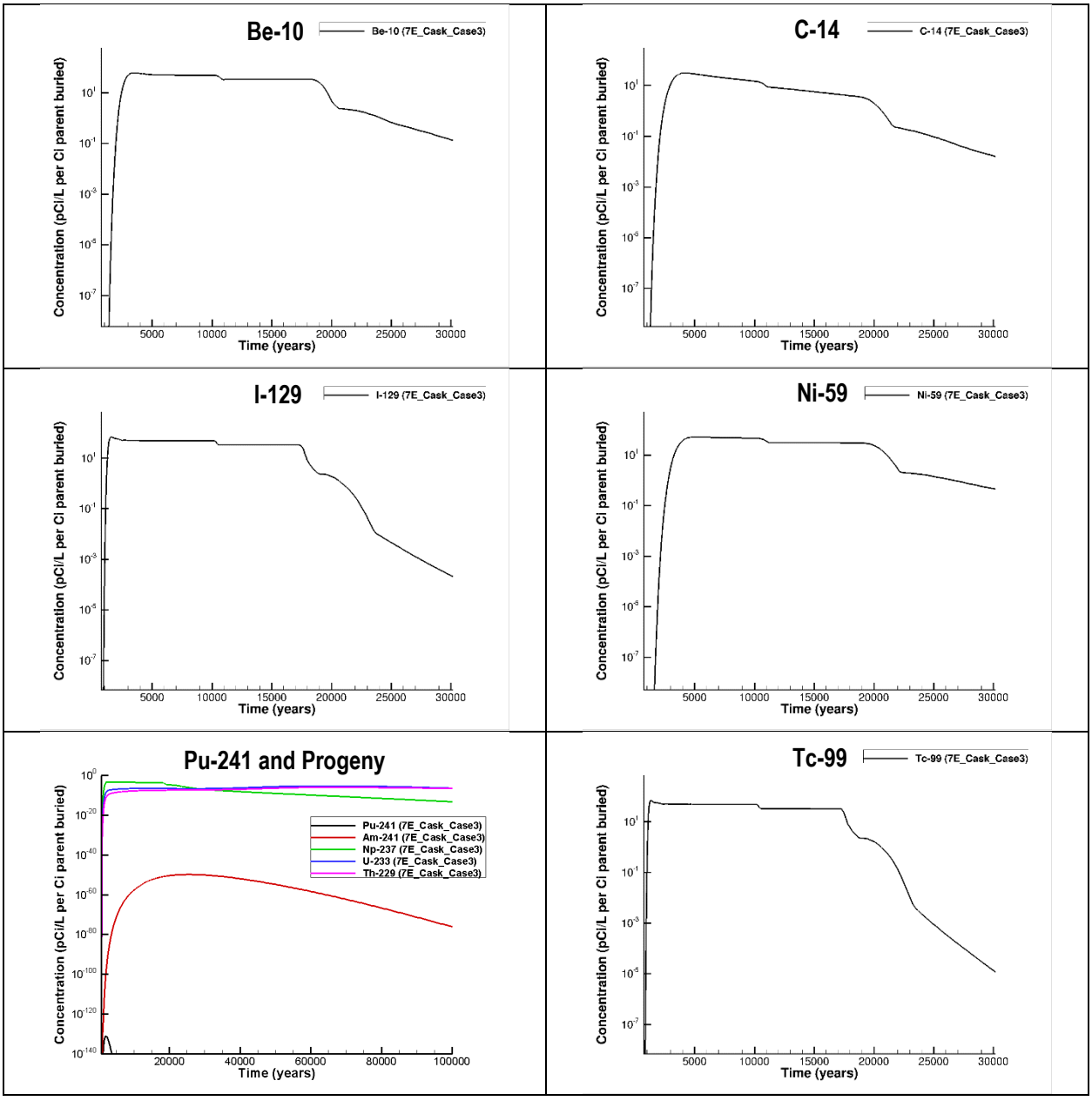

Figure 5-177. NR07E/Case 3 (Special Waste, Activated Inconel, Welded Cask) Maximum Concentration at 100-meter POA

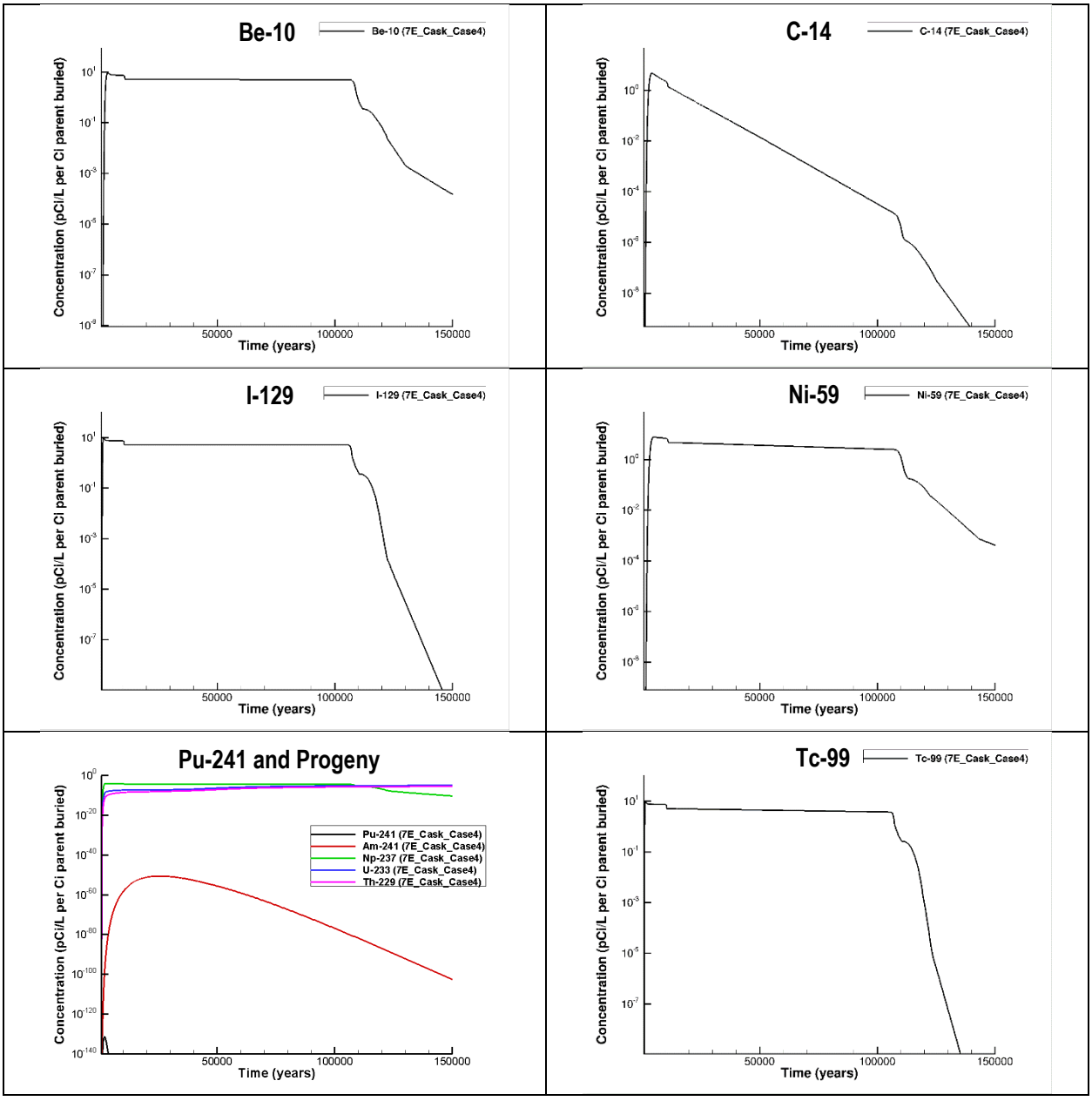

Figure 5-178. NR07E/Case 4 (Special Waste, Activated Zircaloy, Welded Cask) Maximum Concentration at 100-meter POA

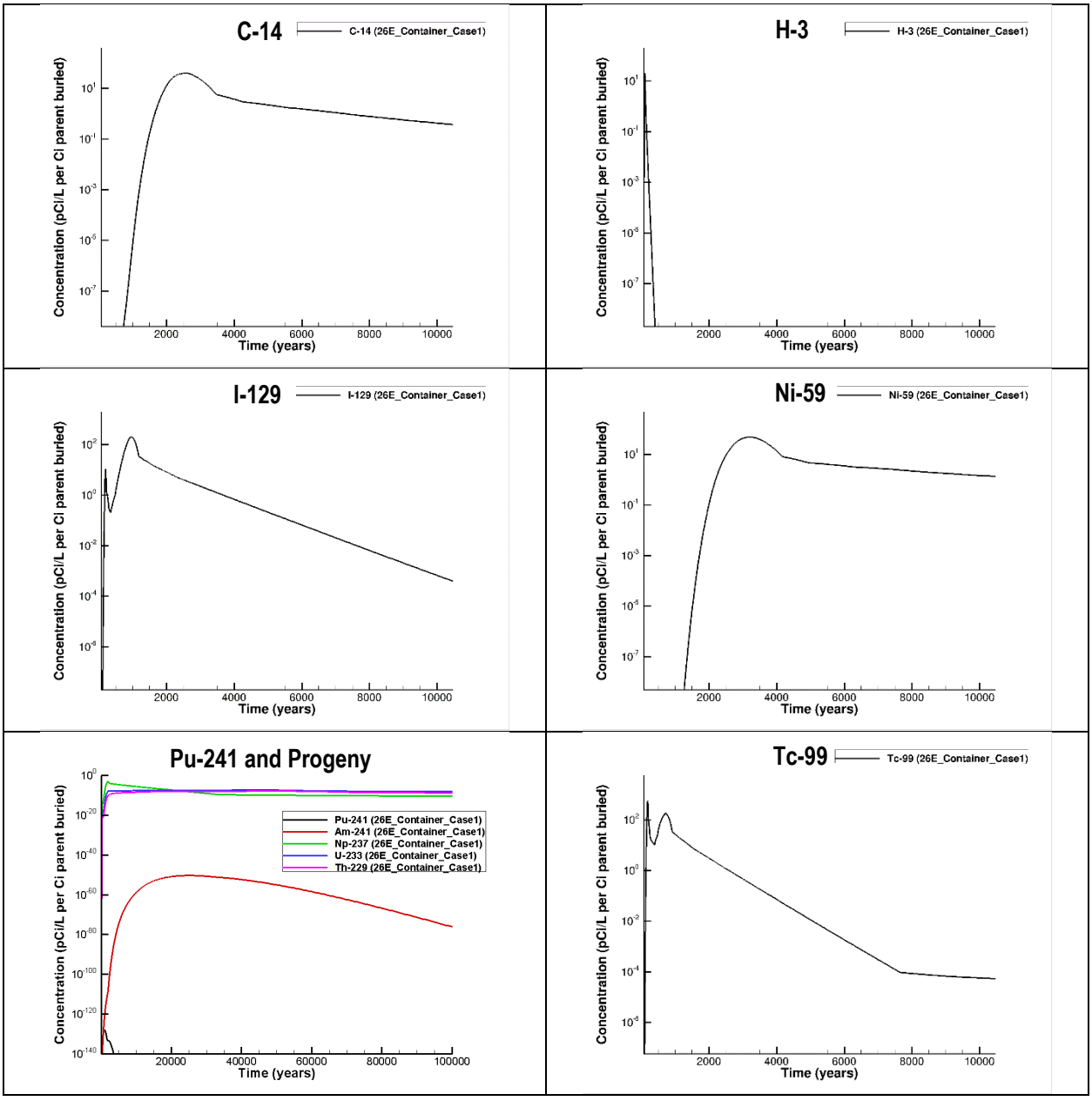

Figure 5-179. NR26E/Case 1 (Generic Waste, Bolted Container) Maximum Concentration at 100-meter POA

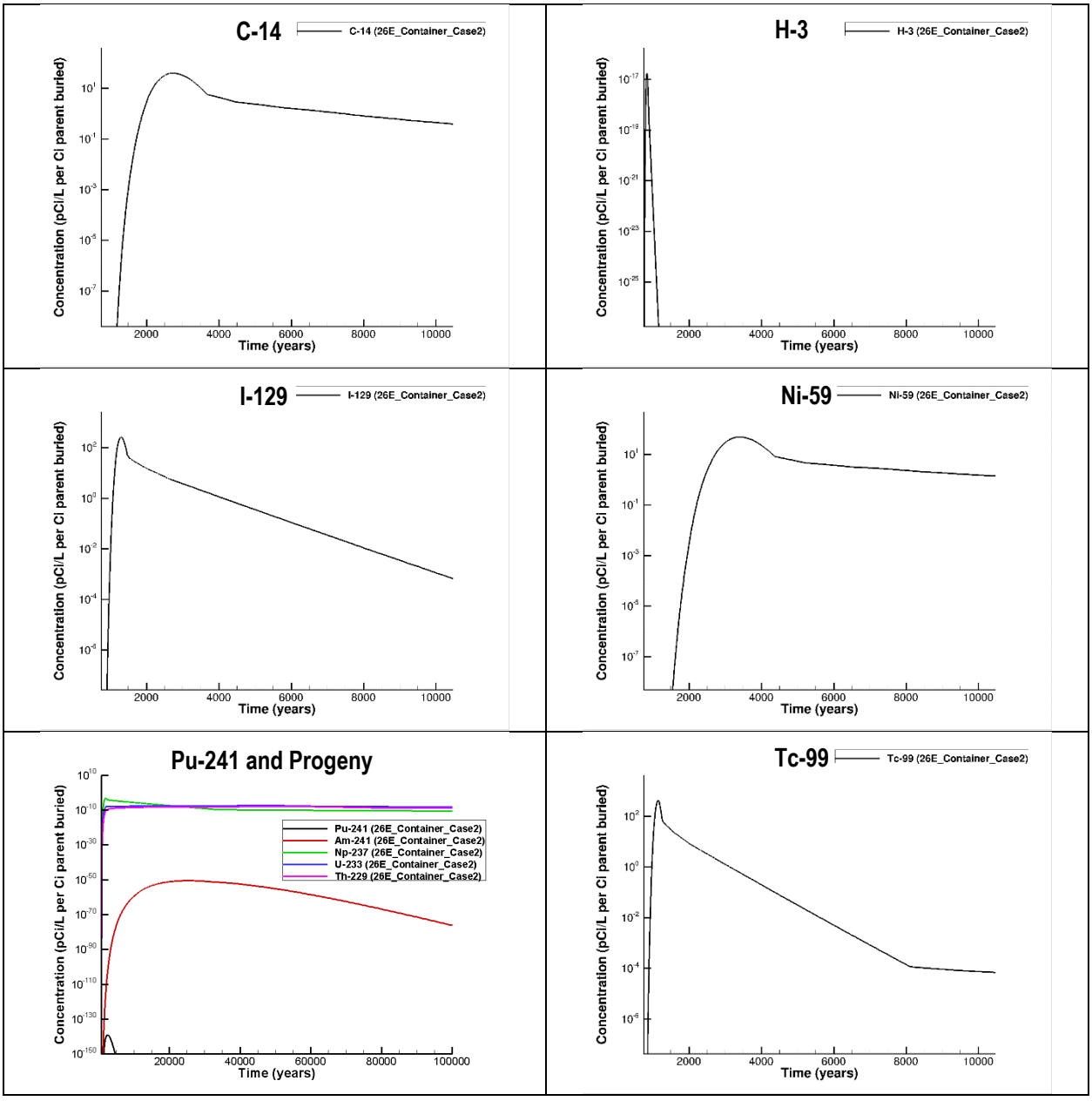

Figure 5-180. NR26E/Case 2 (Generic Waste, Bolted Container) Maximum Concentration at 100-meter POA

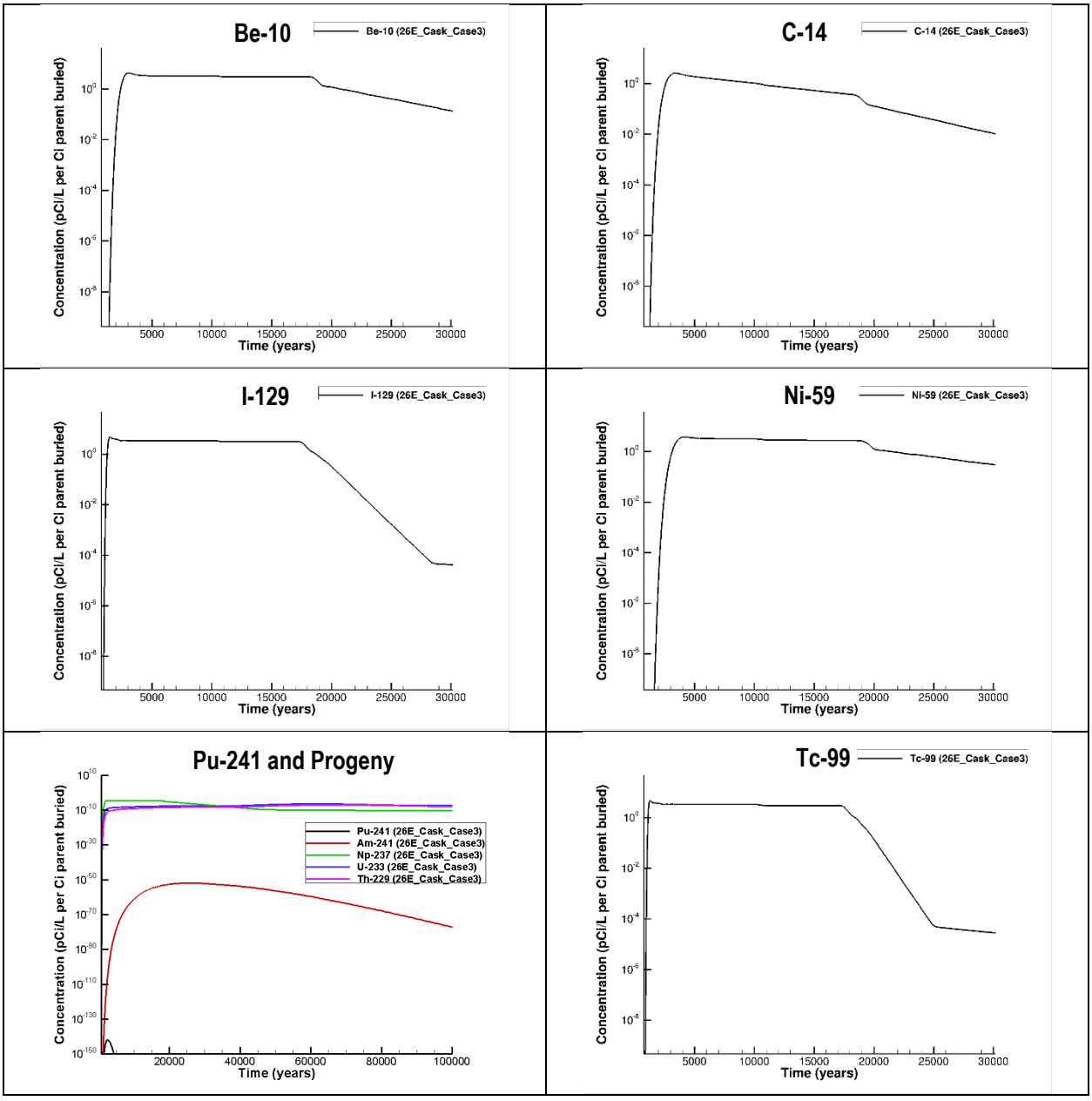

Figure 5-181. NR26E/Case 3 (Special Waste, Activated Inconel, Welded Cask) Maximum Concentration at 100-meter POA

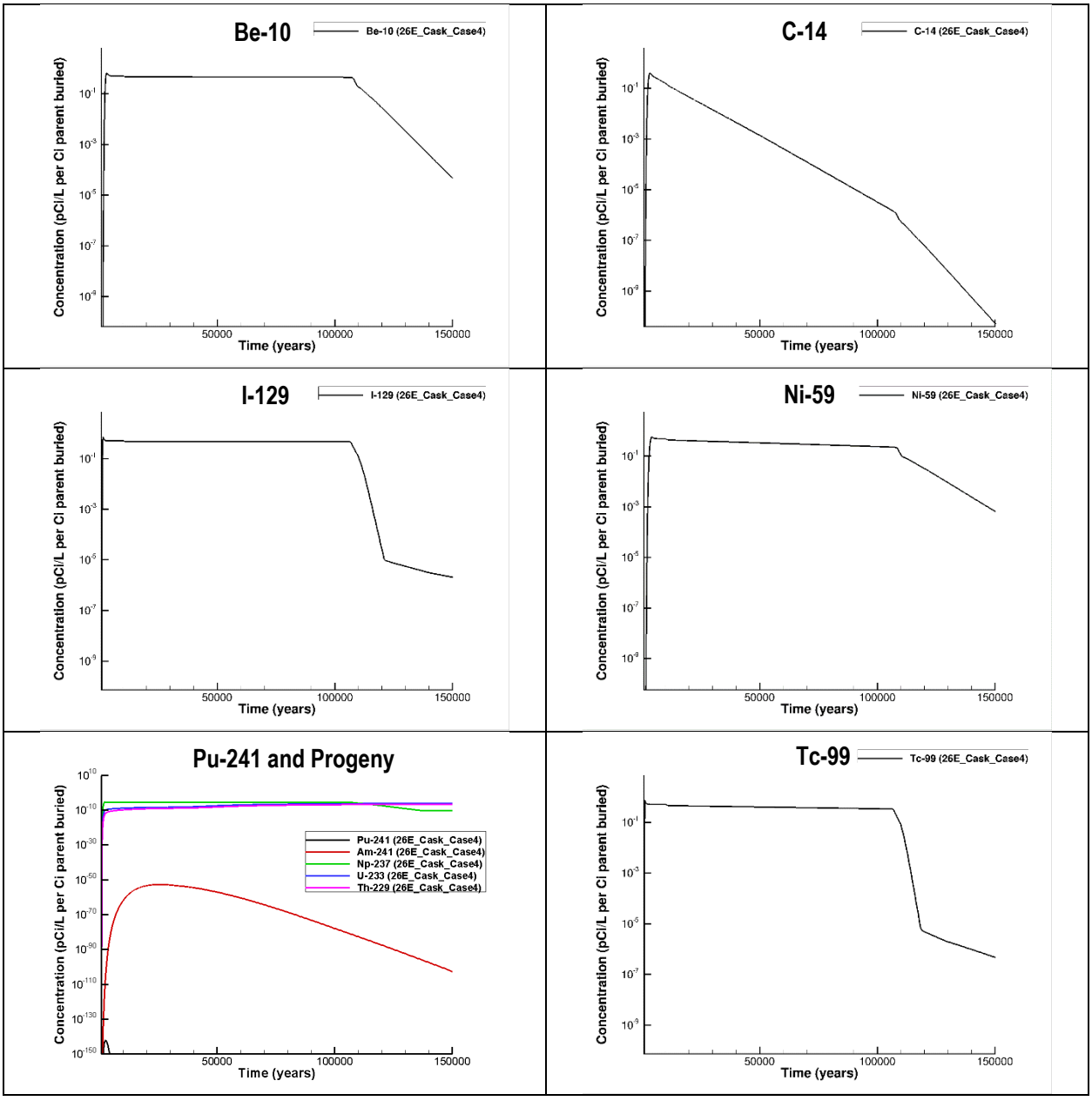

Figure 5-182. NR26E/Case 4 (Special Waste, Activated Zircaloy, Welded Cask) Maximum Concentration at 100-meter POA

Table 5-51. Peak Concentration and Time of Occurrence for NR07E/Case 1 (Bolted Container, Generic Waste)

Radionuclide		Peak Concentration Time (Year)	Peak Concentration (pCi L^{-1} per Ci parent)
Parent	Progeny		
C-14	-	2,935	3.87E+02
H-3	-	37	3.82E+02
I-129	-	205	4.91E+03
Ni-59	-	3,462	5.31E+02
Pu-241	-	554	2.64E-108
-	Am-241	24,902	3.43E-49
-	Np-237	2,047	7.63E-03
-	U-233	4,230	5.44E-07
-	Th-229	46,461	1.53E-07
Tc-99	-	166	1.45E+04

Table 5-52. Peak Concentration and Time of Occurrence for NR07E/Case 2 (Bolted Container, Generic Waste)

Radionuclide		Peak Concentration Time (Year)	Peak Concentration (pCi L^{-1} per Ci parent)
Parent	Progeny		
C-14	-	3,235	3.80E+02
H-3	-	820	3.17E-16
I-129	-	1,347	3.27E+03
Ni-59	-	3,738	5.30E+02
Pu-241	-	2,009	4.18E-129
-	Am-241	25,150	2.13E-49
-	Np-237	2,067	8.61E-03
-	U-233	4,230	5.45E-07
-	Th-229	48,823	1.56E-07
Tc-99	-	1,167	5.92E+03

Table 5-53. Peak Concentration and Time of Occurrence for NR07E/Case 3 (Activated Inconel, Welded Cask, Special Waste)

Radionuclide		Peak Concentration Time (Year)	Peak Concentration (pCi L^{-1} per Ci parent)
Parent	Progeny		
Be-10	-	3,462	5.91E+01
C-14	-	4,137	3.11E+01
I-129	-	1,553	6.82E+01
Ni-59	-	5,082	5.12E+01
Pu-241	-	2,028	9.26E-132
-	Am-241	25,652	1.47E-50
-	Np-237	2,510	4.26E-04
-	U-233	61,297	3.98E-06
-	Th-229	61,297	1.10E-06
Tc-99	-	1,328	6.90E+01

Table 5-54. Peak Concentration and Time of Occurrence for NR07E/Case 4 (Activated Zircaloy, Welded Cask, Special Waste)

Radionuclide		Peak Concentration Time (Year)	Peak Concentration (pCi L^{-1} per Ci parent)
Parent	Progeny		
Be-10	-	3,462	9.11E+00
C-14	-	4,137	4.80E+00
I-129	-	1,553	1.05E+01
Ni-59	-	5,082	7.88E+00
Pu-241	-	2,038	5.12E-132
-	Am-241	25,652	2.26E-51
-	Np-237	2,510	6.56E-05
-	U-233	140,797	8.41E-06
-	Th-229	143,797	2.59E-06
Tc-99	-	1,328	1.06E+01

Table 5-55. Peak Concentration and Time of Occurrence for NR26E/Case 1 (Bolted Container, Generic Waste)

Radionuclide		Peak Concentration Time (Year)	Peak Concentration (pCi L^{-1} per Ci parent)
Parent	Progeny		
C-14	-	2,584	4.00E+01
H-3	-	100	2.04E+01
I-129	-	956	1.99E+02
Ni-59	-	3,214	4.87E+01
Pu-241	-	953	1.15E-128
-	Am-241	25,150	4.63E-51
-	Np-237	1,895	6.18E-04
-	U-233	43,779	4.30E-08
-	Th-229	48,823	1.27E-08
Tc-99	-	184	5.78E+02

Table 5-56. Peak Concentration and Time of Occurrence for NR26E/Case 2 (Bolted Container, Generic Waste)

Radionuclide		Peak Concentration Time (Year)	Peak Concentration (pCi L^{-1} per Ci parent)
Parent	Progeny		
C-14	-	2,742	3.96E+01
H-3	-	834	1.77E-17
I-129	-	1,306	2.66E+02
Ni-59	-	3,415	4.87E+01
Pu-241	-	2,496	7.78E-140
-	Am-241	25,399	3.29E-51
-	Np-237	1,973	7.08E-04
-	U-233	46,003	4.54E-08
-	Th-229	50,797	1.33E-08
Tc-99	-	1,146	4.24E+02

Table 5-57. Peak Concentration and Time of Occurrence for NR26E/Case 3 (Activated Inconel, Welded Cask, Special Waste)

Radionuclide		Peak Concentration Time (Year)	Peak Concentration (pCi L^{-1} per Ci parent)
Parent	Progeny		
Be-10	-	3,110	4.27E+00
C-14	-	3,368	2.59E+00
I-129	-	1,450	4.69E+00
Ni-59	-	4,198	3.72E+00
Pu-241	-	2,525	1.04E-142
-	Am-241	25,906	1.40E-52
-	Np-237	2,298	3.01E-05
-	U-233	61,297	3.85E-07
-	Th-229	66,797	1.09E-07
Tc-99	-	1,304	4.72E+00

Table 5-58. Peak Concentration and Time of Occurrence for NR26E/Case 4 (Activated Zircaloy, Welded Cask, Special Waste)

Radionuclide		Peak Concentration Time (Year)	Peak Concentration (pCi L^{-1} per Ci parent)
Parent	Progeny		
Be-10	-	3,110	6.57E-01
C-14	-	3,368	3.99E-01
I-129	-	1,450	7.22E-01
Ni-59	-	4,198	5.74E-01
Pu-241	-	2,539	5.86E-143
-	Am-241	25,906	2.16E-53
-	Np-237	2,298	4.65E-06
-	U-233	139,797	7.70E-07
-	Th-229	143,797	2.46E-07
Tc-99	-	1,304	7.27E-01

5.4.2.3. Sensitivity Case Results

The sensitivity cases listed in Table 5-49 for the VZ define the aquifer zone sensitivity cases. However, only the Case e parameter change (0.5 K_d) applies in both the VZ and aquifer zone. That is, K_d values for the aquifer soil and clay are reduced by 50%. Parameter changes for the other five sensitivity cases apply to the VZ only. The aquifer parameters remain unchanged from the nominal PA case settings.

Radionuclide fluxes to the water table for all species of interest computed in the VZ sensitivity case simulations serve as source terms for the aquifer zone transport simulations for each NRCDA. The objective of the sensitivity calculations for aquifer zone transport is to quantify the effect of model input parameter perturbations on the peak concentration of each radionuclide at the 100-meter POA. As with the VZ, three radionuclides are selected for demonstration: C-14 (moderate half-life, moderate K_d), I-129 (long half-life, low K_d), and Pu-241 (decay chain nuclide

with daughters Am-241, Np-237, U-233, and Th-229). The sensitivity cases include NR07E/Case 3, NR26E/Case 1, and NR26E/Case 4.

Radionuclide aquifer zone concentrations at the 100-meter POA for the nominal PA case versus sensitivity cases are displayed on the following graphs:

- Figure 5-183 NR07E/Case 3 for C-14 (left) and I-129 (right)
- Figure 5-184 NR26E/Case 1 for C-14 (left) and I-129 (right)
- Figure 5-185 NR26E/Case 4 for C-14 (left) and I-129 (right)
- Figure 5-186 NR07E/Case 3 for Pu-241 and progeny
- Figure 5-187 NR26E/Case 1 for Pu-241 and progeny
- Figure 5-188 NR26E/Case 4 for Pu-241 and progeny

As with the VZ sensitivity cases, Sensitivity Case e ($0.5K_d$) has the greatest impact on the maximum radionuclide concentrations at the 100-meter POA. The reduction in K_d increases peak concentrations; however, concentrations decrease more rapidly with time. For Case 4 (SWF with activated Zircaloy metal; long corrosion time of 104,349 years), the impact of the sensitivity cases on peak concentrations is less pronounced because of the slow nuclide release rate.

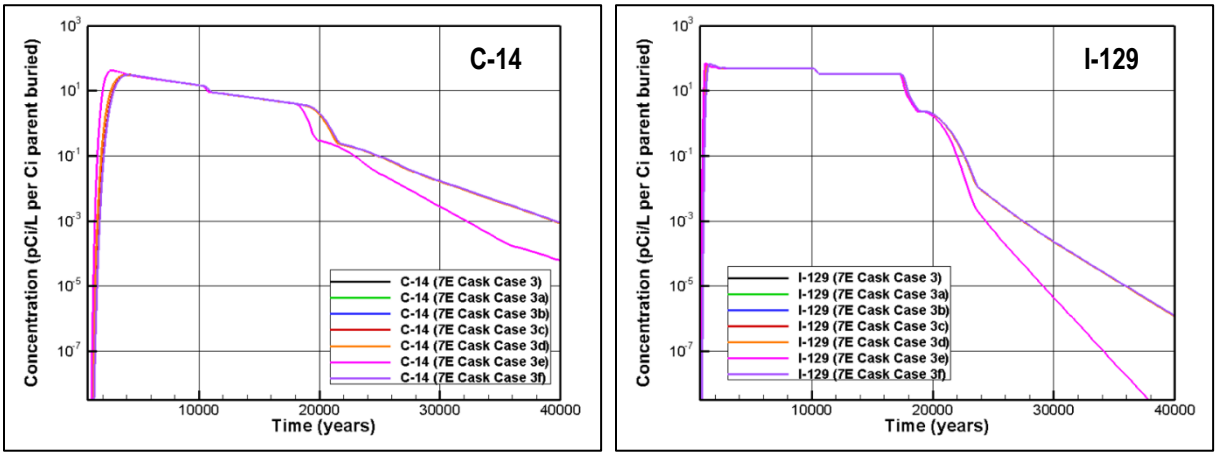

Figure 5-183. Maximum C-14 (left) and I-129 (right) Concentrations at 100-meter POA for Aquifer Nominal PA and Sensitivity Cases for NR07E/Case 3

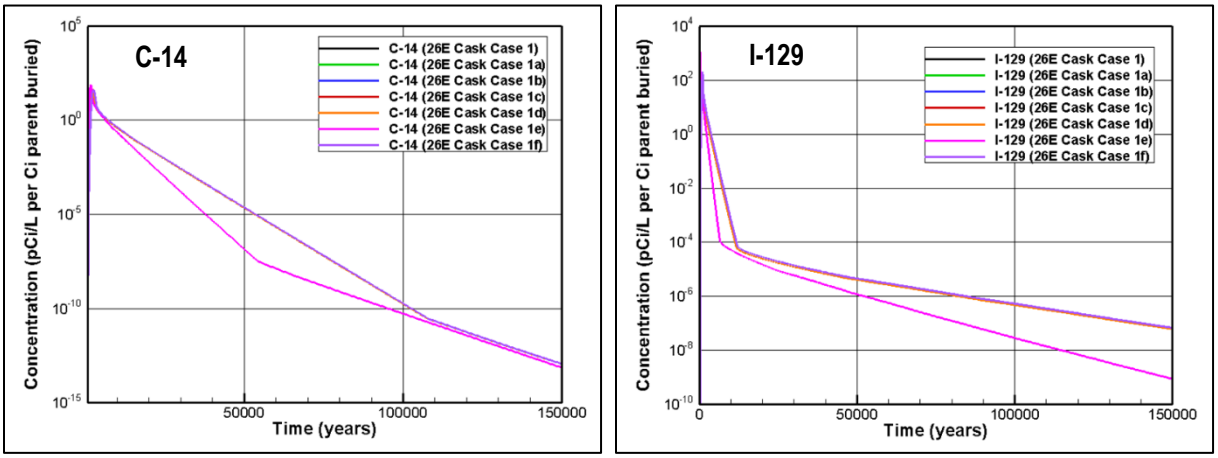

Figure 5-184. Maximum C-14 (left) and I-129 (right) Concentrations at 100-meter POA for Aquifer Nominal PA and Sensitivity Cases for NR26E/Case 1

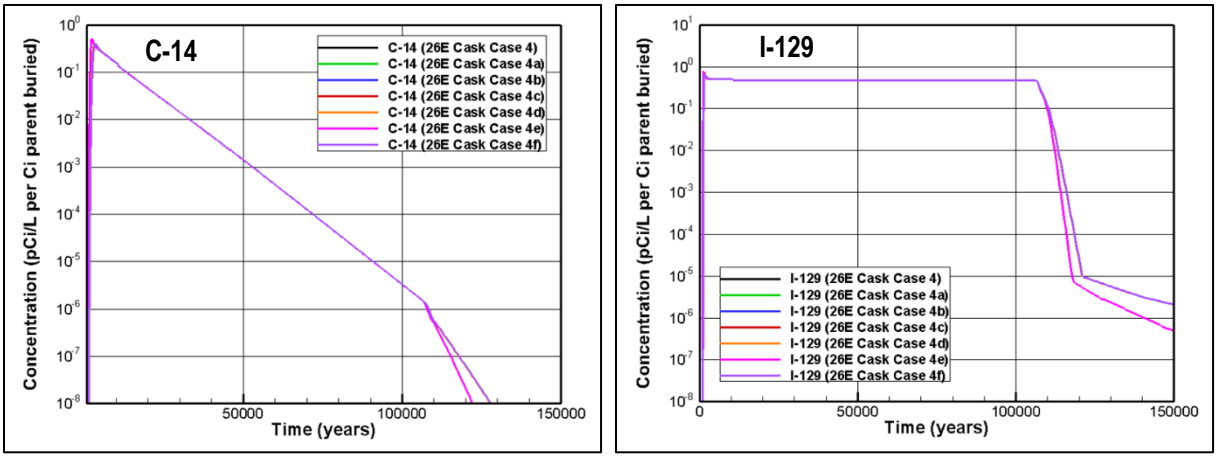

Figure 5-185. Maximum C-14 (left) and I-129 (right) Concentrations at 100-meter POA for Aquifer Nominal PA and Sensitivity Cases for NR26E/Case 4

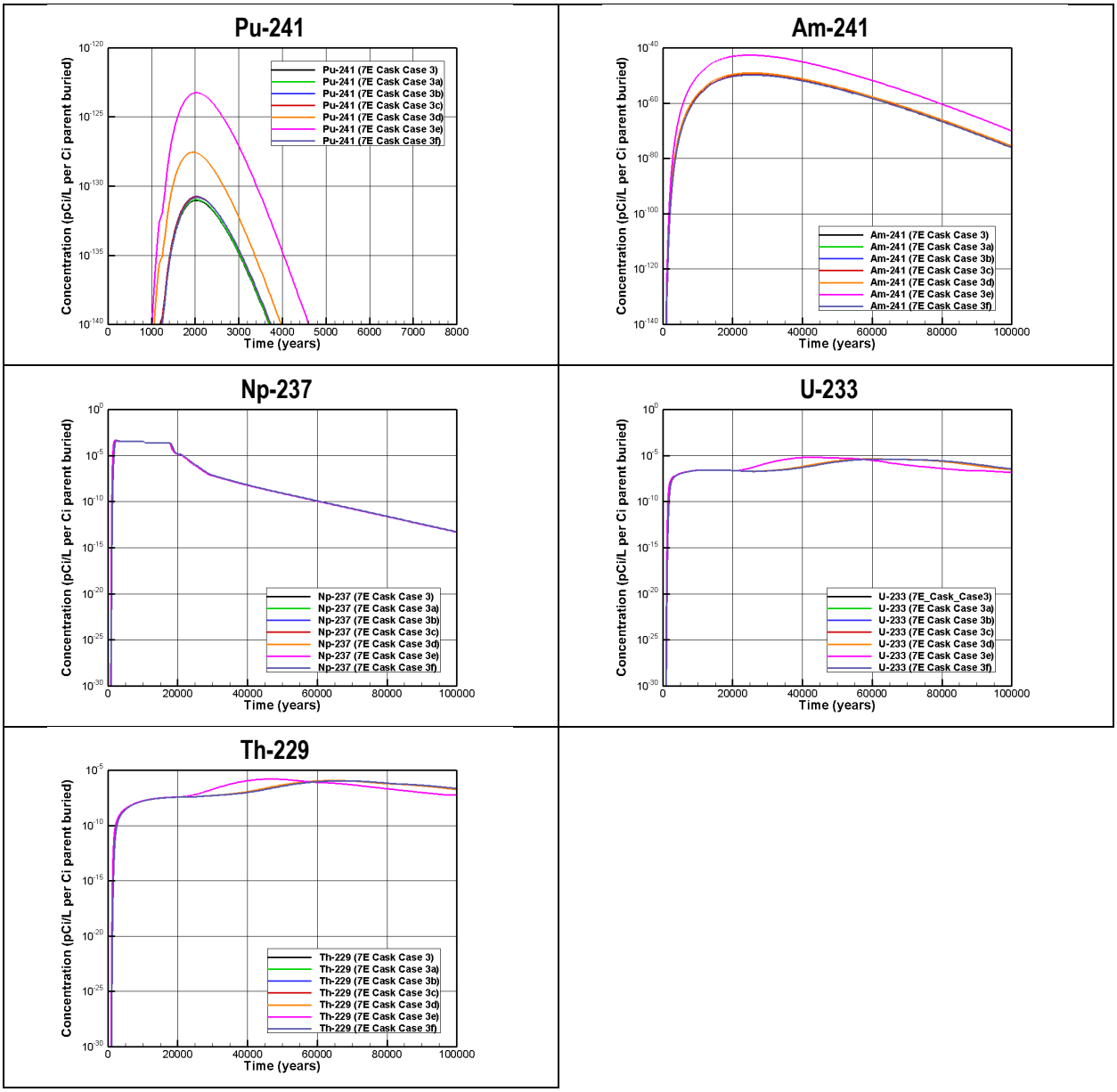

Figure 5-186. Maximum Concentrations of Pu-241 and Progeny at 100-meter POA for Aquifer Nominal PA and Sensitivity Cases for NR07E/Case 3

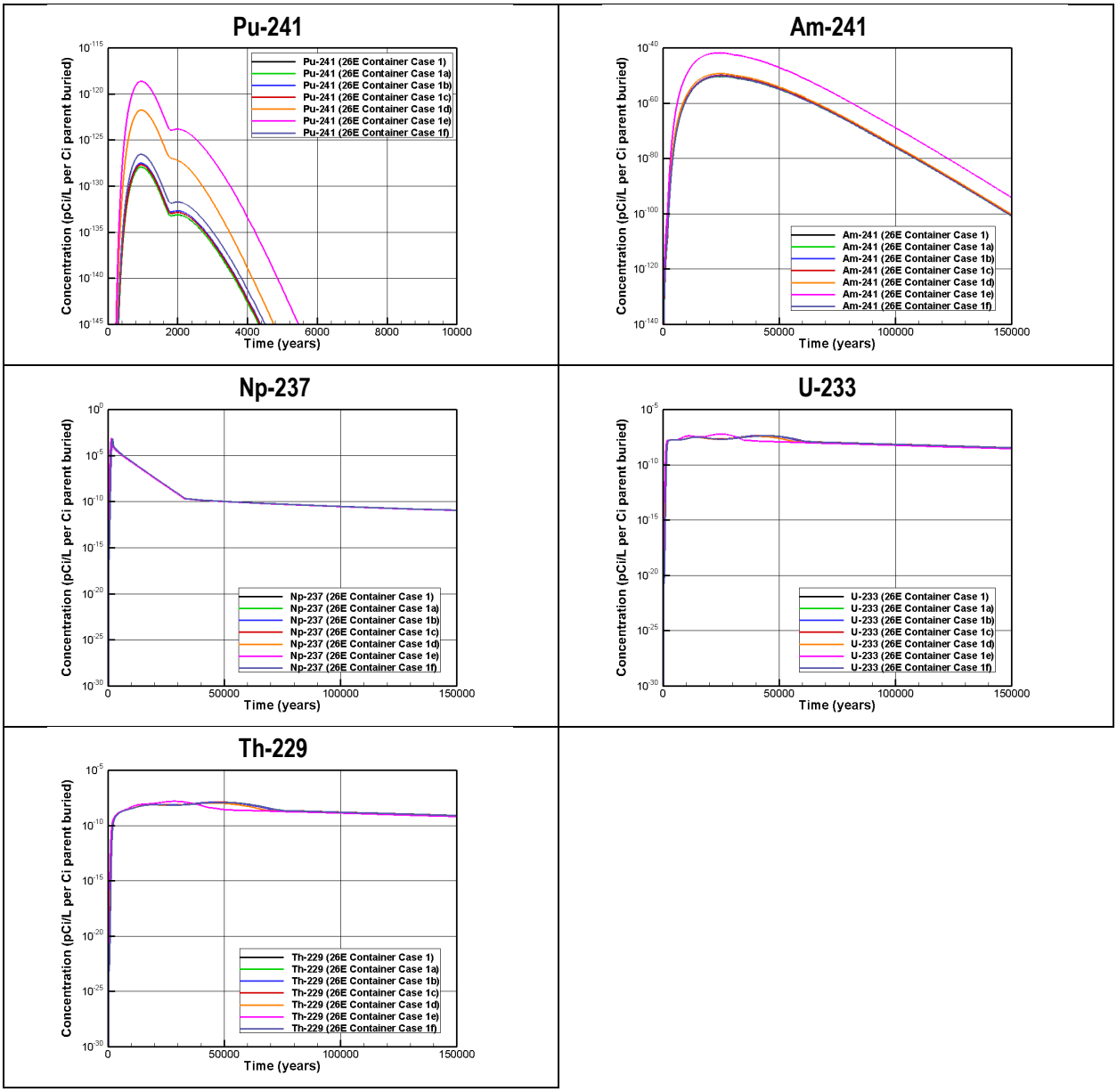

Figure 5-187. Maximum Concentrations of Pu-241 and Progeny at 100-meter POA for Aquifer Nominal PA and Sensitivity Cases for NR26E/Case 1

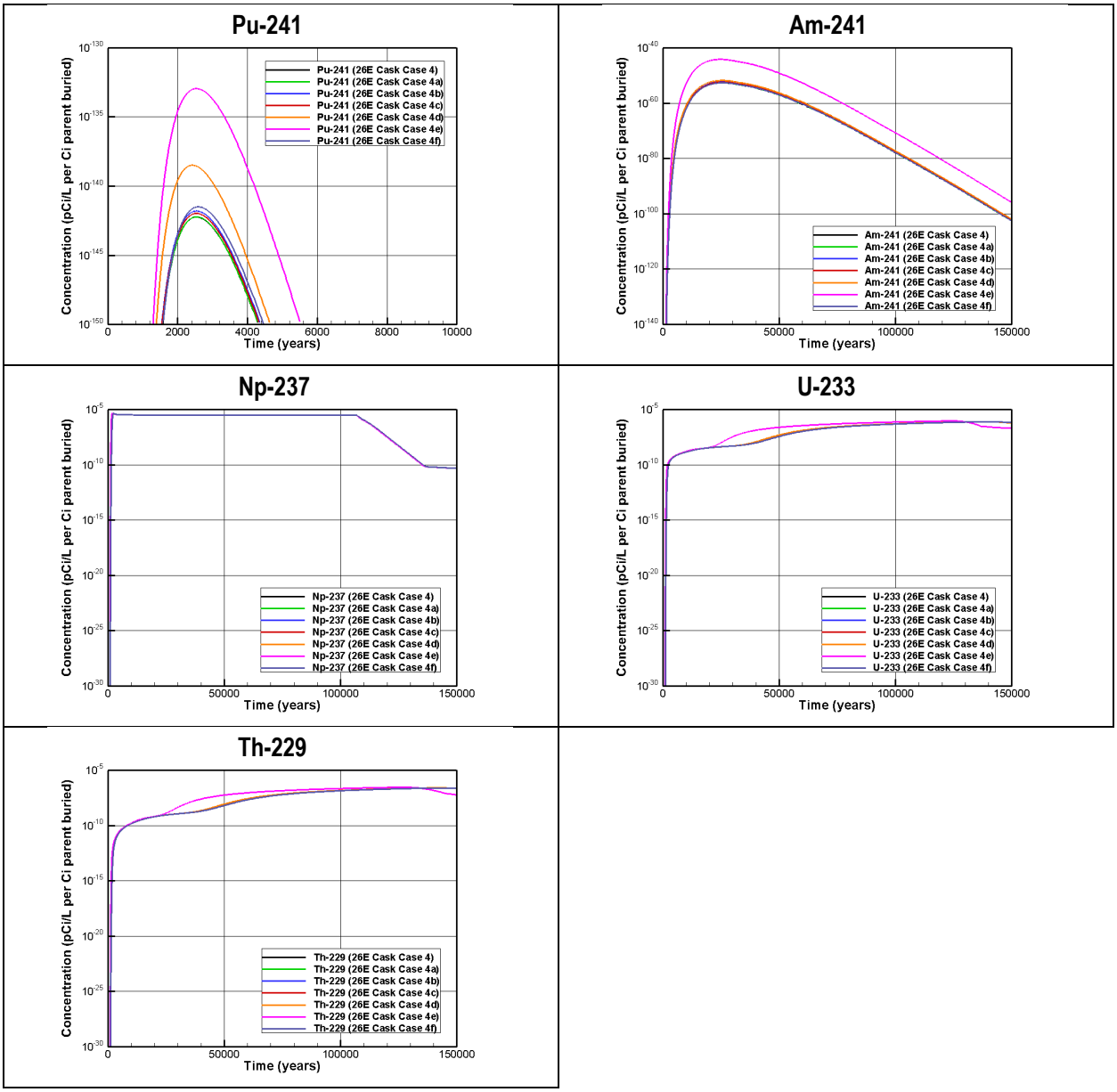

Figure 5-188. Maximum Concentrations of Pu-241 and Progeny at 100-meter POA for Aquifer Nominal PA and Sensitivity Cases for NR26E/Case 4

5.4.3. Air Pathway and Radon Flux Analyses

This section presents the air pathway and radon flux modeling results for the NRCDA. The configuration of the ARM for the NRCDA consists of a 1-D vertical stack of cells from the base of the waste zone to a layer of clean fill. The top of the clean fill is considered the ground surface before closure. Following closure at Year 171, the clean fill is linked to the bottom of the closure cap (Section 3.6.1.9) and the top of the erosion barrier is considered the ground surface. The robust NRCDA waste is assumed to stay intact during the modeled time period. The pertinent information regarding specific material zones, thicknesses, and properties for the NRCDA ARM is presented in Table 5-59. The waste is assumed to be equally distributed throughout the waste zone.

Table 5-59. Layer and Material Properties for Naval Reactor Component Disposal Area Atmospheric Release Model

Layer	Thickness (ft)	Number of Cells	Bulk Dry Density (g cm^{-3})	Porosity	Residual Water Saturation
Before Closure (Year 71 to Year 171)					
Clean Fill	4	10	1.44[a]	0.4561[a]	0.6718[a]
Waste Zone	17	5	0.293[b]	0.889[b]	0.00001[b]
After Closure (Year 171 to Year 1,171)					
Closure Cap	Per Section 3.6.1.9				
Clean Fill	4	10	1.44[a]	0.4561[a]	0.6718[b]
Waste Zone	17	5	0.293[b]	0.889[b]	0.00001[b]

Notes:

[a] From Nichols (2020).

[b] Waste is assumed to be dry resulting in the air-filled porosity equaling the total porosity (WSRC, 2008)

The pads in the NRCDA are split into two waste forms: generic and special. The generic waste form represents the auxiliary equipment, which is primarily contaminated with activated corrosion products (sometimes referred to as "crud" by the U.S. Navy) at low levels and contained within thinner-walled bolted containers. The SWF represents welded casks comprised of highly radioactive components consisting of activated corrosion-resistant metal alloy contained within welded thick steel casks. The only difference between these waste forms in the ARM is the time of breach. The waste in bolted containers is assumed to be available for diffusion immediately following the end of operations. The welded SWF is not breached until 750 years after the end of operations. The waste radionuclides are held in the waste zones until the time of the breach to allow for decay. The waste is assumed to be equally distributed throughout the waste zone. After breach, both waste forms are assigned release rates as metal components corrode. According to data supplied by the NR program, a representative type of activated waste component is the KAPL CB/TS. The KAPL CB/TS was used to represent the various types of activated metal components in the 2002 SA (Yu et al., 2002) and PA2008 (WSRC, 2008) as most of the activity projected for the NR26E NRCDA will be contained in this type of component. The KAPL unit is comprised of six component parts, four made of Inconel and two of Zircaloy. Radionuclides are distributed between the two alloys unequally. Of the radionuclides of interest for the air pathway and radon flux analyses, only the distribution of C-14 is documented in the Special Analysis (88% in Zircaloy and 12% in Inconel). To be conservative, all other radionuclides are modeled to exist entirely in Inconel because of its higher effective corrosion rate (5E-05 cm yr^{-1} versus 5E-06 cm yr^{-1} for Zircaloy). The rate of release of a given radionuclide is calculated by:

$$Rate\_Release = I_a\left(f_I \sum_{i=1}^{i=4} I_i C_i + f_Z \sum_{i=5}^{i=6} I_i C_i\right) \qquad \text{Eq. (5-1)}$$

where:

I_a Inventory of the radionuclide of interest (Ci)
f_I Fraction of the radionuclide inventory in the Inconel metal alloys
f_Z Fraction of the radionuclide inventory in the Zircaloy metal alloys
I_i Fraction of the component part, *i*, in the total alloy
C_i Fraction of the component part, *i*, corroded per year

5.4.3.1. Air Pathway

The surface flux time histories of screened-in air pathway radionuclides (C-14 and H-3; Section 2.3.8) generated by the ARM for the NRCDA are converted to dose by multiplying by the DRFs of the corresponding time period (Section 3.6.2.2.5). The time histories of these doses are used to determine the grouping (immediate, delayed, or non-factor) of the radionuclide-DU pairs to account for temporal differences in dose impact (Section 8.5). The peak dose and grouping-specific effective PO are used to develop a disposal limit for each radionuclide (Section 8.5). Dose results for the NRCDA are presented below.

Naval Reactor Component Disposal Area Generic Waste Form. The surface flux and resultant atmospheric dose of C-14 peaks early because of its immediate availability for transport from the bolted containers (Table 5-60 and Figure 5-189).

Table 5-60. Peak Doses from 1 Curie of C-14 Buried for the Naval Reactor Component Disposal Area Generic Waste Form Air Pathway

Radionuclide	Peak Dose (mrem yr^{-1} Ci^{-1})	Peak Time (Year)
C-14	2.25E-05	71.51

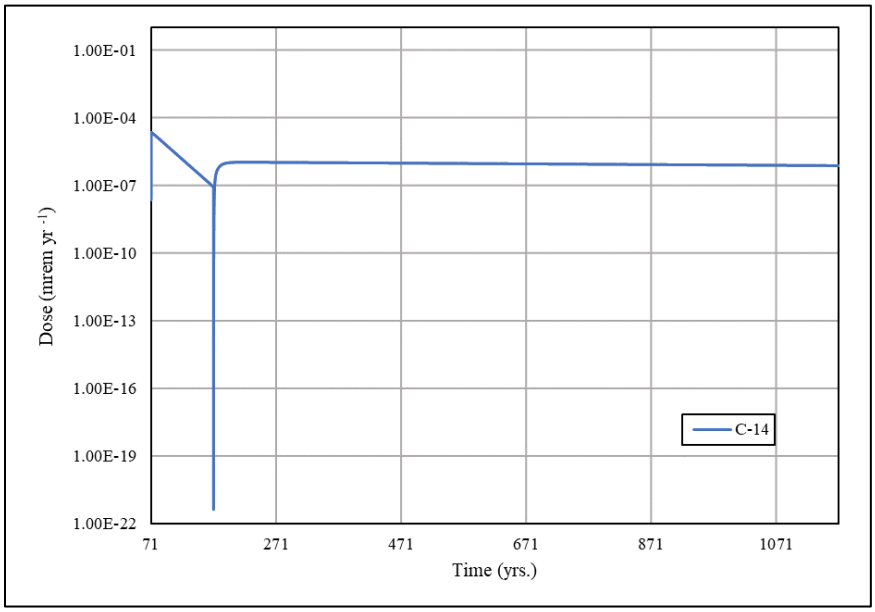

Figure 5-189. Air Pathway Dose Time Histories for 1 Curie of C-14 Buried in Naval Reactor Component Disposal Area Bolted Containers (Generic Waste Form)

Naval Reactor Component Disposal Area Special Waste Form. The surface flux and resultant atmospheric dose of C-14 buried within welded casks does not impact the receptor until after Year 821 (Table 5-61 and Figure 5-190), which is the time of cask breach. The containment of H-3 in the welded cask causes it to decay away before reaching the surface.

Table 5-61. Peak Doses from 1 Curie of C-14 and H-3 Buried for the Naval Reactor Component Disposal Area Special Waste Form Air Pathway

Radionuclide	Peak Dose (mrem yr^{-1} Ci^{-1})	Peak Time (Year)
C-14	1.38E-06	1,171
H-3	---	---

Notes:

--- Peak dose < 10^{-20} mrem yr^{-1}

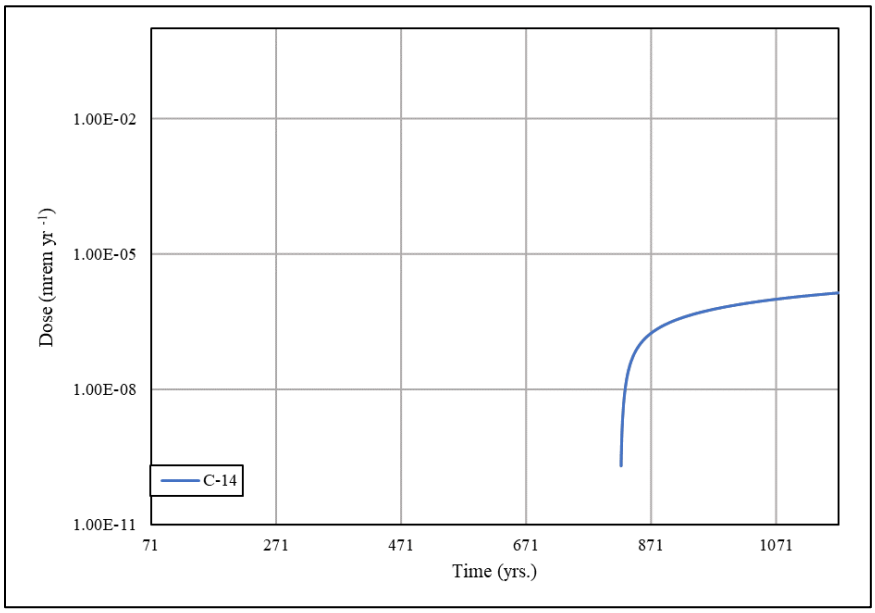

Note: H-3 decays away before the cask is breached and, therefore, is not shown.

Figure 5-190. Air Pathway Dose Time Histories for 1 Curie of C-14 Buried in Naval Reactor Component Disposal Area Welded Casks (Special Waste Form)

5.4.3.2. Radon Pathway

Surface-flux time histories are generated for Rn-222 from each of its 20 parent radionuclides for the NRCDA generic and special waste forms as explained in Section 5.1.5.3.

Naval Reactor Component Disposal Area Generic Waste Form. Rn-222 flux time history characteristics for the NRCDA generic waste form in bolted containers are as detailed for STs and ETs in Section 5.1.5.3 and are like other types of DUs (Figure 5-191). Rn-222 peak fluxes from each parent are provided in Table 5-62. These fluxes are used for radionuclide screening in Section 2.3.8 with all radionuclides being screened out for the NRCDA generic waste form.

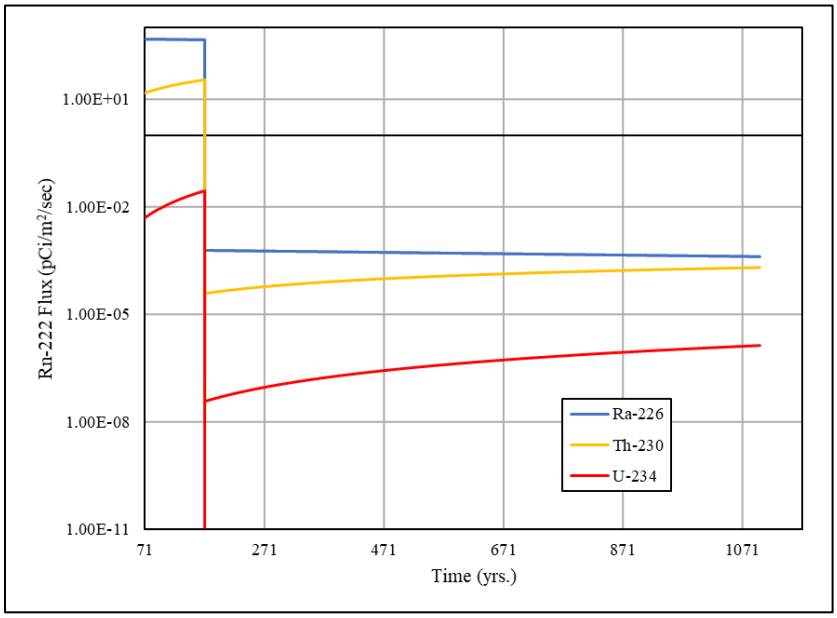

Figure 5-191. Rn-222 Flux Time Histories for 1 Curie of Ra-226, Th-230, and U-234 Buried in Naval Reactor Component Disposal Area Bolted Containers (Generic Waste Form)

Table 5-62. Peak Rn-222 Flux from 1 Curie of Rn-222 Parent Radionuclides and Rn-222 Buried in Naval Reactor Component Disposal Area Bolted Containers (Generic Waste Form)

Radionuclide	Peak Rn-222 Flux (pCi $m^{-2}s^{-1}$)	Peak Time (Year)	Limit or Trigger Required? [a]
Am-242	5.66E-11	170.99	
Am-242m	8.28E-07	170.99	--
Am-246m	0.00E+00	--	--
Bk-250	1.37E-11	170.99	--
Cf-250	3.30E-21	170.99	--
Cm-242	1.67E-08	170.99	--
Cm-246	1.91E-18	170.99	--
Cm-250	3.30E-21	170.99	--
Np-238	2.19E-10	170.99	--
Pa-234	8.66E-11	170.99	--
Pa-234m	2.52E-13	170.99	--
Pu-238	3.32E-06	170.99	--
Pu-242	3.01E-14	170.99	--
Pu-246	0.00E+00	--	--
Ra-226	4.74E+02	72	--
Rn-222	0.00E+00	--	--
Th-230	3.49E+01	170.99	--
Th-234	7.47E-09	170.99	--
U-234	2.78E-02	170.99	--
U-238	4.51E-06	170.99	--

Notes:

[a] Based on radionuclide screening in Section 2.3.8.

Naval Reactor Component Disposal Area Special Waste Form. Rn-222 flux time history characteristics of the NRCDA SWF are like those of the NRCDA generic waste form; however, Rn-222 flux for the SWF is delayed until the welded casks are breached in Year 821 (Figure 5-192). Rn-222 peak fluxes from each parent are provided in Table 5-63. These fluxes are

used for radionuclide screening in Section 2.3.8 with two radionuclides requiring inventory limits (Ra-226 and Th-230) as denoted in Table 5-63 by "Limit" in the last column.

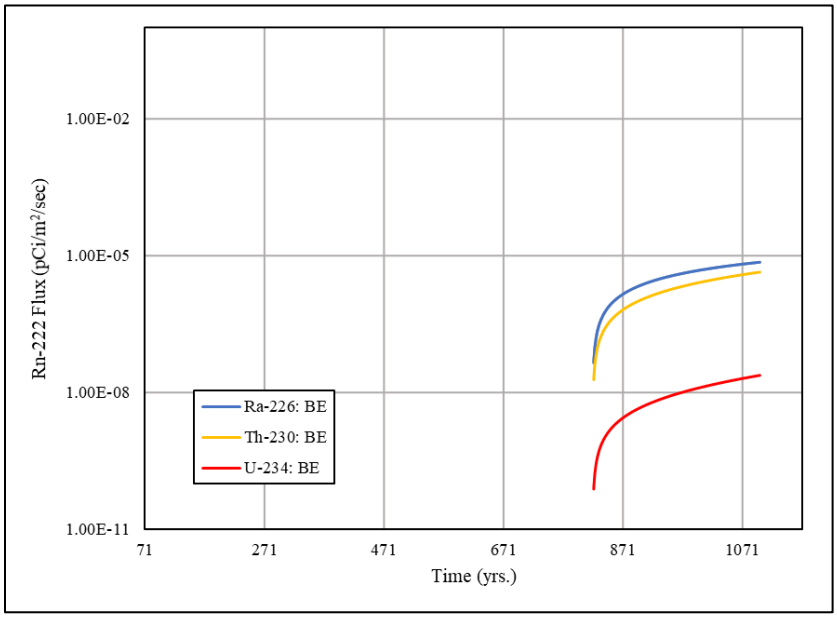

Figure 5-192. Rn-222 Flux Time Histories for 1 Curie of Ra-226, Th-230, and U-234 Buried in Naval Reactor Component Disposal Area Welded Casks (Special Waste Form)

Table 5-63. Peak Rn-222 Flux from 1 Curie of Rn-222 Parent Radionuclides and Rn-222 Buried in Naval Reactor Component Disposal Area Welded Casks (Special Waste Form)

Radionuclide	Peak Rn-222 Flux (pCi $m^{-2}s^{-1}$)	Peak Time (Year)	Limit or Trigger Required? [a]
Am-242	1.68E-16	1,171	--
Am-242m	9.14E-12	1,171	--
Am-246m	0.00E+00	--	--
Bk-250	4.08E-17	1,171	--
Cf-250	0.00E+00	--	--
Cm-242	4.97E-14	1,171	--
Cm-246	7.59E-22	1,171	--
Cm-250	0.00E+00	--	--
Np-238	6.47E-16	1,171	--
Pa-234	1.04E-16	1,171	--
Pa-234m	3.03E-19	1,171	--
Pu-238	9.78E-12	1,171	--
Pu-242	1.78E-18	1,171	--
Pu-246	0.00E+00	--	--
Ra-226	8.73E-06	1,171	Limit
Rn-222	0.00E+00	--	--
Th-230	5.73E-06	1,171	Limit
Th-234	8.99E-15	1,171	--
U-234	3.35E-08	1,171	--
U-238	3.84E-11	1,171	--

Notes:

[a] Based on radionuclide screening in Section 2.3.8.

5.5. REFERENCES

Aleman, S. E., and Hamm, L. L. (2021). "E-Area Low-Level Waste Facility Multitiered Groundwater and Intruder Radionuclide Screening." SRNL-STI-2020-00566, Rev. 0. Savannah River National Laboratory, Aiken, SC. January 2021.

Carey, S. (2005). "Low Activity Waste (LAW) Vault Structural Degradation Prediction." T-CLC-E-00018, Rev. 1. Westinghouse Savannah River Company, Aiken, SC. October 27, 2005.

Danielson, T. L. (2019a). "A Limited-In-Scope Comparison of Subsidence Scenarios for 3D Vadose Zone PORFLOW Trench Models." SRNL-STI-2019-00636, Rev. 1. Savannah River National Laboratory, Aiken, SC.

Danielson, T. L. (2019b). "A Monte Carlo Rectangle Packing Algorithm for Identifying Likely Spatial Distributions of Final Closure Cap Subsidence in the E-Area Low-Level Waste Facility." SRNL-STI-2019-00440, Rev. 0. Savannah River National Laboratory, Aiken, SC.

Danielson, T. L. (2019c). "PORFLOW Implementation of Vadose Zone Conceptual Model for Slit and Engineered Trenches in the E-Area Low Level Waste Facility Performance Assessment." SRNL-STI-2019-00193. Savannah River National Laboratory, Aiken, SC.

Danielson, T. L. (2020a). "A Case Study Using ST06 for Slit and Engineered Trench Model Implementation in the E-Area Low-Level Waste Facility Performance Assessment." SRNL-STI-2019-00750, Rev. 0. Savannah River National Laboratory, Aiken, SC.

Danielson, T. L. (2020b). "Comparison of Slit Trench and Engineered Trench 3D Vadose Zone Conceptual Models." SRNL-STI-2019-00637, Rev. 0. Savannah River National Laboratory, Aiken, SC.

Danielson, T. L. (2021). "PORFLOW Implementation of Special Waste Form Models for Slit and Engineered Trenches in the E-Area Low Level Waste Facility Performance Assessment (T. L. Danielson to D. A. Crowley)." SRNL-STI-2020-00162, Rev. 1. Savannah River National Laboratory, Aiken, SC.

Dyer, J. A. (2019b). "Infiltration Data Package for the E-Area Low-Level Waste Facility Performance Assessment." SRNL-STI-2019-00363, Rev. 0. Savannah River National Laboratory, Aiken, SC. November 2019.

Flach, G. P., Collard, L. B., Phifer, M. A., Crapse, K. P., Dixon, K. L., Koffman, L. D., and Wilhite, E. L. (2005). "Preliminary Closure Analysis for Slit Trenches #1 and #2." WSRC-TR-2005-00093. Westinghouse Savannah River Company, Aiken, SC.

Gorensek, M. B. (2021). "Updated Estimate of Tritium Permeation from TPBAR Disposal Containers in ILV (U)." SRNL-TR-2020-00298, Rev. 1. Savannah River National Laboratory, Aiken, SC. December 7, 2021.

Hamm, L. L., Collard, L. B., Aleman, S. E., Gorensek, M. B., and Butcher, B. T. (2012). "Special Analysis for Slit Trench Disposal of the Reactor Process Heat Exchangers." SRNL-STI-2012-00321, Rev. 0. Savannah River National Laboratory, Aiken, SC.

Hamm, L. L., and Smith, F. G. (2010). "Special Analysis for Slit Trench Disposal of the Heavy Water Components Test Reactor." SRNL-STI-2010-00574, Rev. 0. Savannah River National Laboratory, Aiken, SC.

Hang, T., and Hamm, L. L. (2022). "PORFLOW Implementation of Vadose Zone Conceptual Model for Naval Reactor Component Disposal Areas in the E-Area Low Level Waste Facility Performance Assessment." SRNL-STI-2019-00357, Rev. 1. Savannah River National Laboratory, Aiken, SC. January 2022.

Hiergesell, R. A. (2005). "Special Analysis: Production TPBAR Waste Container Disposal Within the Intermediate Level Vault." WSRC-TR-2005-00531. Westinghouse Savannah River Company, Aiken, SC.

Kaplan, D. I. (2016b). "Geochemical Data Package for Performance Assessment Calculations Related to the Savannah River Site." SRNL-STI-2009-00473, Rev. 1. Savannah River National Laboratory, Aiken, SC.

Lanning, D. D., and Gilbert, E. R. (2005). "Long-Term Release Estimate for TEF Disposal Containers (U)." PNN-TTP-5-683, Rev. 0, S/RD (Extracted information is unclassified). Pacific Northwest National Laboratory, Richland, WA. August 2005.

Nichols, R. L. (2020). "Hydraulic Properties Data Package for the E-Area Soils, Cementitious Materials, and Waste Zones - Update." SRNL-STI-2019-00355, Rev. 0. Savannah River National Laboratory, Aiken, SC.

Nichols, R. L., and Butcher, B. T. (2020). "Hydraulic Properties Data Package for the E-Area Soils, Cementitious Materials, and Waste Zones - Update." SRNL-STI-2019-00355, Rev. 1. Savannah River National Laboratory, Aiken, SC.

Peregoy, W. (2006b). "Structural Evaluation of Intermediate Level Waste Storage Vaults for Long-Term Behavior." T-CLC-E-00024, Rev. 0. Washington Savannah River Company, Aiken, SC. June 27, 2006.

Phifer, M. A., Millings, M. R., and Flach, G. P. (2006). "Hydraulic Property Data Package for the E-Area and Z-Area Vadose Zone Soils, Cementitious Materials, and Waste Zones." WSRC-STI-2006-00198, Rev. 0. Washington Savannah River Company, Aiken, SC.

Smith, F. G. (2020). "GoldSim Modeling of Vadose Zone Transport for E-Area Naval Reactor Component Disposal Areas: Model Description and Benchmarking." SRNL-STI-2020-00214, Rev. 0. Savannah River National Laboratory, Aiken, SC. July 2020.

Smith, F. G., III (2021a). "PORFLOW Modeling of Vadose Zone Flow and Transport for the E-Area Intermediate Level Vault." SRNL-STI-2020-00410, Rev. 1. Savannah River National Laboratory, Aiken, SC. December 2021.

Snider, B. T. (2007). "TEF Waste Containers (U)." M-SPP-H-00418, Rev. 2. Washington Savannah River Company, Aiken, SC. October 8, 2007.

SRNL (2017). "The Hydrostratigraphic Surfaces Data Package [Change Control Rev1 and Rev0 dataset (Appendix 5 to SRNL-STI-2017-00301).xlsx]." Rev. 1. Retrieved August, 2020 from \\godzilla-01\hpc_project\projwork50\QA\Data\ELLWF\SubsurfaceElevDepth. *Last Updated* November 3, 2017. SRNL High Performance Computing File Server Network, Savannah River National Laboratory, Aiken, SC.

SRNL (2018). "The Geochemical Data Package (GeochemPackage_Ver3.1_4-27-18_FINAL.xls)." Version 3.1. Retrieved December, 2018 from \\godzilla-01\hpc_project\projwork50\QA\Data\ELLWF\Rad-Dose. *Last Updated* April 27, 2018. SRNL High Performance Computing File Server Network, Savannah River National Laboratory, Aiken, SC.

SRNL (2019a). "The Infiltration Data Package (Infiltration-Data-Package_Ver1.0_10-16-2019_DRAFT.xlsx)." Version 1.0. Retrieved August, 2020 from \\godzilla-01\hpc_project\projwork50\QA\Data\ELLWF\Infiltration. *Last Updated* October 25, 2019. SRNL High Performance Computing File Server Network, Savannah River National Laboratory, Aiken, SC.

SRNL (2019b). "RadDosePackage_Version-2.0_CLEAN_8-13-19_FINAL.xlsx." Version 2.0. Retrieved August, 2019 from \\godzilla-01\hpc_project\projwork50\QA\Data\ELLWF\Rad-Dose\Current\ Rev1Report_Ver2.0-Database. SRNL High Performance Computing File Server Network, Savannah River National Laboratory, Aiken, SC.

SRNL (2020). "The Hydraulic Properties Data Package (HydraulicProperties_Rev3_12-01-2020.xlsm)." Rev. 3. Retrieved December, 2020 from \\godzilla-01\hpc_project\projwork50\QA\Data\ELLWF\Material\Current. *Last Updated* December 1, 2020. SRNL High Performance Computing File Server Network, Savannah River National Laboratory, Aiken, SC.

U.S. DOE (2021b). "Radioactive Waste Management Manual." DOE M 435.1-1, Chg 3: 1-11-2021. U. S. Department of Energy, Washington, DC. January 11, 2021.

U.S. NRC (2000). "A Performance Assessment Methodology for Low-Level Radioactive Waste Disposal Facilities." NUREG-1573. U.S. Nuclear Regulatory Commission, Washington, DC. October 2000.

Vinson, D. W., Subramanian, K. H., and Clark, E. A. (2004). "Containment Materials Performance for TPBAR Disposal." WSRC-TR-2004-00374. Savannah River National Laboratory, Westinghouse Savannah River Company, Aiken, SC.

WSRC (2008). "E-Area Low-Level Waste Facility DOE 435.1 Performance Assessment." WSRC-STI-2007-00306, Rev. 0. Washington Savannah River Company, Savannah River Site, Aiken, SC.

Yu, A. D., McDowell-Boyer, L. M., Cook, J. R., and Young, K. E. (2002). "Special Analysis: Naval Reactor Waste Disposal Pad (U)." WSRC-RP-2001-00948, Rev. 2. Westingouse Savannah River Company, Aiken, SC. December 2002.